DOI:10.14753/SE.2025.3172

SEMMELWEIS EGYETEM

DOKTORI ISKOLA

Ph.D. értekezések

3172.

KUGLER SZILVIA

Szív- és érrendszeri betegségek élettana és klinikuma

című program

Programvezető: Dr. Merkely Béla, egyetemi tanár

Témavezető: Dr. Radovits Tamás, egyetemi tanár

Dr. Nemeskéri Ágnes, egyetemi docens

DOI:10.14753/SE.2025.3172

HISTOLOGICAL, IMMUNOHISTOCHEMICAL, AND MOLECULAR EXAMINATION OF THE PATHOMECHANISMS OF ATRIAL FIBRILLATION

PhD thesis

Szilvia Kugler, MD

Doctoral School of Theoretical and Translational Medicine
Semmelweis University

Supervisors: Tamás Radovits, MD, Ph.D
Ágnes Nemeskéri, MD, Ph.D

Official reviewers: Márton Ákos Lőrincz, MD, Ph.D
Zoltán Husti, MD, Ph.D

Head of the Complex Examination Committee: István Karádi, MD, Ph.D

Members of the Complex Examination Committee:
Henriette Farkas, MD, Ph.D; Péter Andréka, MD, Ph.D

Budapest
2025

DOI:10.14753/SE.2025.3172

TABLE OF CONTENTS

LIST OF ABBREVIATIONS 4

1. INTRODUCTION 7

1.1. Atrial fibrillation 7

1.1.1. Treatment of atrial fibrillation 7

1.1.2. Pathogenesis of atrial fibrillation 8

1.2. Anatomy of the cardiac pacemaker and conduction system 16

1.3. Markers of the cardiac pacemaker and conduction system 17

1.3.1. Connexins 17

1.3.2. Desmin intermediate filament 18

1.3.3. Hyperpolarization Activated Cyclic Nucleotide Gated Potassium Channel 4 19

1.3.4. Human natural killer-1 19

2. OBJECTIVES 20

2.1. Analysis of the histological and immunohistochemical features of the myocardial sleeves around pulmonary veins, caval veins and coronary sinus ... 20

2.2. Assessment of inflammation in heart failure-associated atrial fibrillation ... 20

3. METHODS 21

3.1. Characterization of the histological and immunohistochemical features of myocardial sleeves in the walls of cardiac veins 21

3.1.1. Human tissues 21

3.1.2. Tissue processing for histology 25

3.1.3. Connexin 45 and connexin 43 immunohistochemistry 25

3.1.4. Desmin immunohistochemistry 26

3.1.5. Double labeling of connexin 45 and desmin 27

3.1.6. Visualization of slides 27

DOI:10.14753/SE.2025.3172

3.1.7. Immunohistochemical quantitative analysis 27

3.2. Investigation of inflammasome activation in end-stage heart failure-associated atrial fibrillation 29

3.2.1. Human samples 29

3.2.2. Assessment of inflammasome activation 30

3.2.3. Assessment of macrophage infiltration 31

3.2.4. Evaluation of fibrosis 32

3.2.5. Statistical analysis 33

4. RESULTS 34

4.1. Histology of the cardiac pacemaker and conduction system of human adults 34

4.2. Histological features of the venous myocardial sleeves and the atria of human adults 36

4.2.1. Myocardial sleeves of the pulmonary veins 36

4.2.2. Myocardial sleeve of the superior vena cava 39

4.2.3. Myocardial sleeve of the inferior vena cava 41

4.2.4. Myocardial sleeve of the coronary sinus 42

4.2.5. Quantitative analysis of desmin immunostaining 45

4.2.6. Right and left atrial structures 48

4.3. Histological features of the human fetal heart 50

4.4. Inflammation and fibrosis in end-stage heart failure-associated atrial fibrillation 51

4.4.1. Inflammasome activation 51

4.4.2. Macrophage infiltration 51

4.4.3. Left atrial fibrosis 54

5. DISCUSSION 55

5.1. Myocardial sleeves of the pulmonary veins, caval veins and coronary sinus 55

DOI:10.14753/SE.2025.3172

5.1.1. Microscopic anatomy of the myocardial sleeves 55

5.1.2. Immunohistochemical characteristics of the myocardial sleeves 58

5.2. Microscopic anatomy of the atria 60

5.3. Developmental explanation for supraventricular specialized cardiomyocytes 61

5.4. The association of inflammation with atrial fibrillation in end-stage heart failure 61

5.5. Atrial fibrosis in end-stage HF-associated atrial fibrillation 64

5.6. Limitations 64

6. CONCLUSIONS 65

7. SUMMARY 66

8. REFERENCES 67

9. BIBLIOGRAPHY OF THE CANDIDATE'S PUBLICATIONS 87

9.1. Publications directly related to the present thesis 87

9.1.1. Publications in international peer–reviewed journals 87

9.1.2. Publications in Hungarian peer–reviewed journals 87

9.2. Publications not directly related to the present thesis 87

9.2.1. Publications in international peer–reviewed journals 87

9.2.2. Publications in Hungarian peer–reviewed journals 88

10. ACKNOWLEDGEMENTS 89

DOI:10.14753/SE.2025.3172

LIST OF ABBREVIATIONS

AF	atrial fibrillation
AIM2	absent in melanoma 2
AO	aortic root
ASC	apoptosis-associated speck-like protein containing a CARD
AV	azygos vein
AVN	atrioventricular node
BMI	body mass index
Bpm	beats per minute
Cav1.3	calcium voltage-gated channel subunit alpha 1 D
Cav3.1	calcium voltage-gated channel subunit alpha 1 G
CFAE	complex fractionated atrial electrogram
CNTN2	contactin 2
CRP	C-reactive protein
CRT	cardiac resynchronization therapy
CS	coronary sinus
CT	crista terminalis
Cx	connexin
DAB	3,3’-diaminobenzidine
DAMPs	damage-associated molecular patterns
DAPI	4′,6-diamidino-2-phenylindole
dsDNA	double-strand deoxyribonucleic acid
E	epicardium
ECG	electrocardiogram
EF	ejection fraction
F	female
FA	formaldehyde
Fig.	figure
GAPDH	glyceraldehyde-3-phosphate dehydrogenase
HCN1	hyperpolarization activated cyclic nucleotide gated potassium channel 1
HCN4	hyperpolarization activated cyclic nucleotide gated potassium channel 4

HE	hematoxylin-eosin
HF	heart failure
HNK1	human natural killer-1
HOCM	hypertrophic obstructive cardiomyopathy
I	interstitial (fibrosis)
IAA	isolated atrial amyloidosis
IAS	interatrial septum
Iba1	ionized calcium-binding adaptor molecule 1
IL	interleukin
IQR	interquartile range
IVC	inferior vena cava
IVS	interventricular septum
LA	left atrium
LAA	left atrial appendage
LAD	left anterior descending artery
LAIW	left atrial inferior wall
LAPW	left atrial posterior wall
LAR	left atrial ridge
LV	left ventricle
M	male / myocardium *(only in figures, clearly defined)*
Max	maximum
MGV	mean gray value
Min	minimum
MRI	magnetic resonance imaging
mRNA	messenger ribonucleic acid
MS	myocardial sleeve
N	number (of patients/ samples)
NA	not available
NALP1	NLR family, pyrin domain containing 1
NFκB	nuclear factor kappa B
NLR	NOD leucine-rich repeat-containing receptor
NLRC4	NLR family CARD domain-containing protein 4

NLRP3	NLR family, pyrin domain containing 3
NS	non-significant
NYHA	New-York Heart Association
PAMPs	pathogen-associated molecular patterns
PAS	periodic acid–Schiff
PCT	procalcitonin
PF	Purkinje fibers
PFA	paraformaldehyde
Pitx	paired-like homeodomain transcription factor
PV	pulmonary vein
Q1	first quartile
Q3	third quartile
RA	right atrium
RAA	right atrial appendage
RV	right ventricle
SAN	sinoatrial node
SD	standard deviation
SNA	sinoatrial nodal artery
SVC	superior vena cava
SR	sinus rhythm
T	total (fibrosis)
TBX	T-box transcription factor
TNF-α	tumor necrosis factor-alpha
TV	tricuspid valve
VEST	left atrial vestibule
WBC	white blood cell
WM	working myocardium

DOI:10.14753/SE.2025.3172

1. INTRODUCTION

1.1. Atrial fibrillation

Atrial fibrillation (AF) is the most prevalent sustained cardiac arrhythmia in the world, with an estimated prevalence of 2-6% in adults (1-3). It is defined as a heart rhythm with no P waves and irregular RR intervals on a 12-lead electrocardiogram (ECG) recording or on a single-lead ECG strip lasting at minimum 30 seconds (provided that atrioventricular conduction is intact) (1, 4). Older age and several comorbidities such as hypertension, heart failure (HF), diabetes mellitus, coronary artery disease, valve disease, hyperthyroidism and obesity contribute to the development and progression of AF (1, 5). It has a significant impact on health care due to the substantial mortality and morbidity associated with HF and ischemic stroke (1). Chest pain, poor effort tolerance, dizziness and disordered sleep are frequent symptoms (1, 6), and the arrhythmia can lead to cognitive decline or depression as well (1, 7, 8). AF has more patterns based on presentation, duration and spontaneous cessation of the episodes. Paroxysmal AF resolves within seven days of onset. In the case of persistent and long-standing persistent AF, rhythm control strategies are applied. Persistent AF lasts beyond 7 days, while long-standing persistent AF persists longer than 12 months. In permanent AF, the arrhythmia is accepted by the patient and physician, and restoration of sinus rhythm (SR) is not a goal (1). Transition from paroxysmal to persistent or permanent AF is commonly characterized by progressive structural remodeling of the atria (1, 9).

1.1.1. Treatment of atrial fibrillation

Treatment of AF targets stroke prevention, rate and rhythm control (1), and management of comorbidities and lifestyle (1, 10). Prevention of ischemic stroke can be achieved by anticoagulation (novel oral anticoagulant drugs, vitamin K antagonists or low-molecular-weight heparin) (1) or, in specific cases, by left atrial appendage (LAA) occlusion (1, 11). The necessity of anticoagulation can be evaluated by stroke risk scores, for example the CHA_2DS_2-VA score, which, unlike the previous scoring system, does not include sex as a risk factor (1). Rate control is often enough to improve the symptoms associated with AF (1), and it can be achieved by drugs (beta-blockers, non-dihydropyridine calcium channel blockers, digoxin) (1, 12) or by atrioventricular node (AVN) ablation and

ventricular pacing (1, 13). Rhythm control aims to restore and maintain SR to reduce AF-related symptoms (1). Compared to rate control alone, rates of AF progression have been shown to be significantly lower with rhythm control strategies (1, 14). Rhythm control can be achieved with antiarrhythmic drugs (propafenone, flecainide, sotalol, amiodarone) (1), electric cardioversion (1, 15) and catheter ablation (1, 16). The main focus of catheter ablation is the isolation of pulmonary veins (PVs) by linear lesions around their antrum, either by point-by-point radiofrequency ablation, single-shot techniques such as cryoballoon ablation or the novel pulsed field ablation (1, 17, 18). PV isolation is recommended as a first-line rhythm control treatment option for patients with paroxysmal AF episodes (1). However, it is not infrequent that AF episodes return after catheter ablation, therefore many patients require several procedures (1, 19). The difficulties of the treatment of AF can be explained by the complexity and progressive nature of the arrhythmia. The recurrence of arrhythmia is caused by an interaction of various factors, such as increasing AF duration, age, left atrial size, presence of extrapulmonary foci, accumulation of epicardial fat tissue, or the presence of other atrial substrates (20). For this reason, particularly in persistent AF, extensive ablation techniques (linear lesions in the atria, ablation of non-PV foci or ganglionated plexi, ablation of sites where complex fractionated electrograms or rotors occur, fibrosis-guided voltage mapping and ablation) may be considered (20-22). Endoscopic (thoracoscopic) and hybrid (endocardial and endoscopic epicardial) ablation should be considered in patients who have drug refractory symptomatic persistent AF (1), as epicardial ablation may result more often in long-standing transmural lesions compared to the endocardial ablation (1, 23).

1.1.2. Pathogenesis of atrial fibrillation

The pathomechanism of AF is highly complex (24-26) (Figure 1). The arrhythmia is presumed to be induced by a focal electrical activation (trigger). Triggers usually originate from the PVs, albeit other supraventricular regions have been also identified as potential sources of AF paroxysms (27, 28). Contrarily, AF recurrences are thought to be associated with more extensive structural and electrical remodeling of the atria, termed the AF substrate (29). Any electrophysiological, structural, architectural or contractile abnormalities affecting the atria that may cause clinically-relevant manifestations are termed atrial cardiomyopathy (30). It has 4 histological subtypes: cardiomyocyte damage

(genetic diseases), fibrotic changes (aging), their combination (HF) and non-collagen deposits (inflammatory infiltrates, atrial amyloidosis) (30). Different stress effects on the atrial myocardium (hemodynamic overload, oxidative stress, pro-inflammatory cytokines, infiltration of adipose tissue) may promote the conversion of atrial cardiomyopathy into an arrhythmogenic substrate (30). Several clinical factors (HF, hypertension, valve disease, atrial septal defect, atrial flutter, obstructive sleep apnea) can facilitate atrial remodeling via increase of atrial stretch (31). Elevated left atrial pressure due to impaired ventricular relaxation, ischemia caused by increased resting heart rate, enhanced atrial ectopic activity, and shortening of the action potential duration and effective refractory period may contribute to the development of hyperthyroidism-induced AF (5). The complex interaction between AF triggers and the remodeled atrial substrate plays essential role in the persistence of AF (31). Atrial remodeling might be reversible following elimination of the inciting cause (31), but irreversible structural alterations can develop as the disease progresses, therefore AF and the underlying disease should be treated as early as possible (32). Numerous data support that AF is itself a progressive disease that causes electrophysiological and structural alterations in the atria that facilitate the initiation or persistence of the arrhythmia. An electrophysiological study on goats verified the shortening of the atrial effective refractory period and of the cycle length of AF during the duration of the arrhythmia. These mechanisms were found to be responsible for the concept that “atrial fibrillation begets atrial fibrillation” (33). It was discussed that general decrease in atrial conduction velocity and formation of local areas of structural intra-atrial conduction block presumably also play a role in chronic electrophysiological adaptation and consequently in the persistence of AF (33). Long-lasting AF episodes induce structural atrial remodeling (fibrosis, dilatation), promoting the perpetuance of the arrhythmia. Structural remodeling can be evaluated in an invasive way by quantifying areas of low-voltage atrial signals, or with magnetic resonance imaging (MRI) (25, 29). Left atrial deformation parameters, such as echocardiographic strain imaging, are highly sensitive for non-invasive indirect detection of left atrial tissue remodeling (30, 34). Global longitudinal atrial strain can even be used to predict future AF in patients with SR (35). It is of note that many patients already have substantial atrial damage at the first AF episode, and the arrhythmia induces further electrical and structural changes in the atria on top of this pre-existing damage (25).

DOI:10.14753/SE.2025.3172

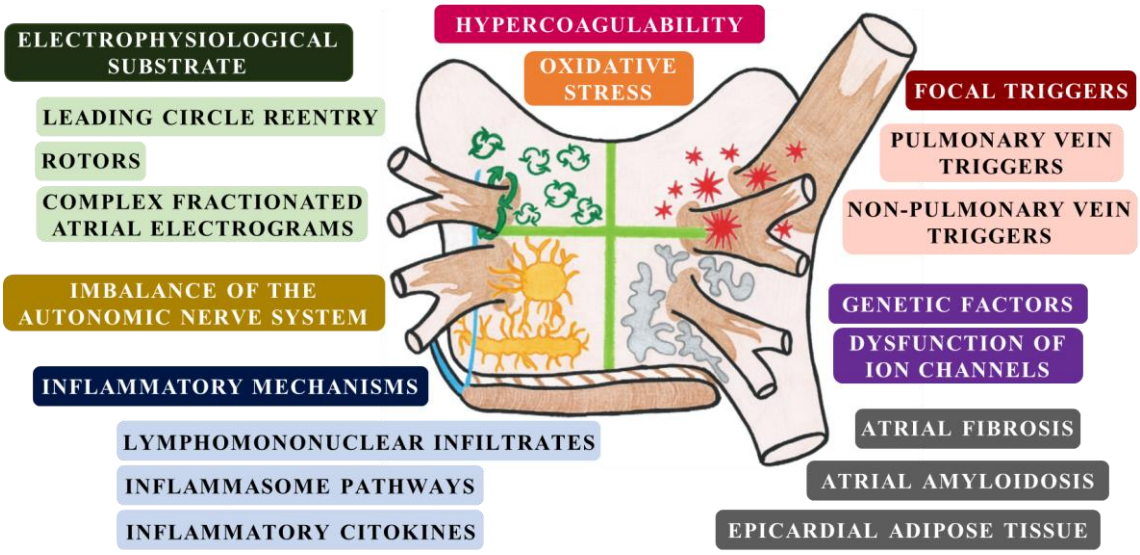

Figure 1. Pathomechanisms of atrial fibrillation.

Pathophysiological factors underlying atrial fibrillation are illustrated in a schematic drawing of the atria, pulmonary veins, caval veins and coronary sinus. Green: rotors; red: focal triggers; yellow: autonomic ganglia; grey: scar (36).

Pulmonary vein triggers

The left atrial myocardium, which extends into the wall of the PVs and forms myocardial sleeves (MSs), is a well-known site of origin of supraventricular tachyarrhythmias. A study of human cardiac electrophysiological examinations published in 1998 verified that the PVs are important sources of ectopic beats, initiating AF paroxysms. These foci responded to radiofrequency ablation treatment (27). Macroscopic (37-39) and microscopic (38, 40-44) features of the MSs around PVs were described previously. MSs were generally longer in the superior than in the inferior PVs (38, 40, 42-44). A study showed significantly higher prevalence of MSs in the PVs of patients with AF compared to patients without AF (42). MSs were documented to be significantly longer in the inferior PVs (44) and in the left superior PVs (41, 42), and significantly thicker in the right superior PVs (41) in patients with AF than in those without AF. However, some studies have shown no differences in the prevalence of MS and its distribution among PVs (43), or in the length and histological feature of MS (38) between patients with and without AF. In rats, electron microscopic examination showed small groups of cardiomyocytes possessing features similar to those of pacemaker cells in the intrapulmonary segments of the PVs (45). For human PVs, only one study is available

that documented the presence of cardiomyocytes displaying ultrastructural morphological characteristics of P-cells and Purkinje fibers (46).

Non-pulmonary vein triggers

Electrophysiological studies indicate that supraventricular regions other than PVs may also trigger arrhythmias. Ectopic beats arising from the superior vena cava (SVC) were reported to initiate arrhythmia in 6% of patients with pre-existing paroxysmal AF (47). Non-PV triggers (crista terminalis, coronary sinus (CS), SVC, left atrial posterior wall) were found in 11% of patients undergoing AF ablation (48), while other reports documented a 20-32% frequency of non-PV triggers of AF (49-52). According to the latter publications, the most common non-PV ectopic areas triggering AF were the SVC (26-40%) and the left atrium (17.5-42%), predominantly its posterior wall. Besides the above-mentioned, the crista terminalis (5-15%), vena obliqua atrii sinistri alias ligament of Marshall (5-15%), interatrial septum (1.5-11%), and the orifice of the CS (1-17%) were also documented as potential sites of AF triggers (49-52). The inferior vena cava (IVC) was identified as the trigger site of AF or paroxysmal atrial tachycardia in a few cases (53-59). Based on electrophysiological mapping, particular cardiomyocytes of the above-mentioned non-PV arrhythmogenic foci may exhibit arrhythmogenic activity due to increased automaticity, triggered activity and microreentrant circuits (28). Despite detailed electrophysiological characterization, few data have been published about the macroscopic (39, 60) and microscopic (61-63) morphology of the MS of caval veins, CS and other non-PV supraventricular arrhythmogenic areas. A previous study found no difference in the characteristics of MS around the caval veins between patients with and without a history of AF (63). For some mammalian species, many pacemaker cell-like cardiomyocytes were documented in the MS throughout the whole length of the CS (64). However, there are no convincing human data on the presence of pacemaker cell-like or Purkinje-like cardiomyocytes in caval veins or CS. For the atrial regions, there is some human and mammalian research documenting the presence of conducting-like cells. Pacemaker cells were identified in the Eustachian ridges of cats (65). A study on human and canine hearts showed the presence of Purkinje-like cardiomyocytes and pacemaker cells in the internodal pathways, the Eustachian ridge and the interatrial conducting pathway (Bachmann’s bundle) (66).

Electrophysiological substrate

Electrophysiological mapping studies revealed complex electrical activations with reentry circuits in the atria during AF, suggesting a heterogeneous electrophysiological substrate (26). During reentry, a cluster of cardiomyocytes that were not activated during the primary depolarization wave regains excitability in time to be discharged before the impulse has died, and these groups serve as a connecting link to reactivate the areas that have just been discharged and have recovered from the initial depolarization (67). The simplest form of functional reentry is the so-called "leading circle reentry". This type of reentry has no excitable gap which results in a permanent centripetal activation of the center of the circuit, rendering it continuously refractory. This refractory area forms a functional barrier that, like scar tissue, maintains reentry. The small wavelength of reentrant circuits due to short atrial refractory period and/or slow conduction velocity, as well as large atria, allow the formation of several reentrant circuits and increase the likelihood of maintaining the AF episode (22). Rotors are a special type of functional reentry where the wavefront is spiral shaped. They can be fixed in one place (often to areas around the PVs) or meander through space and interact with other regions of functional or anatomic inhomogeneity. They fragment and induce multiple disorganized waves, which then induce AF (22). Complex fractionated atrial electrograms (CFAEs) represent areas where myocardial fibers are separated or disorganized resulting in slowed, dyssynchronous, anisotropic local conduction. Termination of AF with ablation of these sites has been documented. However, CFAEs seems to be rather passive electrophysiological manifestations of inter-atrial conduction than real drivers of AF (22).

Inflammatory mechanisms

There is increasing evidence that inflammatory mechanisms are involved in the pathogenesis of AF. Systemic inflammatory conditions, such as psoriasis, rheumatoid arthritis, inflammatory bowel disease or sepsis, as well as local cardiac inflammation in pericarditis and myocarditis, were demonstrated to increase the incidence of AF (68). Emerging evidence supports that not only immune cells but also atrial cardiomyocytes, fibroblasts and adipocytes can produce pro-inflammatory cytokines and express cytokine receptors (68). Inflammatory lymphomononuclear infiltrates and focal myocyte necrosis were found in atrial samples from 66% of patients with lone AF (AF without clinically

evident abnormalities) (69). A study on human and sheep samples suggests that AF is associated with the fibrotic remodeling of subepicardial fatty infiltrates of the atria, and that cytotoxic lymphocytes may be involved in this process (70). Enhanced macrophage infiltration was also shown in the atria of patients with persistent AF (71, 72) and postoperative AF (73). Significantly elevated levels of acute-phase proteins and inflammatory cytokines (C-reactive protein (CRP), tumor necrosis factor-alpha (TNF-α), serum amyloid A, interleukin (IL)-1, IL-6, IL-8, IL-10, IL-18) were detected in blood samples of AF patients compared to the SR group (74-76). Elevated serum levels of IL-18 were significantly associated with AF in the absence of structural heart disease, and IL-18 levels were significantly higher in persistent than in paroxysmal AF (76). Cytokine levels were higher in AF patients with structural heart disease compared to lone AF, and in both persistent and permanent AF compared to paroxysmal AF (74). Polymorphism of the IL-1 receptor antagonist gene was documented to be an independent predictor of lone AF, possibly because of an inadequate restriction of inflammatory responses (77).

Inflammasomes are inflammatory signaling cytoplasmic multiprotein complexes that regulate innate immunity (78, 79). Their activation requires a priming event that induces the synthesis of "NLR family, pyrin domain containing 3" (NLRP3) and pro-IL-1β via toll-like receptor–nuclear factor kappa B (NFκB) signaling, and a subsequent triggering mechanism via inflammasome-related pattern recognition receptors that are expressed among others in macrophages, neutrophils and epithelial cells (80). Trigger signals promote the assembly of NLRP3 sensor protein, an adaptor protein ("apoptosis-associated speck-like protein containing a CARD" [ASC]) and precursor caspase-1, leading to auto-cleavage of precursor caspase-1 into active/cleaved caspase heterodimers consisting of p20 and p10 subunits (79, 81). In immune cells, active caspase-1 cleaves pro-IL-1β and pro-IL-18, releasing active IL-1β and IL-18 (82, 83) (Figure 2).

Role of NLRP3 inflammasome has been established in numerous cardiovascular diseases, including arrhythmias, coronary atherosclerosis, myocardial infarction and cardiomyopathies (68, 84). There is evidence that activation of the NLRP3 inflammasome in atrial cardiomyocytes and infiltrating macrophages plays a role in the initiation and maintenance of AF (85). Hypertension, obesity and diabetes are presumed to promote the development of AF through activation of the NLRP3 inflammasome in atrial cardiomyocytes (85). Increased NLRP3 inflammasome activity was detected in right

atrial appendages (RAAs) from patients with paroxysmal and long-standing persistent AF compared to SR controls (71). A mouse model expressing constitutively active NLRP3 resulted in spontaneous premature atrial contractions and triggerable AF (71). Increased inflammasome priming and triggering (elevated expression of NLRP3, pro-caspase-1, ASC, cleaved caspase-1, toll-like receptor-4 and NFκB) was confirmed in RAAs from patients with SR who underwent open heart surgery and developed AF in the postoperative period compared to those who remained in SR after the operation, suggesting a pre-existing inflammatory substrate for postoperative AF (73). In addition to the NLRP3, other inflammasome pathways, namely "NLR family, pyrin domain containing 1" (NALP1) (86), "NLR family CARD domain-containing protein 4" (NLRC4) (87-89) and "absent in melanoma 2" (AIM2) (87-93) have been identified to play a role in cardiovascular diseases such as atherosclerosis, acute myocardial infarction, cardiomyopathies or stroke (Figure 2).

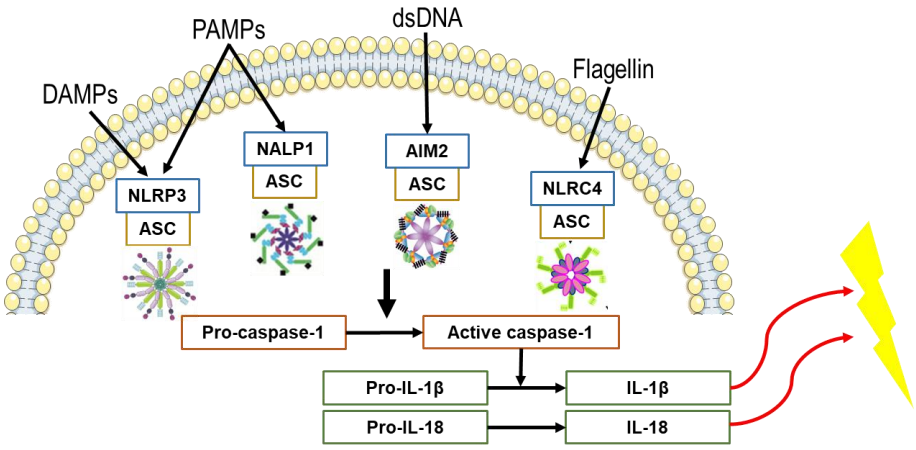

Figure 2. Inflammasome activation.

Specific signals such as damage- or pathogen-associated molecular patterns (DAMPs, PAMPs), double-strand deoxyribonucleic acid (dsDNA) or flagellin induce the assembly of inflammasome complex leading to caspase activation and cleavage of precursor interleukins. The figure was created by Dr. Zsófia Onódi, in part using images from Servier Medical Art (94).

Epicardial adipose tissue and atrial fibrosis

Epicardial fat that directly contacts the myocardium has endocrine and paracrine features that may be associated with myocardial inflammation. It produces a number of adipokines, chemokines and inflammatory cytokines that diffuse into the neighboring

myocardium inducing its fibrotic remodeling. Epicardial fat may extend into the adjacent myocardium, separating myocytes and contributing to its functional disorganization. Increased epicardial adiposity induced myocardial inflammation, atrial fibrosis and altered atrial architecture can predispose to reentry formation and the development of AF (24, 26, 29, 31). Several signaling pathways are known to participate in the pro-fibrotic process (pro-inflammatory cytokines, transforming growth factor-β_1, connective tissue growth factor, oxidative stress, the renin-angiotensin-aldosterone system, endothelin-1, calcium-dependent proteases, extracellular matrix regulatory proteins, hypoxia-inducible factor-1α) (26), and many comorbidities (advancing age, hypertension, diabetes mellitus, HF, ischemic heart disease, obesity, valve disease, obstructive sleep apnea) predispose to atrial fibrosis (26, 95). AF in itself can also induce fibrotic remodeling of the atrial epicardium (26). In human RAA samples, higher degrees of fibrotically remodeled subepicardial fatty infiltrates were found in the case of AF, and the degree of the fibrotic remodeling correlated with the duration of AF (70). Several studies showed an association of total pericardial fat volume with the prevalence and severity of AF, and with the recurrence of the arrhythmia after ablation (31). Higher degree of atrial fibrosis correlated with post-ablation arrhythmia recurrence and increased risk of thromboembolic events (29). It is of interest, that based on an electrophysiological study, right atrial scar burden shows good correlation with left atrial scar burden (96). Fibrosis in the MSs of PVs was also reported to be more severe in patients with AF than in those without (42-44, 97).

Atrial amyloidosis

In case of cardiac amyloidosis, misfolded proteins (predominantly immunoglobulin light chains or transthyretin) accumulate as focal, multifocal, or diffuse interstitial nodules surrounding cardiomyocytes or form subendocardial or perivascular aggregates (98). Atrial amyloidosis can be present as part of cardiac amyloidosis, where atrial involvement is part of the systemic involvement caused by amyloidosis, or it can appear as isolated atrial amyloidosis (IAA) that means the sole infiltration of the atria, without affecting the ventricles (98, 99). In case of IAA, amyloid deposits of atrial natriuretic peptide are formed in the aging human atrium (98, 99), and this accumulation is exacerbated by atrial stretch caused by ventricular diastolic dysfunction, mitral valve disease and/or AF (98). Atrial amyloidosis and IAA have been reported to correlate with the presence and

duration of AF (99-102). The reason for this may be that amyloid accumulation between cardiomyocytes may result in the interruption of normal electrical conduction, thus forming a substrate for atrial tachyarrhythmias (98, 99, 101).

Effects of autonomic nerve system

Both enhanced cholinergic and β-adrenergic tone can induce AF (26). Adrenergic activation promotes focal activity through enhanced automaticity or induction of calcium-dependent triggered activity, while increased vagal tone shortens atrial refractoriness by the induction of the acetylcholine-activated potassium current which predisposes to the formation of reentry circuits. Enhanced calcium current due to adrenergic activation can provoke cardiomyocyte hypertrophy and fibrosis (103). Both long-term vigorous physical training (due to increased parasympathetic tone and atrial dilatation) and lack of physical activity (due to increased heart rate and comorbidities) were shown to be associated with an increased risk of AF, while regular moderate physical activity seemed to have favorable effects regarding supraventricular arrhythmias (104).

Genetic factors

In a prospective cohort study, parental AF was shown to independently predict an increased risk of AF events in offspring, supporting a genetic susceptibility to developing AF (105). Genetic mutations and variants underlying AF were reported to affect among others voltage gated sodium and potassium channels, connexin 40 (Cx40) gap junction protein, lamin, desmin, natriuretic peptide precursor A and atrial myosin light chain 1 (106-109).

1.2. Anatomy of the cardiac pacemaker and conduction system

In human, the crescent-shaped sinoatrial node (SAN) is located at the junction of the SVC and the right atrium, beneath the epicardial surface of the proximal sulcus terminalis. Its tail often penetrates into the crista terminalis. The specialized nodal cells are also striated, but smaller and paler in color than the working cardiomyocytes. They are embedded in a matrix of fibrous tissue (110, 111). The AVN is located at the apex of the triangle of Koch and is directly related to the fibroadipose tissue interposing between the septal portion of the right atrial vestibule and the crest of the muscular interventricular septum (112). A

rightward posterior extension of the AVN frequently continues to the level of the CS ostium (113). The compact node is characterized by a complex architecture of interweaving cells, while posterior extensions are made up of closely spaced, small cells (113). The cells of the compact node bunch together and penetrate to the central fibrous body, forming the bundle of His which then branches on the crest of the muscular interventricular septum. The right bundle branch and the fascicles of the left bundle branch are insulated by fibrous sheaths from the subjacent septal musculature. The terminal ramifications of the ventricular conduction system are the Purkinje fibers (112). Human Purkinje fibers are somewhat larger in diameter (approximately 20 μm) than working cardiomyocytes, and possess a light appearance due to the smaller number of myofibrils (114).

1.3. Markers of the cardiac pacemaker and conduction system

Several markers have been identified that distinguish working myocardium from pacemaker cells and conducting cardiomyocytes in humans, for example, hyperpolarization activated cyclic nucleotide-gated potassium channel 1 (HCN1) and 4 (HCN4) (115-119), Cx45 (120, 121), voltage-gated calcium channel subunit alpha 1 D (Cav1.3) and alpha 1 G (Cav3.1) (115-117, 122) and desmin (114, 123-125). Other markers, namely contactin 2 (CNTN2) (126, 127), human natural killer-1 (HNK1) (128-130) and T-box transcription factor 3 (TBX3) (115, 117, 131, 132) were documented to be present predominantly during embryonic and fetal development.

1.3.1. Connexins

Gap junctions are groups of intercellular channels that provide a direct connection between the cytoplasm of two adjacent cells to mediate intercellular communication (133). These channels are formed by connexin proteins, three main isoforms of which are present in the human heart. Cx40, Cx43 and Cx45 are expressed differently in cardiomyocytes at distinct sites, which determines the properties of conduction velocity (133). Cx43 is expressed throughout the working myocardium, Cx40 is restricted to the atrial myocardium and the ventricular conduction system, whereas Cx45 is mainly expressed in the pacemaker and conduction system of the heart (120, 121, 134). In human adults, only trace amounts of Cx45 was detected in the atrial and ventricular working

myocardium (134), whereas distinct positive signals were found for Cx45 at the AVN and for Cx40 at the AV-bundle and bundle branches (121). For the human SAN, Cx45 mRNA was abundant, while mRNA and protein for Cx40 and Cx43 were less abundant in the SAN than in the right atrial myocardium (115). In human fetal hearts and developing mouse hearts (120), as well as in adult rat and mouse hearts (135), Cx40 and Cx45 labeling was prominent in the ventricular conduction tissues. In rats, the SAN and the AVN proved to be immunopositive for HCN4 and Cx45, but not for Cx43 (136). The compact AVN of rabbits also expressed mainly Cx45 (137). Based on these data, Cx45 appears to be a specific marker for the cardiac pacemaker and conduction system.

Data on the connexin expression patterns of the MSs of PVs and caval veins are based on animal studies and differences between species have been reported. The presence of all cardiac connexins (Cx40, Cx43 and Cx45) was confirmed in the canine SVC, with distinct areas of abundant Cx43 in the center and diffuse Cx40 signals in the periphery. Such regions of atypical connexin expression were mainly localized in the proximal part of the SVC (138). Both Cx40 and Cx43 were detected in isolated cardiac cells from canine SVCs and PVs (139). In rats, a nodal-like tissue was reported at the junction of the SVC and the right atrium. From this site, lightly stained cells exhibiting strong Cx45 but no Cx43 immunoreactivity extended next to both the crista terminalis and the interatrial groove. Atrial walls and PV myocardium showed intense Cx43 immunostaining, while Cx45 was absent (136).

1.3.2. Desmin intermediate filament

Desmin is a muscle-specific intermediate filament that is involved in maintaining the structure of sarcomeres, connecting myofibrils via Z-disks and linking them to the sarcolemma, nucleus and mitochondria (140). Although desmin is not a specific marker of the pacemaker and conduction system of the heart, it was reported to be abundant in the ventricular conduction system and nodal regions in comparison to the ventricular working myocardium. Most evidence are based on mammalian data, but some human studies also support these regional differences. Bovine Purkinje fibers were shown to contain many intermediate filaments, but less myofibrils compared to working cardiomyocytes (141-143). Other mammalian studies demonstrated a stronger desmin immunoreactivity of the ventricular conduction system in comparison to working

cardiomyocytes, both during prenatal development (144, 145) and in the postnatal period (145, 146). Prominent desmin labeling was also observed in the Purkinje fibers of human adults (114) and in the ventricular conduction system of human fetuses (125). Strong desmin immunoreactivity was reported in the developing human SAN and AVN (123) and in the SAN of fetal rats (145). In adult mice and humans, large amounts of desmin were found in the SAN as well (124). In rabbits, the atrioventricular conduction axis was readily identified by the pronounced desmin immunostaining in the cytoplasm of the conducting cardiomyocytes (137).

In fetal rats, intense desmin labeling was noted in the SVC and the PVs (145). In human fetuses, the MSs of the PVs, caval veins and CS were strongly positive for desmin, while the left ventricular working myocardium was immunonegative (125). Studies in human embryos (123) and fetuses (125, 147) reported a strong desmin immunoreactivity of the atria, in contrast to a weaker (147) or absent (123, 125) signal from the ventricular (compact) myocardium. The interatrial conducting pathway displayed intense desmin immunolabeling compared to working cardiomyocytes in monkeys and sheep (148).

1.3.3. Hyperpolarization Activated Cyclic Nucleotide Gated Potassium Channel 4

The hyperpolarization-activated funny current is a crucial regulator of the diastolic depolarization of the heart and plays a key role in heart rate control. The main ion channel responsible for this pacemaker current is the HCN4 which is present abundantly throughout the pacemaker and conduction system of the human heart while its expression is sparse in the working myocardium (115-119). Periodic acid-Schiff (PAS)-positive cardiomyocytes displaying HCN4 immunoreaction, indicating a pacemaking function, were identified in the PV-left atrial junctions of humans both with and without previous AF (97).

1.3.4. Human natural killer-1

In human embryos, HNK-1, a marker of the developing conduction system, was present around the orifice of the common PV primordium, the IVC and the CS, and three HNK-1-positive connections were detected between the SAN and the region of the right atrioventricular ring (128). HNK-1 was also demonstrated in 10% of the MSs around PVs of human adults, both with and without a history of AF (149).

DOI:10.14753/SE.2025.3172

2. OBJECTIVES

We aimed to perform histological and molecular examinations to enhance the knowledge about the pathomechanism of AF.

2.1. Analysis of the histological and immunohistochemical features of the myocardial sleeves around pulmonary veins, caval veins and coronary sinus

We aimed to examine the histological and immunohistochemical features of MSs ensheathing the veins entering the atria of human hearts, namely the SVC, IVC, PVs and CS. We set out to investigate the histological background of the widely documented arrhythmogenic nature of these supraventricular regions by evaluating whether the MSs contain any cardiomyocytes possessing the conducting phenotype. Furthermore, in our first study, we targeted the Cx45 gap junction protein to provide support for the potential arrhythmogenicity of these areas. In a subsequent study, we aimed to investigate regional differences in desmin intermediate filament immunostaining in human hearts with the intention of providing further information about the putative conducting phenotype of the venous MSs.

2.2. Assessment of inflammation in heart failure-associated atrial fibrillation

In this study, we set out to examine the role of atrial substrate in the pathomechanism of HF-associated AF. Our purpose was to assess if any relation exists between inflammation and HF-associated AF in human hearts with end-stage HF. The focus of our research was on inflammasome activation and on infiltration of macrophages into left atrial myocardium and epicardium. We also intended to analyze the fibrotic remodeling of the left atrial myocardium and epicardium in the same population.

3. METHODS

3.1. Characterization of the histological and immunohistochemical features of myocardial sleeves in the walls of cardiac veins

3.1.1. Human tissues

Hearts were removed from 43 adult human cadavers. Age was known in 11/43 cases and it ranged from 22 to 86 years. Clinical data was known in 9/43 cases. We also investigated the heart of a 23-week-old fetus who was born alive but died shortly after birth (Table 1). Eleven hearts were removed from autopsied cadavers. The other 33 hearts were removed from donors who gave written consent before their deaths for their bodies to be used for educational and research purposes at the Department of Anatomy, Histology and Embryology, Semmelweis University {Willed (Whole) Body 77 Program - WWBP}. The most of these hearts were educational material and were not identified as a separate organ, which explains the high proportion of missing demographic and clinical data. The bodies were stored refrigerated at 1-5 ^{o}C until autopsies or fixation, which was carried out 12-72 hours after death. After removal at autopsies, the hearts were immediately fixed.

For adult hearts, PVs were investigated in 26/43, SVC in 34/43, IVC in 18/43 and CS in 19/43 cases, due to technical reasons. For the fetal heart, only the SVC could be analyzed. In some cases, some PVs were missing due to previous postmortem proceedings. The excision was extended into the hilum of the lung for PVs, above the level of the azygos vein for SVCs and to the level of the diaphragm for IVCs. We examined the entire length of the CS from its right atrial orifice to the oblique vein of Marshall. The veins were disconnected from the atria at their ostia and cut transversely into ring-like pieces. Tissue samples were also obtained from the SAN, AVN, left and right atria, interatrial septum, left and right ventricles and interventricular septum (Table 1, Figure 3).

Right and left atrial structures (Figure 3) were systematically investigated in 9 adult cadavers with known demographic data (3 males, median age: 50.0 [IQR 44.0–52.0] years). Medical history was known in 8/9 cases. 6/8 patients had cardiac disease, namely hypertension (n=2), chronic ischemic heart disease (n=1), acute myocardial infarction (n=1), hypertrophic obstructive cardiomyopathy (n=1), dilated cardiomyopathy (n=1), left ventricular hypertrophy (n=1) and pulmonary embolism (n=1). Nevertheless, none of them had previously been diagnosed with AF.

DOI:10.14753/SE.2025.3172

***Table 1*. Demographic and medical data of patients, and data of histological analyses.** *(Adopted from reference (150) with modifications.)*
AVN: atrioventricular node; CS: coronary sinus; FA: formaldehyde; HE: hematoxylin-eosin; HOCM: hypertrophic obstructive cardiomyopathy; IAS: interatrial septum; IVC: inferior vena cava; IVS: interventricular septum; LA: left atrium; LAD: left anterior descending artery; LV: left ventricle; NA: not available; PFA: paraformaldehyde; RA: right atrium; RV: right ventricle; SAN: sinoatrial node; SVC: superior vena cava

Case	Age (years)	Sex	Medical history	Cause of death	Fixation	Investigated tissue	Stain
1-4	NA	NA	NA	NA	FA	SVC	HE, trichrome
5-9	NA	NA	NA	NA	FA	SVC, SAN, RA	HE, trichrome
10	NA	NA	NA	NA	FA	IVC, RA	HE, trichrome
11	NA	NA	NA	NA	FA	CS, RA, IAS, IVS, LV	HE, trichrome
12-14	NA	NA	NA	NA	FA	SVC, IVC, PV	HE, trichrome
15	NA	NA	NA	NA	FA	SVC, PV	HE, trichrome
16, 17	NA	NA	NA	NA	FA	SVC, CS, PV	HE, trichrome
18	NA	NA	NA	NA	FA	IVC, CS, PV	HE, trichrome, iron hematoxylin
19-23	NA	NA	NA	NA	FA	PV	HE, trichrome
24, 25	NA	NA	NA	NA	FA	SVC, IVC, CS, *PV (in case 24)*, SAN, AVN, RA, LA, IAS, IVS, LV	HE, trichrome
26	44	female	hyperthyroidism, cholecystectomy	brain death after prolonged resuscitation from sudden cardiac death due to pulmonary embolism	FA	SVC, IVC, CS, PV, SAN, AVN, RA, LA, IAS, IVS, RV, LV	HE, trichrome
27	NA	NA	NA	NA	frozen	SVC, CS, LV	Cx43 (1:50)
28	81	female	cerebral vascular lesion, cardiac pacemaker, myocardial infarction, percutaneous coronary intervention (LAD)	cachexia due to persistent immobility	methanol	SVC, IVC, CS, PV, LA, IAS	HE, trichrome, Cx45 (1:50)
29	64	male	NA	NA	ethanol	SVC, PV, SAN, AVN, RA, LA, IAS, IVS, RV, LV	HE, trichrome, Carmine, desmin (1:4000–1:5000), Cx45 (1:50–1:100)
30	NA	NA	NA	NA	FA	SVC, RA	HE, desmin (1:200)
31	NA	NA	NA	NA	FA	SVC, RA, RV	HE, desmin (1:200)

32	NA	NA	NA	NA	FA	SVC, SAN, RA, IAS, RV	HE, trichrome, desmin (1:200)
33	NA	NA	NA	NA	FA	SVC, CS, RA, IAS, IVS, LV	HE, trichrome, desmin (1:200)
34	NA	NA	NA	NA	FA	SVC, IVC, CS, PV, LA	HE, trichrome, desmin (1:200)
35	NA	NA	NA	NA	FA	PV	HE, trichrome, desmin (1:200)
36	50	female	NA	suicide by hanging	FA	SVC, IVC, CS, PV, SAN, AVN, RA, LA, IAS, IVS, RV, LV	HE, trichrome, desmin (1:400)
37	22	female	none	suicide by hanging	FA	SVC, IVC, CS, PV, SAN, AVN, RA, LA, IAS, IVS, RV, LV	HE, trichrome, desmin (1:200), iron hematoxylin
38	86	female	hypertension, ischemic stroke, eversion carotid endarterectomy	postoperative left ventricular failure due to chronic ischemic heart disease	FA	SVC, IVC, CS, PV, SAN, AVN, RA, LA, IAS, IVS, LV	HE, trichrome, desmin (1:400), Congo red
39	54	female	HOCM, hypertension, ischemic stroke, liver cirrhosis, small bowel obstruction surgery	postoperative multiorgan failure and vasoplegia; congestive heart failure	FA	SVC, IVC, CS, PV, SAN, AVN, RA, LA, IAS, IVS, RV, LV	HE, trichrome, desmin (1:400), Congo red
40	43	male	chronic alcohol abuse	respiratory failure due to pneumonia; accompanying disease: left ventricular hypertrophy	FA	SVC, IVC, CS, PV, SAN, AVN, RA, LA, IAS, IVS, RV, LV	HE, trichrome, desmin (1:400)
41	48	male	nicotinism	left ventricular failure due to dilated cardiomyopathy	FA	SVC, IVC, CS, PV, SAN, AVN, RA, LA, IAS, IVS, RV, LV	HE, trichrome, desmin (1:400)
42	52	male	master footballer, nicotinism	sudden cardiac death due to acute myocardial infarction caused by severe three coronary vessel disease	FA	SVC, IVC, CS, PV, SAN, AVN, RA, LA, IAS, IVS, RV, LV	HE, trichrome, desmin (1:400)
43	51	female	none	subarachnoid hemorrhage, respiratory sepsis	PFA	SVC, IVC, CS, PV, SAN, RA, LA, IAS, IVS, RV, LV	HE, trichrome, desmin (1:400)
44	23-week fetus	NA	NA	NA	ethanol	SVC, SAN, RA, LV, RV	HE, trichrome, Carmine, desmin (1:5000), Cx45 (1:75)

DOI:10.14753/SE.2025.3172

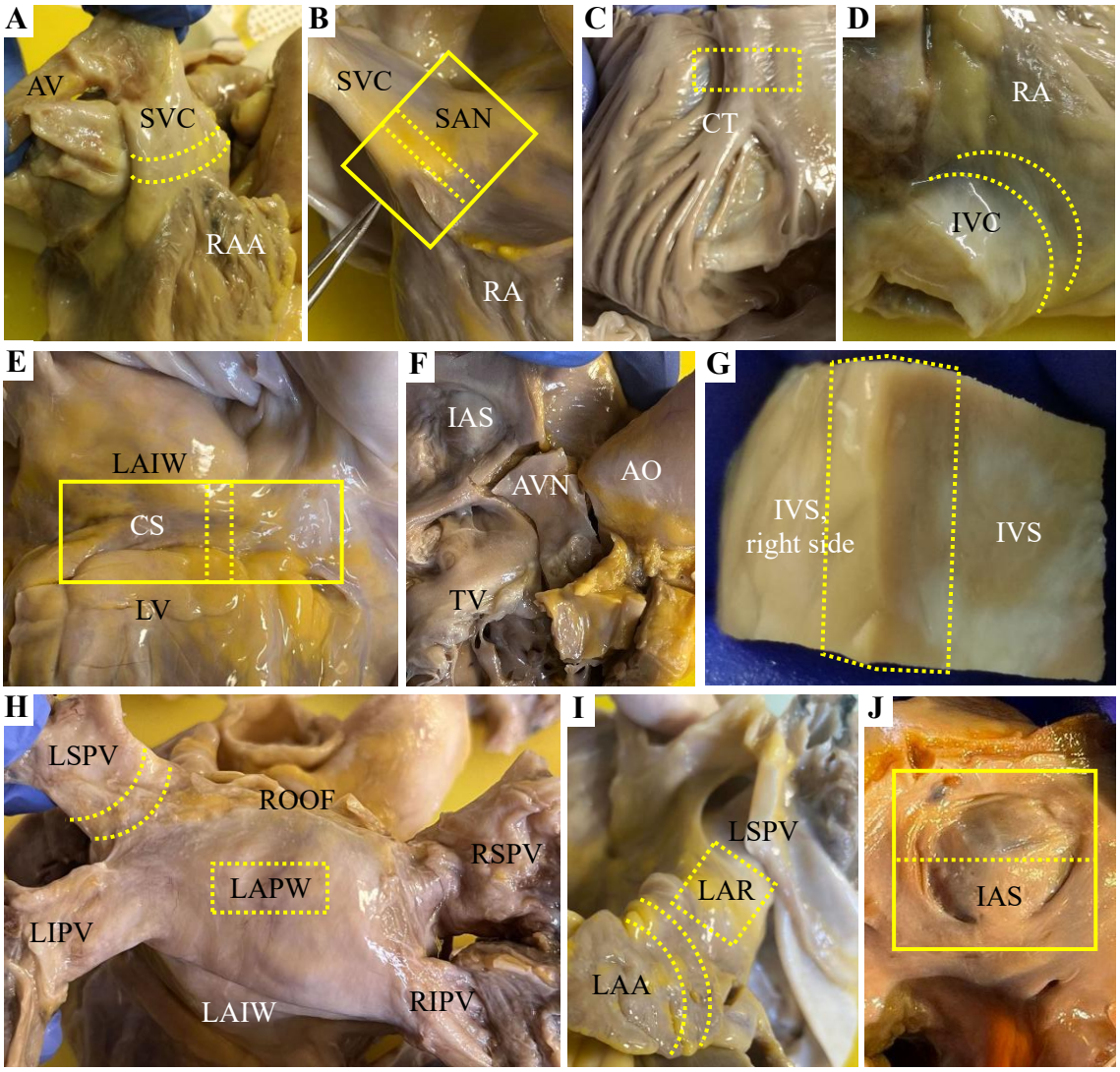

Figure 3. Demonstration of the examined regions of the hearts.

A: *The azygos vein (AV) draining into the superior vena cava (SVC), the SVC and the right atrial appendage (RAA).* ***B:*** *The SVC, the region of the sinoatrial node (SAN) and the right atrium (RA).* ***C:*** *The crista terminalis (CT).* ***D:*** *The RA and the inferior vena cava (IVC).* ***E:*** *The left atrial inferior wall (LAIW), the coronary sinus (CS) and the left ventricle (LV).* ***F:*** *The atrioventricular nodal (AVN) region bordered by the interatrial septum (IAS), the tricuspid valve (TV) and the aortic root (AO).* ***G:*** *The left ventricle (LV), the interventricular septum (IVS) and the right ventricle (RV).* ***H:*** *The left superior (LSPV), inferior (LIPV), right superior (RSPV) and inferior (RIPV) pulmonary veins, the roof of the left atrium and the LAIW.* ***I:*** *The left atrial ridge (LAR) located between the left atrial appendage (LAA) and the LSPV.* ***J:*** *The IAS. Regions of interest are marked by yellow squares. The cutting planes are marked by dotted lines.*

The research was accepted by the Regional and Institutional Committee of Science and Research Ethics, Semmelweis University (No. 122/2016) and the Research Ethics Committee of the Medical Research Council of Hungary (No. IV/1555-1/2021/EKU).

3.1.2. Tissue processing for histology

Except for one heart from which frozen sections were prepared, specimens were fixed in 4% formaldehyde (n=39), in 4% paraformaldehyde (n=1), in 70% ethanol (n=2, including the fetal heart), or in methanol (n=1). After dehydration in ascending concentrations of ethanol, tissue samples were embedded in paraffin and sections of 3-6 μm thickness were made. For general histology, sections were stained with hematoxylin-eosin and Krutsay's trichrome. Intracellular glycogen was shown by Best's Carmine stain (151). Hardly visible muscle striations of the small pacemaker cells were visualized by Heidenhain's iron hematoxylin two steps staining (ferric ammonium sulfate and hematoxylin). Amyloid deposits were demonstrated by Congo red stain (Table 1).

For frozen sections, the specimens were embedded in Cryomatrix (Shandon, Thermo Fisher Scientific, Waltham, Massachusetts, US), frozen in liquid nitrogen, and stored in a deep freezer (-80 ^{o}C). Cryosections of 10 μm thickness were mounted on poly-L-lysine coated slides, fixed in cold (+4 ^{o}C) acetone for 10 minutes and dried in air.

3.1.3. Connexin 45 and connexin 43 immunohistochemistry

Immunostainings were carried out as described in our previous paper (152). Cx45 immunohistochemistry was performed on samples from two adults and the 23-week-old fetus (Table 1). Specimens were fixed in ethanol/methanol and embedded in paraffin. After deparaffinization and rehydration through graded alcohol concentrations, the slides were washed 3 times in phosphate-buffered saline (PBS). Heat-induced citrate-based antigen retrieval (Vector Laboratories; Cat# H-3300) was performed for 30 minutes.

Cx43 immunostaining was carried out on the frozen sections of one adult heart (Table 1). Before immunohistochemistry, the slides were rehydrated in PBS and permeabilized with 0.3% Triton X-100 for 40 minutes.

Cx45 and Cx43 immunostaining were performed as follows: protein blocking was carried out for 15 minutes with 1% bovine serum albumin in PBS, followed by overnight incubation at 4 ^{o}C with primary antibodies. Cx45 was detected using a rabbit polyclonal

antibody (Santa Cruz Biotechnology Inc; Cat# sc-25716; dilution 1:50 or 1:100 for adults and 1:75 for fetal heart), and Cx43 was detected using a goat polyclonal antibody (Santa Cruz Biotechnology Inc; Cat# sc-6560; dilution 1:50). Secondary antibodies (biotinylated goat anti-rabbit immunoglobulin G and biotinylated horse anti-goat immunoglobulin G [Vector Laboratories]) were applied at a dilution of 1:200 for 1 hour. Endogenous peroxidase activity was then quenched with 0.6% hydrogen peroxide (Sigma-Aldrich) in PBS for 10 minutes. After formation of the avidin-biotinylated peroxidase complex (Vectastain Elite ABC kit; Vector Laboratories), the binding sites of the primary antibodies were visualized by 4-chloro-1-naphthol (Sigma-Aldrich; Cat# C8890).

3.1.4. Desmin immunohistochemistry

Desmin immunostaining was performed on samples obtained from 15 adults and the 23-week-old fetus (Table 1), as described in our previous paper (150). Sections fixed with formaldehyde, paraformaldehyde or ethanol were investigated. After deparaffinization and rehydration through graded alcohols, slides were washed three times in PBS.

Desmin immunohistochemistry of the ethanol-fixed sections was prepared as follows: heat-induced citrate-based antigen retrieval was carried out (Vector Laboratories; Cat# H-3300) for 30 minutes. Protein blocking was performed for 20 minutes with 1% bovine serum albumin in PBS, followed by overnight incubation at 4 ^{o}C with mouse monoclonal antibody against human desmin (Dako; Clone D33; Cat# M0760; dilution 1:4000 for adults and 1:5000 for fetal heart). Biotinylated horse anti-mouse IgG (Vector Laboratories; dilution 1:200) was used as a secondary antibody for 1 hour, followed by quenching endogenous peroxidase activity with 0.6% hydrogen peroxide (Sigma-Aldrich) in PBS for 10 minutes. After formation of the avidin-biotinylated peroxidase complex (Vectastain Elite ABC kit; Vector Laboratories), the binding sites of the primary antibody were visualized by 4-chloro-1-naphthol (Sigma-Aldrich; Cat# C8890).

For desmin immunohistochemistry on formaldehyde-fixed, paraffin-embedded tissue sections, a heat-induced Tris-EDTA-based antigen retrieval method was applied (Dako; Target Retrieval Solution pH-9). Desmin was detected using a mouse anti-human desmin monoclonal antibody (Dako; Clone D33; Cat# M0760; dilution 1:200 or 1:400) overnight at 4 ^{o}C. (Similarly to Cx45, different anti-desmin antibody concentrations were used for the individual hearts due to the differences in their histological characteristics. However,

the same antibody dilution was used for different regions of a single heart.) All other steps of the immunohistochemistry protocol (application of peroxidase and protein block, post primary blocking, incubation with secondary antibody, application of 3,3'-diaminobenzidine (DAB) as chromogen, counterstaining of nuclei with hematoxylin) were carried out at room temperature (25 °C) using the Novolink™ Polymer Detection System (Leica Biosystems; Cat# RE7140-K).

3.1.5. Double labeling of connexin 45 and desmin

We performed double immunofluorescence staining for Cx45 and desmin. Cx45 was detected with a rabbit polyclonal antibody (Santa Cruz Biotechnology, Inc.; Cat# sc-25716; dilution 1:50) and desmin with a mouse monoclonal antibody (Dako; Clone D33; Cat# M0760; dilution 1:5000). Goat anti-rabbit IgG conjugated to Alexa Fluor 488 and goat anti-mouse IgG conjugated to Alexa Fluor 594 (Invitrogen) were used as fluorescent secondary antibodies. Cell nuclei were stained with DAPI (Vector Laboratories).

3.1.6. Visualization of slides

Sections were mounted with aqueous Poly/Mount (Polyscience, Inc., Warrington, PA) and examined under a Zeiss Axiophot photomicroscope and/or Zeiss confocal microscope system. Fluorescent images were captured with an Olympus DP50-CU digital camera (Olympus Optical Co., Ltd.), while an automated whole-slide imaging system (3D-Histotech, Budapest, Hungary) was used to visualize other sections.

3.1.7. Immunohistochemical quantitative analysis

Semiquantitative analyses for the intensity of desmin immunostaining of 4 hearts (Case No 37, 40, 41, 42) were performed. The ventricular subendocardial region, ventricular working myocardium, SAN, SVC and CS were investigated in all cases and the PV in 3/4 cases. For each structure of a given heart, three distinct regions with the same sizes were analyzed. These regions were chosen to be representative of the whole section regarding the proportion of conducting-like cardiomyocytes exhibiting strong desmin expression and weakly immunopositive working cardiomyocytes. At first, signal intensity of the strongly immunoreactive cells of the conducting system and the extracardiac MSs was compared with that of weaker labeled ventricular working cardiomyocytes. For this

analysis, twenty cardiomyocytes were chosen from each region (Figure 4A). Thereafter, differences between signal intensity at representative areas of the ventricular conduction system or MSs and the working ventricular myocardium were investigated (Figure 4B). The total size of the analyzed areas was equal for each region.

The ImageJ (Image Processing and Analysis in Java) 1.51 k program (NIH, Bethesda, MD, US) was used to perform semiquantitative analyses. We used the Color Deconvolution plugin for stain separation of hematoxylin-DAB-stained images and selected the derived DAB image for quantification. The software converted each pixel of the Red Green Blue images to grayscale using a special formula, and consequently the desmin signal intensity was expressed in gray values. The software calculated the mean gray values (MGV) for each selected cell and area. MGV was the sum of the gray values of all pixels in the circled area divided by the number of pixels, expressed in gray-level units. A lower MGV indicated a stronger desmin signal intensity.

The amount of the difference in cell or area MGVs among different heart structures was estimated by a mixed effect regression model. We used two separate models for the cell and area MGVs (as outcome variables). The models contained the cardiac structures as explanatory variables and a random intercept was assigned to each heart. (A compound symmetry correlation structure was assumed.) For the estimation of confidence intervals for the difference between the groups and the p-value, a Tukey method adjustment was made to handle the multiple comparisons. All statistical analyses were calculated by *R software* (153) using the *lme4* (154) package for mixed effect regression models, and *emmeans* (155) for multiplicity correction in pairwise comparisons.

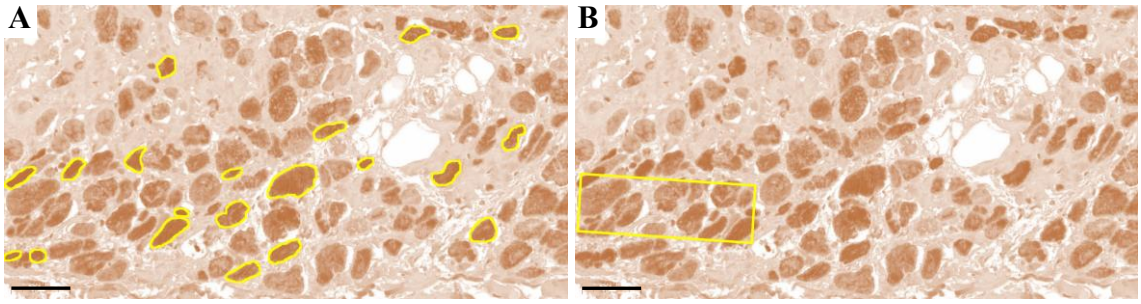

Figure 4. Quantitative analysis of desmin immunostaining for superior vena cava.

A: *Mean gray values of twenty cells displaying strong desmin immunoreactivity framed by yellow were averaged for the sample.* ***B:*** *The mean gray value of a representative area of a given size marked by yellow square was calculated. Scale-bars: 50 µm (150)*

3.2. Investigation of inflammasome activation in end-stage heart failure-associated atrial fibrillation

3.2.1. Human samples

De-identified left atrial specimens from the explanted hearts of 24 patients with end-stage ischemic HF who underwent heart transplantation were acquired from the Transplantation Biobank of the Heart and Vascular Center, Semmelweis University, Budapest, Hungary. The samples were immediately snap frozen in liquid nitrogen after excision and were kept at -80°C until further processing. Formalin-fixed, paraffin-embedded tissue samples were also prepared for histology. The project was approved by the Institutional and National Ethics Committee (ETT TUKEB 7891/2012/EKU (119/PI/12.) and ETT TUKEB IV/10161-1/2020). All patients provided written informed consent. Half of the individuals had no documented AF (SR group, n=12) and the other half had sustained (persistent or permanent) AF (AF group, n=12). All patients were male, aged 43-64 years, with a body mass index of 18.2-33.2 kg/m^2, an ejection fraction of 10-36% and a left atrial length of 47-82 mm. None of the patients suffered from diabetes mellitus. The only significant difference between the two groups was for procalcitonin, which was irrelevant as this value was within the reference range (<0.5 μg/l) in all cases (Table 2).

Table 2. Demographic and medical data of patients enrolled into the analysis of inflammasome activation in end-stage heart failure-associated atrial fibrillation.

Adopted from reference (156) with modifications. Values are presented as number (%), mean (SD) or median [interquartile range]. BMI: body mass index; CRP: C-reactive protein; CRT: cardiac resynchronization therapy; EF: ejection fraction; F: female; LA: left atrial; M: male; NYHA: New-York Heart Association; PCT: procalcitonin; Q1/ Q3: first/ third quartile; SD: standard deviation; WBC: white blood cell

	Patients with sinus rhythm (n=12)	**Patients with atrial fibrillation (n=12)**	**p-value**
Age (years), median [Q1, Q3]	56.5 [48.0 – 60.0]	57.5 [54.5 – 60.5]	0.400
Sex (M / F), n (%)	12 (100) / 0 (0)	12 (100) / 0 (0)	1.00
BMI (kg/m^2), mean (SD)	27.6 (3.8)	25.8 (4.0)	0.278
Etiology of heart failure, n (%)			
Ischemic	12 (100)	12 (100)	1.00
Non ischemic	0 (0)	0 (0)	
NYHA stage, n (%)			
II	0 (0)	1 (9)	
III	7 (58)	7 (64)	0.482
IV	5 (42)	3 (27)	
Missing data	0 (0)	1 (9)	
Echocardiography parameters			
EF (%), mean (SD)	21.7 (8.1)	23.8 (4.0)	0.434

LA length, mean (SD)	58.6 (8.4)	64.2 (7.9)	0.107
Artificial heart valve, n (%)	0 (0)	1 (8)	1.00
CRT, n (%)	3 (25)	5 (42)	0.667
Medication, n (%)			
Parenteral loop diuretics	3 (25)	4 (33)	1.00
Parenteral inotropic support	3 (25)	4 (33)	1.00
Parenteral vasopressor agent	0 (0)	1 (8)	1.00
Sacubitril/valsartan	4 (33)	1 (8)	0.317
Mechanical circulatory support, n (%)	1 (8)	1 (8)	1.00
Mechanical ventilation	0 (0)	1 (8)	1.00
Ventricular tachycardia	1 (8)	4 (33)	0.317
Diabetes mellitus	0 (0)	0 (0)	1.00
Infection			
Presence of infection	4 (33)	4 (33)	1.00
Antibiotic treatment	3 (25)	4 (33)	1.00
WBC (G/l), median [Q1, Q3]	7.6 [6.7 – 9.5]	8.9 [6.6 – 9.4]	0.875
CRP (mg/l), median [Q1, Q3]	4.7 [1.6 – 9.7]	3.0 [2.4 – 4.4]	0.514
PCT (μg/l), median [Q1, Q3]	0.03 [0.02 – 0.05]	0.10 [0.05 – 0.13]	**0.006**
Missing data, n (%)	1 (8)	2 (17)	

3.2.2. Assessment of inflammasome activation

The expression of inflammasome sensors (NALP1, NLRP3, AIM2, NLRC4) and their downstream signaling (ASC, caspase-1, p20/22 subunits of cleaved caspase-1, IL-1β, cleaved IL-1β) was analyzed by Western blot, as described previously (157) with modifications. Left atrial frozen tissue samples were homogenized in 1x radioimmunoprecipitation assay buffer (RIPA; Cell Signaling Technology, Danvers, MA, US) containing 1x HALT Protease and Phosphatase Inhibitor cocktail (Thermo Scientific, Waltham, MA). The protein concentrations of the samples were determined by bicinchoninic acid assay kit (Thermo Scientific). Equal quantities of protein from each of the samples were mixed with 1/4 volume of Laemmli buffer comprising β-mercaptoethanol (Thermo Scientific), loaded onto 4-20% Tris-glycine sodium dodecyl sulfate-polyacrylamide gels (Bio-Rad, Hercules, CA, US) and electrophoresed. Proteins were transferred to a polyvinylidene difluoride membrane (Bio-Rad) using the Trans-Blot® Turbo™ Transfer System (Bio-Rad). Membranes were blocked in 5% bovine serum albumin (Bio-Rad) dissolved in Tris-buffered saline containing 0.05% Tween-20 (0.05% TBS-T; Sigma, St. Louis, MO, US) for 2 hours at room temperature and then incubated overnight at 4°C with primary antibodies (Cell Signaling; NALP1: Cat# 4990S, dilution 1:2500; NLRP3: Cat# 15101S, dilution 1:2500; AIM2: Cat# 12948S, dilution 1:2500; NLRC4: Cat# 12421S, dilution 1:2500; ASC: Cat# 13833S, dilution 1:5000; caspase-1: Cat# 3866S, dilution 1:1000; cleaved caspase-1: Cat# 4199S, dilution 1:1000; IL-1β: Cat# 12703S, dilution 1:1000; cleaved IL-1β: Cat# 83186S, dilution 1:1000). After

three washes in TBS-T, the membranes were probed with corresponding HRP-conjugated secondary antibodies (Cell Signaling) for 2 hours and washed in TBS-T. After incubation with enhanced chemiluminescence kit (Bio-Rad), signals were detected by Chemidoc XRS+ (Bio-Rad). Image analysis was carried out using Image Lab™ 6.0 software (Bio-Rad). Five samples (2 from the SR group and 3 from the AF group) were excluded from analysis due to low-quality homogenates. Glyceraldehyde-3-phosphate dehydrogenase (GAPDH) was used as a loading control.

3.2.3. Assessment of macrophage infiltration

To assess the number of macrophages in the myocardial and epicardial areas of left atrial samples from the SR (myocardium: n=6, epicardium: n=4) and AF (myocardium: n=7, epicardium: n=6) groups, immunohistochemistry was carried out as described previously (158) to stain ionized calcium-binding adaptor molecule 1 (Iba1, marker of monocyte–macrophage lineage) (159, 160). First, antigen retrieval was performed on deparaffinized sections (pH=6 citrate buffer, at 95°C for 15 minutes). After quenching endogenous peroxidase activity (3% H_2O_2 solution in PBS), the sections were blocked in appropriate sera (2.5% goat, bovine serum or milk in PBS). Iba1 was detected by a rabbit polyclonal antibody (Fujifilm Wako; Cat# 019-19741; dilution 1:2000) that was incubated with the sections overnight in diluted blocking solution at 4°C. Sections were then washed three times in PBS and incubated for 1 hour with an anti-rabbit IgG conjugated with a peroxidase polymer (ImmPress reagents, Vector Laboratories, Burlingame, CA, US). After washing three times for 10 minutes, the specific signal was developed with DAB (ImmPACT DAB EqV Peroxidase (HRP) Substrate, Vector Laboratories). Stained slides were mounted with ProLong Gold Mounting Media (Invitrogen, Carlsbad, CA, USA). A Leica DM3000 bright field microscope (Leica Microsystems, Wetzlar, Germany) was used to visualize and image the specific staining.

The number of monocytes and macrophages in left atrial samples was determined by the ImageJ 1.51 k program. The average number of Iba1-positive cells with at least 35 μm^2 size were calculated for unit areas of both the myocardium and the epicardium. The size of unit area was different for the myocardium and the epicardium. For the myocardium, 3-5 unit areas per section were analyzed based on the size of the myocardial area. For epicardial samples, 5-16 unit areas were analyzed in a single section. Sometimes, no

epicardial or myocardial region could be identified. In these cases, Iba1-positive cells were counted only for the existing tissue. Photos were captured at 40x objective magnification. Data were normalized to the mean values of the SR group (Figure 5).

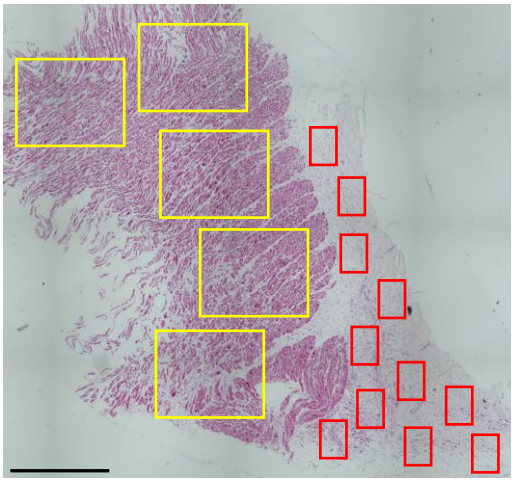

Figure 5. The method for quantitative analysis of macrophage infiltration.

Left atrial macrophages were counted over several unit areas and averaged for the sample. Myocardial (yellow squares) and epicardial (red squares) regions were analyzed separately. Hematoxylin-eosin. Scale bar: 1000 µm (156)

3.2.4. Evaluation of fibrosis

After routine formalin-fixed, paraffin-embedded specimen processing, 4 µm thick sections were prepared and stained with Masson's trichrome (SR group: n=6, AF group: n=7). A Leica DM3000 bright field microscope was used to visualize the sections and take the images. The percentage of total and interstitial fibrosis was assessed by the ImageJ 1.51 k program. The percentage of total fibrosis was defined as the proportion of fibrotic areas in relation to the total area of the section. The RGB Stack plugin was used to split the images into three 8-bit grayscale images, from which the red one was chosen. Thereafter, the threshold was set to mark the whole area of the section which was then measured. After that, the threshold was reset to indicate only the fibrotic regions that were marked by blue on the original images. The area of fibrotic regions was measured as well. Finally, the fibrotic area and total area was divided and multiplied by 100 to get the percentage of total fibrosis. The percentage of interstitial fibrosis was measured by correlating the amount of interstitial fibrosis to a modified area of the section. In case of both the fibrotic and reference area for interstitial fibrosis calculation, the epicardium,

subepicardial fibrotic region and perivascular fibrosis were neglected. These areas were removed at the beginning of the image analysis. The following steps were identical to those described for the quantification of total fibrosis (Figure 6).

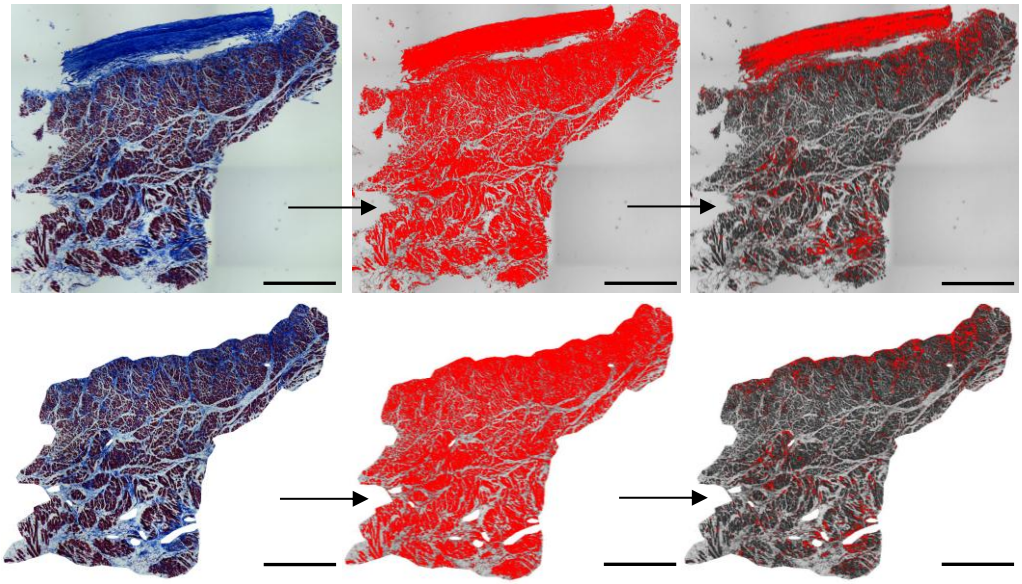

Figure 6. Assessment of total and interstitial fibrosis of left atrial samples.

The method is presented step by step. Masson's trichrome. Scale bars: 1000 µm (156)

3.2.5. Statistical analysis

In the case of categorical data, numbers and percentages were presented and comparisons between two groups were made using the Fisher's exact test or the Chi-square test. For continuous variables, the Shapiro-Wilk test was used to test normality. In the case of a normal distribution, data were presented as mean and standard deviation or mean and standard error of the mean, and comparisons between two groups were made using an unpaired Student's t-test. In the case of a non-normal distribution, data were presented as median with interquartile range, and comparisons between two groups were made using the Mann-Whitney test. Correlation and regression analysis was used to evaluate the correlations of cleaved caspase-1 with the inflammasome sensors and the markers of their downstream signaling. Outlier analysis was performed by ROUT test (Q=1%) for macrophage infiltration and fibrosis. One outlier was identified in both the epicardial macrophage subgroup and the interstitial fibrosis subgroup of SR samples. Outliers were excluded from statistical analysis. All analyses were carried out using GraphPad Prism 8. (GraphPad Software Inc). A P-value <0.05 was considered statistically significant.

DOI:10.14753/SE.2025.3172

4. RESULTS

4.1. Histology of the cardiac pacemaker and conduction system of human adults

The SAN and AVN regions, as well as the ventricular conduction system, were readily identified by hematoxylin-eosin and trichrome stains. Small pacemaker cells embedded within a matrix of fibrous connective tissue around the sinoatrial nodal artery and in the adventitial layer of the artery were characteristic of SAN (Figure 7.A). The compact AVN was identified at the apex of the triangle of Koch, at the base of the interatrial septum. Histologically, the AVN consisted of a nest-like structure of spindle-shaped cells arranged in a network and long, parallel bundles of myocardial fibers around it. Large cardiomyocytes (Purkinje fibers) with pale cytoplasm and peripheral myofibrils were observed in the ventricular conduction system, which was located in the interventricular septum, just beneath the endocardium. These cells were embedded in dense fine fibrous connective tissue and formed the left and right bundle branches of the heart's conducting system (Figure 7.B). Ventricular conducting cardiomyocytes contained large amounts of intracellular glycogen, in contrast to ventricular working cardiomyocytes.

A pronounced Cx45 immunoreactivity could be detected in the SAN (Figure 7.C) and AVN regions. Cx45 was also present in the bundle branches (Figure 7.D). Contrarily, no Cx45 signal was found in the ventricular working myocardium (Figure 7.D). The Cx45 immunostaining of atrial regions was heterogeneous, presumably due to the co-presence of working cardiomyocytes and conductive bundles in the atria. Cx43 immunoreaction was marked at the intercalated discs throughout the ventricular working myocardium (Figure 7.E).

Both pacemaker cells of the SAN (Figure 7.F) and AVN and Purkinje fibers of the ventricular conduction system (Figure 7.G) showed strong desmin immunoreactivity in comparison to the weaker labeling of the adjacent atrial and ventricular working myocardium (Figure 7.G).

DOI:10.14753/SE.2025.3172

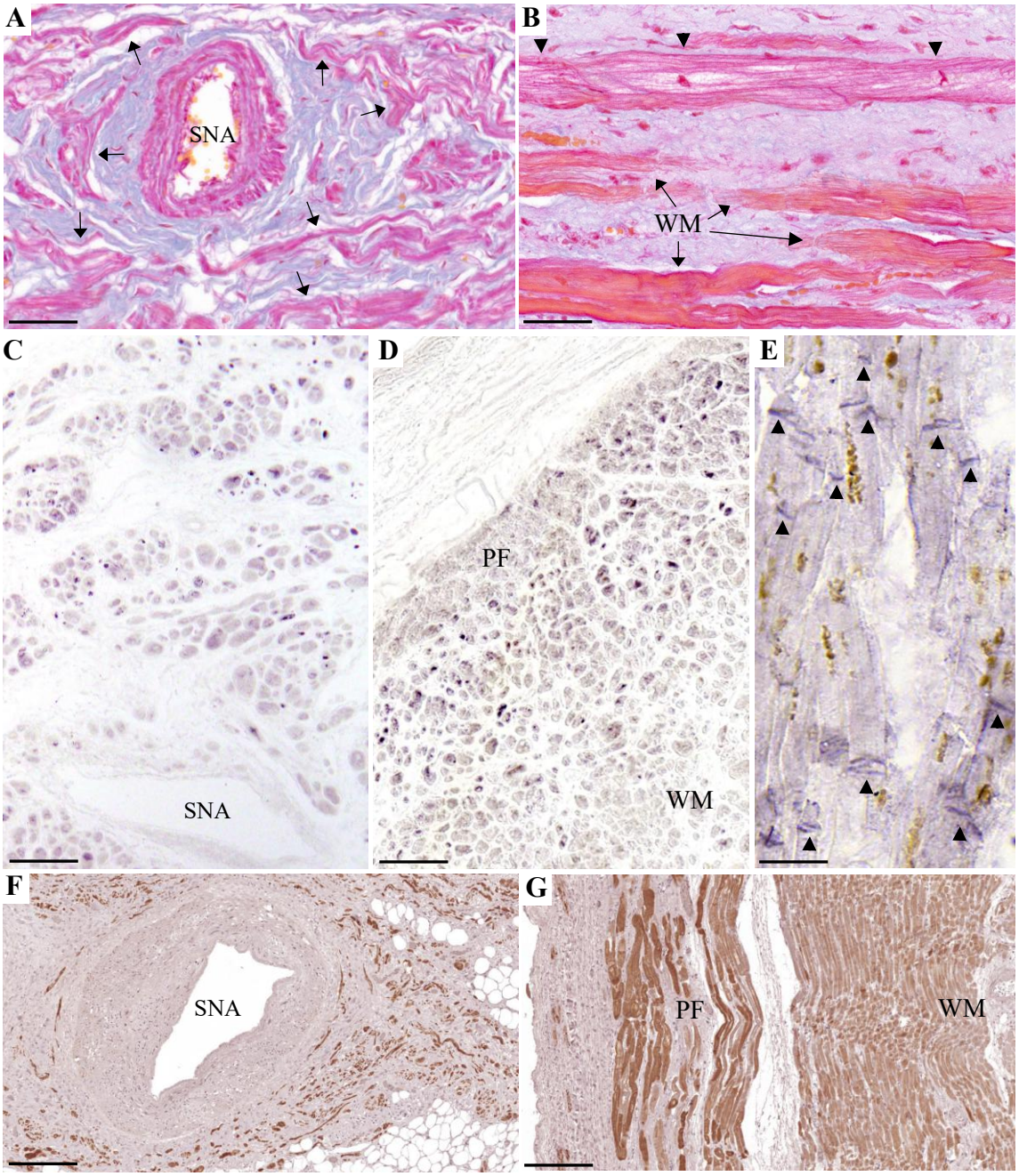

Figure 7. The cardiac pacemaker and conduction system.

A: *Pacemaker cells (arrows) of the sinoatrial node, trichrome (150).* ***B:*** *Purkinje fibers (PF, arrowheads) and ventricular working myocardium (WM), trichrome.* ***C:*** *Presence of Cx45 in the SAN.* ***D:*** *PFs positive for Cx45 and immunonegative ventricular WM (152).* ***E:*** *Ventricular WM immunoreactive for Cx43 (arrowheads); lipofuscin granules are yellow.* ***F:*** *Pacemaker cells of the SAN positive for desmin.* ***G:*** *PFs immunoreactive for desmin and weakly staining ventricular WM. SNA: sinoatrial nodal artery. Scale bar: 50 μm (A, B), 85 μm (C), 100 μm (D), 25 μm (E), 230 μm (F, G)*

4.2. Histological features of the venous myocardial sleeves and the atria of human adults

4.2.1. Myocardial sleeves of the pulmonary veins

Left atrial myocardial extensions forming MSs were observed around the venous wall of the majority of the PVs examined. MSs were present on the outer side of the venous adventitia (Figure 8.A,B) and they consisted of bundles displaying various courses. In the case of 25/26 hearts (96%), at least one PV had MS. All PVs were excised and investigated individually. MS was identified around 12/13 left superior PVs (92%), around 15/17 left inferior PVs (88%), around 12/15 right superior PVs (80%) and around 12/12 right inferior PVs (100%). The MS usually disappeared before the vein reached the hilum of the lung, but in a few cases, it was present at the level of the hilum.

Bundles of large cardiomyocytes with a median diameter of 18.1 μm [IQR 16.5–19.7 μm] were detected in several PVs. These cardiomyocytes possessed lightly stained cytoplasm and peripheral myofibrils similarly to the Purkinje fibers of the ventricular conduction system. Among these cardiomyocytes, a fine collagen fiber network was frequently present (Figure 8.C). Clusters of small and thin cardiomyocytes resembling the pacemaker cells of the SAN were also frequently observed in the MSs of PVs. They were typically embedded in a network of fine dense connective tissue and sometimes showed a reticular arrangement. A small SAN-like structure was identified in the most distal part of the MS around the left superior PV of a 43-year-old man. In the center of the structure was a small artery with a pacemaker cell-like cardiomyocyte in its adventitia. Pacemaker cells embedded in connective tissue clustered around the artery (Figure 8.D). Small SAN-like structures were also identified in the MS of the left inferior PV of an individual with unknown medical history.

Cardiomyocytes displaying a morphology similar to Purkinje fibers or pacemaker cells were identified around the PVs of 24/26 hearts (92%). As for the individual PVs, these cells were present in 10/13 left superior PVs (77%), 11/17 left inferior PVs (65%), 9/15 right superior PVs (60%) and 5/12 right inferior PVs (42%). The amount of the special cardiomyocytes was different in each sample, namely some MSs were composed of exclusively Purkinje-like or pacemaker cell-like cardiomyocytes, while others contained only some groups of these cells. Special cardiomyocytes were present in the samples of young and old female and male patients as well, both with cardiac disease and with no

medical history. Best's Carmine stain confirmed that the MSs of PVs were enriched in cardiomyocytes containing abundant intracellular glycogen supporting their potential conducting phenotype (Figure 8.E). It is of note, however, that 31% of the PVs possessing a MS lacked pacemaker cell-like and Purkinje-like cardiomyocytes.

Intense Cx45 labeling was observed in several regions of the MSs around the examined PVs. Cx45 immunoreaction was predominantly present at the intercalated discs linking the adjacent cardiomyocytes (Figure 8.F). Prominent desmin labeling was also detected in myocardial extensions into PVs. Contrary to Cx45, desmin was present throughout the cytoplasm of the cardiomyocytes (Figure 8.G). Highly immunoreactive cardiomyocytes frequently exhibited a morphological phenotype similar to Purkinje fibers or nodal cardiomyocytes. While several cardiomyocytes showed strong staining for desmin, less immunoreactive cardiomyocytes were also observed. The rate of the highly immunoreactive bundles varied among PV samples. Double immunofluorescence analysis of desmin and Cx45 revealed a strong sarcomeric and junctional pattern for desmin immunostaining. The intense Cx45 labeling was confined to the intercalated discs, where it overlapped to a large extent with desmin (Figure 8.H).

In an 86-year-old female patient with chronic ischemic heart disease and hypertension, amyloid deposits were observed in the vessel walls and MSs of all four PVs, but mainly in the wall of the right inferior PV.

DOI:10.14753/SE.2025.3172

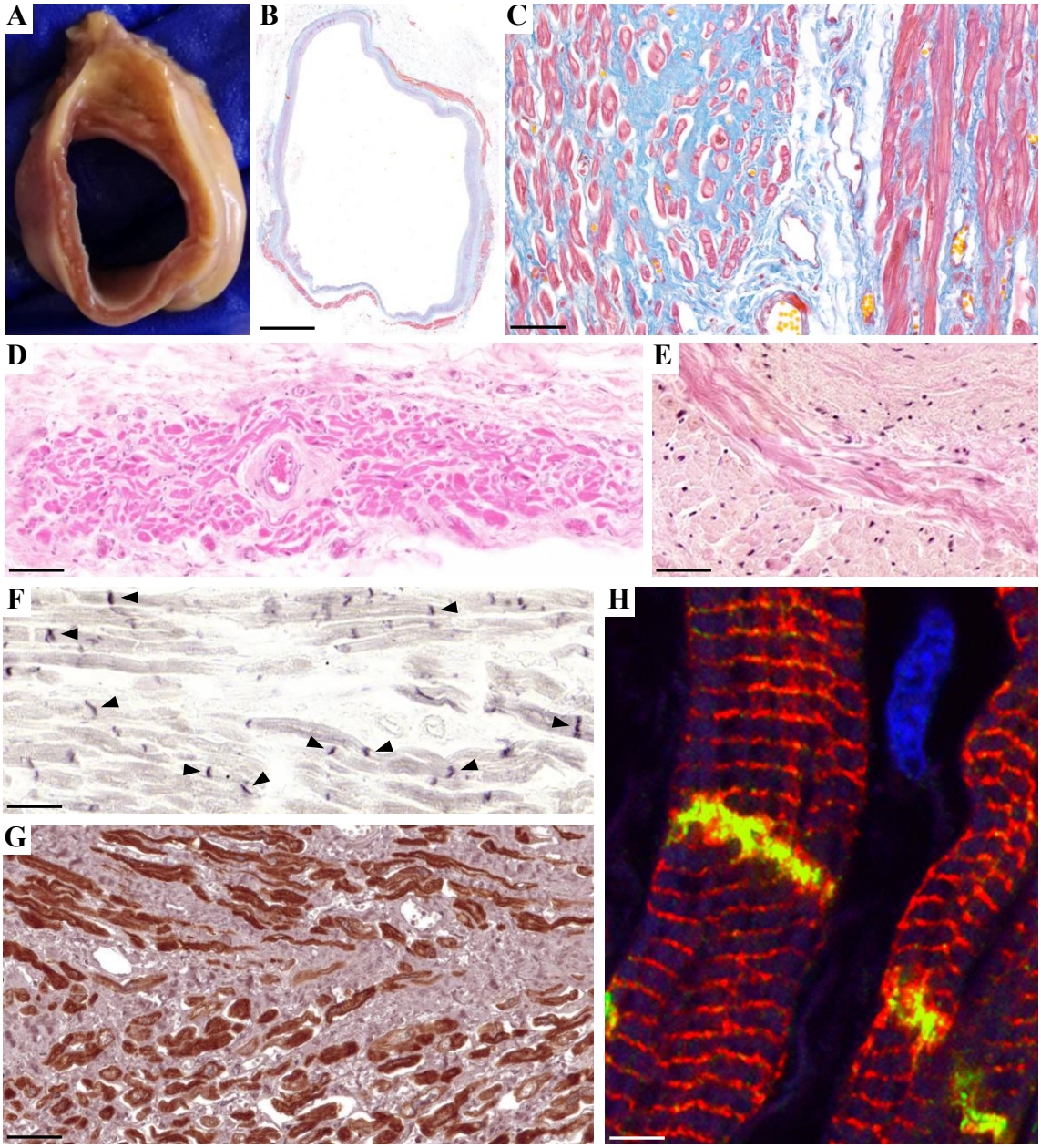

Figure 8. Myocardial sleeves of the pulmonary veins.

A: *Macroscopic image of the cross section of a pulmonary vein (PV) with myocardial sleeve (MS).* ***B:*** *Microscopic image of the cross section of a PV with MS, trichrome.* ***C:*** *Purkinje-like cardiomyocytes in the MS of a PV, trichrome.* ***D:*** *Pacemaker cell-like cardiomyocytes around a small artery in the MS of a PV, hematoxylin-eosin.* ***E:*** *Bundle of glycogen-rich cardiomyocytes, carmine.* ***F:*** *Presence of Cx45 in the MS of a PV (arrowheads).* ***G:*** *Desmin positive cardiomyocytes in the MS of a PV.* ***H:*** *Double labeling of desmin (red) and Cx45 (green) in the MS of a PV; DAPI stains the nucleus blue (150). Scale bar: 2000 µm (B), 50 µm (C, G), 60 µm (D, E), 45 µm (F), 10 µm (H)*

4.2.2. Myocardial sleeve of the superior vena cava

MSs were found around 34/34 SVCs of human adults (100%) (Figure 9.A,B). The MS was lacking from the joining of the azygos vein in every case, therefore only smooth muscle cells were detected at the level of the opening of the azygos vein or beyond it.

Bundles of large cardiomyocytes with a median diameter of 29.4 μm [IQR 27.9–32.5 μm] possessing the phenotypic characteristics of Purkinje fibers were commonly observed in the MSs (Figure 9.C). Small and thin cardiomyocytes resembling pacemaker cells were also identified (Figure 9.D). Purkinje-like or pacemaker cell-like cardiomyocytes were often embedded in networks of fine collagen fibers. Altogether, these cells were identified in 30/34 SVCs (88%), and their numbers were different in each sample. In 3 cases, no cardiomyocytes with special morphological signs were found, while in the case of the frozen sample, the presence of any such cells could not be clearly evaluated due to technical reasons. Special cardiomyocytes were present in the samples of young and old female and male patients as well, both with cardiac disease and with no medical history. Abundant intracellular glycogen content was found in the MS of the SVC (Figure 9.E). In a 54-year-old female, we identified a small SAN-like structure in the MS around the distal part of the SVC.

Cx45 was extensively present at the intercalated discs (Figure 9.F), while Cx43 immunoreaction proved to be weak. MSs of SVCs were frequently strongly immunopositive for desmin (Figure 9.G). Although prominent desmin labeling was detected in a large number of cardiomyocytes, but less immunoreactive myocardial fibers were also observed. The rate of the cardiomyocytes exhibiting strong desmin labeling varied among SVC samples.

Small amyloid deposits were observed in the vessel wall of the SVC of an 86-year-old female patient with chronic ischemic heart disease and hypertension.

DOI:10.14753/SE.2025.3172

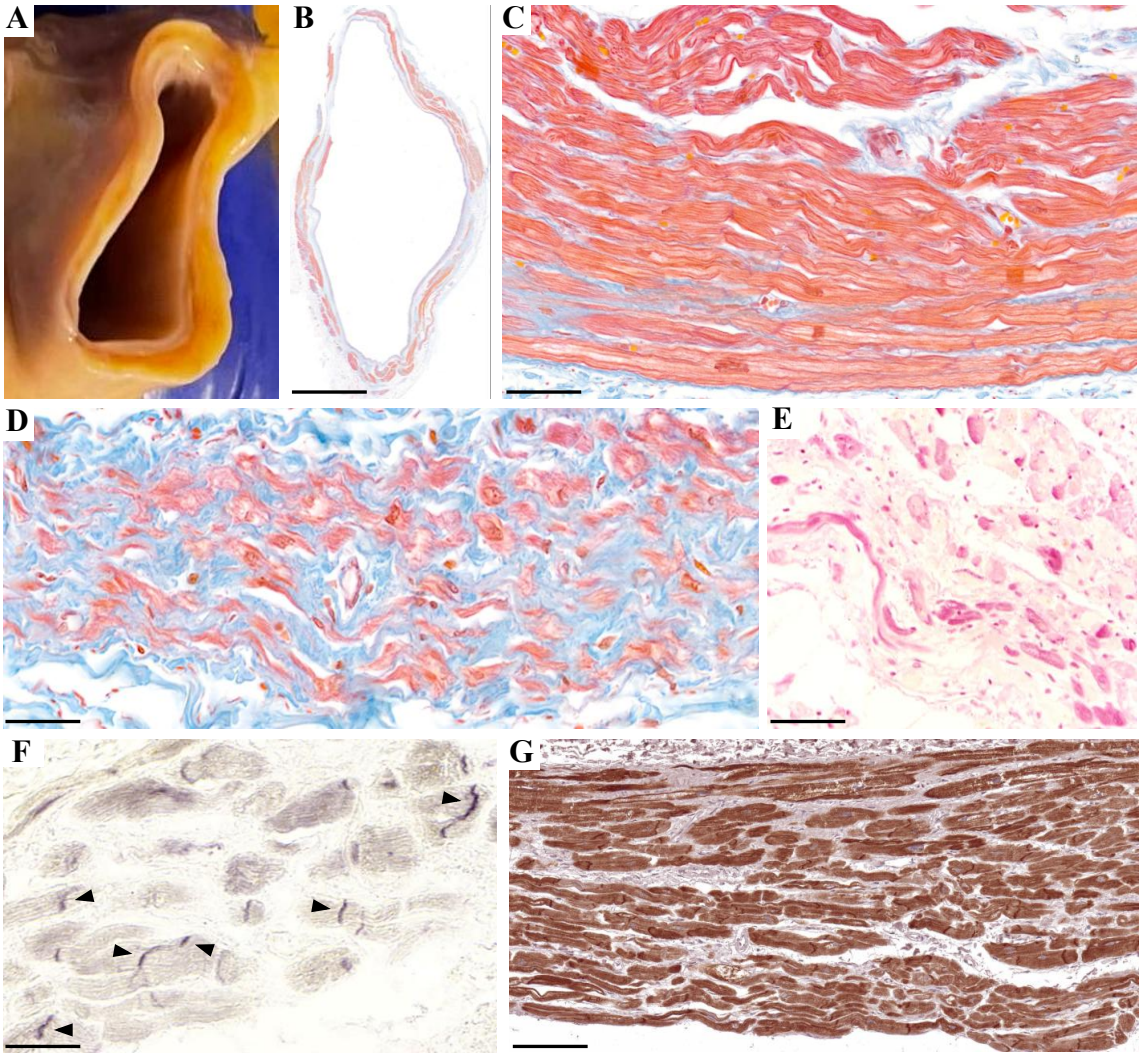

Figure 9. Myocardial sleeve of the superior vena cava.

A: *Macroscopic image of the cross section of a superior vena cava (SVC) with myocardial sleeve (MS).* ***B:*** *Microscopic image of the cross section of a SVC with MS, trichrome.* ***C:*** *Purkinje-like cardiomyocytes in the MS of a SVC, trichrome.* ***D:*** *Pacemaker cell-like cardiomyocytes embedded in dense fibrous tissue in the MS of the SVC of a 54-year-old female with hypertrophic obstructive cardiomyopathy, trichrome.* ***E:*** *Bundle of cardiomyocytes containing abundant intracellular glycogen, carmine.* ***F:*** *Presence of Cx45 in the MS of a SVC (arrowheads).* ***G:*** *Cardiomyocytes immunoreactive for desmin in the MS of a SVC. Scale bar: 3600 µm (B), 50 µm (C), 35 µm (D), 80 µm (E), 60 µm (F), 130 µm (G)*

DOI:10.14753/SE.2025.3172

4.2.3. Myocardial sleeve of the inferior vena cava

MSs were found around 14/18 IVCs (78%) (Figure 10.A,B). Although MS usually covered only the proximal part of the IVC, in some cases it was also present at the level of the diaphragm. Occasionally, cardiomyocytes were also present in the substance of the Eustachian valve (Figure 10.C). Bundles of cardiomyocytes possessing the phenotypic characteristics of Purkinje fibers (Figure 10.D) as well as small and thin cardiomyocytes resembling pacemaker cells (Figure 10.E) were commonly identified in the MSs. These cardiomyocytes were often embedded in fine collagen fiber networks. Purkinje-like or pacemaker cell-like cardiomyocytes were identified in 14/18 IVCs (78%), and their amount was different in each sample. Special cardiomyocytes were present in the samples of young and old female and male patients as well, both with cardiac disease and with no medical history. Small amyloid deposits were observed in the MS around the IVC of an 86-year-old female patient with chronic ischemic heart disease and hypertension.

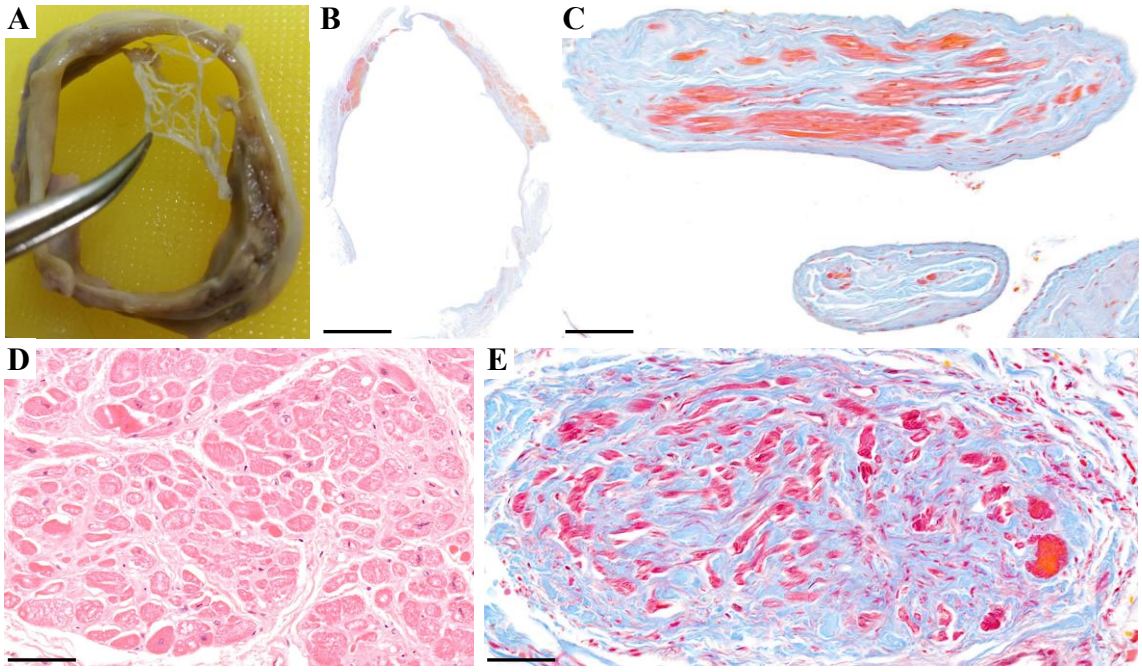

Figure 10. Myocardial sleeve of the inferior vena cava.

A, B: *Macroscopic* ***(A)*** *and microscopic* ***(B****, trichrome****)*** *images of the cross section of an inferior vena cava (IVC) with myocardial sleeve (MS).* ***C:*** *Cross sections of the Eustachian valve containing cardiomyocytes, trichrome.* ***D:*** *Purkinje-like cells in the MS of an IVC, hematoxylin-eosin.* ***E:*** *Pacemaker cell-like cardiomyocytes in the MS of an IVC, trichrome. Scale bar: 5200 μm (B), 100 μm (C), 60 μm (D), 45 μm (E)*

4.2.4. Myocardial sleeve of the coronary sinus

MSs were found around 19/19 CSs (100%) (Figure 11.A,B). The MS thinned towards the distal CS and generally reached the Vieussens valve. Rarely, some cardiomyocytes were present beyond the valve, around the final portion of the great cardiac vein, but none of these showed the morphological features of pacemaker or conducting cells. Bundles of cardiomyocytes with a median diameter of 22.7 μm [IQR 20.7–25.5 μm] possessing the phenotypic features of Purkinje fibers were commonly observed in the MSs (Figure 11.C). Small and thin cardiomyocytes resembling pacemaker cells were also identified (Figure 11.D). Purkinje-like or pacemaker cell-like cardiomyocytes were commonly embedded in fine collagen fiber networks. Altogether, these cells were identified in 17/19 CSs (89%), and their amount was different in each sample. In one case, no special cardiomyocytes were found, while in the frozen sample the presence of such cells could not be clearly distinguished for technical reasons. Special cardiomyocytes were present in young and old females and males as well, both with cardiac disease and with no medical history. Cardiomyocytes, often with a special phenotype, were frequently observed inside the Thebesius valve, at the right atrial orifice of the CS (Figure 11.E).

Cx45 was extensively present at the intercalated discs (Figure 11.F), while Cx43 labeling could barely be observed. Prominent desmin labeling was detected in a large number of cardiomyocytes from many samples (Figure 11.G), albeit less immunoreactive myocardial fibers were also observed. Numerous large amyloid deposits were observed both in the vessel wall and in the MS of the whole CS of an 86-year-old female patient with chronic ischemic heart disease and hypertension (Figure 11.H).

In three samples, small SAN-like structures were identified in the middle part of the CS. In a 22-year-old female, we detected a central artery surrounded by thin cardiomyocytes embedded in connective tissue (Figure 12.A). Pacemaker cell-like cardiomyocytes were also present in the adventitial layer of the artery (Figure 12.B). The diameter of pacemaker cell-like cardiomyocytes was 2-5 μm. Heidenhain's iron hematoxylin stain confirmed the presence of muscle striations inside these cells (Figure 12.C). In a sample with unknown medical history, several pacemaker cell-like cardiomyocytes forming networks were detected in the adventitial layer of an artery within the MS. Muscle striations of these small cells were confirmed by Heidenhain's iron hematoxylin. In the third CS sample, also of unknown medical history, one very small SAN-like structure was identified.

DOI:10.14753/SE.2025.3172

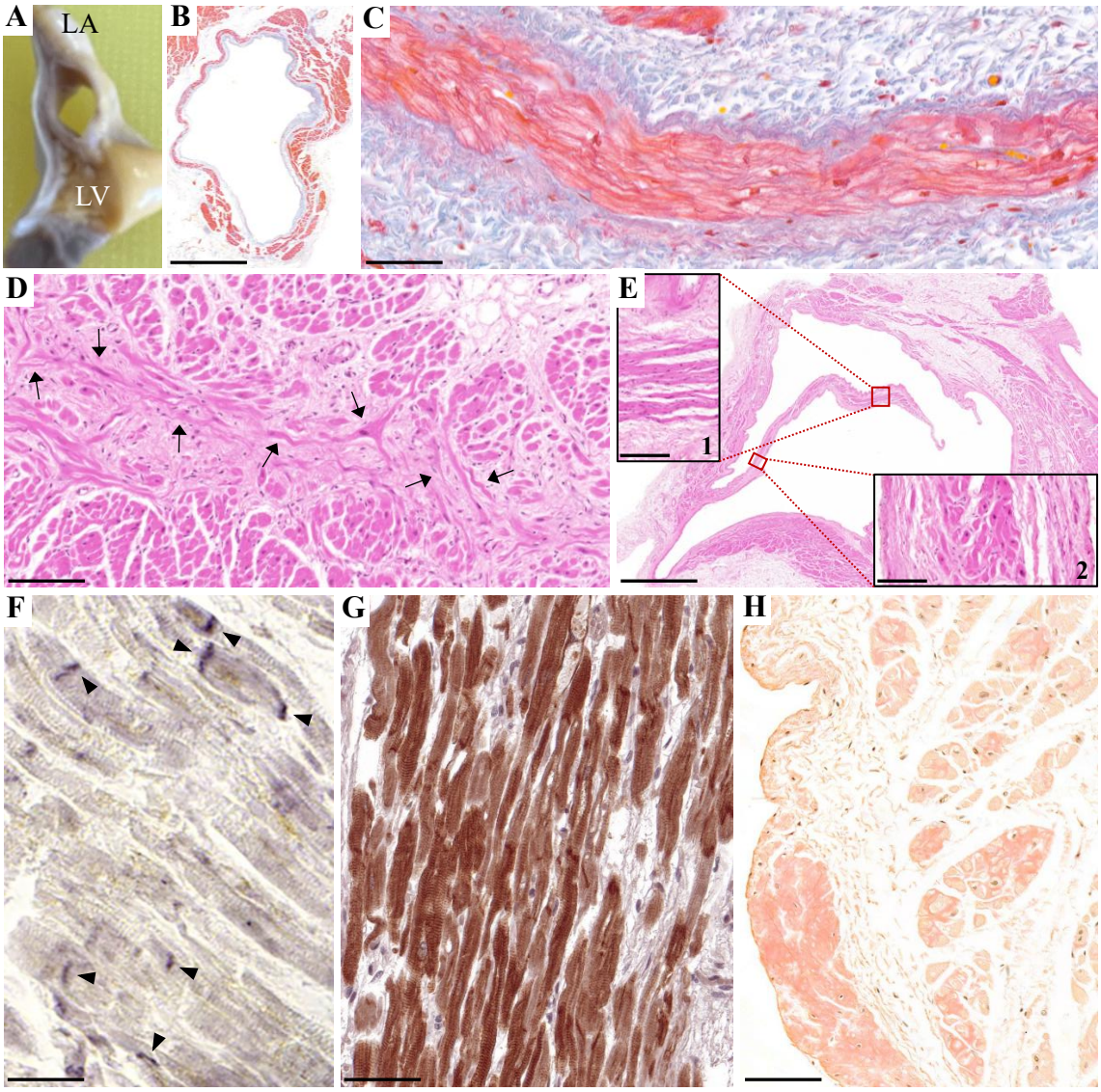

Figure 11. Myocardial sleeve of the coronary sinus.

A: *Macroscopic image of the cross section of a coronary sinus (CS) sample. LA: left atrium; LV: left ventricle.* ***B:*** *Microscopic image of the cross section of a CS with myocardial sleeve (MS), trichrome.* ***C:*** *Purkinje-like cardiomyocytes in the MS of a CS, trichrome.* ***D:*** *Pacemaker cell-like cardiomyocytes (arrows) in the MS of a CS, hematoxylin-eosin.* ***E:*** *Cardiomyocytes within the substance of the Thebesius valve, hematoxylin-eosin.* ***F:*** *Presence of Cx45 in the MS of a CS (arrowheads) (152).* ***G:*** *Cardiomyocytes immunoreactive for desmin in the MS of a CS.* ***H:*** *Amyloid deposits in the vessel wall and within the MS of a CS, Congo red. Scale bar: 1000 µm (B), 50 µm (C), 110 µm (D, E-inset 2), 3000 µm (E), 150 µm (E-inset 1), 35 µm (F), 60 µm (G), 75 µm (H)*

DOI:10.14753/SE.2025.3172

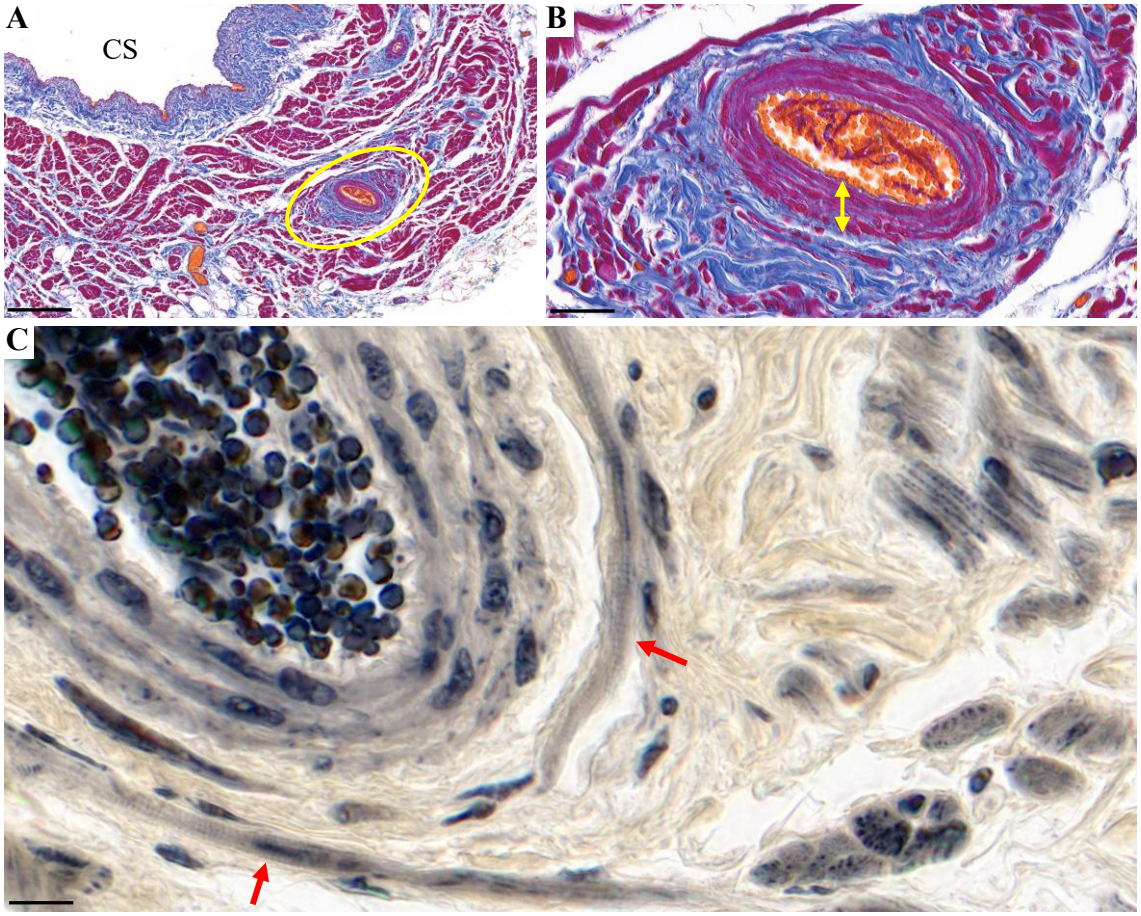

Figure 12. Sinoatrial node-like structure within the myocardial sleeve of the coronary sinus.

A: *A small sinoatrial node-like structure (encircled by yellow line) within the myocardial sleeve of the coronary sinus (CS), trichrome.* ***B:*** *Small cardiomyocytes in the adventitial layer of a small artery and in the dense connective tissue around the artery, trichrome. The tunica media of the artery is marked by double arrow.* ***C:*** *Small pacemaker cell-like striated cardiomyocytes (marked by arrows) in the adventitial layer of the small artery, Heidenhain's iron hematoxylin.*

Scale bar: 200 µm (A), 35 µm (B), 11 µm (C)

DOI:10.14753/SE.2025.3172

4.2.5. Quantitative analysis of desmin immunostaining

Quantitative analysis of desmin immunolabeling on sections of 4 adult hearts showed a significant difference in immunopositivity between ventricular working cardiomyocytes and Purkinje fibers. However, the desmin positivity of the working myocardium was also evident. Highly immunoreactive cardiomyocytes of the MSs around the SVC, PV and CS samples exhibited significantly stronger desmin signal intensity than the ventricular working cardiomyocytes (Figure 13.A).

Less immunoreactive cardiomyocytes (presumably working cardiomyocytes) were also present in the MSs in addition to the strongly stained conducting-like cells, leading to slightly different results when analyzing the signal intensities of representative areas. However, the signal intensity of desmin in all venous MSs was significantly stronger than that of the ventricular working myocardium. Extensive non-staining connective tissue between cardiomyocytes could also result in the higher mean gray value of an area. This problem was particularly present in SAN samples, in which therefore the desmin signal intensity did not differ from that of the working myocardium (Figure 13.B).

As an example, Figure 14 shows the regions analyzed in Case No 37.

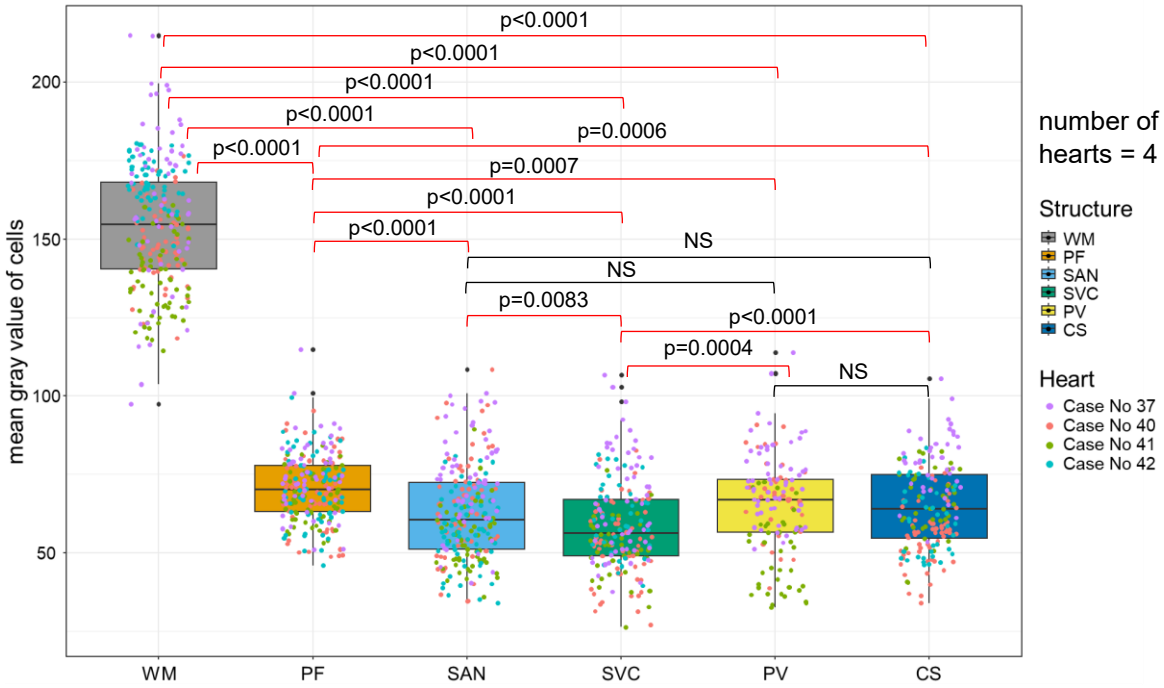

DOI:10.14753/SE.2025.3172

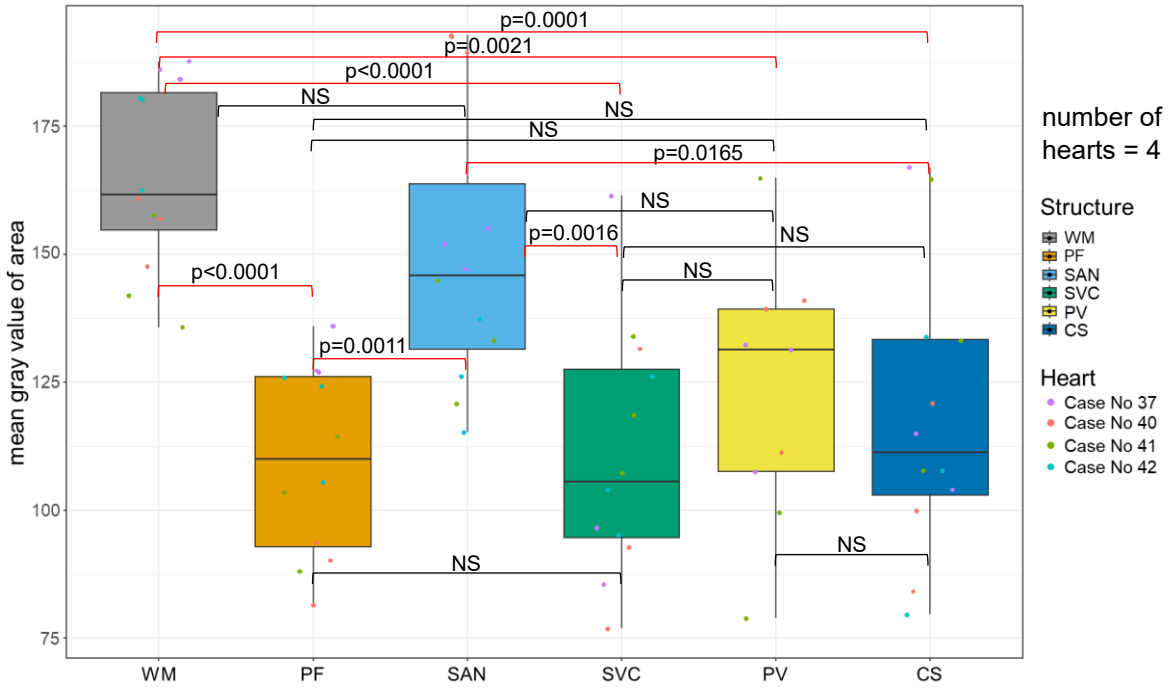

Figure 13. Desmin signal intensity differences between heart structures.

A-B: *Pooled analysis of cells* ***(A)*** *and areas* ***(B)*** *from 4 hearts (cases 37, 40, 41, 42). Lower mean gray value indicates stronger desmin signal intensity. Medians, first and third quartiles as well as minimum and maximum values excluding the outliers are presented for each structure.* ***A:*** *The desmin signal intensity of PF, pacemaker cells of the SAN, and highly immunoreactive cells of the venous MSs was significantly stronger than the desmin signal intensity of ventricular working cardiomyocytes. Due to the large number of particles analyzed, there were significant differences in desmin signal intensity between PF and cardiomyocytes from the MSs, as well as between some venous structures. However, these differences are clinically irrelevant.* ***B:*** *Less pronounced differences were verified between mean gray values of the representative areas. However, the desmin signal intensity of the PF area and all venous MSs was significantly different from WM. CS: coronary sinus; MS: myocardial sleeve; NS: non-significant; PF: Purkinje fibers; PV: pulmonary vein; SAN: sinoatrial node; SVC: superior vena cava; WM: ventricular working myocardium*

DOI:10.14753/SE.2025.3172

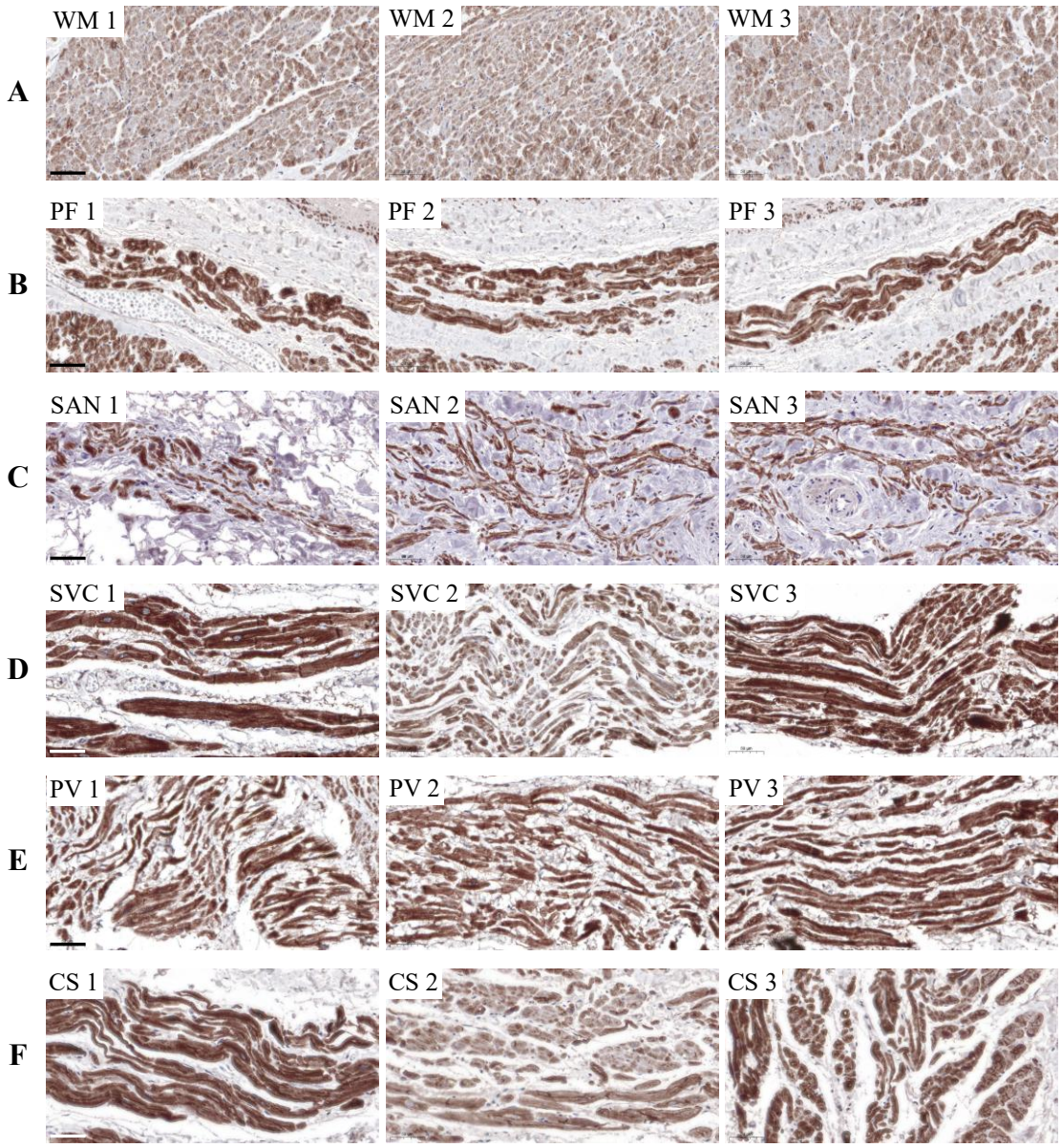

Figure 14. Quantitative analysis of desmin immunostaining.

A-F: *Analyzed regions of Case No 37, desmin immunostaining.* ***A:*** *WM displaying weak immunopositivity.* ***B, C:*** *Strongly immunoreactive PF of the ventricular conduction system ("B" images) and pacemaker cells of the SAN ("C" images).* ***D-F:*** *MS of the SVC ("D" images), PV ("E" images) and CS ("F" images) consists of both strongly immunoreactive and weakly labeled cardiomyocytes. Abbreviations: see legend of Figure 13. Scale bars: 50 μm*

4.2.6. Right and left atrial structures

Purkinje-like or pacemaker cell-like cardiomyocytes were frequently observed in different right and left atrial regions. The occurrence of these special cardiomyocytes differed between the atrial regions of those 9 hearts, whom atrial samples were examined in details. Occurrence of the Purkinje-like or pacemaker cell-like cardiomyocytes was the highest in the interatrial septum (78% of the samples), while 67% of the left atrial posterior wall, left atrial inferior wall and left atrial vestibule (the region between the LAA and the mitral anulus) samples lacked these special cardiomyocytes. It is of note that Purkinje-like or pacemaker cell-like cardiomyocytes were the most numerous in the atrial samples of the 54-year-old female patient with hypertrophic cardiomyopathy. Nevertheless, these cells were also present in each examined atrial regions of the 22-year-old female patient with no medical history (Table 3). In the fossa ovalis and its limbus, networks of thin cardiomyocytes resembling the pacemaker cells of the SAN were frequently observed (Figure 15.A). For the methanol-fixed heart, Cx45 was detected at the intercalated discs in the roof of the left atrium (Figure 15.B) and the limbus fossae ovalis.

Amyloid deposits were observed in the atrial samples of two hearts. For an 86-year-old female patient with hypertension and chronic ischemic heart disease, amyloid deposits were observed in both atria but predominated in the LAA, the left atrial inferior wall and the left atrial vestibule. For the ventricular samples of this heart, amyloid was detected only in arterial walls but not in the myocardium. For a 54-year-old female patient with hypertrophic cardiomyopathy and hypertension, large amyloid deposits were detected in the left atrial ridge (Figure 15.C), but smaller deposits were also present in the interatrial septum, the LAA, the left atrial posterior wall and the left atrial inferior wall. Amyloid was not detected in the ventricular samples.

DOI:10.14753/SE.2025.3172

Table 3. Semiquantitative assessment of the prevalence of cardiomyocytes possessing the phenotype of pacemaker or conducting cells for the atrial regions of 9 adult hearts.

Age, sex, medical history and cause of death are detailed in Table 1.

: none; : few; : several

CT: crista terminalis; IAS: interatrial septum; LAA: left atrial appendage; LAIW: left atrial inferior wall; LAPW: left atrial posterior wall; LAR: left atrial ridge; NA: not available; RAA: right atrial appendage; ROOF: roof of the left atrium; VEST: left atrial vestibule

Case	CT	RAA	IAS	ROOF	LAPW	LAIW	LAA	LAR	VEST
26									
36						NA			NA
37						NA			NA
38									
39									
40									
41	NA							NA	
42	NA								
43	NA			NA		NA			NA

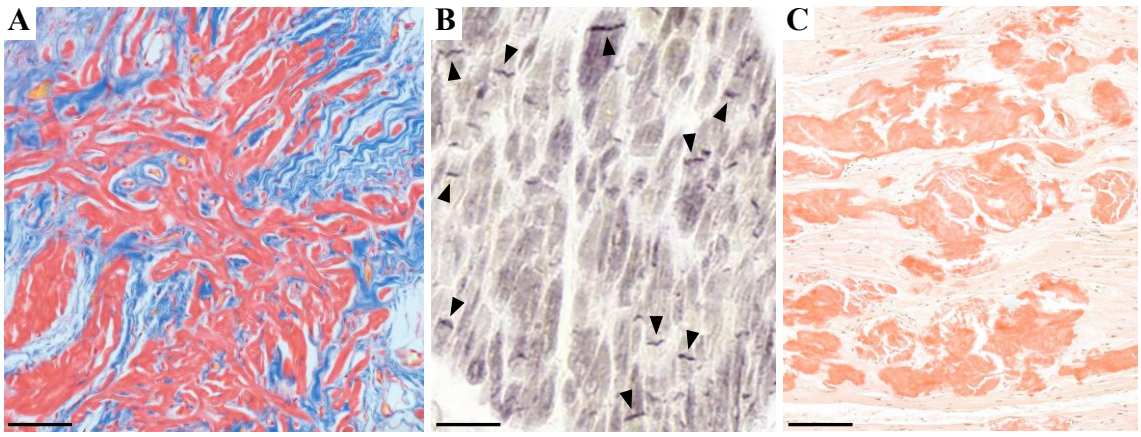

Figure 15. Histological characteristics of atrial regions.

A: *Networks of thin cardiomyocytes resembling the pacemaker cells of the SAN in the fossa ovalis, trichrome.* ***B:*** *Presence of Cx45 in the roof of the left atrium (arrowheads).* ***C:*** *Large amyloid deposits in the left atrial ridge, Congo red.*

Scale bar: 70 µm (A), 55 µm (B), 130 µm (C)

DOI:10.14753/SE.2025.3172

4.3. Histological features of the human fetal heart

In the 23-week-old human fetus, pacemaker cells of the SAN and Purkinje fibers of the ventricular conduction system could not be clearly distinguished from working cardiomyocytes. However, the SAN region could be identified by its localization and its artery. Myocardial extensions into the SVC were observed (Figure 16.A). Strong desmin labeling was detected in the MS of the SVC and at the SAN region (Figure 16.B). The Cx45 immunoreaction was intense in cells surrounding the sinoatrial nodal artery and in the MS of the SVC in comparison to the ventricular working myocardium (Figure 16.C).

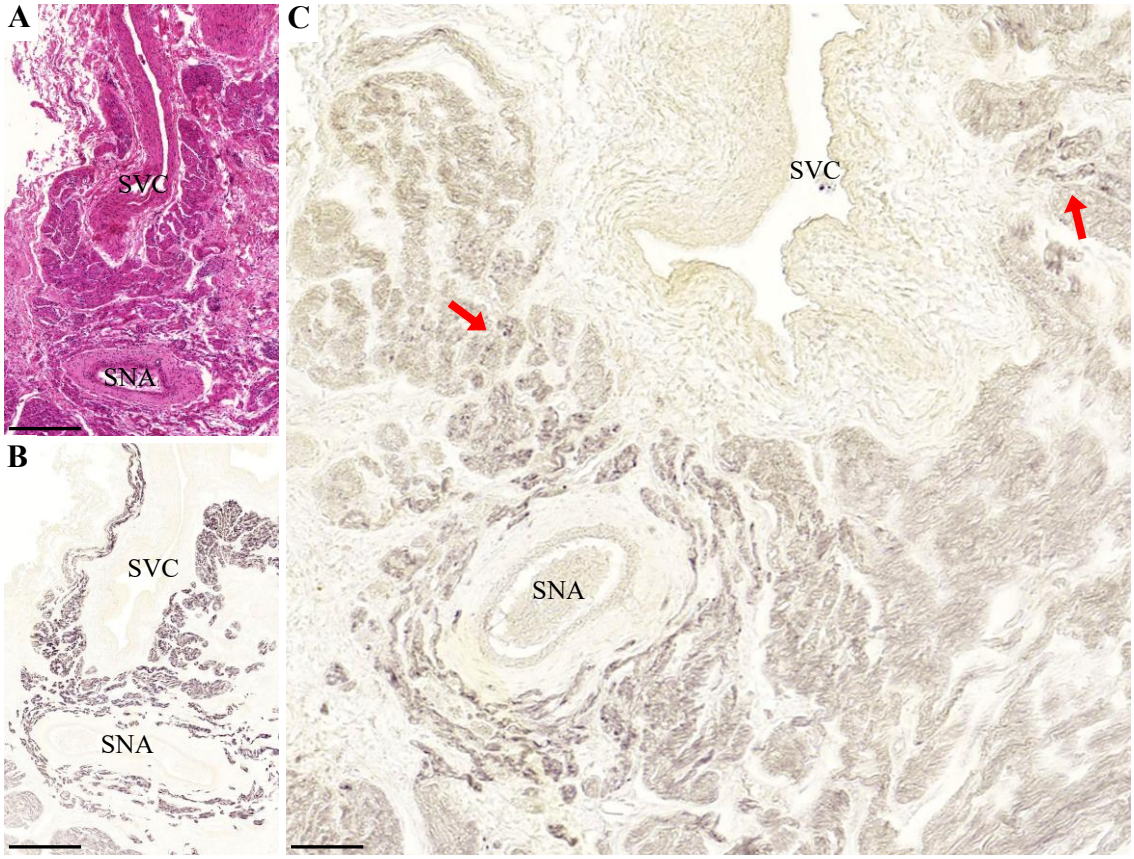

Figure 16. Histological features of a 23-week-old human fetal heart.

A: *Myocardial extensions around the wall of the superior vena cava (SVC). The sinoatrial node (SAN) and its artery (SNA) are located close to the right atrial orifice of the SVC, hematoxylin-eosin (150).* ***B:*** *Strong desmin immunoreaction in the myocardial sleeve of the SVC and at the SAN region (150).* ***C:*** *Intense Cx45 labeling in the cells around the SNA and in some cardiomyocytes (red arrows) around the SVC. Scale bar: 300 µm (A), 330 µm (B), 80 µm (C)*

4.4. Inflammation and fibrosis in end-stage heart failure-associated atrial fibrillation

4.4.1. Inflammasome activation

There was no significant difference in the expression of inflammasome sensors between the AF and SR groups. There was a strong tendency that protein expression of cleaved caspase-1 (p20, p22) was increased in the AF versus SR group (p=0.051). No signal was detected for NALP1 (Figure 17.A,B). The expression of cleaved caspase-1 correlated significantly with the expression of both IL-1β (p=0.005) and its cleaved form (p=0.004) in the whole population. In the AF group, the expression of cleaved caspase-1 correlated significantly with the expression of IL-1β (p=0.01) and its cleaved form (p=0.01) as well, indicating the presence of inflammation in AF patients. However, in the SR group, the expression of cleaved caspase-1 did not correlate with either IL-1β or its cleaved form (p>0.05). Notably cleaved caspase-1 level showed no correlation with the expression of ASC or inflammasome sensors (p>0.05), suggesting a primary effect on inflammasome activity (triggering) rather than on inflammasome priming (Figure 17.C).

Two samples showed pronounced activity of inflammasome sensors and downstream signaling. Patient AF2 did not suffer from any infection close to the heart transplantation, but was an obese smoker. Patient Sinus9 required inotropic support for advanced HF, and was treated for a catheter-related bloodstream infection. However, his inflammatory markers got normal a week before transplantation and control blood culture was negative.

4.4.2. Macrophage infiltration

Enhanced presence of macrophages was found in the left atrial myocardium of the AF group compared to the SR group. The mean of average macrophage number per unit area at the myocardium was 1.80 (min: 0, max: 5.67) in the SR group and 11.9 (min: 0.667, max: 34.8) in the AF group. Likewise, macrophages were more abundant in the left atrial epicardium of the AF group than of the SR group. After the exclusion of an outlier at the SR group, the mean of average macrophage number per unit area at the epicardium was 0.311 (min: 0, max: 0.600) in the SR group and 2.04 (min: 0, max: 5.14) in the AF group (Figure 18.A). Neither difference was significant, however, there was a tendency towards increase for the AF samples (p=0.09 for myocardial samples, p=0.21 for epicardial samples). Distribution of macrophages was heterogeneous within a given sample, both in the AF and in the SR groups (Figure 18.B).

DOI:10.14753/SE.2025.3172

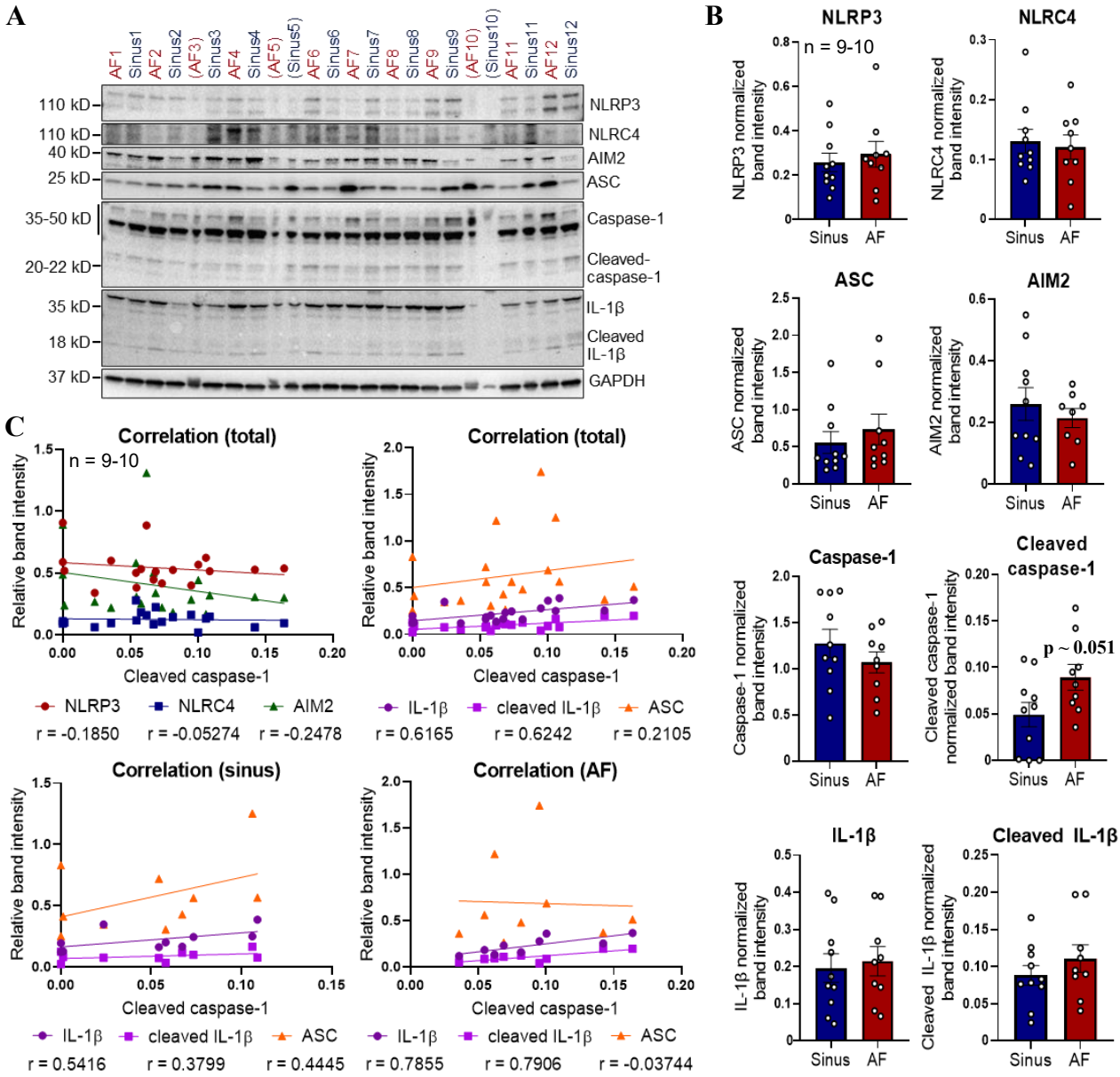

Figure 17. Inflammasome activation in heart failure-associated atrial fibrillation.

A: *Western blot detection of inflammasome markers in left atrium of patients with sinus rhythm and atrial fibrillation (AF). Samples excluded for poor quality homogenates are presented in parentheses.* ***B:*** *Analysis of normalized band intensities of inflammasome markers (p>0.05, Student's t-test; n=9-10). Results are expressed as mean± standard error of the mean.* ***C:*** *Correlation and regression analysis of inflammasome sensors and markers of their downstream signaling. Cleaved caspase-1 was correlated with interleukin-1β and its cleaved form in both the total population (p=0.005 and 0.004, respectively) and the AF group (p=0.01), but not in the sinus rhythm group. No correlation was found with any of the inflammasome sensors (p>0.05). (Pearson-correlation; n=9-10). Continuous data passed the Shapiro-Wilk normality test (156).*

DOI:10.14753/SE.2025.3172

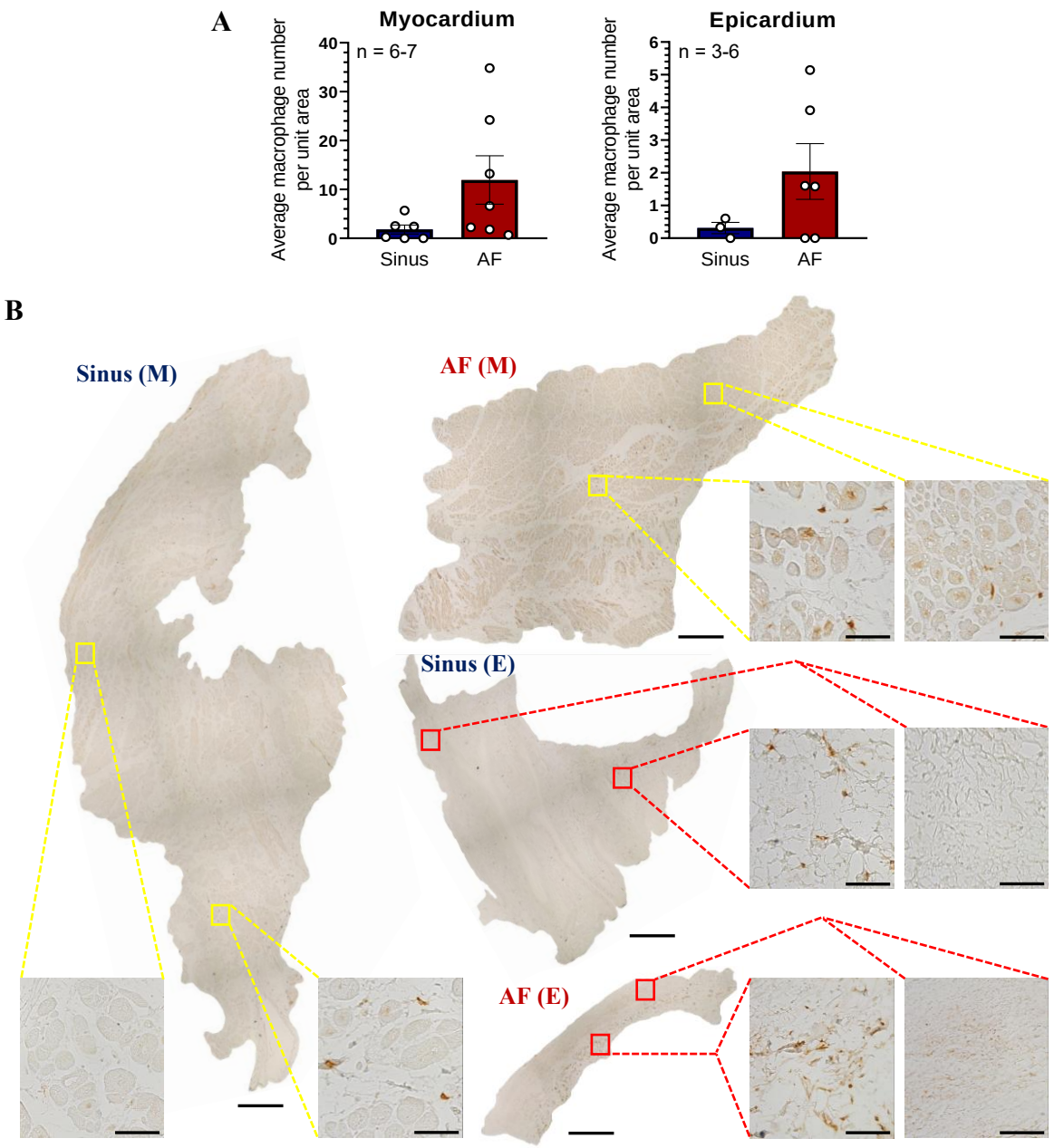

Figure 18. Macrophage infiltration in heart failure-associated atrial fibrillation. ***A****: The average number of macrophages per unit area in both left atrial myocardium and epicardium was higher in the atrial fibrillation (AF) samples than in the sinus rhythm group, but differences were not significant (p>0.05, Student's t-test; n=3-7). Results are expressed as mean ± standard error of the mean.* ***B:*** *Representative images of Iba1-positive macrophages in left atrial myocardium (M) and epicardium (E) of patients with AF and sinus rhythm (scale bars: 500 µm). Heterogeneous accumulation of macrophages within a given sample is shown in the high magnification images (scale bars: 60 µm). Continuous data passed the Shapiro-Wilk normality test (156).*

DOI:10.14753/SE.2025.3172

4.4.3. Left atrial fibrosis

Mean percentage of total fibrosis was 19.5% (min: 6.80%, max: 44.5%) in the SR group and 14.5% (min: 4.92%, max: 24.1%) in the AF group. After the exclusion of an outlier at the SR group, mean percentage of interstitial fibrosis was 7.94% (min: 5.85%, max: 9.81%) in the SR group and 8.74% (min: 4.82%, max: 18.4%) in the AF group (Figure 19.A). Histological examination of left atrial samples showed no relevant difference in the amount of total fibrosis and interstitial fibrosis between the AF and SR groups (p=0.43 for total fibrosis, p=0.73 for interstitial fibrosis) (Figure 19.B).

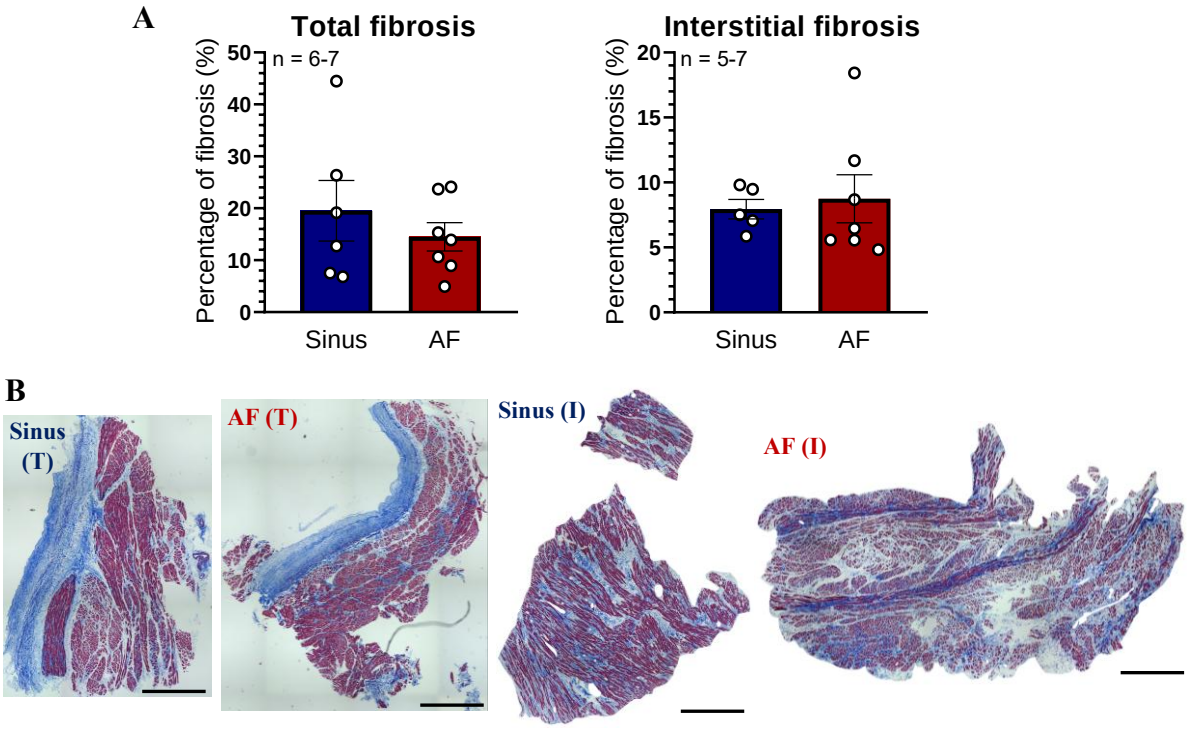

Figure 19. The extent of left atrial fibrosis in heart failure with sinus rhythm or atrial fibrillation.

A: *There was no difference in the percentage of either total or interstitial fibrosis between the two groups (p>0.05, Student's t-test; n=5-7). Results are expressed as mean ± standard error of the mean.* ***B.*** *Representative images of total (T) and interstitial (I) fibrosis in the sinus rhythm and atrial fibrillation (AF) groups (scale bars: 1000 µm). Continuous data passed the Shapiro-Wilk normality test (156).*

5. DISCUSSION

Our results provide a remarkable insight into the histological and molecular characteristics of supraventricular myocardial tissue, and thus contribute to the understanding of the pathophysiological factors responsible for the initiation and maintenance of AF.

5.1. Myocardial sleeves of the pulmonary veins, caval veins and coronary sinus

5.1.1. Microscopic anatomy of the myocardial sleeves

In the current study, the majority of the investigated veins were ensheathed by a MS. MS was present in 89% of the PVs, which is comparable with the literature data. In previous studies, the rate of the human PVs possessing a MS varied between 68-100%, presumably due to the high heterogeneity of the examined specimens (38, 40-44, 149). Similarly to our findings, the MS was detected on the adventitial side of the vein, separated from the venous wall by a fibrofatty tissue layer (38, 41-43). For our samples, the MS has thinned towards the hilum of the lung and it has extended to the hilum only in a few cases. Other human data indicates that MSs may cover the PVs beyond the hilum of the lung (43).

In our study, MS was identified around all SVCs but only around the 78% of the IVCs. Previous papers reported the presence of MS around the SVC in 76-78% of cases (39, 63), while its frequency was quite variable (0-76% of cases) for the IVC (39, 63). The histological results of both the current and previous studies correlate with the literature, that documents SVC as a common origin of atrial arrhythmias (49, 50, 52), compared to the IVC, that has been reported as a trigger site of AF only in a few case reports (53-59). While we did not observe any cardiomyocytes in the azygos veins, a study of 131 samples documented myocardial extensions in 6% of the terminating azygos veins (39).

We found MSs around all CSs, similarly to some previous human reports (60, 61, 161). In contrast, in another study, only 7% of CSs contained myocardial extensions, but this study performed only macroscopic analyses and therefore may have underestimated the true prevalence of MS around CS (39). Given our findings, it is rather strange that CS has been documented as a trigger site of non-PV atrial arrhythmias in only 1-17% of the cases (48-52). We observed cardiomyocytes around the terminal part of the great cardiac vein

only in a few cases, similar to Chauvin et al. (61). It is interesting that Lüdinghausen et al. reported that MS generally covers the terminal part of the great cardiac vein (60).

We identified cardiomyocytes with morphological features of pacemaker cells or Purkinje-fibers in 61% of PVs (69% of PVs with MS), 88% of SVCs of adults, 78% of IVCs (100% of IVCs with MS) and 89% of CSs. These values may underestimate the true incidence of cardiomyocytes with specialized phenotype, as multiple staining procedures did not allow serial sectioning. Our findings of a high number of pacemaker cell-like and Purkinje-like cells in the MSs are a novelty, as the majority of previous microscopic studies have not found similar cells. There is only one human study on the presence of specialized cardiomyocytes in the MSs of PVs (46). The authors identified rows of Purkinje-like cells and clusters of pacemaker cell-like cardiomyocytes in the MSs around the left superior PVs of four patients with AF, while all specimens that had no history of AF lacked these structures. Their findings were confirmed by electron microscopy (46). It is important to note that in our study, pacemaker cell-like and Purkinje-like cardiomyocytes were also present in individuals without a history of AF, suggesting that the presence of these cells alone does not explain the development of AF. In addition, the prevalence of these cells showed no correlation with sex, age and cardiovascular history, again suggesting their general presence. We hypothesize that the presence of pacemaker cell-like and Purkinje-like cardiomyocytes may provide an electrophysiological basis for the development of atrial arrhythmias, but that the manifestation of arrhythmias requires the coexistence of other factors, such as pathophysiological changes in atrial tissue.

To the best of our knowledge, our research is the first to demonstrate the presence of cells displaying the morphological signs of Purkinje fibers and pacemaker-cells in the MSs of human caval veins. As for CS, we found another human study reporting cardiomyocytes with specialized characteristics (161). Barceló et al. reported numerous Purkinje-like cells in CS samples near the entrance of the oblique vein of Marshall, and a group of pacemaker-like cells with much interposed connective tissue, resembling of a nodal structure (161). However, unlike our publications, this article (161) lacked convincing photographic documentation of these structures. Consequently, our study is the first to report conclusive data on the presence of pacemaker cell-like and Purkinje-like cardiomyocytes in caval veins and CS. The fact that these cells are present with almost

the same frequency around caval veins and CS as around PVs underlines the clinical relevance of non-PV arrhythmogenic triggers.

We identified SAN-like structures in the MSs of three CS samples. These structures are probably of embryonic origin, since in the embryonic heart, bilateral pacemaking regions are present in the vicinity of the sinus horns and common cardinal veins (162). During development, the embryonic left pacemaking area may migrate near the CS orifice, where nodal tissue was found repeatedly by histological examinations (163). This is in line with our observations, however, image documentation of the old communications referred by Momma et al. (163) is unavailable, similarly Barceló et al. did not provide photographic documentation of the alleged CS node (161). Double SAN has also been documented in a rare disease called right atrial isomerism (164-169), in which "some paired structures on opposite sides of the left-right axis of the body are symmetrical mirror images of each other, and have the morphology of the normal right-sided structures" (168). The malformation can be explained by the loss of Paired-like homeodomain transcription factor 2c (Pitx2c), a protein physiologically involved in left-right cardiac morphogenesis (167, 169). It is of note that in our cases we excluded right atrial isomerism, as none of the following co-morbidities were present: bilateral SVC (165-167, 170) from which the left one drains to the roof of the left atrium (170), absence of the CS (164, 165, 167, 170), abnormal drainage of the PVs (164, 165, 167, 168, 170), atrial septal defect or common atrium (164, 165, 167, 170) and other major cardiac anomalies (164, 165, 167, 168, 170). Another human study found a small node-like structure consisting of a group of small cells, loose connective tissue and two arteries, but in contrast to our results, this was identified in the LAA of a young patient treated for atrial tachycardia (171). The possible presence of a left SAN has also been theorized to be associated with a persistent left SVC draining into the CS (163). This anomaly has a prevalence of 0.2-3% in the general population (172). The malformation results from persistence of embryonic left common cardinal vein and the caudal part of the left superior cardinal vein (172, 173), therefore its developmental background differs from persistent left SVC with right atrial isomerism (173). We did not confirm persistent left SVC in any of our cases. It is interesting that although several studies have shown that this form of persistent left SVC may be associated with sick sinus syndrome (162), ectopic pacemaker activity triggering supraventricular arrhythmias (28, 162, 174-177) and left P-wave axis suggesting an

ectopic pacemaker in CS (163), histological proof of left SAN in this condition is lacking. Only right SAN was found even in the absence of right SVC (178). In our cases, the presence of left SAN-like structure was independent of any form of left SVC and was also present in a young, healthy subject, raising the suspicion that a remnant of embryonic left SAN may also be present in structurally intact hearts. In addition, we also identified SAN-like structures in samples (1 left superior PV, 1 left inferior PV, 1 SVC) where, to the best of our knowledge, their presence had not been previously published. However, the functional significance of SAN-like structures requires further investigation. Based on the light microscopic similarity between the SAN-like structures in CS and the true SAN, it is possible that these structures could be the source of the so-called low atrial rhythm. However, more detailed studies would be needed to prove this.

We detected amyloid deposits in the MSs of an old female patient, especially around the CS. Although the well-known atrial amyloidosis been shown to predispose to AF (99-102), there is little literature on amyloid deposition in the MSs of PVs (43, 179), IVC (180) and CS (181). Furthermore, there are no publications on amyloid in SVC. We found amyloid deposits in the PVs of only one heart, but the low incidence may be explained by the relatively small number of cases. Contrarily, in high volume human cohorts with a mean age of about 75 years, amyloid deposits were present in 53-55% of the MSs of PVs (43, 179). It is worth noting that although Steiner et al. found a higher frequency of amyloid deposits in patients with AF than in those without AF, the difference was non-significant (43). Consequently, it is a debate whether amyloid deposits in the MSs of PVs pay a role in the pathogenesis of AF, and how often they occur in the caval veins and CS.

5.1.2. Immunohistochemical characteristics of the myocardial sleeves

Given the paucity of data on the immunohistological features of human MSs (97, 128, 149), we performed specific immunostainings to support the specialized phenotype of the Purkinje-like and pacemaker cell-like cardiomyocytes of the MSs.

Connexin 45

We observed strong staining for Cx45 throughout the impulse-generating and conduction system of the heart, but no immunopositivity was detected in the working myocardium. It is in agreement with previous human and mammalian studies that reported Cx45 as a

specific marker for the cardiac pacemaker and conduction system (115, 120, 121, 134-137). Our investigations verified for the first time the presence of Cx45-positive cardiomyocytes in the wall of human PVs, SVC, and CS. Previous data on the connexin expression patterns of the MSs of PVs and caval veins are exclusively based on animal research (136, 138, 139), and human data are lacking. Our findings that ventricular working myocardium lacked Cx45 signal, while the pacemaker and conducting structures and MSs were rich in Cx45, strongly support the hypothesized specialized phenotype of MSs. The abundant presence of Cx45 in MSs may provide a histological basis for supraventricular arrhythmias arising from PVs and non-PV ectopic foci.

Desmin

Based on previous human studies documenting strong desmin immunostaining of the SAN, AVN and ventricular conduction system compared to the weaker labeling of the working myocardium (114, 123-125), we further characterized the MSs, targeting this general myocyte marker. As in previous studies, we observed an apparent difference in the immunostaining of desmin between working cardiomyocytes and cells of the impulse generating and conduction system. Convincing data on desmin labeling in human MSs have been documented only for fetal hearts (125), therefore, we examined specimens both from adult and fetal hearts. In our study of human adults, desmin immunoreactivity was found to be significantly stronger in the MSs of PVs, SVC and CS than in the ventricular working myocardium. Consequently, it is probable that desmin highlights not only the pacemaker and conduction system, but also the supraventricular regions in which arrhythmogenic foci may appear. We identified cardiomyocytes strongly immunoreactive for desmin in the majority of the MSs, irrespective of age, sex and cardiovascular history. Although a human study on PVs showed desmin positive spindle-shaped cardiomyocytes, but the image of this report indicated that these cells were present only dispersedly and other cardiomyocytes were immunonegative for desmin (182). These data are therefore not convincing, as our detailed analyses indicated that strong desmin labeling was present in large bundles of cardiomyocytes instead of discrete myocardial cells. We also observed strong desmin labeling in the MS of fetal SVC. This is in agreement with Yamamoto et al. who documented strong desmin immunopositivity in the PVs, caval veins and CS of human fetal hearts compared to immunonegative left ventricular working myocardium

(125). Our novel finding is that desmin expression is higher in potentially arrhythmogenic foci than in the working myocardium not only in fetuses but also in adults.

The desmin in Purkinje fibers is thought to provide support against mechanical strain (141), bind glycogen and contribute to maintaining the structural integrity of these large cells (114). Desmin may play a role in the cytoarchitecture of the Bachmann's bundle (148) and in mitochondrial function (140, 183). In fetuses, mechanical stress caused by the involvement of venous walls in atrial development was presumed to induce desmin expression (125). Impaired desmin cause abnormal calcium distribution that may result in arrhythmia (109). Consequently, desmin may have an important role in the function of the conduction system. However, the use of desmin as a selective marker for conducting cardiomyocytes seems implausible, as it is also expressed by the working myocardium.

5.2. Microscopic anatomy of the atria

Several atrial regions (crista terminalis, RAA, Eustachian ridge, interatrial septum, left atrial posterior wall, mitral annulus, LAA, ligament of Marshall) have been reported as potential trigger sites of atrial arrhythmias (28, 48). We frequently observed Purkinje-like or pacemaker cell-like cardiomyocytes in the atria, predominantly in the interatrial septum, and they were also present in a young patient without any medical history. We detected Cx45 at the top of the left atrium and in the interatrial septum, further supporting the potential conducting nature of these regions. Similar to our results, previous human studies have shown that certain atrial areas have conducting phenotype. In human embryos, three HNK-1-positive pathways were demonstrated between the SAN and the right atrioventricular ring (128). Studies on human embryos (123) and fetuses (125, 147) reported strong desmin immunoreactivity of the atria compared to weaker (147) or absent (123, 125) signal at the ventricular (compact) myocardium. Although one might assume that these regions lose their conducting properties in the postnatal period, Scherf et al. have shown that Purkinje-like cardiomyocytes and pacemaker cells are also present in adult humans in the internodal pathways, Eustachian ridge and Bachmann's bundle (66). These results, together with ours, suggest that certain atrial regions have conductive properties, which may provide a basis for the arrhythmias that originate from atrial foci.

We observed amyloid in two hearts. In an 86-year-old female, deposits were detected in both atria, but predominantly in the left atrium, while in a 54-year-old female, large

amyloid deposits were found in the left atrial ridge. IAA has been documented in 80% of the elderly population, predominantly in women (43). Atrial amyloidosis has been reported to predispose to AF (99-102), and interestingly, serum amyloid A levels, known to be associated with amyloidosis (184), were shown to correlate with AF (74). However, none of our patients with atrial amyloid had AF, suggesting that other pathophysiological factors are also required for the development of this arrhythmia.

5.3. Developmental explanation for supraventricular specialized cardiomyocytes

There may be a developmental explanation for the conducting phenotype of MSs. The venous pole expressing TBX18 and HCN4 in the primary heart tube shows high pacemaker activity. During later embryonic development (in mice, around embryonic day 9.5), pacemaker activity confines to the SAN, while the myocardium of the sinus venosus and sinus horns adopts an atrial working phenotype. Insufficient "atrialization" of structures derived from the sinus venosus (SVC [right sinus horn), crista terminalis [right venous valve], CS ostium [right atrial orifice of the left sinus horn], ligament of Marshall [left sinus horn]) can result in persisting focal automatic activity. This may explain why we found pacemaker cell-like and Purkinje-like cardiomyocytes in these areas. The PV myocardium develops independently of the sinus venosus and, surprisingly, exhibits an atrial working myocardial phenotype (TBX18/HCN4-negative) (185-187).

5.4. The association of inflammation with atrial fibrillation in end-stage heart failure

It is controversial whether there are differences in the features of MSs in patients with AF and those in SR. HCN4 positive cardiomyocytes, indicative of pacemaking function, have been identified in the PV orifices of humans with and without AF (97). Similarly, we demonstrated the presence of pacemaker-like and conducting-like cardiomyocytes in the MSs of several non-AF individuals. These results suggest that the presence of specialized cardiomyocytes alone does not trigger AF, and the question of which factors are required for the development of AF is still open. We aimed to examine atrial samples from HF patients, in whom it is a particular mystery who develop AF and who remain in SR.

Our research was the first to analyze the differences in inflammation in cardiac tissue samples between HF patients with SR and those with AF. Inflammatory mechanisms are well-known predisposing factors for AF (68). Elevated serum cytokine levels have been

associated with various types of this arrhythmia (74, 76), and increased NLRP3 inflammasome activity has been reported in AF patients (71, 73, 85). HF is a known risk factor for AF and their pathophysiology is similar in many respects. However, numerous patients suffering from HF never develop AF, suggesting pathological differences between HF with AF and HF with SR. Although the role of inflammatory molecules, including the NLRP3 inflammasome (188-191), AIM2 and NLRC4 (88), IL-1 (188, 189, 192, 193) and IL-18 (188, 192), has been demonstrated in the pathomechanism of HF, no publication has addressed the role of inflammatory processes in the pathomechanism of HF-associated AF in atrial tissue. Given the lack of data, we focused on differences in inflammasome activation between HF patients with SR and AF.

We verified increased inflammasome activity in left atrial samples from patients with HF-associated AF compared to HF patients in SR. Some previous studies have also shown higher inflammatory activity in HF patients with AF than in those with SR (194-196), but in contrast to us, they analyzed markers (CRP, IL-6, TNF-α) in blood samples (194-196) instead of atrial tissue. Li et al. reported that patients with paroxysmal, persistent or permanent AF had elevated serum levels of IL-10 and TNF-α compared to those with AF only, but after adjusting for variables such as sex, age and HF, the difference was not significant (75). This finding was explained by the high rates of comorbidities such as HF in the first three groups, compared to structurally intact hearts in the lone AF group (75). Elevated CRP and IL-6 levels in AF patients have been associated with an increased risk of HF-related hospitalization (197). These studies also suggest higher inflammatory activity in HF-associated AF, but like the above reports, they analyzed blood samples. The uniqueness of our study is that it was the first to analyze myocardial rather than serum samples to investigate the inflammatory processes underlying HF-associated AF.

It is unclear which phase of inflammasome activation is involved in AF. We confirmed a strong tendency towards increase in the expression of cleaved caspase-1 and its significant correlation with IL-1β and cleaved IL-1β expression in persistent AF samples. These findings suggest an enhanced triggering for inflammasome activation in persistent AF associated with end-stage HF. Yao et al. observed an increase in active caspase-1 protein levels in the RAAs from paroxysmal and long-standing persistent AF patients compared to SR controls, suggesting that triggering is an important mechanism in both paroxysmal and persistent AF (71). They showed that NLRP3-inflammasome priming

also plays a role in persistent AF (as supported by increased protein levels of NLRP3, ASC and NFκB compared to controls) (71). In contrast, we observed no significant differences in the expression of any type of inflammasome sensor between AF and SR groups, and cleaved caspase-1 levels did not correlate with inflammasome sensor expression, suggesting that inflammasome priming has no relevant role in HF-associated sustained AF. Interestingly, RAAs from SR patients who underwent heart surgery and developed postoperative AF showed increased inflammasome priming and triggering (increased expression of NLRP3, pro-caspase-1, ASC, cleaved caspase-1, toll-like receptor-4, NFκB) compared to patients who remained in SR, suggesting a pre-existing inflammatory substrate for postoperative AF (73). These results altogether support a role for inflammasome activation in various forms of AF, but there is no consensus on the role of priming and triggering processes in each type of AF. Although a prominent role of inflammasome activity in the maintenance of AF in patients with end-stage HF seems plausible, there is no strong evidence that this factor is responsible for this particular form of AF. Further studies are needed to determine possible causal relationships, correlations and consequences, to identify possible prognostic factors and to assess whether inflammasome activation has a diagnostic role in end-stage HF-associated AF.

Both the current and some other studies (194-196) suggest that inflammation in the presence of HF may induce the development and persistence of AF. We found that not only inflammasome activity but also macrophage infiltration was more pronounced in left atrial samples from AF patients compared to the SR group, although the number of macrophages was not significantly different. A recent review on NLRP3 signaling in AF raised the question: “does activation of cardiomyocyte inflammatory signalling recruit and activate macrophages and other inflammation-associated leukocytes in the heart?” (68). Our study seems to support this theory. Other studies have also shown increased infiltration of macrophages in atrial samples from AF patients, both in persistent (71, 72) and postoperative (73) AF. Lymphomononuclear infiltrates were more frequent in the PV-left atrial junction of patients with AF than in patients with SR (97). Taken together, these data suggest a possible role for macrophage infiltration in the pathogenesis of AF. In HF patients, serum levels of certain macrophage-secreted markers [TNF-α (196), IL-6 (195)] have been shown to be higher in AF than in SR. In our study, cleaved caspase-1 was correlated with the expression of IL-1β, a macrophage-secreted cytokine, in HF-

associated AF. Measurement of serum levels of these markers may help predict the occurrence of HF-associated AF, but further studies are needed before clinical use.

Despite the proven role of NLRP3 inflammasome activation in the pathomechanism of AF, drug targeting is still in its infancy. Currently, the main focus is on inhibiting NLRP3 transcription or post-translational modifications, as well as inhibiting IL-1β, ASC or caspase-1. The major drawbacks of these strategies are the off-target effects due to lack of specificity (85). NLRP3-mediated anti-inflammatory colchicine reduced AF recurrence after cardiac surgery or PV isolation (198, 199). In a pilot trial, treatment with canakinumab (anti-IL-1β antibody) was associated with a non-significantly lower incidence of AF recurrence after electrical cardioversion (200). Our results also suggest that a drug that selectively targets the inflammasome signaling pathway could potentially reduce the incidence of persistent AF in HF patients.

5.5. Atrial fibrosis in end-stage HF-associated atrial fibrillation

We found no difference in the amount of left atrial fibrosis in patients with AF and SR. There is conflicting literature on the relationship between fibrosis and AF in HF. In advanced HF, extensive atrial fibrosis expressed by collagen volume fraction has been reported to be present regardless of the presence or absence of AF (201). This correlates with our results. However, another study in HF patients has shown that collagen type-I synthesis indicating increased severity of myocardial fibrosis, is independently associated with coexisting AF (202). Although it cannot be clearly stated that the extent of atrial fibrosis in HF patients is not related to the occurrence of AF, our results suggest that the role of other factors, such as inflammatory processes, must be taken into account.

5.6. Limitations

Histological characterization of MSs in the wall of cardiac veins was limited by the small number of cases and the high proportion of hearts with unknown medical history.

The evaluation of inflammation in HF-associated AF was limited by the high heterogeneity of patients with end-stage HF undergoing heart transplantation. Some of those included in the study were treated for infection, had renal or hepatic failure, or required mechanical ventilation or circulatory support shortly before transplantation. The possible impact of these factors on inflammatory pathways cannot be clearly excluded.

DOI:10.14753/SE.2025.3172

6. CONCLUSIONS

In the present studies, we investigated the potential pathomechanisms of AF. In the MSs of human PVs, caval veins and CS, as well as in some atrial regions, we found cardiomyocytes that microscopically show features of cardiac pacemaker and conduction system cells. Our study is the first to show pronounced Cx45 immunoreactivity in the MSs, further supporting the hypothesis that these regions have arrhythmogenic properties. Immunostaining for desmin was apparently stronger in the pacemaker and conduction system of the heart and in supraventricular arrhythmogenic regions than in the ventricular working myocardium. Although desmin cannot be used as a selective marker of the pacemaker and conduction system of the heart, it is noteworthy that the prominent desmin immunostaining coincides with MSs ensheathing the veins entering the heart, which are the sites of arrhythmogenic foci. Taken together, these morphological and molecular findings support the hypothesis that arrhythmogenic foci are present in several supraventricular regions that are well-known trigger sites of atrial tachyarrhythmias.

We investigated inflammation-related differences in failing human hearts with SR and AF. Our study was the first to investigate this issue in cardiac tissue samples. We found tendency towards increase in the expression of cleaved caspase-1 and its significant correlation with the expression of interleukin-1β and its cleaved form in the AF samples. These findings indicate that enhanced inflammasome activity (triggering) may cause AF in patients with end-stage HF. Tendentiously higher macrophage infiltration also indicates higher levels of inflammation in AF samples, whereas HF-associated AF seems to be independent of cardiac fibrosis.

Our studies suggest that pacemaker- and Purkinje-like cardiomyocytes present in venous MSs do not induce AF per se. Similarly, the degree of left atrial fibrosis in HF patients is not associated with AF. Only inflammatory processes were associated with the prevalence of AF in a group of HF patients, suggesting that an increased inflammatory state is necessary for the development of AF, at least in certain patient populations.

DOI:10.14753/SE.2025.3172

7. SUMMARY

Prevalence of AF is about 3% in the adult population and it is often associated with HF. The cornerstone of the rhythm control therapy for AF is catheter ablation targeting the isolation of the PVs, which, however, has a one-year success rate of only 70%, even despite multiple interventions. Long-term efficacy of catheter ablation therapy is limited by the structural remodeling of the atria that facilitates the perpetuance of the arrhythmia. Several factors have been implicated in the pathomechanism of AF, such as epicardial fat accumulation, atrial fibrosis and inflammation, imbalance of the autonomic nerve system, and arrhythmogenic foci in PVs and other supraventricular areas. However, the microscopic and molecular basis of arrhythmogenic supraventricular foci and the predisposing factors for the development of HF-associated AF are rarely investigated. Therefore, we focused on these two issues.

We have shown that glycogen-positive cardiomyocytes displaying morphological features of SAN pacemaker-cells and ventricular Purkinje fibers, are present in MSs of human PVs, caval veins and CSs. Compared to the working cardiomyocytes, many of these cells showed a strong immunoreaction for Cx45 gap junction protein and desmin intermediate filament, similarly to SAN, AVN and ventricular conduction system. These findings were observed irrespective of sex, age and medical history. The prominent staining of Cx45 and desmin suggests a pacemaker and/or conducting phenotype of the venous MSs, which, however, does not always trigger arrhythmias by itself.

Inflammatory mechanisms were investigated in left atrial samples from patients with end-stage ischemic HF who either had sustained AF or no AF episodes. No differences were observed in the expression of inflammasome sensors between the two groups. Nevertheless, cleaved caspase-1 increased near significantly and showed significant correlation with the expression of interleukin-1β and its cleaved form in the AF group. A trend toward increase in the number of left atrial macrophages was observed in the AF group compared to the SR group as a sign of the inflammatory state. The amount of fibrosis did not differ between the two groups. Our observations were the first to show increased inflammasome activity in left atrial samples from patients with HF-associated AF compared to patients with HF and SR. These results may have therapeutic relevance for patients with HF and concomitant AF.

8. REFERENCES

1. Van Gelder IC, Rienstra M, Bunting KV, Casado-Arroyo R, Caso V, Crijns H, et al. 2024 ESC Guidelines for the management of atrial fibrillation developed in collaboration with the European Association for Cardio-Thoracic Surgery (EACTS). Eur Heart J. 2024;45(36):3314-414.
2. Benjamin EJ, Muntner P, Alonso A, Bittencourt MS, Callaway CW, Carson AP, et al. Heart Disease and Stroke Statistics-2019 Update: A Report From the American Heart Association. Circulation. 2019;139(10):e56-e528.
3. Alonso A, Alam AB, Kamel H, Subbian V, Qian J, Boerwinkle E, et al. Epidemiology of atrial fibrillation in the All of Us Research Program. PLoS One. 2022;17(3):e0265498.
4. Steinberg JS, O'Connell H, Li S, Ziegler PD. Thirty-Second Gold Standard Definition of Atrial Fibrillation and Its Relationship With Subsequent Arrhythmia Patterns: Analysis of a Large Prospective Device Database. Circ Arrhythm Electrophysiol. 2018;11(7):e006274.
5. Bielecka-Dabrowa A, Mikhailidis DP, Rysz J, Banach M. The mechanisms of atrial fibrillation in hyperthyroidism. Thyroid Res. 2009;2(1):4.
6. Wynn GJ, Todd DM, Webber M, Bonnett L, McShane J, Kirchhof P, et al. The European Heart Rhythm Association symptom classification for atrial fibrillation: validation and improvement through a simple modification. Europace. 2014;16(7):965-72.
7. Kalantarian S, Stern TA, Mansour M, Ruskin JN. Cognitive impairment associated with atrial fibrillation: a meta-analysis. Ann Intern Med. 2013;158(5 Pt 1):338-46.
8. Schnabel RB, Michal M, Wilde S, Wiltink J, Wild PS, Sinning CR, et al. Depression in atrial fibrillation in the general population. PLoS One. 2013;8(12):e79109.
9. Nattel S, Guasch E, Savelieva I, Cosio FG, Valverde I, Halperin JL, et al. Early management of atrial fibrillation to prevent cardiovascular complications. Eur Heart J. 2014;35(22):1448-56.
10. Rienstra M, Hobbelt AH, Alings M, Tijssen JGP, Smit MD, Brugemann J, et al. Targeted therapy of underlying conditions improves sinus rhythm maintenance in

patients with persistent atrial fibrillation: results of the RACE 3 trial. Eur Heart J. 2018;39(32):2987-96.

11. Reddy VY, Mobius-Winkler S, Miller MA, Neuzil P, Schuler G, Wiebe J, et al. Left atrial appendage closure with the Watchman device in patients with a contraindication for oral anticoagulation: the ASAP study (ASA Plavix Feasibility Study With Watchman Left Atrial Appendage Closure Technology). J Am Coll Cardiol. 2013;61(25):2551-6.
12. Nikolaidou T, Channer KS. Chronic atrial fibrillation: a systematic review of medical heart rate control management. Postgrad Med J. 2009;85(1004):303-12.
13. Lim KT, Davis MJ, Powell A, Arnolda L, Moulden K, Bulsara M, et al. Ablate and pace strategy for atrial fibrillation: long-term outcome of AIRCRAFT trial. Europace. 2007;9(7):498-505.
14. Zhang YY, Qiu C, Davis PJ, Jhaveri M, Prystowsky EN, Kowey P, et al. Predictors of progression of recently diagnosed atrial fibrillation in REgistry on Cardiac Rhythm DisORDers Assessing the Control of Atrial Fibrillation (RecordAF)-United States cohort. Am J Cardiol. 2013;112(1):79-84.
15. Sandhu RK, Smigorowsky M, Lockwood E, Savu A, Kaul P, McAlister FA. Impact of Electrical Cardioversion on Quality of Life for the Treatment of Atrial Fibrillation. Can J Cardiol. 2017;33(4):450-5.
16. Calkins H, Hindricks G, Cappato R, Kim YH, Saad EB, Aguinaga L, et al. 2017 HRS/EHRA/ECAS/APHRS/SOLAECE expert consensus statement on catheter and surgical ablation of atrial fibrillation: Executive summary. Europace. 2018;20(1):157-208.
17. Kuck KH, Brugada J, Furnkranz A, Metzner A, Ouyang F, Chun KR, et al. Cryoballoon or Radiofrequency Ablation for Paroxysmal Atrial Fibrillation. N Engl J Med. 2016;374(23):2235-45.
18. Reddy VY, Gerstenfeld EP, Natale A, Whang W, Cuoco FA, Patel C, et al. Pulsed Field or Conventional Thermal Ablation for Paroxysmal Atrial Fibrillation. N Engl J Med. 2023;389(18):1660-71.
19. Wokhlu A, Hodge DO, Monahan KH, Asirvatham SJ, Friedman PA, Munger TM, et al. Long-term outcome of atrial fibrillation ablation: impact and predictors of very late recurrence. J Cardiovasc Electrophysiol. 2010;21(10):1071-8.

20. Hindricks G, Potpara T, Dagres N, Arbelo E, Bax JJ, Blomstrom-Lundqvist C, et al. 2020 ESC Guidelines for the diagnosis and management of atrial fibrillation developed in collaboration with the European Association for Cardio-Thoracic Surgery (EACTS): The Task Force for the diagnosis and management of atrial fibrillation of the European Society of Cardiology (ESC) Developed with the special contribution of the European Heart Rhythm Association (EHRA) of the ESC. Eur Heart J. 2021;42(5):373-498.
21. Haissaguerre M, Hocini M, Sanders P, Sacher F, Rotter M, Takahashi Y, et al. Catheter ablation of long-lasting persistent atrial fibrillation: clinical outcome and mechanisms of subsequent arrhythmias. J Cardiovasc Electrophysiol. 2005;16(11):1138-47.
22. Waks JW, Josephson ME. Mechanisms of Atrial Fibrillation - Reentry, Rotors and Reality. Arrhythm Electrophysiol Rev. 2014;3(2):90-100.
23. Gehi AK, Kiser AC, Mounsey JP. Atrial Fibrillation Ablation by the Epicardial Approach. J Atr Fibrillation. 2014;6(5):979.
24. Auer J. Fat: an emerging player in the field of atrial fibrillation. Eur Heart J. 2017;38(1):62-5.
25. Kirchhof P, Calkins H. Catheter ablation in patients with persistent atrial fibrillation. Eur Heart J. 2017;38(1):20-6.
26. Lau DH, Schotten U, Mahajan R, Antic NA, Hatem SN, Pathak RK, et al. Novel mechanisms in the pathogenesis of atrial fibrillation: practical applications. Eur Heart J. 2016;37(20):1573-81.
27. Haissaguerre M, Jais P, Shah DC, Takahashi A, Hocini M, Quiniou G, et al. Spontaneous initiation of atrial fibrillation by ectopic beats originating in the pulmonary veins. N Engl J Med. 1998;339(10):659-66.
28. Santangeli P, Marchlinski FE. Techniques for the provocation, localization, and ablation of non-pulmonary vein triggers for atrial fibrillation. Heart Rhythm. 2017;14(7):1087-96.
29. Gal P, Marrouche NF. Magnetic resonance imaging of atrial fibrosis: redefining atrial fibrillation to a syndrome. Eur Heart J. 2017;38(1):14-9.
30. Goette A, Kalman JM, Aguinaga L, Akar J, Cabrera JA, Chen SA, et al. EHRA/HRS/APHRS/SOLAECE expert consensus on atrial cardiomyopathies:

Definition, characterization, and clinical implication. Heart Rhythm. 2017;14(1):e3-e40.

31. Nalliah CJ, Sanders P, Kottkamp H, Kalman JM. The role of obesity in atrial fibrillation. Eur Heart J. 2016;37(20):1565-72.
32. Van Gelder IC, Hemels ME. The progressive nature of atrial fibrillation: a rationale for early restoration and maintenance of sinus rhythm. Europace. 2006;8(11):943-9.
33. Wijffels MC, Kirchhof CJ, Dorland R, Allessie MA. Atrial fibrillation begets atrial fibrillation. A study in awake chronically instrumented goats. Circulation. 1995;92(7):1954-68.
34. Marincheva G, Iakobishvili Z, Valdman A, Laish-Farkash A. Left atrial strain: clinical use and future applications—a focused review article. Rev Cardiovasc Med. 2022;23(5):154.
35. Mészáros H, Vámosi P, Merkely B. Left atrial strain can predict the occurrence of atrial fibrillation: a systematic review and meta-analysis. Heart Rhythm 2023 Annual Meeting; New Orleans, Louisiana: Heart Rhythm; 2023. p. S305.
36. Kugler S, Duray G, Preda I. Új felismerések a pitvarfibrilláció genezisében és fenntartásában: az egyénre szabott kezelés lehetőségei [Novel mechanisms in the initiation and maintenance of atrial fibrillation: tailored individual treatment]. Orv Hetil. 2018;159(28):1135-45.
37. Nathan H, Eliakim M. The junction between the left atrium and the pulmonary veins. An anatomic study of human hearts. Circulation. 1966;34(3):412-22.
38. Saito T, Waki K, Becker AE. Left atrial myocardial extension onto pulmonary veins in humans: anatomic observations relevant for atrial arrhythmias. J Cardiovasc Electrophysiol. 2000;11(8):888-94.
39. DeSimone CV, Noheria A, Lachman N, Edwards WD, Gami AS, Maleszewski JJ, et al. Myocardium of the superior vena cava, coronary sinus, vein of Marshall, and the pulmonary vein ostia: gross anatomic studies in 620 hearts. J Cardiovasc Electrophysiol. 2012;23(12):1304-9.
40. Ho SY, Cabrera JA, Tran VH, Farre J, Anderson RH, Sanchez-Quintana D. Architecture of the pulmonary veins: relevance to radiofrequency ablation. Heart. 2001;86(3):265-70.

41. Kholova I, Kautzner J. Anatomic characteristics of extensions of atrial myocardium into the pulmonary veins in subjects with and without atrial fibrillation. Pacing Clin Electrophysiol. 2003;26(6):1348-55.
42. Hassink RJ, Aretz HT, Ruskin J, Keane D. Morphology of atrial myocardium in human pulmonary veins: a postmortem analysis in patients with and without atrial fibrillation. J Am Coll Cardiol. 2003;42(6):1108-14.
43. Steiner I, Hajkova P, Kvasnicka J, Kholova I. Myocardial sleeves of pulmonary veins and atrial fibrillation: a postmortem histopathological study of 100 subjects. Virchows Arch. 2006;449(1):88-95.
44. Tagawa M, Higuchi K, Chinushi M, Washizuka T, Ushiki T, Ishihara N, et al. Myocardium extending from the left atrium onto the pulmonary veins: a comparison between subjects with and without atrial fibrillation. Pacing Clin Electrophysiol. 2001;24(10):1459-63.
45. Masani F. Node-like cells in the myocardial layer of the pulmonary vein of rats: an ultrastructural study. J Anat. 1986;145:133-42.
46. Perez-Lugones A, McMahon JT, Ratliff NB, Saliba WI, Schweikert RA, Marrouche NF, et al. Evidence of specialized conduction cells in human pulmonary veins of patients with atrial fibrillation. J Cardiovasc Electrophysiol. 2003;14(8):803-9.
47. Tsai CF, Tai CT, Hsieh MH, Lin WS, Yu WC, Ueng KC, et al. Initiation of atrial fibrillation by ectopic beats originating from the superior vena cava: electrophysiological characteristics and results of radiofrequency ablation. Circulation. 2000;102(1):67-74.
48. Santangeli P, Zado ES, Hutchinson MD, Riley MP, Lin D, Frankel DS, et al. Prevalence and distribution of focal triggers in persistent and long-standing persistent atrial fibrillation. Heart Rhythm. 2016;13(2):374-82.
49. Lin WS, Tai CT, Hsieh MH, Tsai CF, Lin YK, Tsao HM, et al. Catheter ablation of paroxysmal atrial fibrillation initiated by non-pulmonary vein ectopy. Circulation. 2003;107(25):3176-83.
50. Lee SH, Tai CT, Hsieh MH, Tsao HM, Lin YJ, Chang SL, et al. Predictors of non-pulmonary vein ectopic beats initiating paroxysmal atrial fibrillation: implication for catheter ablation. J Am Coll Cardiol. 2005;46(6):1054-9.

51. Yamaguchi T, Tsuchiya T, Miyamoto K, Nagamoto Y, Takahashi N. Characterization of non-pulmonary vein foci with an EnSite array in patients with paroxysmal atrial fibrillation. Europace. 2010;12(12):1698-706.
52. Chang HY, Lo LW, Lin YJ, Chang SL, Hu YF, Li CH, et al. Long-term outcome of catheter ablation in patients with atrial fibrillation originating from nonpulmonary vein ectopy. J Cardiovasc Electrophysiol. 2013;24(3):250-8.
53. Mizobuchi M, Enjoji Y, Shibata K, Funatsu A, Yokouchi I, Kambayashi D, et al. Case report: Focal ablation for atrial fibrillation originating from the inferior vena cava and the posterior left atrium. J Interv Card Electrophysiol. 2006;16(2):131-4.
54. Katsivas AG, Manolis AG, Vassilopoulos C, Ioannidis P, Giotopoulou A, Kyriakides Z. Electroanatomical mapping of a right atrial tachycardia originating within the inferior vena cava. Hellenic J Cardiol. 2004;45:187-90.
55. Tao Y, Yang D, Chen L. Paroxysmal Atrial Fibrillation Originating From the Inferior Vena Cava: A Case Report and Literature Review. Front Cardiovasc Med. 2022;9:935524.
56. Alonso-Martin C, Garcia Mancebo S, Campos Garcia B, Guerra Ramos J, Moreno Weidman Z, Mendez Zurita F, et al. Atrial Fibrillation Originating in the Inferior Vena Cava: A Typical Presentation of an Atypical Location. JACC Case Rep. 2021;3(18):1918-23.
57. Mansour M, Ruskin J, Keane D. Initiation of atrial fibrillation by ectopic beats originating from the ostium of the inferior vena cava. J Cardiovasc Electrophysiol. 2002;13(12):1292-5.
58. Scavee C, Jais P, Weerasooriya R, Haissaguerre M. The inferior vena cava: an exceptional source of atrial fibrillation. J Cardiovasc Electrophysiol. 2003;14(6):659-62.
59. Yamane T, Miyazaki H, Inada K, Matsuo S, Miyanaga S, Date T, et al. Focal source of atrial fibrillation arising from the ostium of the inferior vena cava. Circ J. 2005;69(6):756-9.
60. Lüdinghausen M, Ohmachi N, Boot C. Myocardial coverage of the coronary sinus and related veins. Clin Anat. 1992;5(1):1-15.

61. Chauvin M, Shah DC, Haissaguerre M, Marcellin L, Brechenmacher C. The anatomic basis of connections between the coronary sinus musculature and the left atrium in humans. Circulation. 2000;101(6):647-52.
62. Hashizume H, Ushiki T, Abe K. A histological study of the cardiac muscle of the human superior and inferior venae cavae. Arch Histol Cytol. 1995;58(4):457-64.
63. Kholova I, Kautzner J. Morphology of atrial myocardial extensions into human caval veins: a postmortem study in patients with and without atrial fibrillation. Circulation. 2004;110(5):483-8.
64. Coakley JB, King TS. Cardiac muscle relations of the coronary sinus, the oblique vein of the left atrium and the left precaval vein in mammals. J Anat. 1959;93(1):30-5.
65. Rubenstein DS, Fox LM, McNulty JA, Lipsius SL. Electrophysiology and ultrastructure of eustachian ridge from cat right atrium: a comparison with SA node. J Mol Cell Cardiol. 1987;19(10):965-76.
66. Sherf L, James TN. Fine structure of cells and their histologic organization within internodal pathways of the heart: clinical and electrocardiographic implications. Am J Cardiol. 1979;44(2):345-69.
67. Rubart M, Zipes DP. Genesis of cardiac arrhythmias: electrophysiological considerations. In: Zipes DP, Libby P, Bonow RO, Braunwald E, editors. Braunwald's heart disease A textbook of cardiovascular medicine. Philadelphia, PA: Elsevier Saunders; 2005. p. 653-87.
68. Dobrev D, Heijman J, Hiram R, Li N, Nattel S. Inflammatory signalling in atrial cardiomyocytes: a novel unifying principle in atrial fibrillation pathophysiology. Nat Rev Cardiol. 2023;20(3):145-67.
69. Frustaci A, Chimenti C, Bellocci F, Morgante E, Russo MA, Maseri A. Histological substrate of atrial biopsies in patients with lone atrial fibrillation. Circulation. 1997;96(4):1180-4.
70. Haemers P, Hamdi H, Guedj K, Suffee N, Farahmand P, Popovic N, et al. Atrial fibrillation is associated with the fibrotic remodelling of adipose tissue in the subepicardium of human and sheep atria. Eur Heart J. 2017;38(1):53-61.

71. Yao C, Veleva T, Scott L, Jr., Cao S, Li L, Chen G, et al. Enhanced Cardiomyocyte NLRP3 Inflammasome Signaling Promotes Atrial Fibrillation. Circulation. 2018;138(20):2227-42.
72. Hulsmans M, Schloss MJ, Lee IH, Bapat A, Iwamoto Y, Vinegoni C, et al. Recruited macrophages elicit atrial fibrillation. Science. 2023;381(6654):231-9.
73. Heijman J, Muna AP, Veleva T, Molina CE, Sutanto H, Tekook M, et al. Atrial Myocyte NLRP3/CaMKII Nexus Forms a Substrate for Postoperative Atrial Fibrillation. Circ Res. 2020;127(8):1036-55.
74. Cheng T, Wang XF, Hou YT, Zhang L. Correlation between atrial fibrillation, serum amyloid protein A and other inflammatory cytokines. Mol Med Rep. 2012;6(3):581-4.
75. Li J, Solus J, Chen Q, Rho YH, Milne G, Stein CM, et al. Role of inflammation and oxidative stress in atrial fibrillation. Heart Rhythm. 2010;7(4):438-44.
76. Luan Y, Guo Y, Li S, Yu B, Zhu S, Li S, et al. Interleukin-18 among atrial fibrillation patients in the absence of structural heart disease. Europace. 2010;12(12):1713-8.
77. Gungor B, Ekmekci A, Arman A, Ozcan KS, Ucer E, Alper AT, et al. Assessment of interleukin-1 gene cluster polymorphisms in lone atrial fibrillation: new insight into the role of inflammation in atrial fibrillation. Pacing Clin Electrophysiol. 2013;36(10):1220-7.
78. Haneklaus M, O'Neill LA, Coll RC. Modulatory mechanisms controlling the NLRP3 inflammasome in inflammation: recent developments. Curr Opin Immunol. 2013;25(1):40-5.
79. Lamkanfi M, Dixit VM. Inflammasomes and their roles in health and disease. Annu Rev Cell Dev Biol. 2012;28:137-61.
80. Martinon F, Mayor A, Tschopp J. The inflammasomes: guardians of the body. Annu Rev Immunol. 2009;27:229-65.
81. Guo H, Callaway JB, Ting JP. Inflammasomes: mechanism of action, role in disease, and therapeutics. Nat Med. 2015;21(7):677-87.
82. Martinon F, Burns K, Tschopp J. The inflammasome: a molecular platform triggering activation of inflammatory caspases and processing of proIL-beta. Mol Cell. 2002;10(2):417-26.

83. Lu A, Magupalli VG, Ruan J, Yin Q, Atianand MK, Vos MR, et al. Unified polymerization mechanism for the assembly of ASC-dependent inflammasomes. Cell. 2014;156(6):1193-206.
84. An N, Gao Y, Si Z, Zhang H, Wang L, Tian C, et al. Regulatory Mechanisms of the NLRP3 Inflammasome, a Novel Immune-Inflammatory Marker in Cardiovascular Diseases. Front Immunol. 2019;10:1592.
85. Ajoolabady A, Nattel S, Lip GYH, Ren J. Inflammasome Signaling in Atrial Fibrillation: JACC State-of-the-Art Review. J Am Coll Cardiol. 2022;79(23):2349-66.
86. Zong J, Li FF, Liang K, Dai R, Zhang H, Yan L, et al. Nuclear Localization Leucine-Rich-Repeat Protein 1 Deficiency Protects Against Cardiac Hypertrophy by Pressure Overload. Cell Physiol Biochem. 2018;48(1):75-86.
87. Denes A, Coutts G, Lenart N, Cruickshank SM, Pelegrin P, Skinner J, et al. AIM2 and NLRC4 inflammasomes contribute with ASC to acute brain injury independently of NLRP3. Proc Natl Acad Sci U S A. 2015;112(13):4050-5.
88. Onodi Z, Ruppert M, Kucsera D, Sayour AA, Toth VE, Koncsos G, et al. AIM2-driven inflammasome activation in heart failure. Cardiovasc Res. 2021;117(13):2639-51.
89. Durga Devi T, Babu M, Makinen P, Kaikkonen MU, Heinaniemi M, Laakso H, et al. Aggravated Postinfarct Heart Failure in Type 2 Diabetes Is Associated with Impaired Mitophagy and Exaggerated Inflammasome Activation. Am J Pathol. 2017;187(12):2659-73.
90. Wang X, Pan J, Liu H, Zhang M, Liu D, Lu L, et al. AIM2 gene silencing attenuates diabetic cardiomyopathy in type 2 diabetic rat model. Life Sci. 2019;221:249-58.
91. Paulin N, Viola JR, Maas SL, de Jong R, Fernandes-Alnemri T, Weber C, et al. Double-Strand DNA Sensing Aim2 Inflammasome Regulates Atherosclerotic Plaque Vulnerability. Circulation. 2018;138(3):321-3.
92. Fidler TP, Xue C, Yalcinkaya M, Hardaway B, Abramowicz S, Xiao T, et al. The AIM2 inflammasome exacerbates atherosclerosis in clonal haematopoiesis. Nature. 2021;592(7853):296-301.

93. Lusebrink E, Goody PR, Lahrmann C, Flender A, Niepmann ST, Zietzer A, et al. AIM2 Stimulation Impairs Reendothelialization and Promotes the Development of Atherosclerosis in Mice. Front Cardiovasc Med. 2020;7:582482.
94. Servier Medical Art [Internet]. 2024 [cited 2024 September 17]. Available from: https://smart.servier.com/.
95. Platonov PG. Atrial fibrosis: an obligatory component of arrhythmia mechanisms in atrial fibrillation? J Geriatr Cardiol. 2017;14(4):233-7.
96. Herczeg S, Galvin J, Keaney JJ, Keelan E, Byrne R, Howard C, et al. The Value of Voltage Histogram Analysis Derived Right Atrial Scar Burden in the Prediction of Left Atrial Scar Burden. Cardiol Res Pract. 2020;2020:3981684.
97. Nguyen BL, Fishbein MC, Chen LS, Chen PS, Masroor S. Histopathological substrate for chronic atrial fibrillation in humans. Heart Rhythm. 2009;6(4):454-60.
98. Vergaro G, Aimo A, Rapezzi C, Castiglione V, Fabiani I, Pucci A, et al. Atrial amyloidosis: mechanisms and clinical manifestations. Eur J Heart Fail. 2022;24(11):2019-28.
99. Ariyarajah V, Steiner I, Hajkova P, Khadem A, Kvasnicka J, Apiyasawat S, et al. The association of atrial tachyarrhythmias with isolated atrial amyloid disease: preliminary observations in autopsied heart specimens. Cardiology. 2009;113(2):132-7.
100. Sanchis K, Cariou E, Colombat M, Ribes D, Huart A, Cintas P, et al. Atrial fibrillation and subtype of atrial fibrillation in cardiac amyloidosis: clinical and echocardiographic features, impact on mortality. Amyloid. 2019;26(3):128-38.
101. Rocken C, Peters B, Juenemann G, Saeger W, Klein HU, Huth C, et al. Atrial amyloidosis: an arrhythmogenic substrate for persistent atrial fibrillation. Circulation. 2002;106(16):2091-7.
102. Leone O, Boriani G, Chiappini B, Pacini D, Cenacchi G, Martin Suarez S, et al. Amyloid deposition as a cause of atrial remodelling in persistent valvular atrial fibrillation. Eur Heart J. 2004;25(14):1237-41.
103. Chen PS, Chen LS, Fishbein MC, Lin SF, Nattel S. Role of the autonomic nervous system in atrial fibrillation: pathophysiology and therapy. Circ Res. 2014;114(9):1500-15.

104. Nielsen JR, Wachtell K, Abdulla J. The Relationship Between Physical Activity and Risk of Atrial Fibrillation-A Systematic Review and Meta-Analysis. J Atr Fibrillation. 2013;5(5):789.
105. Fox CS, Parise H, D'Agostino RB, Sr., Lloyd-Jones DM, Vasan RS, Wang TJ, et al. Parental atrial fibrillation as a risk factor for atrial fibrillation in offspring. JAMA. 2004;291(23):2851-5.
106. Lubitz SA, Ozcan C, Magnani JW, Kaab S, Benjamin EJ, Ellinor PT. Genetics of atrial fibrillation: implications for future research directions and personalized medicine. Circ Arrhythm Electrophysiol. 2010;3(3):291-9.
107. Tucker NR, Ellinor PT. Emerging directions in the genetics of atrial fibrillation. Circ Res. 2014;114(9):1469-82.
108. Gudbjartsson DF, Holm H, Sulem P, Masson G, Oddsson A, Magnusson OT, et al. A frameshift deletion in the sarcomere gene MYL4 causes early-onset familial atrial fibrillation. Eur Heart J. 2017;38(1):27-34.
109. Su W, van Wijk SW, Brundel B. Desmin variants: Trigger for cardiac arrhythmias? Front Cell Dev Biol. 2022;10:986718.
110. Ho SY, Sanchez-Quintana D. Anatomy and pathology of the sinus node. J Interv Card Electrophysiol. 2016;46(1):3-8.
111. Kawashima T, Sato F. First in situ 3D visualization of the human cardiac conduction system and its transformation associated with heart contour and inclination. Sci Rep. 2021;11(1):8636.
112. Anderson RH, Mori S, Spicer DE, Sanchez-Quintana D, Jensen B. The Anatomy, Development, and Evolution of the Atrioventricular Conduction Axis. J Cardiovasc Dev Dis. 2018;5(3).
113. Inoue S, Becker AE. Posterior Extensions of the Human Compact Atrioventricular Node. A Neglected Anatomic Feature of Potential Clinical Significance. Circulation. 1998;97(2):188-93.
114. Yoshimura A, Yamaguchi T, Kawazato H, Takahashi N, Shimada T. Immuno-histochemistry and three-dimensional architecture of the intermediate filaments in Purkinje cells in mammalian hearts. Med Mol Morphol. 2014;47(4):233-9.

115. Chandler NJ, Greener ID, Tellez JO, Inada S, Musa H, Molenaar P, et al. Molecular architecture of the human sinus node: insights into the function of the cardiac pacemaker. Circulation. 2009;119(12):1562-75.
116. Gaborit N, Le Bouter S, Szuts V, Varro A, Escande D, Nattel S, et al. Regional and tissue specific transcript signatures of ion channel genes in the non-diseased human heart. J Physiol. 2007;582(Pt 2):675-93.
117. Greener ID, Monfredi O, Inada S, Chandler NJ, Tellez JO, Atkinson A, et al. Molecular architecture of the human specialised atrioventricular conduction axis. J Mol Cell Cardiol. 2011;50(4):642-51.
118. Li N, Csepe TA, Hansen BJ, Dobrzynski H, Higgins RS, Kilic A, et al. Molecular Mapping of Sinoatrial Node HCN Channel Expression in the Human Heart. Circ Arrhythm Electrophysiol. 2015;8(5):1219-27.
119. Xu Y, Peng Y, Qu R, Zheng G, Feng F, Feng Y, et al. Locating the Human Cardiac Conduction System Using a 3D Model of Its Nutritious Arteries. Sci Rep. 2017;7(1):344.
120. Coppen SR, Kaba RA, Halliday D, Dupont E, Skepper JN, Elneil S, et al. Comparison of connexin expression patterns in the developing mouse heart and human foetal heart. Mol Cell Biochem. 2003;242(1-2):121-7.
121. Kreuzberg MM, Liebermann M, Segschneider S, Dobrowolski R, Dobrzynski H, Kaba R, et al. Human connexin31.9, unlike its orthologous protein connexin30.2 in the mouse, is not detectable in the human cardiac conduction system. J Mol Cell Cardiol. 2009;46(4):553-9.
122. Mangoni ME, Couette B, Bourinet E, Platzer J, Reimer D, Striessnig J, et al. Functional role of L-type Cav1.3 Ca2+ channels in cardiac pacemaker activity. Proc Natl Acad Sci U S A. 2003;100(9):5543-8.
123. Liu HX, Jing YX, Wang JJ, Yang YP, Wang YX, Li HR, et al. Expression patterns of intermediate filament proteins desmin and lamin A in the developing conduction system of early human embryonic hearts. J Anat. 2020;236(3):540-8.
124. Mavroidis M, Athanasiadis NC, Rigas P, Kostavasili I, Kloukina I, Te Rijdt WP, et al. Desmin is essential for the structure and function of the sinoatrial node: implications for increased arrhythmogenesis. Am J Physiol Heart Circ Physiol. 2020;319(3):H557-H70.

125. Yamamoto M, Abe S, Rodriguez-Vazquez JF, Fujimiya M, Murakami G, Ide Y. Immunohistochemical distribution of desmin in the human fetal heart. J Anat. 2011;219(2):253-8.
126. Kim EE, Shekhar A, Lu J, Lin X, Liu FY, Zhang J, et al. PCP4 regulates Purkinje cell excitability and cardiac rhythmicity. J Clin Invest. 2014;124(11):5027-36.
127. Shekhar A, Lin X, Liu FY, Zhang J, Mo H, Bastarache L, et al. Transcription factor ETV1 is essential for rapid conduction in the heart. J Clin Invest. 2016;126(12):4444-59.
128. Blom NA, Gittenberger-de Groot AC, DeRuiter MC, Poelmann RE, Mentink MM, Ottenkamp J. Development of the cardiac conduction tissue in human embryos using HNK-1 antigen expression: possible relevance for understanding of abnormal atrial automaticity. Circulation. 1999;99(6):800-6.
129. Blom NA, Ottenkamp J, Deruiter MC, Wenink AC, Gittenberger-de Groot AC. Development of the cardiac conduction system in atrioventricular septal defect in human trisomy 21. Pediatr Res. 2005;58(3):516-20.
130. Ikeda T, Iwasaki K, Shimokawa I, Sakai H, Ito H, Matsuo T. Leu-7 immunoreactivity in human and rat embryonic hearts, with special reference to the development of the conduction tissue. Anat Embryol (Berl). 1990;182(6):553-62.
131. van Eif VWW, Stefanovic S, van Duijvenboden K, Bakker M, Wakker V, de Gier-de Vries C, et al. Transcriptome analysis of mouse and human sinoatrial node cells reveals a conserved genetic program. Development. 2019;146(8).
132. Hoogaars WM, Tessari A, Moorman AF, de Boer PA, Hagoort J, Soufan AT, et al. The transcriptional repressor Tbx3 delineates the developing central conduction system of the heart. Cardiovasc Res. 2004;62(3):489-99.
133. Severs NJ, Rothery S, Dupont E, Coppen SR, Yeh HI, Ko YS, et al. Immunocytochemical analysis of connexin expression in the healthy and diseased cardiovascular system. Microsc Res Tech. 2001;52(3):301-22.
134. Vozzi C, Dupont E, Coppen SR, Yeh HI, Severs NJ. Chamber-related differences in connexin expression in the human heart. J Mol Cell Cardiol. 1999;31(5):991-1003.
135. Coppen SR, Dupont E, Rothery S, Severs NJ. Connexin45 expression is preferentially associated with the ventricular conduction system in mouse and rat heart. Circ Res. 1998;82(2):232-43.

136. Yamamoto M, Dobrzynski H, Tellez J, Niwa R, Billeter R, Honjo H, et al. Extended atrial conduction system characterised by the expression of the HCN4 channel and connexin45. Cardiovasc Res. 2006;72(2):271-81.
137. Ko YS, Yeh HI, Ko YL, Hsu YC, Chen CF, Wu S, et al. Three-dimensional reconstruction of the rabbit atrioventricular conduction axis by combining histological, desmin, and connexin mapping data. Circulation. 2004;109(9):1172-9.
138. Yeh HI, Lai YJ, Lee SH, Lee YN, Ko YS, Chen SA, et al. Heterogeneity of myocardial sleeve morphology and gap junctions in canine superior vena cava. Circulation. 2001;104(25):3152-7.
139. Yeh HI, Lai YJ, Lee YN, Chen YJ, Chen YC, Chen CC, et al. Differential expression of connexin43 gap junctions in cardiomyocytes isolated from canine thoracic veins. J Histochem Cytochem. 2003;51(2):259-66.
140. Capetanaki Y, Bloch RJ, Kouloumenta A, Mavroidis M, Psarras S. Muscle intermediate filaments and their links to membranes and membranous organelles. Exp Cell Res. 2007;313(10):2063-76.
141. Eriksson A, Thornell LE. Intermediate (skeletin) filaments in heart Purkinje fibers. A correlative morphological and biochemical identification with evidence of a cytoskeletal function. J Cell Biol. 1979;80(2):231-47.
142. Eriksson A, Thornell LE, Stigbrand T. Cytoskeletal filaments of heart conducting system localized by antibody against a 55,000 dalton protein. Experientia. 1978;34(6):792-4.
143. Thornell LE, Eriksson A. Filament systems in the Purkinje fibers of the heart. Am J Physiol. 1981;241(3):H291-305.
144. Franco D, Icardo JM. Molecular characterization of the ventricular conduction system in the developing mouse heart: topographical correlation in normal and congenitally malformed hearts. Cardiovasc Res. 2001;49(2):417-29.
145. Ya J, Markman MW, Wagenaar GT, Blommaart PJ, Moorman AF, Lamers WH. Expression of the smooth-muscle proteins alpha-smooth-muscle actin and calponin, and of the intermediate filament protein desmin are parameters of cardiomyocyte maturation in the prenatal rat heart. Anat Rec. 1997;249(4):495-505.

146. Vitadello M, Matteoli M, Gorza L. Neurofilament proteins are co-expressed with desmin in heart conduction system myocytes. J Cell Sci. 1990;97 (Pt 1):11-21.
147. Grigore A, Arsene D, Filipoiu F, Cionca F, Enache S, Ceausu M, et al. Cellular immunophenotypes in human embryonic, fetal and adult heart. Rom J Morphol Embryol. 2012;53(2):299-311.
148. Yamaguchi T, Yi SQ, Tanaka S, Ono K, Shimada T. Ultrastructure and cytoarchitecture of Bachmann's bundle in the mammalian heart. Journal of Arrhythmia. 2009;25(1):24-31.
149. Kholova I, Niessen HW, Kautzner J. Expression of Leu-7 in myocardial sleeves around human pulmonary veins. Cardiovasc Pathol. 2003;12(5):263-6.
150. Kugler S, Tokes AM, Nagy N, Fintha A, Danics K, Saghi M, et al. Strong desmin immunoreactivity in the myocardial sleeves around pulmonary veins, superior caval vein and coronary sinus supports the presumed arrhythmogenicity of these regions. J Anat. 2024;244(1):120-32.
151. Totty BA. Mucins. In: Bancroft JD, Gamble M, editors. Theory and Practice of Histological Techniques. London, UK: Churchill Livingstone; 2007. p. 163–200.
152. Kugler S, Nagy N, Racz G, Tokes AM, Dorogi B, Nemeskeri A. Presence of cardiomyocytes exhibiting Purkinje-type morphology and prominent connexin45 immunoreactivity in the myocardial sleeves of cardiac veins. Heart Rhythm. 2018;15(2):258-64.
153. R Core Team. R: A language and environment for statistical computing [Internet]. Vienna, Austria: R Foundation for Statistical Computing; 2024 [updated 2024 June 14; cited 2024 July 28]. Available from: https://www.R-project.org/.
154. Bates D, Maechler M, Bolker B, Walker S. lme4: Linear mixed-effects models using eigen and S4 [Internet]. 2024 [updated 2017 Nov 13; cited 2024 July 28]. Available from: https://github.com/lme4/lme4/.
155. Lenth RV. Emmeans: Estimated marginal means, aka least-squares means [Internet]. 2024 [updated 2024 July 22; cited 2024 July 28]. Available from: https://rvlenth.github.io/emmeans/.
156. Kugler S, Onodi Z, Ruppert M, Sayour AA, Olah A, Benke K, et al. Inflammasome activation in end-stage heart failure-associated atrial fibrillation. ESC Heart Fail. 2022;9(4):2747-52.

157. Baranyai T, Herczeg K, Onodi Z, Voszka I, Modos K, Marton N, et al. Isolation of Exosomes from Blood Plasma: Qualitative and Quantitative Comparison of Ultracentrifugation and Size Exclusion Chromatography Methods. PLoS One. 2015;10(12):e0145686.
158. Varga ZV, Erdelyi K, Paloczi J, Cinar R, Zsengeller ZK, Jourdan T, et al. Disruption of Renal Arginine Metabolism Promotes Kidney Injury in Hepatorenal Syndrome in Mice. Hepatology. 2018;68(4):1519-33.
159. Ito D, Imai Y, Ohsawa K, Nakajima K, Fukuuchi Y, Kohsaka S. Microglia-specific localisation of a novel calcium binding protein, Iba1. Brain Res Mol Brain Res. 1998;57(1):1-9.
160. Ohsawa K, Imai Y, Kanazawa H, Sasaki Y, Kohsaka S. Involvement of Iba1 in membrane ruffling and phagocytosis of macrophages/microglia. J Cell Sci. 2000;113 (Pt 17):3073-84.
161. Barceló A, De La Fuente LM, Stertzer SH. Anatomic and histologic review of the coronary sinus. International Journal of Morphology. 2004;22(4):331-8.
162. Morgan DR, Hanratty CG, Dixon LJ, Trimble M, O'Keeffe DB. Anomalies of cardiac venous drainage associated with abnormalities of cardiac conduction system. Europace. 2002;4(3):281-7.
163. Momma K, Linde LM. Abnormal rhythms associated with persistent left superior vena cava. Pediatr Res. 1969;3(3):210-6.
164. Dickinson DF, Wilkinson JL, Anderson KR, Smith A, Ho SY, Anderson RH. The cardiac conduction system in situs ambiguus. Circulation. 1979;59(5):879-85.
165. Smith A, Ho SY, Anderson RH, Connell MG, Arnold R, Wilkinson JL, et al. The diverse cardiac morphology seen in hearts with isomerism of the atrial appendages with reference to the disposition of the specialised conduction system. Cardiol Young. 2006;16(5):437-54.
166. Ho SY, Seo JW, Brown NA, Cook AC, Fagg NL, Anderson RH. Morphology of the sinus node in human and mouse hearts with isomerism of the atrial appendages. Br Heart J. 1995;74(4):437-42.
167. Ammirabile G, Tessari A, Pignataro V, Szumska D, Sutera Sardo F, Benes J, Jr., et al. Pitx2 confers left morphological, molecular, and functional identity to the sinus venosus myocardium. Cardiovasc Res. 2012;93(2):291-301.

168. Kim SJ. Heterotaxy syndrome. Korean Circ J. 2011;41(5):227-32.
169. Mommersteeg MT, Hoogaars WM, Prall OW, de Gier-de Vries C, Wiese C, Clout DE, et al. Molecular pathway for the localized formation of the sinoatrial node. Circ Res. 2007;100(3):354-62.
170. Tremblay C, Loomba RS, Frommelt PC, Perrin D, Spicer DE, Backer C, et al. Segregating bodily isomerism or heterotaxy: potential echocardiographic correlations of morphological findings. Cardiol Young. 2017;27(8):1470-80.
171. Iwa T, Ichihashi T, Hashizume Y, Ishida K, Okada R. Successful surgical treatment of left atrial tachycardia. Am Heart J. 1985;109(1):160-2.
172. Azizova A, Onder O, Arslan S, Ardali S, Hazirolan T. Persistent left superior vena cava: clinical importance and differential diagnoses. Insights Imaging. 2020;11(1):110.
173. Miraldi F, di Gioia CR, Proietti P, De Santis M, d'Amati G, Gallo P. Cardinal vein isomerism: an embryological hypothesis to explain a persistent left superior vena cava draining into the roof of the left atrium in the absence of coronary sinus and atrial septal defect. Cardiovasc Pathol. 2002;11(3):149-52.
174. Hsu LF, Jais P, Keane D, Wharton JM, Deisenhofer I, Hocini M, et al. Atrial fibrillation originating from persistent left superior vena cava. Circulation. 2004;109(7):828-32.
175. Fujino T, Yuzawa H, Kinoshita T, Shinohara M, Okishige K, Ikeda T. A case of successful cryoballoon ablation of paroxysmal atrial fibrillation originating from a persistent left superior vena cava. J Cardiol Cases. 2019;20(3):77-80.
176. Elayi CS, Fahmy TS, Wazni OM, Patel D, Saliba W, Natale A. Left superior vena cava isolation in patients undergoing pulmonary vein antrum isolation: impact on atrial fibrillation recurrence. Heart Rhythm. 2006;3(9):1019-23.
177. Ozcan EE, Szeplaki G, Merkely B, Geller L. Isolation of persistent left superior vena cava during atrial fibrillation ablation. Indian Pacing Electrophysiol J. 2015;15(2):130-2.
178. Lenox CC, Hashida Y, Anderson RH, Hubbard JD. Conduction tissue anomalies in absence of the right superior caval vein. Int J Cardiol. 1985;8(3):251-60.

179. Satoh F, Seto Y, Tsuboi A, Osawa M. Regressive Changes of the Myocardial Sleeves in Elderly Victims of Sudden Bathtub Death. Forensic Medicine and Anatomy Research. 2015;3(2):57-65.
180. Fujiyoshi K, Maeda I, Tojo T. Echocardiographic findings focused on the inferior vena cava partly aid the diagnosis of cardiac amyloidosis. Eur Heart J. 2023;44(25):2349.
181. Eliot RS, McGee HJ, Blount SG. Cardiac Amyloidosis. Circulation. 1961;23:613-22.
182. Weiss C, Gocht A, Willems S, Hoffmann M, Risius T, Meinertz T. Impact of the distribution and structure of myocardium in the pulmonary veins for radiofrequency ablation of atrial fibrillation. Pacing Clin Electrophysiol. 2002;25(9):1352-6.
183. Capetanaki Y. Desmin cytoskeleton: a potential regulator of muscle mitochondrial behavior and function. Trends Cardiovasc Med. 2002;12(8):339-48.
184. Soric Hosman I, Kos I, Lamot L. Serum Amyloid A in Inflammatory Rheumatic Diseases: A Compendious Review of a Renowned Biomarker. Front Immunol. 2020;11:631299.
185. Christoffels VM, Moorman AF. Development of the cardiac conduction system: why are some regions of the heart more arrhythmogenic than others? Circ Arrhythm Electrophysiol. 2009;2(2):195-207.
186. Christoffels VM, Smits GJ, Kispert A, Moorman AF. Development of the pacemaker tissues of the heart. Circ Res. 2010;106(2):240-54.
187. van Weerd JH, Christoffels VM. The formation and function of the cardiac conduction system. Development. 2016;143(2):197-210.
188. Mezzaroma E, Abbate A, Toldo S. The inflammasome in heart failure. Curr Opin Physiol. 2021;19:105-12.
189. Bracey NA, Beck PL, Muruve DA, Hirota SA, Guo J, Jabagi H, et al. The Nlrp3 inflammasome promotes myocardial dysfunction in structural cardiomyopathy through interleukin-1beta. Exp Physiol. 2013;98(2):462-72.
190. Butts B, Gary RA, Dunbar SB, Butler J. The Importance of NLRP3 Inflammasome in Heart Failure. J Card Fail. 2015;21(7):586-93.

191. Chen G, Chelu MG, Dobrev D, Li N. Cardiomyocyte Inflammasome Signaling in Cardiomyopathies and Atrial Fibrillation: Mechanisms and Potential Therapeutic Implications. Front Physiol. 2018;9:1115.
192. Abbate A, Toldo S, Marchetti C, Kron J, Van Tassell BW, Dinarello CA. Interleukin-1 and the Inflammasome as Therapeutic Targets in Cardiovascular Disease. Circ Res. 2020;126(9):1260-80.
193. Pascual-Figal DA, Bayes-Genis A, Asensio-Lopez MC, Hernandez-Vicente A, Garrido-Bravo I, Pastor-Perez F, et al. The Interleukin-1 Axis and Risk of Death in Patients With Acutely Decompensated Heart Failure. J Am Coll Cardiol. 2019;73(9):1016-25.
194. Targonski R, Salczynska D, Sadowski J, Cichowski L. Relationship between inflammatory markers and clinical patterns of atrial fibrillation in patients with congestive heart failure. Kardiol Pol. 2008;66(7):729-36; discussion 37-9.
195. Nessler B, Nessler J, Kitliñski M, Gackowski A, Piwowarska W. Inflammatory markers (TNF-alpha, IL-6, CRP), BNP and spiroergometric stress test parameters in patients with heart failure and atrial fibrillation. 4th Asian Pacific Congress of Heart Failure; Melbourne, Australia: Heart, Lung and Circulation; 2008. p. S34.
196. Putko BN, Wang Z, Lo J, Anderson T, Becher H, Dyck JR, et al. Circulating levels of tumor necrosis factor-alpha receptor 2 are increased in heart failure with preserved ejection fraction relative to heart failure with reduced ejection fraction: evidence for a divergence in pathophysiology. PLoS One. 2014;9(6):e99495.
197. Benz AP, Aeschbacher S, Krisai P, Moschovitis G, Blum S, Meyre P, et al. Biomarkers of Inflammation and Risk of Hospitalization for Heart Failure in Patients With Atrial Fibrillation. J Am Heart Assoc. 2021;10(8):e019168.
198. Varghese B, Feldman DI, Chew C, Valilis E, Blumenthal RS, Sharma G, et al. Inflammation, atrial fibrillation, and the potential role for colchicine therapy. Heart Rhythm O2. 2021;2(3):298-303.
199. Kommu S, Arepally S. The Effect of Colchicine on Atrial Fibrillation: A Systematic Review and Meta-Analysis. Cureus. 2023;15(2):e35120.
200. Krisai P, Blum S, Schnabel RB, Sticherling C, Kuhne M, von Felten S, et al. Canakinumab After Electrical Cardioversion in Patients With Persistent Atrial

Fibrillation: A Pilot Randomized Trial. Circ Arrhythm Electrophysiol. 2020;13(7):e008197.

201. Aldhoon B, Kucera T, Smorodinova N, Martinek J, Melenovsky V, Kautzner J. Associations between cardiac fibrosis and permanent atrial fibrillation in advanced heart failure. Physiol Res. 2013;62(3):247-55.
202. Lofsjogard J, Persson H, Diez J, Lopez B, Gonzalez A, Edner M, et al. Atrial fibrillation and biomarkers of myocardial fibrosis in heart failure. Scand Cardiovasc J. 2014;48(5):299-303.

9. BIBLIOGRAPHY OF THE CANDIDATE'S PUBLICATIONS

9.1. Publications directly related to the present thesis

9.1.1. Publications in international peer–reviewed journals

Kugler S, Nagy N, Rácz G, Tőkés AM, Dorogi B, Nemeskéri Á. (2018) Presence of cardiomyocytes exhibiting Purkinje-type morphology and prominent connexin45 immunoreactivity in the myocardial sleeves of cardiac veins. Heart Rhythm, 15(2): 258-264. doi: 10.1016/j.hrthm.2017.09.044. (SJR D1, IF=5.225)

Kugler S*, Onódi Z*, Ruppert M, Sayour AA, Oláh A, Benke K, Ferdinandy P, Merkely B, Radovits T, Varga ZV. (2022) Inflammasome activation in end-stage heart failure-associated atrial fibrillation. ESC Heart Fail, 9(4): 2747-2752. doi: 10.1002/ehf2.13972. *Contributed equally. (SJR Q1, IF=3.8)

Kugler S, Tőkés AM, Nagy N, Fintha A, Danics K, Sághi M, Törő K, Rácz G, Nemeskéri Á. (2024) Strong desmin immunoreactivity in the myocardial sleeves around pulmonary veins, superior caval vein and coronary sinus supports the presumed arrhythmogenicity of these regions. J Anat, 244(1): 120-132. doi: 10.1111/joa.13947. (SJR Q1, IF=1.8)

9.1.2. Publications in Hungarian peer–reviewed journals

Kugler S, Duray G, Préda I. (2018) Új felismerések a pitvarfibrilláció genezisében és fenntartásában: az egyénre szabott kezelés lehetőségei. Orv Hetil, 159(28): 1135-1145. doi: 10.1556/650.2018.31087. (SJR Q3, IF=0.564)

9.2. Publications not directly related to the present thesis

9.2.1. Publications in international peer–reviewed journals

Kugler S, Pólos M, Király Á, Pataki Á, Koppányi Á, Varga T, Szakál-Tóth Z, Parázs N, Teszák T, Tarjányi Z, Prinz G, Hartyánszky I, Szabolcs Z, Merkely B, Sax B. (2021) Pseudoaneurysm of the ascending aorta: case report of a donor-derived Pseudomonas infection in a heart transplant recipient. BMC Infect Dis, 21(1): 847. doi: 10.1186/s12879-021-06557-y. (SJR Q2, IF=3.669)

Szabo D, Szabo A, Magyar L, Banhegyi G, **Kugler S**, Pinter A, Juhasz V, Ruppert M, Olah A, Ruzsa Z, Edes IF, Szekely A, Becker D, Merkely B, Hizoh I. (2022) Admission lactate level and the GRACE 2.0 score are independent and additive predictors of 30-day mortality of STEMI patients treated with primary PCI-Results of a real-world registry. PLoS One, 17(11): e0277785. doi: 10.1371/journal.pone.0277785. (SJR Q1, IF=3.7)

Kugler S, Vári DK, Veres DS, Király Á, Teszák T, Parázs N, Tarjányi Z, Drobni Z, Szakál-Tóth Z, Prinz G, Miheller P, Merkely B, Sax B. (2023) Seroconversion after SARS-CoV-2 vaccination is protective against severe COVID-19 disease in heart transplant recipients. Immun Inflamm Dis, 11: e1086. doi: 10.1002/iid3.1086. (SJR Q2, IF=3.1)

Szécsi B, Sinkó R, Vereb A, Khochanskiy D, Benke K, Radovits T, Lakatos B, Kőszegi A, Losoncz E, **Kugler S**, Szabó M, Merkely B, Székely A*, Gereben B*. (2024) The perioperative period of heart transplantation is affected by thyroid hormone status. Thyroid, 34(6): 774-784. doi: 10.1089/thy.2023.0628. (SJR D1, IF=5.8)

*Contributed equally.

9.2.2. Publications in Hungarian peer–reviewed journals

Parázs N, Lakatos BK, Kovács A, Assabiny A, Király Á, Tarjányi Z, Szakál-Tóth Z, Teszák T, Tokodi M, Ujvári A, **Kugler S**, Szücs N, Merkely B*, Sax B*. (2021) Jobbszívfél-elégtelenség évekkel a szívtranszplantációt követően: Egy ritka etiológiai tényező esete. Cardiol Hung, 51: 69-72. doi: 10.26430/CHUNGARICA.2021.51.1.69. *Contributed equally.

DOI:10.14753/SE.2025.3172

10. ACKNOWLEDGEMENTS

I am grateful to several people for their support, without whom this thesis could not have been written.

I would like to thank my supervisors, Dr. Ágnes Nemeskéri and Prof. Dr. Tamás Radovits, for their continuous support and dedicated help in acquiring the skills and approach necessary for scientific work, in organizing the research steps efficiently and in preparing the manuscripts on which the thesis is based.

I would like to thank Dr. Ágnes Nemeskéri and Dr. Nándor Nagy for their special attention to my professional and personal development during my students' scientific research.

I express my gratitude to Prof. Dr. Béla Merkely, who provided an excellent background and time for my research and supported me in my scientific and clinical work.

I thank all my co-authors, especially Dr. Anna-Mária Tőkés, Dr. Attila Fintha, Dr. Zsófia Gulyás-Onódi, Dr. Zoltán Varga, Dr. Mihály Ruppert and Dr. Alex Ali Sayour, for their professional help, outstanding expertise and for teaching me many important scientific skills in the histological and molecular studies of the human heart.

I also thank the current and former laboratory assistants, namely Judit Fogarasi, Ferenc Kilin, Erzsébet Kovács, Edit Orbán, Lili Orbán, Mária Bakó, Andrea Kovács, Benjamin Prokaj, Dorottya Csernus-Horváth and Rebeka Bertalan for the outstanding technical assistance.

I thank to Dr. Dániel Sándor Veres, Dr. Zsófia Gulyás-Onódi and Dr. Ádám Pál-Jakab for their outstanding help with the statistical analyses. I thank to Dr. János Apostol for his professional assistance during the information technology difficulties.

I thank my colleagues and friends, especially Dr. Marianna Németh, Dr. Györgyi Apponyi, Dr. Zsuzsanna Ulakcsai, Dr. Fanni Hegedűs, Dr. Eszter Pálinkás, Dr. Márton Sághi, Dr. Lili Róbert and Márta Mészár-Kosztolányi for their continued support.

I would also like to thank my parents, my grandmother and my sister for giving me so much love, encouragement and support, not only in my current job, but also in the years before. I dedicate this thesis to my 19-month-old niece, Sztella.

DOI:10.14753/SE.2025.3172

Presence of cardiomyocytes exhibiting Purkinje-type morphology and prominent connexin45 immunoreactivity in the myocardial sleeves of cardiac veins

Szilvia Kugler, MD,*† Nándor Nagy, PhD,* Gergely Rácz, MD, PhD,‡ Anna-Mária Tőkés, PhD,§ Bence Dorogi, MD,* Ágnes Nemeskéri, MD, PhD*

*From the *Department of Anatomy, Histology and Embryology, Faculty of Medicine, Semmelweis University, Budapest, Hungary, †Heart and Vascular Center, Semmelweis University, Budapest, Hungary, ‡1st Department of Pathology and Experimental Cancer Research, Faculty of Medicine, Semmelweis University, Budapest, Hungary, and §2nd Department of Pathology, Faculty of Medicine, Semmelweis University, Budapest, Hungary.*

BACKGROUND Pulmonary vein (PV) myocardium is a known source of atrial fibrillation. A debated question is whether myocardial extensions into caval veins and coronary sinus (CS) have similar properties. No studies have documented specific pacemaker and/or conducting properties of human extracardiac myocardium.

OBJECTIVE The purpose of this study was to characterize the histology and immunohistochemical features of myocardial sleeves in the wall of cardiac veins.

METHODS Sections of 32 human hearts were investigated. Specimens of PVs, superior caval vein (SVC), CS, sinoatrial and atrioventricular nodes, and left ventricle were stained with Best's Carmine for selective staining of intracellular glycogen. Anti-connexin45 (Cx45)– and Cx43–specific antibodies were used to determine the conduction properties of extracardiac myocardium.

RESULTS Myocardial sleeve was found in the wall of PVs of 15 of 16 hearts, 21 of 22 SVCs, and 8 of 8 CSs. Bundles of glycogen-positive cardiomyocytes exhibiting pale cytoplasm and peripheral myofibrils were observed in the venous sleeves. Strong Cx45 and weak Cx43 labeling was detected in the extracardiac myocardium. Similar staining pattern was observed for the pacemaker and conduction system, whereas ventricular myocardium exhibited prominent Cx43 and no Cx45 immunoreactivity.

CONCLUSION Myocardial fibers of PVs, SVC, and CS exhibit morphology similar to that of Purkinje fibers and are enriched in glycogen. We provide data for the first time on prominent positive staining for Cx45 in the extracardiac myocardium, indicating its potential pacemaker and/or conducting nature.

KEYWORDS Cardiac muscle sleeve; Caval vein; Connexin45; Coronary sinus; Glycogen; Immunohistochemistry; Pulmonary vein; Purkinje-type morphology

(Heart Rhythm 2018;15:258–264)

Introduction

Myocardial sleeves of pulmonary veins (PV) play a critical role in the mechanism of atrial fibrillation (AF). Macroscopic features of these areas were described previously.[1–3] During the last decade, growing attention has prompted investigation into the microscopic properties of the extracardiac myocardial sleeves.[2,4–6] Perez-Lugones et al[7] documented the presence of cardiomyocytes exhibiting ultrastructural morphology of P-cells and Purkinje fibers (PFs) in the wall of human PVs. Although it is accepted that atrial tachyarrhythmias are frequently triggered from caval veins and coronary sinus (CS),[8–12] limited data have been published about the macroscopic[3] and microscopic morphology[13,14] of the myocardial sleeves of these regions. Moreover, there is a general lack of research on the immunohistochemical characterization of caval and CS myocardial sleeves.

Immunohistochemical markers to distinguish working myocardium and pacemaker or conducting cells have been established. In addition to several determinants of conduction in the heart, such as HCN4 and HNK-1 (CD57), connexin (Cx) isoforms, of which gap junction channels are composed, are also proteins characteristic of cardiac pacemaker tissues. Cx40, Cx43, and Cx45 are found differentially expressed in cardiomyocytes at various sites, which determine the characteristics of conduction velocity.[15] Cx43 is present throughout the working myocardium, whereas Cx40 is confined to the atrial myocardium and the ventricular conduction system. Cx45 is predominantly expressed in the impulse generating

This work was supported by institutional funds and by István Apáthy Foundation's Research Grant 2014-2016. **Address reprint requests and correspondence:** Dr. Ágnes Nemeskéri, Semmelweis University, H-1085 Budapest, Üllői út 26, Hungary. E-mail address: nemeskeri.agnes@med.semmelweis-univ.hu.

1547-5271/$-see front matter https://doi.org/10.1016/j.hrthm.2017.09.044

DOI:10.14753/SE.2025.3172

and conduction system but is present in substantially lower amounts in working myocardium.[16,17]

Methods

Human tissues

Thirty-two adult human hearts were removed from cadavers at 12–72 hours postmortem age that were maintained at 1°–5°C until fixation. The ages of deceased individuals ranged from 60 and 81 years. Their medical histories were unknown. Prior to death, donors had provided written consent for the use of their bodies for education and research (Willed Whole Body Program). The work was approved by the Regional and Institutional Committee of Science and Research Ethics, Semmelweis University (Research Ethics committee approval 122/2016).

Because of technical reasons, the heart could be excised together with PVs in only 16 of 33 subjects and with superior caval vein (SVC) in 22 of 33 subjects. The excision was extended into the lung hilum in the case of PVs, above the level of the azygos vein in the case of SVC, and as far as the orifice of great cardiac vein in the case of CS. The veins were then separated from the atria at the level of their ostia and cut transversely. CSs of 8 of 33 subjects were suitable for further tissue processing. Tissue samples were obtained from the sinoatrial and atrioventricular nodes, the atria, the anterior wall of the left ventricle, and the interventricular septum. Specimens were fixed in either 4% formaldehyde, or in 70% ethanol or methanol. After dehydration in graded concentrations of alcohol, tissue samples were embedded in paraffin, and 3- to 4-μm sections were made.

Tissue processing for histology

For general histology, paraffin sections were stained with hematoxylin and eosin or trichrome. Intracellular glycogen was demonstrated by Best's Carmine stain, which is a stain specific for glycogen content. Best's Carmine staining was performed as described.[18]

Immunohistochemistry

For Cx45 immunohistochemistry, specimens were fixed in ethanol/methanol and embedded in paraffin. After deparaffinization and rehydration through graded alcohols, the slides were washed 3 times in phosphate-buffered saline (PBS). Heat-induced antigen retrieval method was applied using Tris-based (Target Retrieval Solution pH-9; Dako, Santa Clara, California, US) or citrate-based (Sigma, Rocklin, California, US; H-3300) antigen unmasking solution, respectively. For Cx43 immunohistochemistry, frozen sections were prepared. Specimens were embedded in Cryomatrix (Shandon, Thermo Fisher Scientific, Waltham, Massachusetts, US), frozen in liquid nitrogen, and stored in a deep freezer (–80°C). Cryosections 10-μm thick were mounted on poly-L-lysine coated slides, fixed in cold (+4°C) acetone for 10 minutes, and air-dried. Before immunostaining, the slides were rehydrated in PBS and, permeabilization with 0.3% Triton X-100 was performed for 40 minutes.

Cx45 and Cx43 immunostaining were performed as follows. Protein blocking was carried out for 15 minutes with 1% bovine serum albumin in PBS, followed by overnight incubation at 4°C with primary antibodies. Cx45 was detected using a rabbit polyclonal antibody (sc-25716; dilution 1:100; Santa Cruz Biotechnology Inc), and Cx43 was detected using a goat polyclonal antibody (sc-6560; dilution 1:50; Santa Cruz Biotechnology Inc). Secondary antibodies, which included biotinylated goat anti-rabbit immunoglobulin G and biotinylated horse anti-goat immunoglobulin G (Vector Labs) were used, followed by endogenous peroxidase activity quenching step using 3% hydrogen peroxide (Sigma) in PBS. After formation of the avidin-biotinylated peroxidase complex (Vectastain Elite ABC kit; Vector), the binding sites of the primary antibodies were visualized by 4-chloro-1-naphthol (Sigma).

The sections were covered by aqueous Poly/Mount (Polyscience Inc, Warrington, PA) and examined using a Zeiss Axiophot photomicroscope. An automated whole-slide imaging system (3D-Histech, Budapest, Hungary) was used to visualize the sections.

Results

Myocardial sleeve of the PVs

Extensions of left atrial myocardium could be observed in the PVs of 15 of 16 hearts (94%) and formed bundles displaying various courses (Figures 1A and 1B). Bundles of large cardiac cells (median diameter 18.1 μm; interquartile range [IQR] 16.5–19.7 μm) resembling PFs based on their lightly stained cytoplasm and peripheral myofibrils were detected in the PVs of 14 hearts. Among these cardiomyocytes, a dense network of fine collagen bundles was present (Figures 1C and 1D). Best's Carmine staining confirmed that PV myocardium was enriched in cardiomyocytes containing abundant glycogen (Figure 1E). Intense Cx45 labeling was observed in the myocardial sleeve of PVs. The Cxs were clustered in intercalated discs (Figure 1F).

Myocardial sleeve of the SVC

Myocardial sleeve composed of fibers displaying a mainly spiral course was found around 21 of 22 SVCs (95%) (Figures 2A and 2B). In 1 case, some groups of myocardial fibers were present at the root of the azygos vein, but no cardiac cells were found in the portion distal to this point. Bundles of Purkinje-like cardiomyocytes (median diameter 29.4 μm; IQR 27.9–32.5 μm) embedded in connective tissue were identified in 20 SVCs (Figure 2C). Similar to the PVs, abundant intracellular glycogen content was found in SVC myocardium (Figure 2D). Intense Cx45 positivity with a pattern similar to that shown in Figure 1F was observed (Figure 2E). No Cx43 staining in the sinoatrial node, sparse labeling in the vicinity of the sinoatrial node (mixed population of atrial and pacemaker cells), and marked positivity were detected in the atrial working myocardium (data not shown).

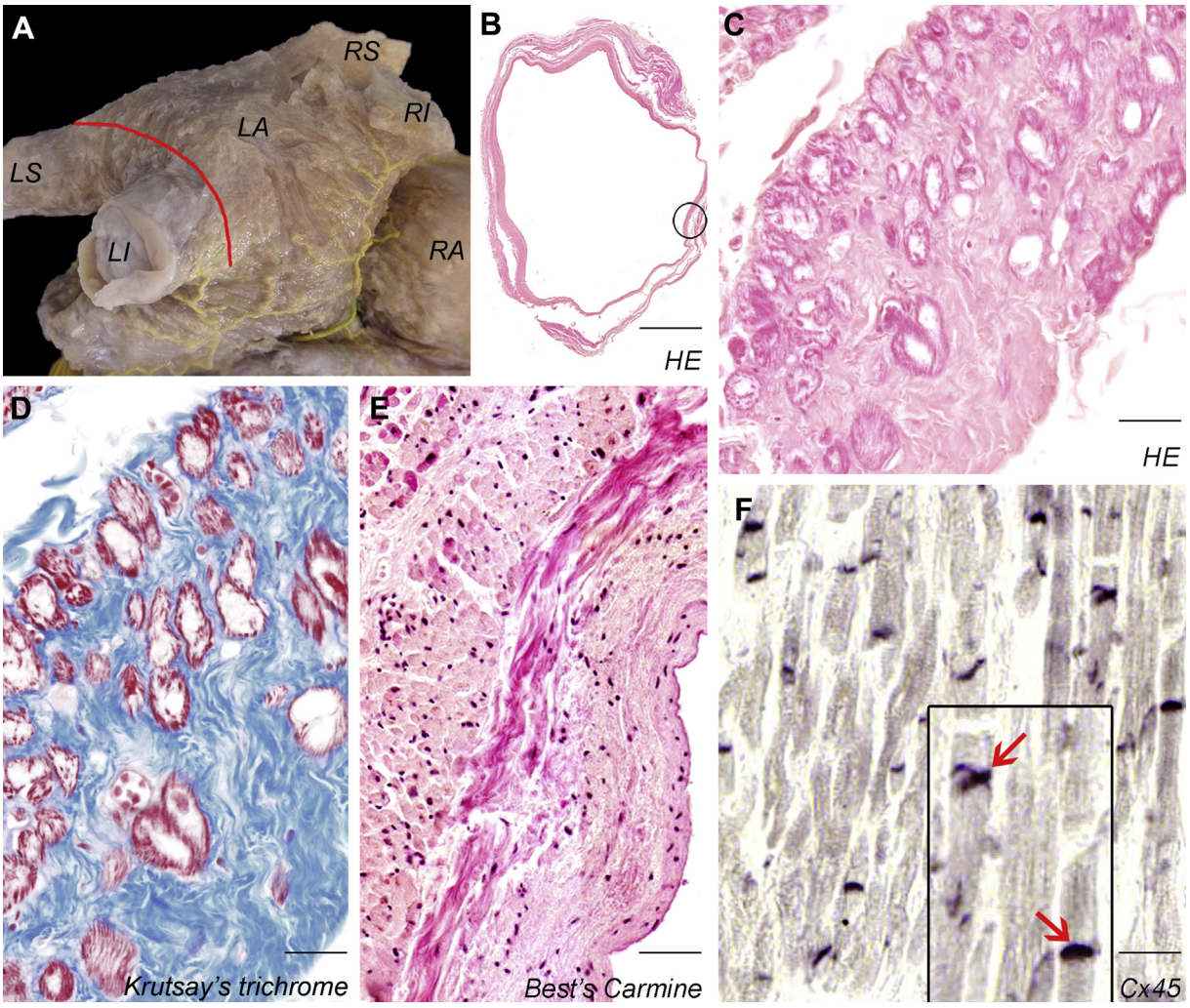

Figure 1 Histology of the PV myocardium. **A:** Myocardial extensions into the wall of PVs (LS, LI, RS, RI). Circumflex artery is filled with yellow resin mixture. *Red line* indicates the area that was cut out for histology. **B:** Transverse section of PV with myocardial sleeve. HE = hematoxylin and eosin. **C:** Large cardiomyocytes with lightly staining cytoplasm at the area indicated by the *circle* in panel B. **D:** Trichrome stain showing myocardial fibers *(red)* isolated by fibrous tissue *(blue)*. **E:** Bundle of myocardial cells containing large amount of glycogen. **F:** Prominent connexin 45 (Cx45) positivity in intercalated discs *(inset, arrows)*. Scale bar: 5000 μm (B); 40 μm (C); 30 μm (D); 70 μm (E); 30 μm (F); 20 μm (F, inset). LA = left atrium; LI = left inferior; LS = left superior; PV = pulmonary vein; RA = right atrium; RI = right inferior; RS = right superior.

Myocardial sleeve of the CS

Cardiac muscle was present in 8 of 8 CS specimens (100%) (Figure 3A). The course of cardiomyocyte bundles was spiral closer to the venous lumen and predominantly longitudinal at the outer circumference (Figure 3B). Purkinje-like myocardial fibers (median diameter 22.7 μm; IQR 20.7–25.5 μm) embedded in a network of collagen fibers were identified in 7 CSs (Figures 3C and 3D). Immunostaining revealed that Cx45 labeling was as prominent in intercalated discs as in PV and SVC (Figure 3E). Cx43 labeling could barely be observed in the myocardial sleeve of CS (data not shown).

Histology of the working myocardium and conduction system of the heart

Ventricular conducting cells were rich in glycogen in contrast to ventricular working myocardium (Figures 4A–4C). Compared to the extracardiac myocardium, no Cx45 signal could be detected in working myocardium, whereas conducting cells proved to be strongly positive (Figure 4D). Weak Cx45 immunoreactivity was present in the atria. Cx43 label was marked throughout ventricular working myocardium (Figure 4E). Prominent Cx45 immunoreactivity was detected in the region of the sinoatrial node. Cx45 was present at the atrioventricular nodal region and in the atrioventricular bundle as well (data not shown).

Discussion

Characteristics of myocardial extensions around PVs

Left atrial myocardium has been demonstrated to extend into the wall of PVs in 68%–100% of cases.[2,4–6] No specialized cells were observed in these previous studies; however, Perez-Lugones et al[7] analyzed electron microscopic images of human PV myocardium and reported the presence of P-cells and PFs.

DOI: 10.14753/SE.2025.3172

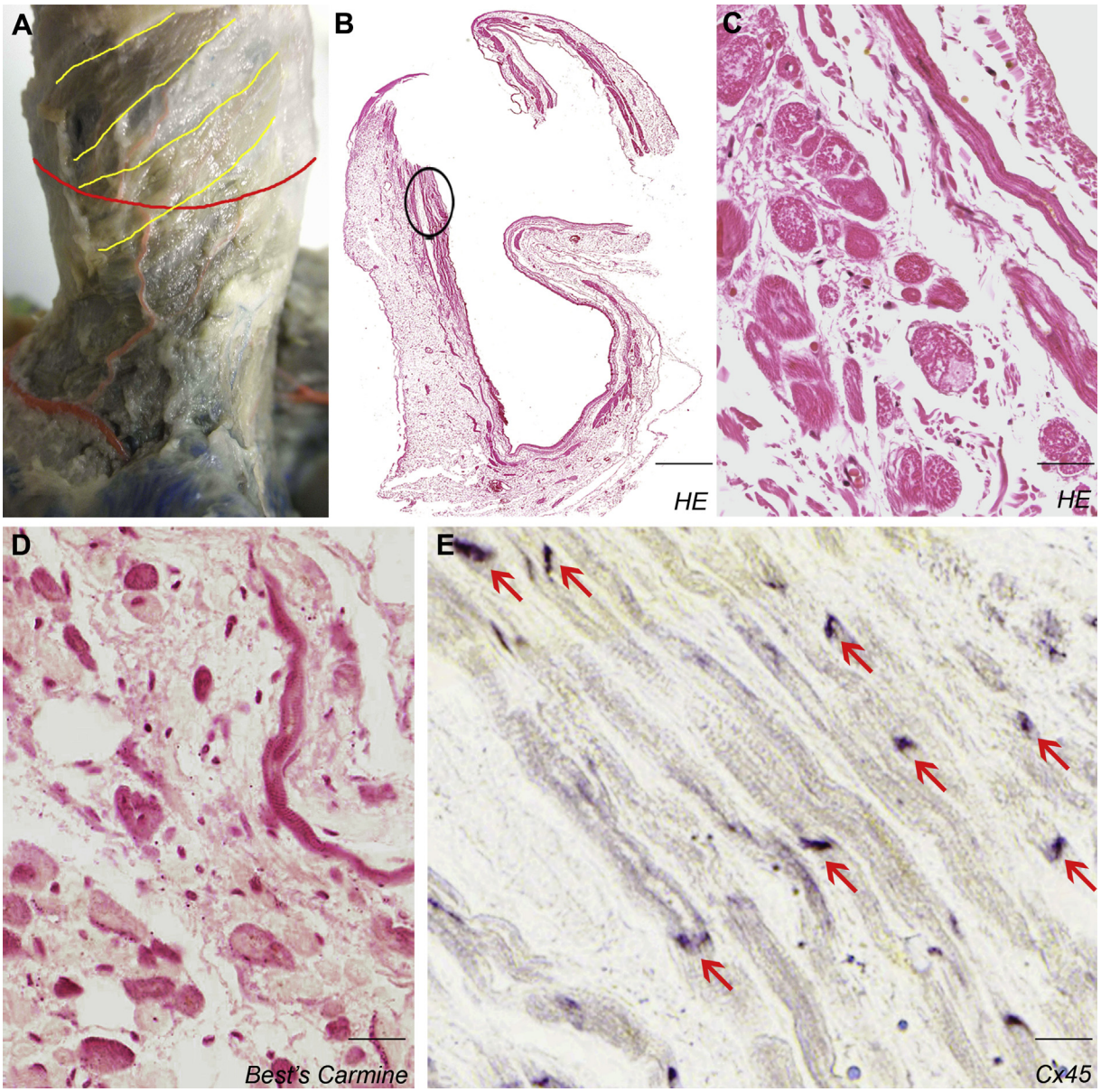

Figure 2 Histology of the SVC myocardium. **A:** Cardiomyocyte bundles with spiral course *(yellow lines).* Sinoatrial nodal artery is with red resin mixture. *Red line* indicates area that was cut out for histology. **B:** Transverse section of SVC with myocardial sleeve. HE = hematoxylin and eosin. **C:** Purkinje-like myocardial cells at the area indicated by the *circle* in panel B. **D:** Glycogen-containing cardiomyocytes. **E:** Prominent connexin45 (Cx45) immunoreactivity in intercalated discs *(arrows).* Scale bar: 1750 μm (B); 30 μm (C); 30 μm (D); 20 μm (E). SVC = superior caval vein

Nguyen et al[19] found PAS-positive cells, further supporting specialized characteristics of PVs. In the current study, bundles of cardiomyocytes displaying the characteristic features of PFs were identified in almost all PV, SVC, and CS samples. These cells contained high amounts of glycogen in their cytoplasm and were found to be embedded in a dense network of fine collagen fibers.

Potential arrhythmogenic role of caval veins and CS

Increasing interest recently has been devoted to non-PV ectopic beats, which proved to be responsible for 20%–32% of all AF cases.[11,12] Among patients with non-PV–initiating AF, SVC triggers were found in about 40%.[9,11,12] In the SVC wall, myocardial sleeve was detected in 76%–78% of all cases.[3,14] The CS area were recognized as a site of tachyarrhythmias in 1%–17% of all non-PV ectopies.[11,12] Two studies noted the presence of myocardium in all CSs examined,[20,21] whereas DeSimone et al[3] reported that only 7% of CSs contained myocardial extensions from the right atrium. To the best of our knowledge, the present study demonstrates for the first time that cells displaying PF morphology are present in human SVC and CS myocardium. The question arises whether this may indicate possible arrhythmogenicity of these regions. We intend to investigate hearts removed

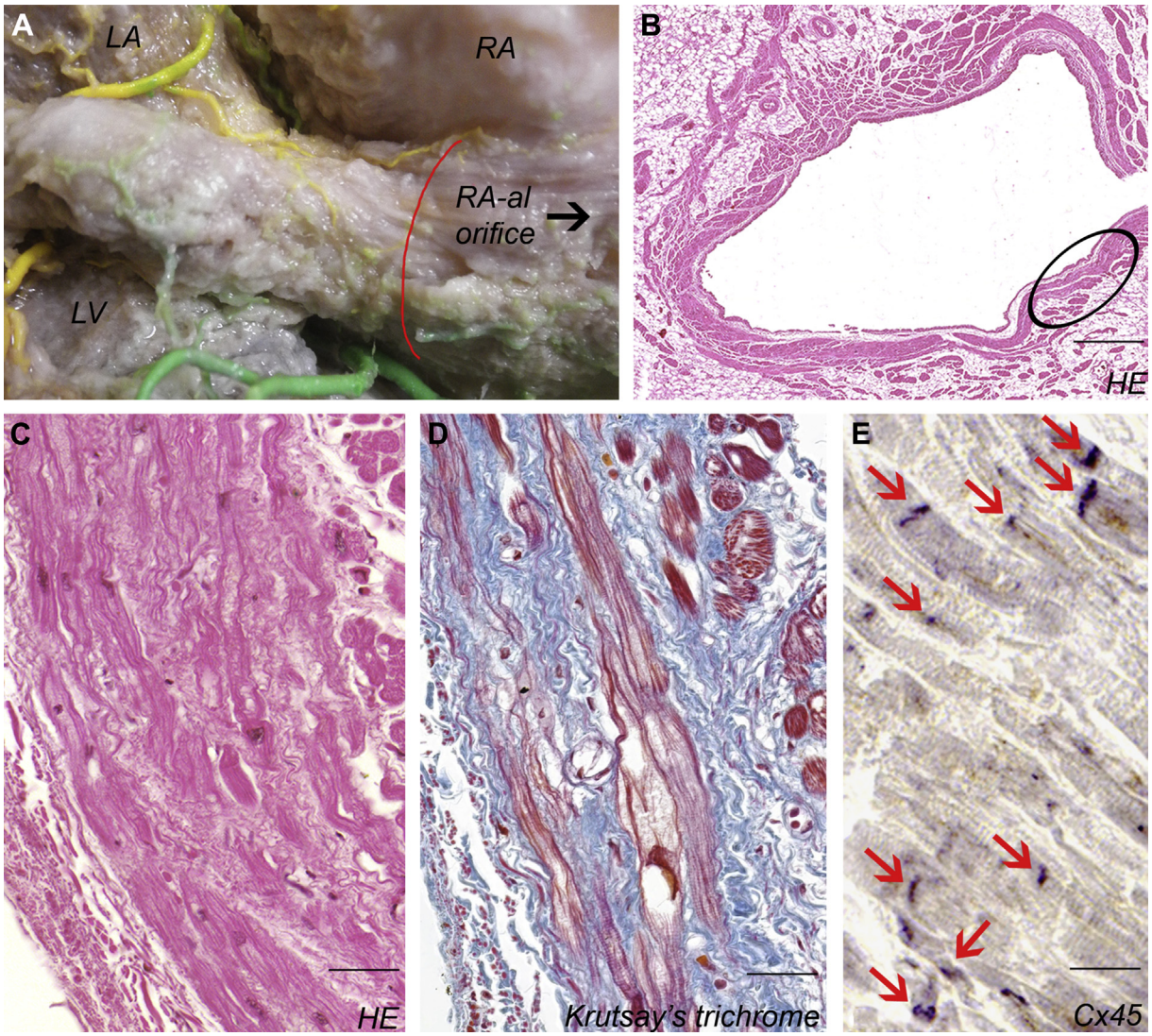

Figure 3 Histology of the CS myocardium. **A:** Myocardial sleeve around wall of the CS. Right coronary artery *(green)* and circumflex artery *(yellow)* are filled with synthetic resin. *Red line* indicates area that was cut out for histology. **B:** Cross-section of the CS orifice. HE = hematoxylin and eosin. **C:** Bundles of Purkinje-like cardiomyocytes run around the lumen at the area indicated by the *circle* in panel B. **D:** Trichrome stain showing myocardial fibers having lightly staining cytoplasm *(red)* are separated by connective tissue *(blue)*. **E:** Connexin45 (Cx45) immunoreactivity is prominent in intercalated discs *(arrows)*. Scale bar: 900 μm (B); 45 μm (C); 40 μm (D); 30 μm (E). LA = left atrium; LV = left ventricle; RA = right atrium.

from deceased patients with evidence of extracardiac loci of atrial arrhythmias to clarify this issue.

Immunohistochemical characterization of extracardiac myocardial sleeves

In this study, immunostaining was performed in order to characterize the immunophenotype of extracardiac myocardium. To date, positivity for HNK-1 (CD57), which is an antigen to the developing conduction system,[22] and reactivity for the cardiac pacemaker antigen HCN4 have been detected in human studies.[19,23]

According to previous data, Cx45 was detected at very low levels in atrial and ventricular working myocardium,[16] whereas distinct positive signal was found at the atrioventricular node of human adults.[17] Therefore, Cx45 seems to be a specific marker of the conduction system. In the current study, strong staining for Cx45 was observed throughout the impulse-generating and conduction system of the heart, whereas almost no immunopositivity could be detected in working myocardium.

Data on the Cx expression patterns of cardiac veins are based on animal research, and differences among distinct species have been reported. In canine SVC, the presence of all cardiac Cxs (including Cx45) were reported, with distinct areas characterized by abundance of Cx43 in the center and diffuse Cx40 signals in the periphery. Such areas of atypical Cx expression were mainly present in the proximal portion of the SVC, usually in the outer circumference of the myocardial sleeve.[24] Both Cx40 and Cx43 were observed in isolated cardiac cells from canine great veins, with a higher amount of Cx43 in the SVC than in the PVs. The absence of Cx45 signal was presumably caused by paraformaldehyde fixation or injury of the cell membrane.[25] In rat, a nodal-like tissue

DOE:10.14753/SE.2025.3172

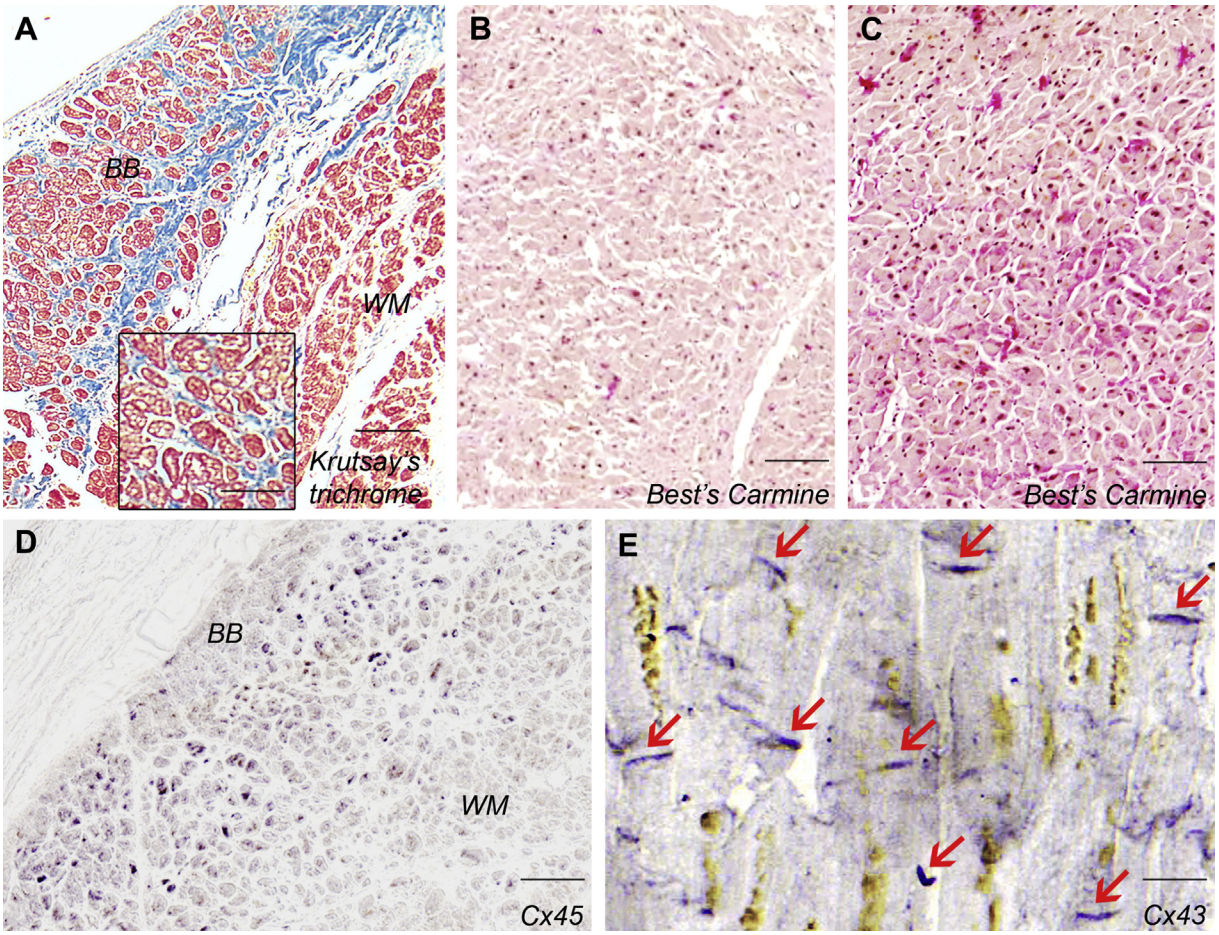

Figure 4 Histology of left ventricular myocardium. **A:** Trichrome staining of working myocardium (WM) and a bundle branch (BB) *(inset)* composed of cardiomyocytes with pale cytoplasm. **B**, **C:** WM shows almost no sign with glycogen-specific Best's Carmine staining **(B),** whereas a large amount of glycogen is recognized at the BB **(C)**. **D:** Connexin45 (Cx45) immunoreactivity is prominent at the BB but barely detectable in the WM. **E:** At the WM, marked positivity for Cx43 is detectable in the intercalated discs (arrows). Yellow-brown intracellular granules in the vicinity of nuclei are lipofuscin pigments. Scale bar: 80 μm (A); 40 μm (A-inset); 160 μm (B); 100 μm (C); 90 μm (D); 12 μm (E).

looping around the junction of right atrium and SVC was reported. From the junction, lightly stained cells extended next to both the crista terminalis and the interatrial groove. Although nodal-like cells proved to be strongly positive for Cx45 and negative for Cx43, atrial walls and PV myocardium exhibited intense Cx43 but no Cx45 immunostaining in rat.[26]

The current study documents for the first time the presence of Cx45-positive myocardial fibers in the wall of human PVs, SVC, and CS. Based on the difference between Cx45 immunopositivity of working myocardium and pacemaker and/or conducting structures, our findings regarding the prominent Cx45 staining of extracardiac myocardial fibers might provide some support for the presumed specialized nature of these areas. Because Cx43 labeling was weak in the myocardial sleeves, it can be hypothesized that extracardiac myocardium in PVs, SVC, and CS contains predominantly cardiomyocytes with pacemaker and/or conducting properties.

Study limitation

Immunohistochemistry is not an adequate method for reporting amounts of protein expression. Therefore, quantitative western blot analysis, which is suitable for determining the relative abundance of distinct proteins, would add weight to our observations.

Conclusion

The presence of Purkinje-like cardiomyocytes exhibiting strong glycogen positivity was documented in the myocardial sleeves of human PVs, SVC and CS. This research is the first to demonstrate pronounced Cx45 positivity of extracardiac myocardium, which may provide some support for the presumed arrhythmogenicity of the myocardial sleeves ensheathing PVs, caval veins, and the CS.

Acknowledgment

We thank the technical staff of Department of Anatomy, Histology and Embryology and 2nd Department of Pathology, Faculty of Medicine, Semmelweis University for important contributions.

References

1. Nathan H, Eliakim M. The junction between the left atrium and the pulmonary veins: an anatomic study of human hearts. Circulation 1966;34:412–422.

2. Saito T, Waki K, Becker AE. Left atrial myocardial extensions onto pulmonary veins in humans: anatomic observations relevant for atrial arrhythmias. J Cardiovasc Electrophysiol 2000;11:888–894.
3. DeSimone CV, Noheria A, Lachman N, Edwards WD, Gami AS, Maleszewski JJ, Friedman PA, Munger TM, Hammill SC, Packer DL, Asirvatham SJ. Myocardium of the superior vena cava, coronary sinus, vein of Marshall, and the pulmonary vein ostia: gross anatomic studies in 620 hearts. J Cardiovasc Electrophysiol 2012;23:1304–1309.
4. Ho SY, Cabrera JA, Tran VH, Farré J, Anderson RH, Sánchez-Quintana D. Architecture of the pulmonary veins: relevance to radiofrequency ablation. Heart 2001;86:265–270.
5. Kholová I, Kautzner J. Anatomic characteristics of extensions of atrial myocardium into pulmonary veins in subjects with and without atrial fibrillation. Pacing Clin Electrophysiol 2003;26:1348–1355.
6. Hassink RJ, Aretz HT, Ruskin J, Keane D. Morphology of atrial myocardium in human pulmonary veins. A postmortem analysis in patients with and without atrial fibrillation. J Am Coll Cardiol 2003;42:1108–1114.
7. Perez-Lugones A, McMahon JT, Ratliff NB, Saliba WI, Schweikert RA, Marrouche NF, Saad EB, Navia JL, McCarthy PM, Tchou P, Gillinov AM, Natale A. Evidence of specialized conduction cells in human pulmonary veins of patients with atrial fibrillation. J Cardiovasc Electrophysiol 2003;14:803–809.
8. Tsai CF, Tai CT, Hsieh MH, Lin WS, Yu WC, Ueng KC, Ding YA, Chang MS, Chen SA. Initiation of atrial fibrillation by ectopic beats originating from the superior vena cava. Circulation 2000;102:67–74.
9. Lin WS, Tai CT, Hsieh MH, Tsai CF, Lin YK, Tsao HM, Huang JL, Yu WC, Yang SP, Ding YA, Chang MS, Chen SA. Catheter ablation of paroxysmal atrial fibrillation initiated by non–pulmonary vein ectopy. Circulation 2003;107:3176–3183.
10. Katsivas AG, Manolis AG, Vassilopoulos C, Ioannidis P, Giotopoulou A, Kyriakides Z. Electroanatomical mapping of a right atrial tachycardia originating within the inferior vena cava. Hellenic J Cardiol 2004;45:187–190.
11. Lee SH, Tai CT, Hsieh MH, Tsao HM, Lin YJ, Chang SL, Huang JL, Lee KT, Chen YJ, Cheng JJ, Chen SA. Predictors of non-pulmonary vein ectopic beats initiating paroxysmal atrial fibrillation: implication for catheter ablation. J Am Coll Cardiol 2005;46:1054–1059.
12. Chang HY, Lo LW, Lin YJ, et al. Long-term outcome of catheter ablation in patients with atrial fibrillation originating from nonpulmonary vein ectopy. J Cardiovasc Electrophysiol 2013;24:250–258.
13. Hashizume H, Ushiki T, Ahe K. A histological study of the cardiac muscle of the human superior and inferior venae cavae. Arch Histol Cytol 1995;58:457–464.
14. Kholová I, Kautzner J. Morphology of atrial myocardial extensions into human caval veins: a postmortem study in patients with and without atrial fibrillation. Circulation 2004;110:483–488.
15. Severs NJ, Rothery S, Dupont E, Coppen SR, Yeh HI, Ko YS, Matsushita T, Kaba R, Halliday D. Immunocytochemical analysis of connexin expression in the healthy and diseased cardiovascular system. Microsc Res Tech 2001;52:301–322.
16. Vozzi C, Dupont E, Coppen SR, Yeh HI, Severs NJ. Chamber-related differences in connexin expression in the human heart. J Mol Cell Cardiol 1999;31:991–1003.
17. Kreuzberg MM, Liebermann M, Segschneider S, Dobrowolski R, Dobrzynski H, Kaba R, Rowlinson G, Dupont E, Severs NJ, Willecke K. Human connexin31.9, unlike its orthologous protein connexin30.2 in the mouse, is not detectable in the human cardiac conduction system. J Mol Cell Cardiol 2009;46:553–559.
18. Totty BA. Mucins. In: Bancroft JD, Gamble M, eds. Theory and Practice of Histological Techniques. London, UK: Churchill Livingstone; 2007. p. 163–200.
19. Nguyen BL, Fishbein MC, Chen LS, Chen PS, Masroor S. Histopathological substrate for chronic atrial fibrillation in humans. Heart Rhythm 2009;6:454–460.
20. Lüdinghausen M, Ohmachi N, Boot C. Myocardial coverage of the coronary sinus and related veins. Clin Anat 1992;5:1–15.
21. Chauvin M, Shah DC, Haïssaguerre M, Marcellin L, Brechenmacher C. The anatomic basis of connections between the coronary sinus musculature and the left atrium in humans. Circulation 2000;101:647–652.
22. Blom NA, Gittenberger-de Groot AC, DeRuiter MC, Poelmann RE, Mentink MMT, Ottenkamp J. Development of the cardiac conduction tissue in human embryos using HNK-1 antigen expression: possible relevance for understanding of abnormal atrial automaticity. Circulation 1999;99:800–806.
23. Kholová I, Niessen HWM, Kautzner J. Expression of Leu-7 in myocardial sleeves around human pulmonary veins. Cardiovasc Pathol 2003;12:263–266.
24. Yeh HI, Lai YJ, Lee SH, Lee YN, Ko YS, Chen SA, Severs NJ, Tsai CH. Heterogeneity of myocardial sleeve morphology and gap junctions in canine superior vena cava. Circulation 2001;104:3152–3157.
25. Yeh HI, Lai YJ, Lee YN, Chen YJ, Chen YC, Chen CC, Chen SA, Lin CI, Tsai CH. Differential expression of connexin43 gap junctions in cardiomyocytes isolated from canine thoracic veins. J Histochem Cytochem 2003;51:259–266.
26. Yamamoto M, Dobrzynski H, Tellez J, Niwa R, Billeter R, Honjo H, Kodama I, Boyett MR. Extended atrial conduction system characterised by the expression of the HCN4 channel and connexin45. Cardiovasc Res 2006;72:271–281.

DOI:10.14753/SE.2025.3172
ÖSSZEFOGLALÓ KÖZLEMÉNY

Új felismerések a pitvarfibrilláció genezisében és fenntartásában: az egyénre szabott kezelés lehetőségei

Kugler Szilvia dr.[1] ▪ Duray Gábor dr.[2] ▪ Préda István dr.[1, 2]

[1]**Semmelweis Egyetem, Általános Orvostudományi Kar, Városmajori Szív- és Érgyógyászati Klinika, Budapest**
[2]**Magyar Honvédség Egészségügyi Központ, Kardiológiai Osztály, Budapest**

A pitvarfibrilláció prevalenciája a felnőttkorosztályban körülbelül három százalék. A ritmuskontroll céljából alkalmazott katéterablatiós terápia alapját jelenleg a pulmonalis vénák izolációja képezi, amelynek egyéves sikeraránya azonban többszöri beavatkozással sem emelhető 70% fölé. A beavatkozás hosszú távú eredményességét a pitvarokban bekövetkező elektromos és strukturális remodelláció korlátozza, amely az arrhythmia tartós fennmaradásához vezet. Az epicardialis zsírszöveti akkumuláció, a pitvari fibrosis, az autonóm idegrendszeri hatások, valamint a különféle arrhythmogen gócok lehetséges szerepét számos tanulmány elemezte. A pitvari epicardialis zsírszövet mennyisége, gyulladás indukálta fibroticus átalakulása és a myocardium zsíros infiltrációja, például obesitas esetén, pitvarfibrilláció fellépésére hajlamosít. Az autonóm szabályozás egyensúlyának megváltozása, például rendszeres sporttevékenység hatására, a triggerelt aktivitás fokozódása, valamint a pitvari refrakter periódus csökkenése révén indukálhat ritmuszavart. Hatékony terápia a lehetséges arrhythmogen trigger és szubsztrátmechanizmusok egyénre szabott komplex befolyásolása által valósulhat meg. A fibroticus folyamatok a renin-angiotenzin-aldoszteron rendszer gátlása révén lassíthatók. A neuromodulációs lehetőségek magukban foglalják a renalis denervációt, illetve a ganglionablatiót, és az antikoaguláns terápia pitvari remodellációt gátló hatásáról is ismertek adatok. A katéterablatiós beavatkozások lehetséges új irányait a jobb és bal pitvari lineáris laesiók alkalmazása, a heges területek homogenizálása mellett a komplex frakcionált pitvari elektrogramok, rotorok és az ectopiás fókuszok ablatiója képezik. Mindezek mellett kiemelt fontosságú a fennálló rizikófaktorok, úgymint obesitas, hyperlipidaemia, hypertonia, diabetes mellitus és obstruktív alvási apnoe hosszú távú, tervezett kezelése.
Orv Hetil. 2018; 159(28): 1135–1145.

Kulcsszavak: pitvarfibrilláció, pitvari remodelláció, zsírszövet, autonóm idegrendszer, egyénre szabott kezelés

Novel mechanisms in the initiation and maintenance of atrial fibrillation: tailored individual treatment

Atrial fibrillation affects approximately three percent of the adults. Ablation strategies targeting the isolation of the pulmonary veins are the up-to-date cornerstones for atrial fibrillation ablations. However, a one-year success rate of repeated interventions is not more than 70%. Long-term efficacy of catheter ablation is presumably limited by electrical and structural remodeling of the atria, which results in a progressive increase in the duration of atrial fibrillation to become sustained. The potential pathophysiological importance of the epicardial adipose tissue, atrial fibrosis, autonomic nervous system and arrhythmogenic foci are documented by several studies. Increased volume, inflammation induced transformation to fibrosis and myocardial infiltration of atrial subepicardial fat in obese patients result in higher risk of atrial fibrillation development. Changes in atrial autonomic innervation under some conditions including regular physical exercise strongly promote arrhythmogenesis *via* the mechanism of enhanced triggered activity or abbreviated atrial refractoriness. Individualized management of possible trigger and substrate mechanisms are proposed to provide a novel basis for the effective treatment of atrial fibrillation. Pro-fibrotic signalling pathways can be inhibited by the suppression of renin-angiotensin-aldosterone system. Neuromodulation strategies include renal sympathetic denervation and ganglionic plexi ablation. Anticoagulation therapy has also been shown to reduce the burden of abnormal atrial remodeling. Possible novel catheter ablation techniques are used for right or left atrial linear lesions, scar homogenization and catheter ablation of complex fractionated atrial electrograms, rotors or ectopic foci. Beside these new management strategies, clinical consideration of factors of particular risks as obesity, hyperlipidaemia, hypertension, diabetes and obstructive sleep apnoe are also essential.

DOI:10.14753/SE.2025.3172
ÖSSZEFOGLALÓ KÖZLEMÉNY

Keywords: atrial fibrillation, atrial remodeling, adipose tissue, autonomic nervous system, tailored individual treatment

Kugler Sz, Duray G, Préda I. [Novel mechanisms in the initiation and maintenance of atrial fibrillation: tailored individual treatment]. Orv Hetil. 2018; 159(28): 1135–1145.

(Beérkezett: 2018. február 12.; elfogadva: 2018. március 27.)

Semmelweis Ignác születésének 200. évfordulója évében a *Szerkesztőség* felkérésére készített tanulmány.

Rövidítések

BMI = (body mass index) testtömegindex; CFAE = (complex fractionated atrial electrogram) komplex frakcionált pitvari elektrogram; DE-MRI = (delayed enhancement MRI) késői kontraszthalmozásos technikával végzett szív-MRI; FACM = (fibrotic atrial cardiomyopathy) „kötőszövetes pitvari szívizomelfajulás"; FIRM = (focal impulse and rotor modulation) fokális impulzus- és rotormoduláció; HMG-CoA = (3-hydroxy-3-methyl-glutaryl-coenzyme A) 3-hidroxi-3-metil-glutaril-koenzim-A; LOM = (ligament of Marshall) Marshall-ligamentum; MRI = (magnetic resonance imaging) mágneses rezonanciás képalkotás; NOAC = (novel oral anticoagulant) új típusú orális antikoaguláns; OSAS = (obstructive sleep apnea syndrome) obstruktív alvási apnoe szindróma; PAR = (protease-activated receptor) proteáz aktiválta receptor; PF = pitvarfibrilláció; PVI = (pulmonary vein isolation) pulmonalisvéna-izoláció; RAAS = (renin-angiotensin-aldosterone system) renin-angiotenzin-aldoszteron rendszer; SC = sinus coronarius; VCI = vena cava inferior; VCS = vena cava superior; VP = vena pulmonalis

A pitvarfibrilláció (PF) a leggyakoribb szívritmuszavar, amelynek prevalenciája a felnőttkorosztályban körülbelül 3%, a betegségben 80 éves életkor felett pedig minden negyedik ember érintett. 2010-ben világszerte körülbelül 33,5 millió egyén szenvedett PF-ban [1]. Jellemzően progresszív lefolyású, vagyis a kezdetben csupán alkalmanként fellépő ritmuszavar az idő múlásával állandósul.

Általánosan elfogadott, hogy a ritmuszavart fokális elektromos aktiváció (trigger) váltja ki, amely nagyrészt a tüdővénák (vena pulmonalisok, VP-ok) területéről származik. Ezzel szemben a PF fenntartásában kiterjedt elektromos és strukturális pitvari remodelláció (arrhythmogen szubsztrát) szerepét feltételezik [2]. A PF-triggerek, valamint a remodellált pitvari szubsztrát komplex interakciójának fontos szerepet tulajdonítanak a perzisztens PF fennmaradásában.

A pitvari remodelláció kezdetben vélhetően reverzíbilis folyamat, amelynek előidézői között olyan tényezőket tartanak nyilván, mint a hypertonia, a szívelégtelenség, a billentyűbetegség, a pitvar kötőszövetes átalakulása (fibrosis), az obstruktív alvási apnoe szindróma (OSAS), valamint a pitvari flattern, pitvari septumdefektus, amelyek a falfeszülés fokozása révén fejtik ki hatásukat [3]. Számos esetben már az első PF-epizód jelentkezése előtt bekövetkezik a pitvarok károsodása, remodellációja. A remodellált pitvarban fellépő PF napok–hetek alatt elektromos és strukturális változásokat idéz elő [4].

A pitvari károsodás és a következményes PF patomechanizmusában közrejátszik a renin-angiotenzin-aldoszteron rendszer (RAAS) aktivációja által kiváltott fibrosis, zsíros infiltráció, gyulladásos folyamatok, az autonóm idegrendszer egyensúlyának megbomlása, az ioncsatornák működészavara, a fokozott alvadékonyság, valamint az oxidatív stressz által mediált folyamatok. A szöveti szinten történő szerkezeti változásokat működésbeli funkciózavar kíséri, amely az elektrofiziológiai sajátosságok megváltozása révén fokozza a PF kialakulásának kockázatát és a ritmuszavar állandósulását. A PF hátterében álló szubsztrát a primer folyamat progresszióját okozva korlátozza a katéterablatiós beavatkozások sikerarányát [4–6] *(1. táblázat)*.

1. táblázat | A pitvari remodelláció hátterében szerepet játszó tényezők

Klinikai faktorok	Szövettani faktorok	Patofiziológiai faktorok
Hypertonia	Zsíros infiltráció	RAAS
Obesitas	Fibrosis	Oxidatív stressz
Diabetes mellitus	Gyulladás	Ioncsatornák
Szívelégtelenség		Alvadási faktorok
Billentyűbetegség		Autonóm idegrendszer
COPD		Elektrofiziológiai tényezők
OSAS		

COPD = krónikus obstruktív tüdőbetegség; OSAS = obstruktív alvási apnoe szindróma; RAAS = renin-angiotenzin-aldoszteron rendszer

A továbbiakban szeretnénk bemutatni a PF kiváltásában és fenntartásában jelenleg ismert patológiai folyamatokat, a triggerforrásként szolgáló anatómiai struktúrákat, elektromos kiváltó tényezőket, az epicardialis zsírszövet és a pitvarfal zsíros infiltrációját, az autonóm idegrendszer és az alvadási faktorok szerepét, valamint különféle genetikai tényezőket *(1. ábra)*.

A pitvarfibrilláció kiváltásában (trigger) forrásként szolgáló anatómiai struktúrák

Vena pulmonalis eredetű fokális impulzusok

A VP-ok körül a bal pitvari myocardium nyúlványai által képzett szívizomhüvely területén jelen lévő ectopiás ingerképző fókuszok a PF kiváltása szempontjából kiemel-

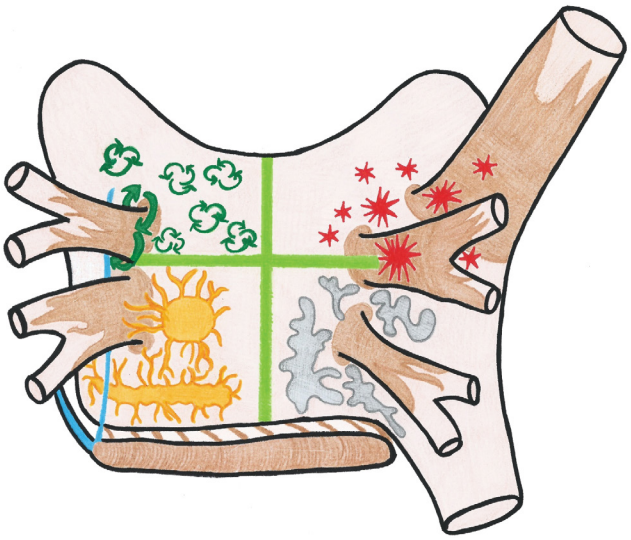

1. ábra A pitvarfibrilláció hátterében álló lehetséges mechanizmusok

A sémás ábra hátsó nézetben ábrázolja a bal és a jobb pitvart. A bal felső pulmonalis véna körüli terület a reentrymechanizmust, a bal alsó negyed az autonóm ganglionok szerepét, a jobb felső pulmonalis véna a fokális triggereket, míg a jobb alsó negyed a heg jelentőségét szemlélteti

kedő jelentőséggel bírnak. Egy 1998-ban publikált, elektrofiziológiai vizsgálaton alapuló humán tanulmány eredményei arra utalnak, hogy a PF-paroxizmusok hátterében álló arrhythmogen gócok többsége a bal oldali, illetve a felső VP-ok területére lokalizálható, és a PF-t triggerelő ectopiás jelek rádiófrekvenciás ablatiót követően megszűnnek [7]. A VP falában jelen lévő ectopiás pacemaker-sejtcsoportok a ritmuszavart fokozott automáciájuk révén válthatják ki, amelynek sejtélettani alapját a maximális diasztolés potenciál abszolút értékének csökkenése képezi [8].

Haïssaguerre és mtsai közleményének megjelenése óta a PF katéterablatiós terápiájának alapját a VP-szájadékok körkörös izolálása jelenti [7]. Ismert azonban, hogy a pulmonalisvéna-izoláció (PVI) egyéves sikeraránya – antiarrhythmiás gyógyszer alkalmazása nélkül – több beavatkozás esetén sem emelhető 70% fölé [9]. A sikerarány független az alkalmazott módszertől (cryoablatio *versus* rádiófrekvenciás ablatio) [10].

A hatékonyságot több tényező korlátozza. Egyrészt a jelenlegi eszközökkel nem minden esetben hozható létre tartós laesio, következésképpen gyakran kiújul a VP-ok és a bal pitvar között kapcsolatot teremtő szívizomhüvely vezetőképessége, az ablatio során létesített hegben ingerületvezetésre képes rések keletkeznek. Másrészt jelenleg még nem ismertek kellően a PF-t fenntartó mechanizmusok [11].

Nem vena pulmonalis eredetű fokális impulzusok

Egy tanulmány tanúsága szerint a PF-ablatióban részesülő betegek esetében akár 11%-ban nem VP-eredetű góc az indukált tartós PF forrása [12]. Az indukált nem tartós pitvari arrhythmiák esetén ez az arány még jelentősebb, akár 60% is lehet [13]. Más közlemények a nem VP-eredetű PF gyakoriságát 20–32% között határozzák meg. A nem VP-eredetű pitvarfibrilláló betegek csoportjában a leggyakoribb ectopiás ingerképző góc a vena cava superior (VCS, 26–40%), valamint a bal pitvar területe (17,5–42%-ban), a leggyakrabban a hátsó szabad fal. Emellett a crista terminalis (5–15%), a vena obliqua atrii sinistri (Marshall-ligamentum [LOM], 5–15%), a septum interatriale (1,5–11%), valamint az ostium sinus coronarii (1–7%) szerepét is leírták a nem VP-eredetű PF vonatkozásában [14–17].

Az elektroanatómiai térképezések arra utalnak, hogy a nem VP-lokalizációjú triggerek jól meghatározott anatómiai régiókba (alsó mitralis gyűrű, bal pitvar hátsó fala, interatrialis septum [fossa ovalis és annak limbusa], crista terminalis, Eustach-billentyű, sinus coronarius [SC], VCS, bal fülcse, perzisztáló bal VCS, LOM) tömörülnek *(2. ábra)*. E területeken olyan szívizomrostok vannak jelen, amelyek fokozott automácia, triggerelt aktivitás és lokális microreentrykörök együttes hatása következtében arrhythmogen aktivitással bírhatnak [18].

Kugler és mtsai Purkinje-rost morfológiájú, glikogénben gazdag szívizomrostokat figyeltek meg a VP, a VCS, valamint a SC körüli myocardium területén. A szerzők ezekben a régiókban a szív ingerképző és ingerületvezető rendszerében a magas expressziót mutató connexin-45 fehérje kifejezett pozitivitását tapasztalták, amely az extracardialis myocardium lehetséges ingerképző/ingerületvezető természetére utalhat [19].

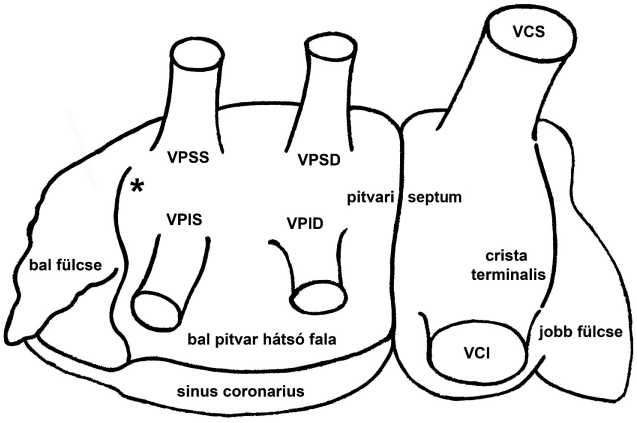

2. ábra Fokális triggerek kiindulási helyeként azonosított jobb és bal pitvari régiók

Pulmonalisvéna-eredetű triggerek eredete: bal felső (VPSS) és alsó (VPIS), jobb felső (VPSD) és alsó (VPID) tüdővénák. Nem pulmonalisvéna-eredetű bal pitvari triggerek forrásai: Marshall-ligamentum (*), bal fülcse, a bal pitvar hátsó fala. Jobbpitvar-eredetű arrhythmogen gócok kiindulási helyei: crista terminalis, jobb fülcse, vena cava superior (VCS) és inferior (VCI). A sinus coronarius, valamint a pitvari septum arrhythmogen tulajdonsága is ismert

Jobbpitvar-eredetű triggerek

A nem VP-eredetű triggerek egyik legjelentősebb forrásaként számon tartott VCS területén az embrionális sinus venosusra jellemző spontán ingerképzésre képes szövet van jelen. A jobb felső VP anatómiai közelsége miatt nehézséget jelenthet az ezen régiókból származó triggerek elkülönítése. Az arrhythmogen fókusz a leggyakrabban szegmentális ablatióval izolálható, amelynek során a góctól proximálisan, annak közvetlen közelében hozzák létre a laesiót. Ritkán előforduló szövődményként a sinuscsomó vagy a nervus phrenicus sérülését, illetve a VCS szűkületét írták le, viszonylag kevés esetben [18].

A crista terminalis eredetű PF-triggerek a legkorábbi aktiváció helyén végzett fokális ablatióval eliminálhatók. Szövődményként a jobb oldali nervus phrenicus sérülése fordulhat elő. Az Eustach-billentyű a crista terminalis alsó folytatása, amely elkülöníti a vena cava inferior (VCI) szájadékát a SC-tól. Egy macskán végzett tanulmány [20] pacemakersejtek jelenlétét írta le az Eustach-billentyű területén. A VCI csupán néhány tanulmány esetén bizonyult PF-trigger kiindulási helyének. Ennek magyarázata az, hogy az embrionális fejlődés során a VCI atrialisatiója csupán részlegesen következik be. Azonosított góc esetén fokális ablatio végzendő [18].

Alkalmanként a jobb fülcse lateralis részéről, valamint a tricuspidalis gyűrű területéről eredő triggerek is azonosításra kerülnek [18].

Balpitvar-eredetű triggerek

A bal pitvar hátsó fala embrionális, anatómiai és elektrofiziológiai szempontból a VP-ok folytatásának tekinthető, ezáltal kifejezett arrhythmogen tulajdonsággal bír. A hátsó fal elektromos izolációja a széles antralis VP-izolációs vonalaknak a bal pitvar tetején (roof) és alján (floor) létrehozott vonalszerű laesiókkal történő összekötésével végezhető. Az eljárás során ügyelni kell arra, hogy a rádiófrekvenciás energia leadása során ne károsodjon a közelben elhelyezkedő oesophagus [18].

A SC pitvari szívizommal behüvelyezett szakasza 3–5,5 cm hosszúságú. Ez a szakasz PF-triggerként, illetve reentrykörök részeként egyaránt szolgálhat. A LOM a bal VCS anatómiai maradványa, és a Vieussens-billentyű szintjében nyílik a SC-ba. A SC-eredetű triggerek fokális ablatióval vagy a SC teljes izolációja révén eliminálhatók. A SC izolációja az endocardialis (bal pitvar), valamint az epicardialis felszín (SC belfelszíne) felől egyaránt elvégezhető [18].

Az interatrialis septum, különösen a fossa ovalis/limbus, továbbá a mitralis gyűrű területén azonosított PF-triggerek eliminálása fokális ablatióval lehetséges [18].

A bal fülcse szájadékának hátsó részéről eredő triggerek esetenként valójában a bal oldali VP-ok vagy a LOM területéről származnak. Valódi bal fülcsei trigger azonosítása esetén a fülcse mechanikus funkciózavarának kivédése céljából fokális ablatio végzendő [18].

A LOM-ból származó triggerek azonosítása a SC-on keresztül történő kanülálással lehetséges. Trigger azonosítása esetén endocardialis úton (a bal pitvar felől) végzett elektromos izoláció javasolt. Ritkán szükséges a SC-on keresztül végzett direkt kanülálás vagy etanol LOM-ba injektálása az izoláció komplettálásához. Az esetenként perzisztáló bal VCS, amely a LOM embrionális megfelelője, csakugyan PF-triggerként szolgálhat. A bal VCS a bal fülcse és a bal oldali VP-ok között helyezkedik el, és közvetlen kapcsolatban áll a SC-val. A típusos esetben kitágult SC-on keresztül a véna retrográd úton érhető el [18, 21].

Elektrofiziológiai mechanizmusok

Valószínű, hogy a PF elindításáért VP-eredetű triggerek felelnek [7], a ritmuszavar fenntartásának mechanizmusai azonban nem ismertek pontosan. Az elmúlt években több ezzel kapcsolatos elmélet látott napvilágot. Elektroanatómiai térképezésre alapuló feltételezések felvetették annak lehetőségét, hogy az ectopiás fókuszokon kívül egyéb mechanizmusok is szerepet játszanak a PF kiváltásában és fenntartásában [5].

Kimutatták, hogy PF során a pitvarokban olyan reentrykörökkel jellemezhető komplex elektromos aktiváció zajlik, amely heterogén elektrofiziológiai szubsztrát jelenlétét feltételezi [5]. A reentry létrejöttének elektroanatómiai alapja, hogy a szívizomrostok egy csoportja nem aktiválódik a kezdeti depolarizációs folyamat hatására, hanem az eredeti impulzus megszűnése előtt válik újra ingerelhetővé. Ezeken a szívizomrostokon keresztül olyan sejtcsoportok juthatnak újra ingerületbe, amelyekben éppen csak lezajlott az eredeti depolarizációs folyamat [8].

„Leading circle reentry”

A funkcionális reentry legegyszerűbb formája az arrhythmiaszubsztrátum nélküli ingerület-körforgás („leading circle reentry”). Az ilyen típusú reentrykör nem tartalmaz ingerelhető rést, ezáltal az aktiváció állandóan a kör közepe felé irányul, amelyet így az ingerülethullámok folyamatosan refrakter állapotban tartanak. Ez a refrakter terület olyan funkcionális gátat képez, amely az állandó anatómiai barrierekhez (heg) hasonlóan képes fenntartani a reentrykört [8, 22].

„Multiple wavelet” elmélet

Kitágult pitvar, valamint rövid hullámhosszú (lassú vezetési sebesség/rövid refrakter periódus) reentrykörök esetén lehetővé válik, hogy egyidejűleg számos reentrykör legyen jelen, amelyek folyamatosan vándorolva egymással találkoznak, és vagy kialszanak, vagy újabb hullámocskákat képeznek [8, 22]. Ez a „multiple wavelet” elmélet, amely szerint a PF annál tartósabb, minél több

hullámocska van jelen a pitvarokban. Az együttesen előforduló hullámok száma a pitvar összfelületétől és a pitvari impulzus hullámhosszától függ. Mivel kitágult és változó ingerületvezetési tulajdonságokkal bíró pitvarizomzatban több „wavelet" lehet jelen, a pitvartágulat a PF fontos rizikófaktora. A nervus vagus stimulációja a pitvari akciós potenciálnak a teljes szívciklushoz képest történt relatív rövidülése miatt hajlamosít PF-ra. A széles/bifázisos P-hullámok, késői potenciálok, fragmentált pitvari elektrogramok fokozott rizikót jelentenek PF kialakulására [23].

Rotorelmélet

A rotorok a funkcionális reentry specifikus formái, amelyeknek szerepet tulajdonítanak a PF fenntartásában. A rotorok esetében a hullámfrontnak spirális formája van, és a hullámfront és a hullám vége egy gyújtópontban találkozik. A hullámfront terjedési sebessége a gyújtópont helyén a legalacsonyabb, ezért itt a hullámfront képtelen ingerelni a rotor központjában elhelyezkedő szövetet. Ez a mag a „leading circle" reentryközpontjához hasonlóan funkcionális blokkot képez azzal a különbséggel, hogy a rotor központjában lévő szövet valójában nem refrakter, csupán a gyújtópontban fennálló alacsony vezetési sebesség miatt nehezen ingerelhető. Mindebből az következik, hogy míg a „leading circle" modell esetén a reentrykör a középső terület ingerelhetetlensége miatt állandóan ugyanazon a helyen marad, addig a rotor igen összetett módon képes a térben vándorolni. A rotorok képződéséhez szükséges, hogy a hullámfront valamiféle barrierrel találkozzon, amely lehet strukturális akadály (például heg) vagy valamiféle funkcionális elektromos inhomogenitás, anizotrópia a myocardiumban (például pitvari extraszisztolé hatására). Anizotrópián azt értjük, amikor a szívizomszövet ingerületvezető képessége a szívizomrostok lefutási irányának függvényében jelentős változatosságot mutat. A rotorok esetenként egy meghatározott területen (például VP-ok körüli terület) stabilan rögzülhetnek. A hullámfrontok a myocardium organikus vagy funkcionális inhomogén területeivel interakcióba lépve feltöredezhetnek, majd számos rendezetlen hullámot indukálva kaotikus elektromos aktivitást idézhetnek elő a pitvarokban [22]. A több ezer cikluson keresztül stabil vagy átmeneti, instabil rotorok feltérképezése endocardialis térképezés útján (64 elektródás „basket catheter"), valamint testfelszíni elektródákat (például 252 db) magában foglaló térképezőrendszer révén egyaránt lehetséges [5].

A FIRM- (fokális impulzus- és rotormoduláció) terápia lényege a fokális impulzusok és rotorok katéterablatiós eliminációja. Tartósan pitvarfibrilláló betegek esetében 97%-ban igazolták rotor vagy fokális impulzusok jelenlétét. Az arrhythmogen forrást 24%-ban jobb pitvari régiókra lokalizálták [11]. *Hocini és mtsai* arra utalnak, hogy a jobb pitvari ablatióval kiegészített beavatkozásoknak magasabb a sikerarányuk, mint a hagyományos eljárásoknak [24]. Összegzésképpen megállapítható, hogy néhány lokalizált arrhythmogen forrás hatására a pitvarban elektromos dezorganizáció következik be, amely a PF kialakulása szempontjából fokozott rizikót jelent. A FIRM-ablatio révén ezen arrhythmogen források aktivitása megszüntethető vagy mérsékelhető [11].

Komplex frakcionált pitvari elektrogramok

Perzisztens PF esetén a folyamatos pitvari elektromos aktivitással jellemezhető komplex frakcionált pitvari elektrogramok (CFAE) lehetséges ablatiós célpontként ismertek [25]. A CFAE-k kialakulása számos mechanizmussal magyarázható. A myocardiumnak olyan területein fordulnak elő, ahol a szívizomrostok egymástól elkülönülten, rendezetlenül vannak jelen. Valószínűsíthető, hogy a CFAE-k a pitvaron belüli ingerületvezetés passzív megnyilvánulásai, nem pedig a PF kiváltói [22].

Perzisztens PF esetén a CFAE-ket tartalmazó régiók gyakran a bal pitvar >50%-ára kiterjednek. Mivel a CFAE-helyek jelentős hányada nem specifikus, indokolttá vált a PF fenntartásában kritikus szereppel bíró területek azonosítása, a CFAE-k morfológiáján alapuló szelektív eljárások kidolgozása [26].

Egy állatmodell tanúsága szerint ibutilid (III-as osztályú antiarrhythmiás szer) alkalmazása mérsékli a pitvari reentrymechanizmusokat, ellenben a PF-t generáló fokális gócok aktivitására nincs hatással. Elképzelhető, hogy az ibutilid alkalmazását követően is fennmaradó CFAE-k területén végzett ablatióval eliminálhatók a PF fenntartásában kritikus szereppel bíró régiók, ami a beavatkozás hatékonyságának és a hosszú távú arrhythmiamentességnek a fokozódását eredményezheti. Egy randomizált-kontrollált, kettős vaktanulmány során perzisztensen pitvarfibrilláló, korábban PVI-n átesett betegek körében a CFAE-ablatiót megelőzően alkalmazott ibutilid hatására a bal pitvar CFAE-t tartalmazó felszíne nagyobb mértékben csökkent (8% *versus* 1%), továbbá a PF gyakrabban terminálódott (71% *versus* 56%), mint placebo adása esetén [26].

A pitvarfibrilláció-ablatio okozta arrhythmogen és egyéb hosszú távú hatások

Ismert, miszerint a PF-ablatiót követően hetekkel–hónapokkal gyógyszeres terápiára nehezen reagáló, gyakran tartós pitvari tachycardia vagy atípusos pitvari flattern alakulhat ki, amely ismételt katéterablatiós beavatkozás elvégzését teheti szükségessé. Ezek a ritmuszavarok legfőképpen kiterjedt pitvari lineáris laesiók képzése esetén lépnek fel, és szubsztrátjukat az inkomplett hegvonalak talaján kifejlődő reentrykörök képezik [27].

Emellett több vizsgálat eredménye utal arra, hogy a kiterjedt ablatio a bal pitvar szisztolés funkciójának károsodásához vezethet, amelynek következtében magasabb thromboemboliás kockázattal kell számolni [28, 29].

Epicardialis zsírszövet és pitvari fibrosis

Az epicardialis zsírszövet a mesenterialis zsírhoz hasonlóan endokrin funkcióval is rendelkezik, továbbá gyulladásos folyamatok helyszínéül szolgálhat. Ezzel szemben a parietalis pericardiumon kívül eső paracardialis zsírszövet vélhetően nem játszik szerepet endokrin és gyulladásos folyamatokban. Az epicardialis zsírszövet által szekretált adipokinek, chemokinek és gyulladásos citokinek szabadon diffundálhatnak az alatta fekvő myocardiumba, annak fibroticus elváltozását előidézve. Obesitas esetén a zsírszövet fibroticus átalakulásra való hajlama fokozott. A subepicardialis zsírszövet arrhythmogen volta a gyulladásos mediátorok, adipokinek által közvetített parakrin hatással, valamint a gyulladás indukálta fibrosis talaján végbemenő remodellációval magyarázható. A myocardiumba infiltráló subepicardialis zsírszövet fibrosisának talaján bekövetkező szerkezeti átalakulás az érintett területeken elektromos disszociációt okoz, az ingerületvezetés lassul és heterogénné válik, unidirekcionális blokkok és reentrykörök képződnek, ezáltal fokozódik a PF kialakulásának és fennmaradásának valószínűsége [2, 3, 5, 6].

A pitvari fibrosis szempontjából rizikótényezőként tekintendő az időskor, a hypertonia, a szívelégtelenség, az obesitas, a szívbillentyű-betegség, az OSAS fennállása, továbbá maga a PF is hajlamosít epicardialis túlsúlyú kötőszövetes elfajulásra a pitvarokban. A fibrosist előidéző folyamatban számos tényező (gyulladáskeltő citokinek, oxidatív stressz, transzformáló növekedési faktor-béta, RAAS, kalciumdependens proteázok, extracelluláris mátrixot szabályozó fehérjék, hypoxia indukálta faktor-1-alfa, endothelin-1) szerepet játszik. A fokozott fizikai terhelés vagy gyulladás okozta következményes fibrosis [30] szerepe szintén jelentős.

Haemers és mtsai szívműtéten átesett betegek jobb fülcséből származó szövetmintáin vizsgálták az esetenként jelentősen fibroticus (remodellált) zsíros infiltrátumoknak a PF patomechanizmusában betöltött szerepét. A PF az epicardialis remodelláció szignifikáns klinikai prediktorának bizonyult. CD8+ citotoxikus T-lymphocyták aggregátumait is leírták a subepicardialis zsírszövetben, ami arra utal, hogy a zsíros-kötőszövetes infiltrátumok területén immunreakció is zajlik. Mivel a pitvari zsírszövet fibrosisában számos klinikai tényezőnek szerepe lehet, a szerzők juhoknál gyors pitvari ingerléssel perzisztens PF-t kiváltva is végeztek elemzéseket. Ezt a modellt alkalmazva a PF szöveti szintű hatásai jelentős bal kamrai funkciózavar hiányában vizsgálhatók. A pitvarfibrilláló juhok esetén a zsíros infiltrátumok területén nagyobb arányban voltak jelen lymphocytaaggregátumok, mint a kontrollállatokban [31].

A pitvari fibrosis kiemelt jelentőségére utal, hogy felmerült a „kötőszövetes pitvari szívizom-elfajulás" (FACM) mint önálló fogalom alkalmazása. A pericardialis zsírszövet össztérfogata arányos a PF gyakoriságával és súlyosságával, továbbá az ablatiót követő arrhythmia-visszatérés valószínűségével [3]. A pitvari fibrosisnak mindemellett a kriptogén stroke-ok kialakulásában is szerepet tulajdonítanak. Fokozott pitvari fibrosis esetén gyakrabban észlelhető a bal fülcsében spontán echókontraszt, valamint thrombus [2].

A pitvari fibrosis mértékének jelentősége a katéterablatio sikerességére

Számos katéterablatiós vizsgálat elemezte a pitvari fibrosis mértékének jelentőségét. A pitvari fibrosis kimutatható szövettani úton, elektrofiziológiai módszerekkel (pitvari feszültségértékek csökkenése), továbbá késői kontraszthalmozásos technikával végzett szív-MRI (DE-MRI)-vizsgálattal. A DE-MRI lehetőséget nyújt a pitvari fibrosis noninvazív úton történő mennyiségi meghatározására. Az eljárás lehetővé teszi a fibroticus és az ép myocardium differenciálását. Meghatározható a fibroticus myocardium teljes pitvarfali térfogathoz viszonyított %-os mennyisége. A százalékos értékeken alapuló Utah-klasszifikáció négyfokozatú skálán jellemzi a pitvari fibrosis kiterjedtségét: I.: <10% fibrosis; II.: 10–20% fibrosis; III.: 20–30% fibrosis; IV.: >30% fibrosis. PF-ban szenvedő populációban a késői kontraszthalmozású területek jellegzetes lokalizációi a bal VP-antrum, továbbá a bal pitvar hátsó és oldalsó fala. Perzisztens PF esetén ezek a régiók, különösen a bal pitvar elülső és hátsó falát illetően, fokozottabb kiterjedést mutatnak. A pitvari fibrosis mértéke, továbbá a legnagyobb fibroticus terület mérete jelentős hatással van az ablatiót követő arrhythmia-visszatérésre. Eszerint magas ablatiós sikerarány várható Utah I. stádiumban, továbbá kisméretű fibroticus területekkel bíró Utah II. és III. stádiumban. Nagyméretű fibroticus régiók, továbbá Utah IV. stádium esetén a sikeres ablatio esélye csekélyebb [2, 5, 32].

Az ablatiót követően fennmaradó residualis fibrosis szerepe

A katéterablatio célja krónikus transmuralis laesio létrehozatala. A DE-MRI lehetővé teszi az ablatio során képzett hegek, valamint a residualis fibrosis megítélését. A visszatérő ritmuszavarmentes túlélés igazoltan összefügg a residualis fibrosissal [33]. Amíg a stabil heges laesio az ablatiót követő arrhythmiamentesség szempontjából kedvező, addig progresszív fibrosis esetén a ritmuszavar visszatérése várható [2].

Autonóm idegrendszeri hatások

Az autonóm idegrendszer aktivációja jelentős elektrofiziológiai változásokat idézhet elő a pitvarokban, pitvari tachyarrhythmiák indukcióját előidézve [22, 34].

A szív vegetatív beidegzése

A szív vegetatív beidegzésében a szíven kívüli (extrinsic), valamint a szíven belüli (intrinsic) ganglionoknak egya-

ránt jelentős szerepük van. Az intrinsic autonóm idegrostok főként a pitvarokban, különösképpen a bal pitvar-VP junkció közelében, az epicardium alatt találhatók. Az itt elhelyezkedő ganglionplexusoknak közvetítő szerepük van az autonóm stimulusok arrhythmogenesisében. A ganglionsejtek mintegy 30%-a adrenerg és kolinerg immunfenotípussal egyaránt rendelkezik, emiatt a szimpatikus és paraszimpatikus idegrostok szelektív rádiófrekvenciás ablatiója nehézségekbe ütközhet [22, 34].

Autonóm hatások sejtszintű mechanizmusai

Az autonóm pitvari remodelláció magában foglalja az extrinsic (szimpatikus és paraszimpatikus), valamint a komplex idegi hálózatot képező intrinsic ganglionok szintjén történő funkcionális változásokat. A béta-adrenerg, illetve a kolinerg tónus fokozódása, a katecholaminerg és a vagustónus egyensúlyának megváltozása egyaránt PF-t indukálhat [5]. A fokozott adrenerg tónus a fokális ectopiás gócok automáciájának fokozása, illetve kalciumdependens triggerelt aktivitás növelése révén válthat ki ritmuszavart, míg a kifejezett vagustónus az acetilkolindependens káliumáramot indukálva a pitvari refrakter periódus csökkenése révén reentrykörök kialakulásának kedvez. A vagustónus fokozódása során a refrakteritás csökkenése jelentős regionális különbségeket mutat, ami hozzájárul a fokozott vagustónus PF-t indukáló hatásához. A PF tartóssá válásában kiemelt szerep jut a strukturális remodellációnak. A béta-adrenerg stimuláció által kiváltott fokozott kalciumáram géntranszkripciós változásokat indukálva szívizomsejt-hypertrophiát és fibrosist idéz elő [34].

Társbetegségek és életmódbeli tényezők szerepe az autonóm idegrendszeri hatásokon keresztül

Az autonóm idegrendszeri hatásokat különféle társbetegségek befolyásolják [22]. Egyes kórállapotok (például myocardialis infarctus) esetén az autonóm idegrostok aktivitása fokozódhat, ami pitvari és kamrai arrhythmiák fellépését idézheti elő. Jellemző a pitvari szimpatikus innerváció fokozódása magas frekvenciájú tartós PF kialakulásában [34].

Az utóbbi években több vizsgálat foglalkozott a fizikai aktivitás és a PF összefüggésével. A mérsékelt testedzés kedvező hatásával ellentétben az állóképességi sportok versenyszintű űzése esetén a PF hajlama magasabbnak bizonyult. Noha az időskorban végzett rendszeres séta a ritmuszavar kialakulása szempontjából minden bizonnyal kedvező, napi szinten végzett futás esetén fiatal férfiaknál a PF gyakorisága magasabbnak bizonyult. *Nielsen és mtsai* metaanalízise hasonló eredményeket igazolt. Eszerint a hosszú távú, intenzív sporttevékenység, továbbá a fizikai aktivitás teljes hiánya egyaránt fokozza a PF rizikóját, míg a rendszeres mérsékelt testmozgás a PF szempontjából kedvező hatással bírhat. A PF kialakulása szempontjából kedvezőtlen fizikai aktivitás pontos mértéke ugyanakkor igen nehezen határozható meg [35, 36]. Egy hazai közlemény tanúsága szerint heti 3–5 órányi testmozgás számos pozitív egészségi előnye mellett nem növeli a PF kockázatát [37].

A fizikai aktivitásnak az általános egészségi állapotra és a cardiovascularis rendszerre, így a PF kialakulására kifejtett hatásában számos patofiziológiai tényező játszik szerepet. Az aerob testedzés során a paraszimpatikus tónus, a baroreceptorok érzékenysége, valamint a szívizomrostok kolinerg érzékenysége fokozódik, ami együttesen a pitvari refrakteritás csökkenését előidézve PF-t indukálhat. Újabban az epidemiológiai adatokon kívül [38] humán biokémiai és MRI-vizsgálatokkal is igazolták [39, 40], hogy az elhúzódó bal és jobb pitvari fizikai terhelés és a következményes emelkedett pulmonalis nyomás élsportolókban fokozott pitvari fibrosist is okoz, amely a PF kiváltásában is szerepet játszik. A nem extrém sportterhelés (testedzés) során megnyilvánuló paraszimpatikus tónusfokozódás ugyanakkor a PF szempontjából protektív hatással is bírhat [5, 34]. Ezzel szemben, amint *Nielsen és mtsai* kifejtik, a mozgásszegény életmód elhízáshoz, diabeteshez, hypertoniához és coronariabetegséghez vezethet, valamint a szívfrekvencia növekedését okozhatja, ezáltal fokozva a PF előfordulási gyakoriságát. A rendszeres mérsékelt fizikai terhelés a felsorolt tényezők mérséklésével csökkenti a PF kockázatát [36].

Az autonóm idegrendszeren keresztül ható terápiás lehetőségek

Az autonóm idegrendszer modulációja lehetőséget nyújt a pitvari remodelláció folyamatának befolyásolására. Az autonóm idegrendszer túlzott aktivitása gátolható gyógyszerek révén, eszközös úton, emellett a rendszeres sporttevékenység is kedvező hatású. Az antiarrhythmiás gyógyszeres terápiák jelentős része hatással van az autonóm idegrendszerre. A béta-blokkolók széles körben alkalmazott, a szimpatikus idegi aktivitást gátló gyógyszerek, amelyek az elektromos cardioversio után visszatérő, valamint a posztoperatív PF megelőzése szempontjából is kedvező hatásúnak bizonyultak. Az elsőként alkalmazandó gyógyszeres kezelés mellett az alábbiakban ismertetett eszközös beavatkozások is a neuromodulációs terápiás lehetőségek közé sorolandók. Mivel a szívre ható autonóm idegi struktúrák egymással jelentős mértékben együttműködnek, a neuromodulációs terápiák során egy adott területet célzó beavatkozások egyéb struktúrákra is hatással lehetnek. A szimpatikus denerváció hosszú távú hatásai jelenleg nem ismertek [5, 34].

A szimpatikus beidegzés gátlása elérhető átmeneti úton a nervus vagus cervicalis szakaszának stimulációjával, vagy végleges módon, a ganglion stellatum denervációjával. A baroreflex eszközös aktiválása a sinus caroticus direkt úton történő stimulálása révén lehetséges. A nervus vagus stimulációhoz hasonlóan ez az eljárás is jelentősen csökkenti a szimpatikus idegi aktivitást. Enyhe

fokú stimuláció során a pitvari refrakter periódus nagyfokú, kedvezőtlen csökkenése nem következik be. A szomatikus idegek transzkután stimulációja (például a tragus területén) autonómreflex-válaszokat eredményezhet [34].

A PVI során gyakran a VP-ok körüli ganglionplexus részleges ablatiója is bekövetkezik. Ez járulékosan történik, de ezenfelül vizsgálták a célzott ganglionablatio hatását is, változó eredménnyel. Egyes vizsgálatok tanúsága szerint ganglionablatióval kiegészített PVI esetén magasabb sikerarány várható, mint kizárólagos PVI-t követően. Más tanulmányok ugyanakkor arról tesznek említést, hogy a terápiás célú ganglionablatiónak olykor paradox hatása is lehet [5, 22, 34].

Az endovascularis úton végzett renalis szimpatikus denerváció gyógyszeres terápiára nem reagáló hypertensio esetén kísérleti kezelési módszer. Az eljárás a szimpatikus idegi aktivitás csökkentése révén a PF neuromodulációs terápiájában is használatos lehet. A renalis szimpatikus denerváció közvetlen hatást gyakorolhat a pitvari szubsztrátra. A beavatkozás következtében a RAAS aktivitása csökken, a pitvari fibrosis, gyulladás, apoptózis mérséklődik [5, 34]. Az atrioventricularis csomóra ható paraszimpatikus idegek stiumulálása a gyógyszeres kezelésre nem reagáló magas kamrafrekvenciájú PF frekvenciakontroll-terápiájának lehetséges invazív megoldása lehet [41, 42].

Fokozott alvadékonyság

A PF fennállása fokozott alvadékonysággal járó állapot. A fokozott alvadékonyság szintén arrhythmogen hatású. A PF idején fennálló ischaemia aktiválja az alvadási faktorokat, amelyek proteáz aktiválta receptorokat (PARs) stimulálva szívizomsejt-hypertrophiát, gyulladásos reakciót, valamint fibroblastaktiváció talaján pitvari fibrosist idéznek elő. A fokozott alvadékonyság által aktivált folyamatok a pitvarok strukturális remodellációját előidézve megzavarják a szívizomrostok közötti ingerületvezetést, és ezáltal a PF szubsztrátjául szolgálnak [5, 43].

Patkányból izolált pitvari fibroblastokban thrombin hatására a fibrosist és gyulladást indukáló folyamatok fokozódását figyelték meg. A thrombint gátló dabigatrán mérsékelte ezeket a hatásokat. Thrombomodulinmutáció miatt fokozott alvadékonyságra hajlamos fenotípusú transzgenikus egerek esetén könnyebben lehetett PF-epizódokat indukálni, és azok tartósabb ideig álltak fenn, mint a vad fenotípusban. Mindezek az adatok arra utalnak, hogy a fokozott alvadékonysággal járó állapotoknak szerepük lehet a PF-szubsztrát kialakulásában. A NOAC-ok eredményesen gátolják a pitvari fibroticus folyamatokat és a PF szubsztrátjának kialakulását, ezáltal késleltethetik a PF progresszióját, továbbá a pitvari thrombusképződést és a következményes stroke kialakulását [43].

Genetikai tényezők

A „Framingham Heart Study” tanulmány igazolta, hogy PF-ban szenvedő egyének leszármazottainak egyéb PF-ra hajlamosító kórállapotok fennállásától függetlenül fokozódott a PF-rizikójuk [44]. Egyes nukleotidpolimorfizmusok (például a 4q25-ös kromoszómalocuson) feltételezhetően hajlamosítanak PF kialakulására. A 4q25-ös locus a PITX2-es (paired-like homeodomain transzkripciós faktor-2) géntől nem messze helyezkedik el, amelynek az embrionális szívfejlődés során kulcsszerepe van a VP körüli myocardiumhüvely kialakulásában [45].

Az elmúlt években számos feszültségfüggő nátrium- és káliumcsatornát érintő mutációt, illetve variációt azonosítottak a PF hátterében. A PF-hoz társuló káliumcsatornavariánsok többsége a csatorna fokozott működését idézi elő, aminek következtében a pitvarban a repolarizáció hamarabb következik be, az akciós potenciál időtartama és a refrakter periódus rövidül, s ez reentrykörök kialakulásának kedvez. A káliumcsatornák funkcióvesztő mutációja a pitvari akciós potenciál időtartamának megnyúlásán keresztül, korai utódepolarizációt okozva vált ki PF-t. A feszültségfüggő nátriumcsatornák funkciónyerő, -vesztő variációi egyaránt arrhythmogen szubsztrátot eredményeznek. A connexin 40 gap junction proteint kódoló gén mutációja a pitvarokban az ingerületvezetési sebesség csökkenéséhez vezet, ami reentrykörök képződésének kedvez. Jelátviteli faktoroknak és egyéb (lamin, natriureticus peptid prekurzor) molekuláknak a variációit is azonosították a PF hátterében [46, 47].

A pitvari miozinkönnyűláncot kódoló MYL4-génen belüli deletiónak a recesszíven öröklődő, korai kezdetű PF patogenezisében tulajdonítanak szerepet [48].

A pitvarfibrilláció szerepe a pitvarfibrilláció patomechanizmusában

Egy tanulmány tanúsága szerint társbetegségekkel nem rendelkező, paroxismalisan pitvarfibrilláló betegeknél átlagosan 15 év alatt 18%-ban fejlődik ki tartós PF [49]. Rövidebb ideig tartó paroxismusok esetén kisebb, míg hosszabb fennállás esetén nagyobb gyakorisággal alakul ki krónikus ritmuszavar [50]. Kémiai vagy elektromos cardioversio nagyobb sikeránnyal végezhető rövid ideje fennálló PF esetén. Ezek a megfigyelések arra utalnak, hogy a PF a háttérben álló tényezőktől függetlenül, önmagában progresszív betegség, és lefolyása során olyan elektrofiziológiai és szerkezeti elváltozásokat okoz, amelyek elősegítik újabb PF-epizódok kialakulását, valamint a ritmuszavar állandósulását [23].

Wijffels és mtsai (1995) 12 kecske pitvari epicardiumára számos elektródát varrtak, majd 2–3 hét múlva egy külsőleg csatlakoztatott pacemaker segítségével mesterséges úton PF-t idéztek elő. Amíg a folyamat elején, sinusritmus fennállása mellett, az indukált PF-epizódok csupán néhány másodpercig tartottak, és jellemzően

spontán szűntek, addig a ritmuszavar hosszan tartó mesterséges fenntartása a PF időtartamának progresszív növekedését okozta, míg végül a ritmuszavar tartóssá vált, és többé nem szűnt meg magától. 24 órán keresztül fenntartott PF hatására a PF indukálhatósága 24%-ról 76%-ra fokozódott. A pitvari effektív refrakter periódus az első 24 órában pitvarszerte jelentősen csökkent. A krónikus PF kialakulásával párhuzamosan a pitvari elektrogramok morfológiája is megváltozott, az amplitúdó csökkenése mellett nagyfokú fragmentáció és az izoelektromos szakaszok megszűnése vált jellemzővé [23].

A tanulmány során azt is megfigyelték, hogy hosszan fennálló PF esetén a pitvari refrakter periódus a fiziológiás reakciótól eltérően nem csökken az ingerlési frekvencia növelésének hatására. Ennek jelentőségét az adja, hogy amennyiben cardioversiót követően a jelentős frekvenciacsökkenést nem kíséri a refrakter periódus kellő megnyúlása, a helyreállított sinusritmus ideje alatt a pitvarban kritikusan rövid marad a refrakter periódus, ami a PF korai újraindulását okozhatja egy pitvari extraszisztolé hatására [23].

A tanulmány során tapasztalt pitvari refrakteritás csökkenése és az ezzel párhuzamosan rövidülő fibrillációs ciklushossz mellett vélhetően egyéb tényezők (a pitvarok tágulata, a pitvaron belüli ingerületvezetési sebesség általános csökkenése, helyi ingerületvezetési blokkok) is szerepet játszhatnak a krónikus elektrofiziológiai adaptációban és ezáltal a PF tartóssá válásában [23].

A *Wijffels és mtsai* (1995) által közölt „atrial fibrillation begets atrial fibrillation" (a PF újranemzi önmagát) elmélet értelmében tehát a PF talaján olyan elektrofiziológiai változások következnek be, amelyek az effektív refrakter periódus csökkenése révén a ritmuszavar további fennmaradását okozzák [23]. Hosszú ideje fennálló PF esetén a bal pitvarban remodellációs folyamatok következnek be, amelyek elektrofiziológiai (bal pitvari szignálok alacsony feszültségértéke), valamint képalkotó (MRI-) módszerekkel is igazolhatók. Fontos tényező, hogy a PF folyamatos fennállásának időtartamával arányosan a pitvari elektromos aktivitás egyre komplexebbé válik, a PF indukálta pitvari remodelláció pedig a ritmuszavar késői stádiumában egyre inkább elősegíti az újabb epizódok kialakulását [4]. Emellett nyilvánvalóvá vált, hogy a PF strukturális változásokhoz (pitvari fibrosis, bal pitvari dilatáció) is vezet, ezáltal is elősegítve a ritmuszavar állandósulását. A pitvari remodelláció tehát kiváltja, majd fenntartja a ritmuszavart, ami önrontó kör módjára felgyorsítja a remodelláció folyamatát. Fontos tényező azonban, hogy a PF klinikai megjelenése és lefolyása egyénenként igen változatos, továbbá az említett strukturális remodelláció nem pitvarfibrilláló betegek esetében is jelen lehet [2]. A sinusritmus fenntartásának előnyeként tartják számon a PF indukálta pitvari károsodás mérséklődését, az elektromos és strukturális remodelláció esetleges visszafordítását (reverz remodelláció).

A társbetegségek szerepe

Az elmúlt évtizedekben számos rizikófaktort azonosítottak a PF kialakulásában, valamint a PF-epizódok visszatérésének hátterében, úgymint idős életkor, hypertonia, obesitas, szívelégtelenség, krónikus vesebetegség, OSAS, az aortabillentyű meszesedése, dohányzás, intenzív sporttevékenység, a testedzés hiánya, PF-ban eltöltött idő, genetikai faktorok, pericardialis zsírszövet [4, 5]. Egy nemrégiben megjelent közlemény adatai szerint a praehypertensio, valamint az emelkedett éhomi vércukorszint normál testsúlyú egyének esetén is hajlamosít új keletű PF kialakulására [51]. Hosszú ideje fennálló PF, valamint cardiovascularis társbetegségek jelenléte esetén a bal pitvarban remodellációs folyamatok következnek be [4]. Az akut myocardialis infarctust követő időszakban 6–21% gyakorisággal lép fel PF [52].

Az obesitas jelentősége a pitvarfibrilláció patogenezisében

A Danish Diet, Cancer, and Health Study tanulmány kimutatta, hogy a testtömegindex (BMI) növekedésével párhuzamosan a véletlenül felfedezett PF kockázata fokozódott [53].

Nalliah és mtsai részletesen ismertetik az elhízásnak a PF patogenezisében feltételezett szerepét. Az elhízás hemodinamikai, szerkezeti és elektromos működészavart okoz a pitvarokban, a pitvar fibroticus átalakulása jellemző, ezáltal fokozza a PF kialakulásának és progressziójának rizikóját. Obesitas esetén nemritkán alakul ki diasztolés diszfunkció, amely mellett a PF gyakrabban jelentkezik perzisztens formában, súlyosabb tünetekkel. Állatmodell esetén azt tapasztalták, hogy testsúlygyarapodás hatására pitvari megnagyobbodással, kamrai hypertrophiával, pericardialis zsírdepozícióval, heterogén ingerületvezetéssel jellemezhető progresszív remodelláció következik be, amelynek talaján a PF gyakoribbá válik. A pericardialis zsír tartós obesitas esetén leginkább a bal pitvar hátsó falát infiltrálja [3].

Az obstruktív alvási apnoe szerepe a pitvarfibrilláció patomechanizmusában

Az OSAS jellemzője a felső légutak alvás közbeni átmeneti kollapszusa, amely hypoxiát, hypercapniát, kóros mellűri nyomásváltozást, valamint autonóm idegrendszeri túlműködést okoz. Ezek a patofiziológiai mechanizmusok kölcsönös egymásra hatással növelhetik a PF rizikóját. Ráadásul OSAS esetén fokozott cardialis remodellációt és szisztémás gyulladást igazoltak, amely tényezőknek szintén szerepük lehet a PF genezisében és fenntartásában [54].

A társbetegségek kezelésének szerepe a pitvarfibrilláció terápiájában

A rendellenes pitvari remodellációért felelős kockázati tényezők jelentős csökkentését célzó terápia lehetővé teszi a PF-szubsztrát mérséklését. Intenzív testsúlycsökkentés, valamint az egyéb társuló rizikófaktorok (csökkent ejekciós frakciójú szívelégtelenség, revascularisatiót igénylő ischaemiás szívbetegség, mitralisbillentyű-betegség) evidenciákon alapuló, hatékony kezelése reverz szubsztrátremodellációt előidézve a PF-ban eltöltött idő csökkenését és az ablatio sikerarányának javulását eredményezheti. Pitvarfibrilláló betegeknél, eredményes billentyű- vagy coronariaműtét után érdemes a sinusritmus visszaállítását megpróbálni. Kimutatták, hogy a pitvari fibroticus folyamatok mérsékelhetők a RAAS és a HMG-CoA-reduktáz gátlása (angiotenzinkonvertálóenzim-gátlók, angiotenzinreceptor-blokkolók, statinok), továbbá többszörösen telítetlen zsírsavak alkalmazása révén. A csökkent ejekciós frakciójú szívelégtelenség gyógyszeres terápiája (angiotenzinkonvertálóenzim-gátlók, béta-blokkolók, mineralokortikoidreceptor-antagonisták) mellett a központi szimpatikus tónusra ható moxonidinnek is szerepet tulajdonítanak a PF prevenciója szempontjából [3–5].

Következtetések

A PVI a PF általánosan elfogadott, széles körben alkalmazott terápiás módszere, amelynek sikeraránya azonban, különösen perzisztensen pitvarfibrilláló egyének esetén, a javuló eredmények ellenére sem emelhető egy bizonyos határ fölé. Noha az ablatiót követő arrhythmiavisszatérés oka a korai időszakban a VP-ok szájadékánál képzett heg vezetőképességének a helyreállása, később a PF-szubsztrát progrediálása miatt újul ki a ritmuszavar. PF esetén a terápiás siker növelése érdekében tehát olyan kezelési stratégiákra is szükség lehet, amelyek a PF patomechanizmusában szerepet játszó számos lehetséges tényezőt figyelembe véve célozzák meg a ritmuszavar eliminálását. A PF fenntartásában jelentőséggel bíró, újonnan felismert faktorok (pitvari epicardialis zsírszövet és fibrosis, nem VP-eredetű arrhythmogen gócok, rotorok, autonóm idegrendszeri hatások) mértéke nagyfokú egyéni változatosságot mutat. Ezeknek a tényezőknek a vizsgálatára egyre több noninvazív módszer (CT, DE-MRI, testfelszíni térképezés) áll rendelkezésre. Az arrhythmogen trigger- és szubsztrátmechanizmusok azonosítása olyan egyénre szabott terápiás módszerek (fibrosis mérséklése a RAAS gátlásán keresztül, hegek homogenizálása, rotorok és nem VP-eredetű fókuszok ablatiója, neuromoduláció) kidolgozását teszik lehetővé, amelyek alkalmazása a jelenleg evidenciákon alapuló VP-ablatio hosszú távú eredményességére is kedvező hatással lehet. Mindezek mellett, a tartós terápiás siker érdekében, elengedhetetlen a fennálló kockázati tényezők hatékony csökkentése, illetve kezelése.

Anyagi támogatás: A közlemény megírása, illetve a kapcsolódó kutatómunka anyagi támogatásban nem részesült.

Szerzői munkamegosztás: K. Sz.: Szakirodalmi adatok gyűjtése, a kézirat piszkozatának megírása, ábrák elkészítése. D. G.: Szakirodalmi adatok gyűjtése, a kézirat piszkozatának megírása. P. I.: A dolgozat koncepciójának kialakítása, a megfogalmazottak pontosítása. A cikk végleges változatát valamennyi szerző elolvasta és jóváhagyta.

Érdekeltségek: A szerzőknek nincsenek érdekeltségeik.

Irodalom

[1] Chugh SS, Havmoeller R, Narayanan K, et al. Worldwide epidemiology of atrial fibrillation: a Global Burden of Disease 2010 Study. Circulation 2014; 129: 837–847.
[2] Gal P, Marrouche NF. Magnetic resonance imaging of atrial fibrosis: redefining atrial fibrillation to a syndrome. Eur Heart J. 2017; 38: 14–19.
[3] Nalliah CJ, Sanders P, Kottkamp H, et al. The role of obesity in atrial fibrillation. Eur Heart J. 2016; 37: 1565–1572.
[4] Kirchhof P, Calkins H. Catheter ablation in patients with persistent atrial fibrillation. Eur Heart J. 2017; 38: 20–26.
[5] Lau DH, Schotten U, Mahajan R, et al. Novel mechanisms in the pathogenesis of atrial fibrillation: practical applications. Eur Heart J. 2016; 37: 1573–1581.
[6] Auer J. Fat: an emberging player in the field of atrial fibrillation. Eur Heart J. 2017; 38: 62–65.
[7] Haïssaguerre M, Jaïs P, Shah DC, et al. Spontaneous initiation of atrial fibrillation by ectopic beats originating in the pulmonary veins. N Engl J Med. 1998; 339: 659–666.
[8] Rubart M, Zipes DP. Genesis of cardiac arrhythmias: Electrophysiological considerations. In: Zipes DP, Libby P, Bonow RO, et al. (eds.) Braunwald's heart disease. A textbook of cardiovascular medicine. Elsevier Saunders, Philadelphia, PA, 2005; pp. 653–688.
[9] Cappato R, Calkins H, Chen SA, et al. Updated worldwide survey on the methods, efficacy, and safety of catheter ablation for human atrial fibrillation. Circ Arrhythm Electrophysiol. 2010; 3: 32–38.
[10] Kuck KH, Brugada J, Fürnkranz A, et al. Cryoballoon or radiofrequency ablation for paroxysmal atrial fibrillation. N Engl J Med. 2016; 374: 2235–2245.
[11] Narayan SM, Krummen DE, Shivkumar K, et al. Treatment of atrial fibrillation by the ablation of localized sources. J Am Coll Cardiol. 2012; 60: 628–636.
[12] Santangeli P, Zado ES, Hutchinson MD, et al. Prevalence and distribution of focal triggers in persistent and long-standing persistent atrial fibrillation. Heart Rhythm 2016; 13: 374–382.
[13] Di Biase L, Burkhardt JD, Mohanty P, et al. Left atrial appendage: an underrecognized trigger site of atrial fibrillation. Circulation 2010; 122: 109–118.
[14] Lin WS, Tai CT, Hsieh MH, et al. Catheter ablation of paroxysmal atrial fibrillation initiated by non-pulmonary vein ectopy. Circulation 2003; 107: 3176–3183.
[15] Lee SH, Tai CT, Hsieh MH, et al. Predictors of non-pulmonary vein ectopic beats initiating paroxysmal atrial fibrillation: Implication for catheter ablation. J Am Coll Cardiol. 2005; 46: 1054–1059.
[16] Yamaguchi T, Tsuchiya T, Miyamoto K, et al. Characterization of non-pulmonary vein foci with an EnSite array in patients with paroxysmal atrial fibrillation. Europace 2010; 12: 1698–1706.
[17] Chang HY, Lo LW, Lin YJ, et al. Long-term outcome of catheter ablation in patients with atrial fibrillation originating from non-

pulmonary vein ectopy. J Cardiovasc Electrophysiol. 2013; 24: 250–258.
[18] Santangeli P, Marchlinski FE. Techniques for the provocation, localization, and ablation of non-pulmonary vein triggers for atrial fibrillation. Heart Rhythm 2017; 14: 1087–1096.
[19] Kugler Sz, Nagy N, Rácz G, et al. Presence of cardiomyocytes exhibiting Purkinje-type morphology and prominent connexin 45 immunoreactivity in the myocardial sleeves of cardiac veins. Heart Rhythm 2018; 15: 258–264.
[20] Rubenstein DS, Fox LM, McNulty JA, et al. Electrophysiology and ultrastructure of Eustachian ridge from cat right atrium: a comparison with SA node. J Mol Cell Cardiol. 1987; 19: 965–976.
[21] Ozcan EE, Széplaki G, Merkely B, et al. Isolation of persistent left superior vena cava during atrial fibrillation ablation. Indian Pacing Electrophysiol J. 2015; 15: 130–132.
[22] Waks JW, Josephson ME. Mechanisms of atrial fibrillation – Reentry, rotors and reality. Arrhythm Electrophysiol Rev. 2014; 3: 90–100.
[23] Wijffels MC, Kirchhof CJ, Dorland R, et al. Atrial fibrillation begets atrial fibrillation. A study in awake chronically instrumented goats. Circulation 1995; 92: 1954–1968.
[24] Hocini M, Nault I, Wright M, et al. Disparate evolution of right and left atrial rate during ablation of long-lasting persistent atrial fibrillation. J Am Coll Cardiol. 2010; 55: 1007–1016.
[25] Nademanee K, McKenzie J, Kosar E, et al. A new approach for catheter ablation of atrial fibrillation: mapping of the electrophysiologic substrate. J Am Coll Cardiol. 2004; 43: 2044–2053.
[26] Singh SM, d'Avila A, Kim YH, et al. The modified stepwise ablation guided by low-dose ibutilide in chronic atrial fibrillation trial (the MAGIC-AF study). Eur Heart J. 2016; 37: 1614–1621.
[27] Sághy L, Tutuianu C, Szilágyi J. Atrial tachycardias following atrial fibrillation ablation. Curr Cardiol Rev. 2015; 11: 149–156.
[28] Wylie JV Jr, Peters DC, Essebag V, et al. Left atrial function and scar after catheter ablation of atrial fibrillation. Heart Rhythm 2008; 5: 656–662.
[29] Nori D, Raff G, Gupta V, et al. Cardiac magnetic resonance imaging assessment of regional and global left atrial function before and after catheter ablation for atrial fibrillation. J Interv Card Electrophysiol. 2009; 26: 109–117.
[30] Platonov PG. Atrial fibrosis: an obligatory component of arrhythmia mechanisms in atrial fibrillation? J Geriatr Cardiol. 2017; 14: 233–237.
[31] Haemers P, Hamdi H, Guedj K, et al. Atrial fibrillation is associated with the fibrotic remodelling of adipose tissue in the subepicardium of human and sheep atria. Eur Heart J. 2017; 38: 53–61.
[32] Higuchi K, Cates J, Gardner G, et al. The spatial distribution of late gadolinium enhancement of left atrial magnetic resonance imaging in patients with atrial fibrillation. JACC Clin Electrophysiol. 2018; 4: 49–58.
[33] Akoum N, Wilber D, Hindricks G, et al. MRI assessment of ablation-induced scarring in atrial fibrillation: analysis from the DECAAF study. J Cardiovasc Electrophysiol. 2015; 26: 473–480.
[34] Chen PS, Chen LS, Fishbein MC, et al. Role of the autonomic nervous system in atrial fibrillation. Pathophysiology and therapy. Circ Res. 2014; 114: 1500–1515.
[35] La Gerche A, Schmied CM. Atrial fibrillation in athletes and the interplay between exercise and health. Eur Heart J. 2013; 34: 3599–3602.
[36] Nielsen JR, Wachtell K, Abdulla J. The relationship between physical activity and risk of atrial fibrillation – A systematic review and meta-analysis. J Atr Fibrillation 2013; 5: 789.
[37] Apor P. Atrial fibrillation and physical activity. [Pitvarfibrilláció és a fizikai aktivitás.] Orv Hetil. 2013; 154: 503–509. [Hungarian]
[38] Mokhayeri Y, Nashemi-Nazari SS, Mansournia MA, et al. The association between physical activity and atrial fibrillation applying the Heaviside function in survival analysis: the Multi-Ethnic Study of Atherosclerosis. Epidemiol Health 2017; 39: e2017024.
[39] Turagam MK, Flaker GC, Velagapudi P, et al. Atrial fibrillation in athletes: pathophysiology, clinical presentation, evaluation and management. J Atr Fibrillation 2015; 8: 1309.
[40] Wilson M, O'Hanlon R, Prasad S, et al. Diverse patterns of myocardial fibrosis in lifelong, veteran endurance athletes. J Appl Physiol (1985). 2011; 110: 1622–1626.
[41] Vágó H, Róka A, Acsády Gy, et al. Parasympathetic cardiac nerve stimulation with implanted coronary sinus lead. J Cardiovasc Electrophysiol. 2004; 15: 588–590.
[42] Soós P, Merkely B, Horvát PM, et al. Determinants and effects of electrical stimulation of the inferior interatrial parasympathetic plexus during atrial fibrillation. J Cardiovasc Electrophysiol. 2005; 16: 1362–1367.
[43] Spronk HM, De Jong AM, Verheule S, et al. Hypercoagulability causes atrial fibrosis and promotes atrial fibrillation. Eur Heart J. 2017; 38: 38–50.
[44] Fox CS, Parise H, D'Agostino RB, et al. Parental atrial fibrillation as a risk factor for atrial fibrillation in offspring. JAMA 2004; 291: 2851–2855.
[45] Mommersteeg MT, Brown NA, Prall OW, et al. *Pitx2c* and *Nkx2-5* are required for the formation and identity of the pulmonary myocardium. Circ Res. 2007; 101: 902–909.
[46] Lubitz SA, Ozcan C, Magnani JW, et al. Advances in the genetics of atrial fibrillation: Implications for future research directions and personalized medicine. Circ Arrhythm Electrophysiol. 2010; 3: 291–299.
[47] Tucker NR, Ellinor PT. Emerging directions in the genetics of atrial fibrillation. Circ Res. 2014; 114: 1469–1482.
[48] Gudbjartsson DF, Holm H, Sulem P, et al. A frameshift deletion in the sarcomere gene *MYL4* causes early-onset familial atrial fibrillation. Eur Heart J. 2017; 38: 27–34.
[49] Kopecky SL, Gersh BJ, McGoon MD, et al. The natural history of lone atrial fibrillation: a population-based study over three decades. N Engl J Med. 1987; 317: 669–674.
[50] Godtfredsen J. (ed.) Atrial fibrillation: Etiology, course and prognosis: A follow-up study of 1212 cases. Munksgaard International Publishers Ltd., Copenhagen, 1975.
[51] Lee SS, Kong KA, Kim D, et al. Clinical implication of an impaired fasting glucose and prehypertension related to new onset atrial fibrillation in a healthy Asian population without underlying disease: a nationwide cohort study in Korea. Eur Heart J. 2017; 38: 2599–2607.
[52] Schmitt J, Duray G, Gersh BJ, et al. Atrial fibrillation in acute myocardial infarction: a systematic review of the incidence, clinical features and prognostic implications. Eur Heart J. 2009; 30: 1038–1045.
[53] Frost L, Hune LJ, Vestergaard P. Overweight and obesity as risk factors for atrial fibrillation or flutter: the Danish Diet, Cancer, and Health Study. Am J Med. 2005; 118: 489–495.
[54] Zhang L, Hou Y, Po SS. Obstructive sleep apnoea and atrial fibrillation. Arrhythm Electrophysiol Rev. 2015; 4: 14–18.

(Kugler Szilvia dr.,
Budapest, Városmajor u. 68., 1122
e-mail: kugler.szilvia@med.semmelweis-univ.hu)

DOI:10.14753/SE.2025.3172
ESC HEART FAILURE
SHORT COMMUNICATION
ESC Heart Failure 2022; **9**: 2747–2752
Published online 18 May 2022 in Wiley Online Library (wileyonlinelibrary.com) **DOI:** 10.1002/ehf2.13972

Inflammasome activation in end-stage heart failure-associated atrial fibrillation

Szilvia Kugler[1†], Zsófia Onódi[2,3,4†], Mihály Ruppert[1], Alex Ali Sayour[1], Attila Oláh[1], Kálmán Benke[1], Péter Ferdinandy[2,5], Béla Merkely[1†], Tamás Radovits[1†] and Zoltán V. Varga[2,3,4*†]

[1]*Heart and Vascular Center, Semmelweis University, Budapest, Hungary;* [2]*Department of Pharmacology and Pharmacotherapy, Semmelweis University, Budapest, Hungary;* [3]*HCEMM-SU Cardiometabolic Immunology Research Group, Budapest, Hungary;* [4]*MTA-SE "Momentum" Cardio-Oncology and Cardioimmunology Research Group, Budapest, Hungary; and* [5]*Pharmahungary Group, Szeged, Hungary*

Abstract

Aims Inflammatory pathways are increasingly recognized as an important factor in the pathophysiology of both heart failure (HF) and atrial fibrillation (AF). However, there is no data about inflammation-related histological and molecular alterations in HF-associated AF. The objective of our study was to investigate inflammatory pathways and fibrosis in end-stage HF-associated AF.

Methods and results Left atrial samples of 24 male patients with end stage ischemic HF undergoing heart transplantation were analysed. Twelve patients suffered from sustained AF while the others had no documented AF. The expression of inflammasome sensors and their downstream signalling were investigated by Western blot. No differences were observed in the expression of inflammasome sensors between the two groups, while cleaved caspase-1 increased tendentiously in the AF group ($P = 0.051$). Cleaved caspase-1 also showed significant correlation with the expression of interleukin-1β and its cleaved form in the total population and in the AF group ($P < 0.05$). The presence of myocardial and epicardial macrophages were assessed by ionized calcium-binding adaptor molecule 1 (Iba1) immunostaining. Number of macrophages showed a tendency towards elevation in the left atrial myocardium and epicardium of AF compared with SR group. The amount of total and interstitial fibrosis was determined on Masson's trichrome-stained sections. Histological assessment revealed no difference between AF and SR groups in the amount of either total or interstitial fibrosis.

Conclusions This is the first study on inflammation-related differences between HF with SR or AF showing elevated inflammasome activity and enhanced macrophage infiltration in left atrial samples of patients with AF.

Keywords Heart failure; Atrial fibrillation; Inflammasome; Macrophages; Fibrosis

Received: 30 November 2021; Revised: 23 April 2022; Accepted: 4 May 2022
**Correspondence to: Zoltán V. Varga, Department of Pharmacology and Pharmacotherapy, Semmelweis University, Nagyvárad tér 4, H-1089 Budapest, Hungary.*
Tel: +36-1-210-4412; Fax: +36-1-210-4416. Email: varga.zoltan@med.semmelweis-univ.hu
The work was performed at the following institutions: Heart and Vascular Center, Semmelweis University, Budapest, Hungary; Department of Pharmacology and Pharmacotherapy, Semmelweis University, Budapest, Hungary.
[†]These authors contributed equally to this work.

Background

Atrial fibrillation (AF) is the most common sustained cardiac arrhythmia. Heart failure (HF) is a known risk factor for AF; however, numerous HF patients never develop AF indicating presumable pathological differences between the types of HF associated with AF or sinus rhythm (SR). There is a growing number of evidence that inflammatory mechanisms contribute to the pathogenesis of AF.[1,2] Although inflammasome activity is observed among patients with HF generally,[3] there is lack of publications investigating whether the presence of AF is associated with enhanced inflammation in atrial tissues of HF patients.

Aims

We aimed to assess whether there is a relationship between inflammation and HF-associated AF in failing human

hearts. The focus of our research was on canonical inflammasome activation.

Methods

De-identified human left atrial samples from explanted hearts of 24 patients with end-stage ischemic HF undergoing heart transplantation were obtained from the Transplantation Biobank of the Heart and Vascular Center at Semmelweis University, Budapest, Hungary. The project complies with the Declaration of Helsinki and it was approved by the institutional and national ethics committee (ethical permission numbers: ETT TUKEB 7891/2012/EKU (119/PI/12.) and ETT TUKEB IV/10161–1/2020). All patients provided written informed consent. Half of the patients had no documented AF (SR, *n* = 12) and the other half suffered from persistent AF (AF, *n* = 12). All individuals were male between 43–64 years of age (SR: median 56.5 [IQR 48–60] years, AF: median 57.5 [IQR 54.5–60.5] years) with body mass index of 18.2–33.2 kg/m^2 (SR: median 28.9 [IQR 25.0–30.2]kg/m^2, AF: median 25.8 [IQR 23.5–28.8]kg/m^2), ejection fraction of 10–36% (SR: median 20 [IQR 18–25]%, AF: median 24 [IQR: 22–26]%) and left atrial length of 47-82 mm (SR: median 58 [IQR 52–65]mm, AF: median 63 [IQR 59–66]mm). None of them suffered from diabetes mellitus (*Table 1*).

Inflammasome activation was assessed by Western blot from tissue lysates prepared from left atrial samples as previously described.[3] The expression of inflammasome sensors (NLR family, pyrin domain containing 1 and 3 [NALP1, NLRP3], absent in melanoma 2 [AIM2], NLR family CARD domain-containing protein 4 [NLRC4]) and their downstream signalling (apoptosis-associated speck-like protein containing a CARD [ASC], caspase-1, interleukin-1β) were analysed (Supplementary Figure). Five samples (two from SR and three from AF) were excluded due to low-quality homogenates (*Figure 1A*). Image analysis was performed using Image Lab™ 6.0 software (Bio-Rad, Hercules, CA, USA).

To assess the presence of macrophages in the epicardial and myocardial areas of left atrial samples (*Figure 2A*) from SR (myocardium: *n* = 6, epicardium: *n* = 4) and AF (myocardium: *n* = 7, epicardium: *n* = 6) groups, immunohistochemistry was performed to stain ionized calcium-binding adaptor

Table 1 Patient characteristics

	Patients with sinus rhythm (*n* = 12)	Patients with atrial fibrillation (*n* = 12)
Age (years)	56.5 (48.0–60.0)	57.5 (54.5–60.5)
Sex (M/F)	12 (100)/0 (0)	12 (100)/0 (0)
BMI (kg/m^2)	28.9 (25.0–30.2)	25.8 (23.5–28.8)
Aetiology of heart failure		
Ischemic	12 (100)	12 (100)
Non-ischemic	0 (0)	0 (0)
NYHA stage		
II	0 (0)	1 (9)
III	7 (58)	7 (64)
IV	5 (42)	3 (27)
Echocardiography parameters		
EF (%)	20 (18–25)	24 (22–26)
LA length	58 (52–65)	63 (59–66)
Artificial heart valve	0 (0)	1 (8)
CRT	3 (25)	5 (42)
Medication		
Parenteral loop diuretics	3 (25)	4 (33)
Parenteral inotropic support	3 (25)	4 (33)
Parenteral vasopressor agent	0 (0)	1 (8)
Mechanical circulatory support	1 (8)	1 (8)
Mechanical ventilation	0 (0)	1 (8)
Ventricular tachycardia	1 (8)	4 (33)
Diabetes mellitus	0 (0)	0 (0)
Infection		
Presence of infection	4 (33)	4 (33)
Antibiotic treatment due to infection	3 (25)	4 (33)
White blood cell count (G/L)	7.6 (6.7–9.5)	8.9 (6.6–9.4)
CRP (mg/L)	4.7 (1.6–9.7)	3.0 (2.4–4.4)
PCT (μg/L)	0.03 (0.02–0.05)	0.10 (0.05–0.13)

The most relevant baseline characteristics of the patients whom left atrial tissues were examined are listed. All patients were male with ischemic cardiomyopathy. In case of categorical variables, data are presented as number (%), while in case of continuous variables, median values (interquartile range) are shown.
BMI, body mass index; CRP, C-reactive protein; CRT, cardiac resynchronisation therapy; EF, ejection fraction; F, female; LA, left atrial; M, male; NYHA, New-York Heart Association; PCT, procalcitonin.

DOI:10.14753/SE.2025.3172

Figure 1 Inflammasome activation in heart failure-associated atrial fibrillation. (A) Western blot detection of inflammasome markers in left atrial samples of ischemic HF patients with SR (blue) and AF (red). Samples excluded due to low-quality homogenates are shown in parentheses. GAPDH is shown as loading control. No signal could be detected for NALP1 (not shown). (B) Analysis of normalized band intensities of inflammasome markers ($P > 0.05$, Student's *t*-test; $n = 9–10$). (C) Correlation and regression analysis of inflammasome sensors and markers of their downstream signalling based on Western blot detection. Cleaved caspase-1 showed correlation with interleukin-1β and its cleaved form both in the total population ($P = 0.005$ and 0.004, respectively) and in AF group ($P = 0.01$), but not in SR group. No correlation was found with any inflammasome sensors ($P > 0.05$, Pearson-correlation; $n = 9–10$). Continuous data passed the Shapiro–Wilk normality test.

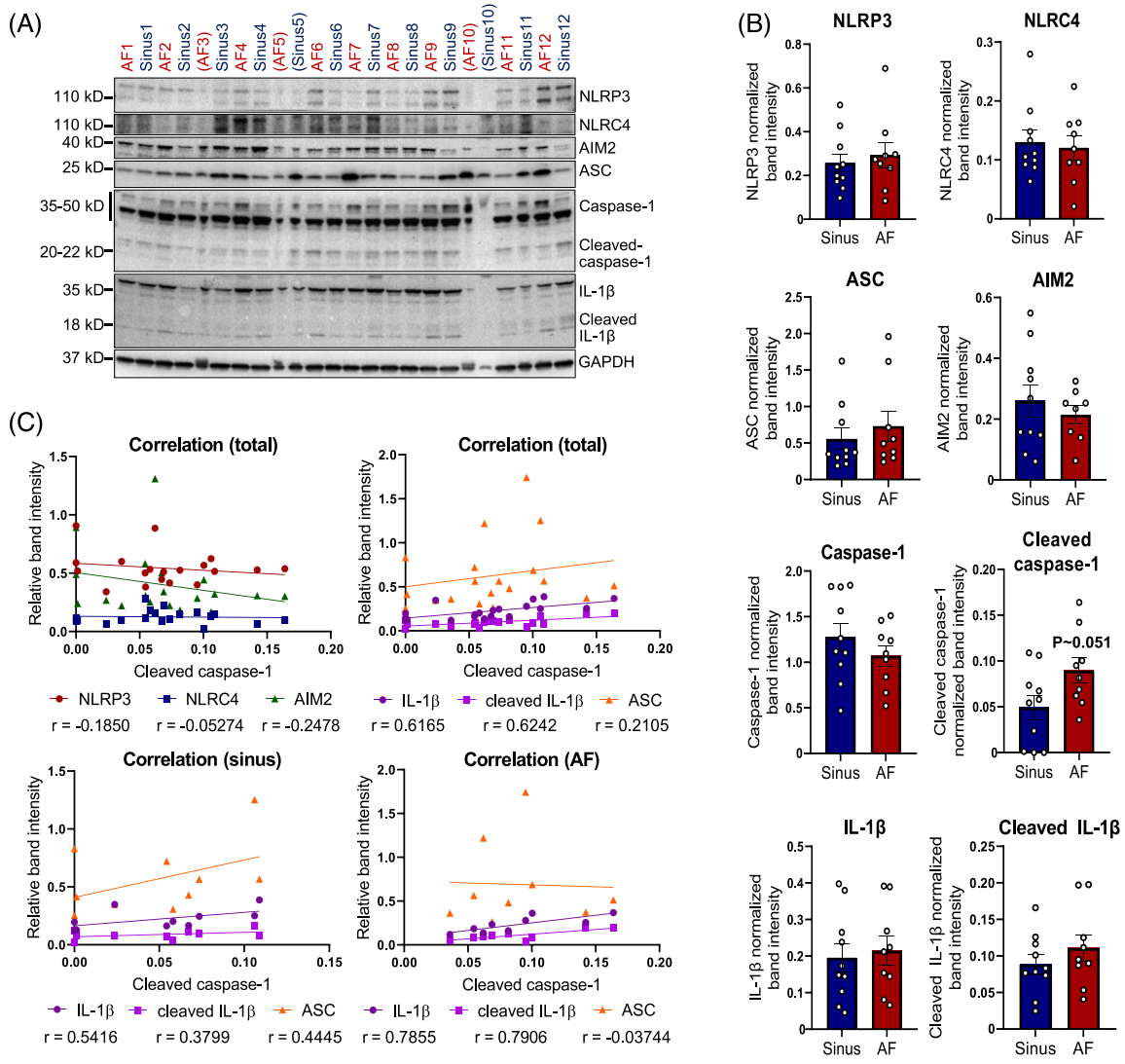

molecule 1 (Iba1, marker of monocyte–macrophage lineage). An outlier was identified by ROUT test (Q = 1%) in the epicardial subgroup of SR and was excluded from data analysis.

The amount of total and interstitial fibrosis was determined on Masson's trichrome-stained sections (SR: $n = 6$, AF: $n = 7$). Percentage of total fibrosis was defined as the amount of fibrotic regions compared with the whole area of the section, while the amount of interstitial fibrosis was correlated to a modified area which did not include the epicardium, subepicardial fibrotic area and fibrosis surrounding vascular structures (*Figure 3A*). An outlier at the interstitial fibrosis subgroup of SR was excluded from statistical analysis.

Stained sections were visualized and images were acquired using Leica DM3000 bright field microscope (Leica Microsystems, Wetzlar, Germany). For fibrosis and macrophage quantification, ImageJ (Image Processing and Analysis in Java) 1.51 k program was applied. Continuous data were presented as mean ± standard error of the mean or median with interquartile range. Categorical data were presented as numbers (percentages). Comparisons of two groups were performed using unpaired Student's *t*-test. All analyses were

Figure 2 Left atrial macrophage infiltration in heart-failure associated atrial fibrillation. (A) The method for quantitative analysis of macrophage infiltration is demonstrated on a haematoxylin–eosin stained section. Left atrial macrophages were counted at several unit areas and averaged for the sample. Myocardial (yellow squares) and epicardial (red squares) regions were investigated separately (scale bar: 1000 μm). (B) Average macrophage number per unit area was higher at both the myocardium and the epicardium of the AF samples compared with the SR group. However, this difference was not significant ($P > 0.05$, Student's *t*-test; $n = 3–7$). (C) Representative images about the presence of Iba1 positive macrophages in the myocardium (M) and epicardium (E) of AF and SR patients. Different amount of macrophage accumulation at the high-magnification images indicates heterogeneous distribution of these cells within a given sample (scale bars: 60 μm). Continuous data passed the Shapiro–Wilk normality test.

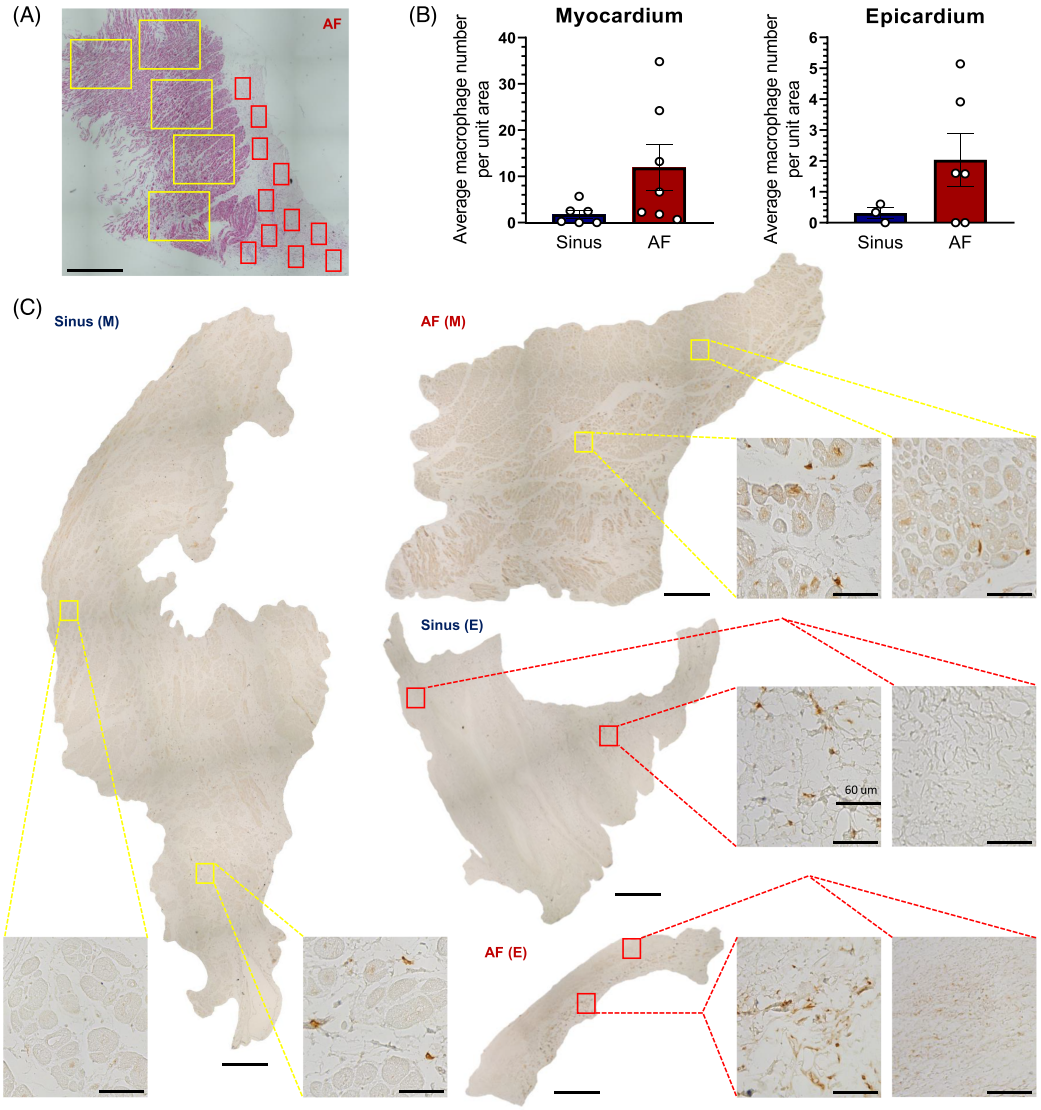

conducted using GraphPad Prism 8. (GraphPad Software Inc). We considered a *P*-value of <0.05 to be statistically significant.

Results

No significant differences were observed in the expression of any types of inflammasome sensors between AF and SR groups. There was a strong tendency that cleaved caspase-1 was increased in the AF group versus the SR group ($P = 0.051$) (*Figure 1B*). Furthermore, it showed significant correlation with the expression of interleukin-1β and its cleaved form ($P < 0.05$). This correlation was observed in the total population and in AF group alone but not in SR group. In contrast, cleaved caspase-1 level showed no correlation with the expression of inflammasome sensors, suggesting overall a primary effect on inflammasome activity rather than on inflammasome priming (*Figure 1C*).

Figure 3 Amount of left atrial fibrosis in heart failure with sinus rhythm or atrial fibrillation (A) Assessment of total and interstitial fibrosis after Masson's trichrome-staining of left atrial samples (scale bars: 1000 μm). (B) Percentages of both total and interstitial fibrosis proved to be the same at the two groups ($P > 0.05$, Student's *t*-test; $n = 5–7$). (C) Representative images of total (T) and interstitial (I) fibrosis from SR and AF groups (scale bars: 1000 μm). Continuous data passed the Shapiro–Wilk normality test.

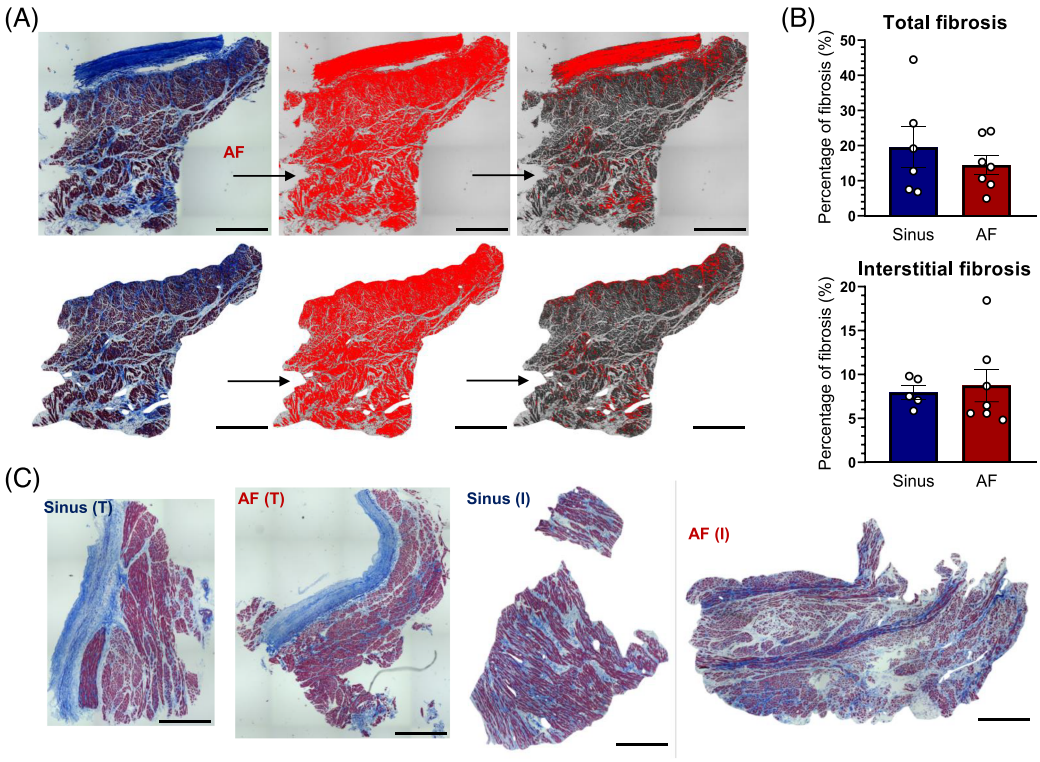

We found enhanced macrophage presence in the left atrial myocardium of AF compared with SR group. Likewise, macrophages were present in a higher number in the left atrial epicardium of AF than of SR. Neither differences were however significant due to high variability (*Figure 2B,C*).

Histological assessment of left atrial samples revealed no relevant difference between AF and SR groups in the amount of total fibrosis and interstitial fibrosis (*Figure 3B,C*).

Discussion and conclusions

Inflammasomes are well-characterized signalling complexes that regulate immune responses. Their activation involves priming (transcription of inflammasome components and effectors) and triggering (enhancing the assembly of the inflammasome complex). Elevated protein levels of active caspase-1 and NLRP3 as well as enhanced macrophage infiltration in atrial tissue were reported in chronic and postoperative AF, suggesting that NLRP3 inflammasome activation might contribute to these phenomena.[1,2] Additionally, some previous studies verified elevated inflammatory markers (C-reactive protein, interleukin-6, tumour necrosis factor-alpha) in venous blood samples of HF patients suffering from AF compared with HF patients with SR,[4–6] while another group showed that patients with typical (paroxysmal/persistent/permanent) AF had significantly elevated serum concentrations of interleukin-10 and tumour necrosis factor-alpha compared with patients with AF only. This result was explained by the relatively high (20%) presence of HF in typical AF group compared with the absence of any structural heart diseases in the case of lone AF.[7] Elevated serum levels of high-sensitivity C-reactive protein and interleukin-6 were demonstrated to strongly associate with the risk of HF-related hospitalization among patients with AF.[8] The current research was the first that analysed inflammation-related differences between HF patients with SR and AF in cardiac tissue samples. In our study, protein levels of inflammasome sensors were unaltered between AF and SR groups, indicating unaffected priming signal. However, tendency towards increase in the expression of cleaved caspase-1 and its significant correlation with the expression of (cleaved) interleukin-1β in AF samples suggest enhanced triggering for inflammasome activation in end-stage HF-associated AF.

The main limitation of this study is the lack of enough evidence that inflammasome activity contributes directly to maintaining AF in patients with end-stage HF. Further studies

are needed to define any causalities, correlations and consequences, to determine possible prognostic factors and to evaluate whether inflammasome activation has a diagnostic role in end-stage HF-associated AF.

In conclusion, this is the first study on inflammation-related differences in failing human hearts with SR and AF that analysed cardiac tissues. It verified that inflammasome activity may associate with AF in patients with end-stage HF. Enhanced macrophage infiltration also indicates higher levels of inflammation in AF samples, while HF-associated AF may be independent of cardiac fibrosis.

Acknowledgements

We are grateful to Andrea Kovács, Edina Urbán, Kincső Gulyás, Benjamin Prokaj, Gábor Kapus, Zsolt Bári, Imre J. Barabás, and Krisztián Z. Maró for their excellent technical assistance.

Conflict of interest

P.F. is the founder and CEO of Pharmahungary Group, a group of R&D companies. All other authors have nothing to disclose.

Funding

This work was supported by NVKP_16-1-2016-0017 ('National Heart Program'), which has been implemented with the support provided from the National Research, Development and Innovation Fund of Hungary, financed under the NVKP_16 funding scheme. The research was also financed by the Thematic Excellence Programme of the Ministry for Innovation and Technology in Hungary: NKFIH-1277-2/2020, 2020-4.1.1.-TKP2020, TKP2021-NVA/TKP2021-NKTA, and TKP2021-EGA-23. The work was supported by the European Union's Horizon 2020 research and innovation programme under grant agreement no. 739593. Further support was provided by grant VEKOP-2.3.2-16-2016-00002 and by 2020-1.1.6-JÖVŐ-2021-00013 ('Befektetés a jövőbe' NFKIH). This project was supported by grants from the National Research, Development and Innovation Office (NKFIH) of Hungary (K134939 to T.R. and FK134751 to Z.V.V.). Z.V.V. is supported by the New National Excellence Program of the Ministry of Human Capacities (ÚNKP-21-5) and by the János Bolyai Research Scholarship of the Hungarian Academy of Sciences. Z.O. was supported by EFOP-3.6.3-VEKOP-16-2017-00009, 'Az orvos-, egészségtudományi- és gyógyszerészképzés tudományos műhelyeinek fejlesztése'.

Supporting information

Additional supporting information may be found online in the Supporting Information section at the end of the article.

Data S1. Supporting information.

References

1. Yao C, Veleva T. Enhanced cardiomyocyte NLRP3 inflammasome signaling promotes atrial fibrillation. *Circulation*. 2018; **138**: 2227–2242.
2. Heijman J, Muna AP, Veleva T, Molina CE, Sutanto H, Tekook M, Wang Q, Abu-Taha IH, Gorka M, Künzel S, El-Armouche A, Reichenspurner H, Kamler M, Nikolaev V, Ravens U, Li N, Nattel S, Wehrens XHT, Dobrev D. Atrial myocyte NLRP3/CaMKII nexus forms a substrate for postoperative atrial fibrillation. *Circ Res*. 2020; **127**: 1036–1055.
3. Onódi Z, Ruppert M, Kucsera D, Sayour AA, Tóth VE, Koncsos G, Novák J, Brenner GB, Makkos A, Baranyai T, Giricz Z, Görbe A, Leszek P, Gyöngyösi M, Horváth IG, Schulz R, Merkely B, Ferdinandy P, Radovits T, Varga ZV. AIM2-driven inflammasome activation in heart failure. *Cardiovasc Res*. 2021; **117**: 2639–2651.
4. Nessler B, Nessler J, Kitlinski M, Gackowski A, Piwowarska W. Inflammatory markers (TNF-alpha, IL-6, CRP), BNP and spiroergometric stress test parameters in patients with heart failure and atrial fibrillation. In *4th Asian Pacific Congress of Heart Failure, Melbourne, Australia*. Australia: Elsevier Masson SAS; 2008. Abstract 17S. p S34.
5. Targoński R, Salczyńska D, Sadowski J, Cichowski L. Relationship between inflammatory markers and clinical patterns of atrial fibrillation in patients with congestive heart failure. *Kardiol Pol*. 2008; **66**: 729–736.
6. Putko BN, Wang Z, Lo J, Anderson T, Becher H, Dyck JRB, Kassiri Z, Oudit GY, Alberta HEART Investigators. Circulating levels of tumor necrosis factor-alpha receptor 2 are increased in heart failure with preserved ejection fraction relative to heart failure with reduced ejection fraction: Evidence for a divergence in pathophysiology. *PLoS One*. 2014; **9**: e99495.
7. Li J, Solus J, Chen Q, Rho YH, Milne G, Stein CM, Darbar D. Role of inflammation and oxidative stress in atrial fibrillation. *Heart Rhythm*. 2010; **7**: 438–444.
8. Benz AP, Aeschbacher S, Krisai P, Moschovits G, Blum S, Meyre P, Blum MR, Rodondi N, Di Valentino M, Kobza R, De Perna ML, Bonati LH, Beer JH, Kühne M, Osswald S, Conen D, BEAT-AF, Swiss-AF Investigators. Biomarkers of inflammation and risk of hospitalization for heart failure in patients with atrial fibrillation. *J Am Heart Assoc* 2021; **10**:e019168.

Received: 30 August 2022 | Revised: 4 August 2023 | Accepted: 5 August 2023
DOI: 10.1111/joa.13947
DOI:10.14753/SE.2025.3172

Journal of Anatomy
ANATOMICAL SOCIETY WILEY

ORIGINAL ARTICLE

Strong desmin immunoreactivity in the myocardial sleeves around pulmonary veins, superior caval vein and coronary sinus supports the presumed arrhythmogenicity of these regions

Szilvia Kugler[1] | Anna-Mária Tőkés[2] | Nándor Nagy[3] | Attila Fintha[4] | Krisztina Danics[2] | Márton Sághi[4] | Klára Törő[2] | Gergely Rácz[4] | Ágnes Nemeskéri[3]

[1]Heart and Vascular Centre, Semmelweis University, Budapest, Hungary
[2]Department of Pathology, Forensic and Insurance Medicine, Semmelweis University, Budapest, Hungary
[3]Department of Anatomy, Histology and Embryology, Semmelweis University, Budapest, Hungary
[4]Department of Pathology and Experimental Cancer Research, Semmelweis University, Budapest, Hungary

Correspondence
Szilvia Kugler, Heart and Vascular Centre, Semmelweis University, Budapest, Hungary.
Email: kugler.szilvia@med.semmelweis-univ.hu

Funding information
Hungarian Science Foundation NKFI grant, Grant/Award Number: 138664; István Apáthy Foundation's Research Grant; Research Excellence Programme of the Ministry for Innovation and Technology in Hungary, TKP2021-EGA-25 thematic programme of the Semmelweis University

Abstract

Myocardial sleeve around human pulmonary veins plays a critical role in the pathomechanism of atrial fibrillation. Besides the well-known arrhythmogenicity of these veins, there is evidence that myocardial extensions into caval veins and coronary sinus may exhibit similar features. However, studies investigating histologic properties of these structures are limited. We aimed to investigate the immunoreactivity of myocardial sleeves for intermediate filament desmin, which was reported to be more abundant in Purkinje fibers than in ventricular working cardiomyocytes. Sections of 16 human (15 adult and 1 fetal) hearts were investigated. Specimens of atrial and ventricular myocardium, sinoatrial and atrioventricular nodes, pulmonary veins, superior caval vein and coronary sinus were stained with anti-desmin monoclonal antibody. Intensity of desmin immunoreactivity in different areas was quantified by the ImageJ program. Strong desmin labeling was detected at the pacemaker and conduction system as well as in the myocardial sleeves around pulmonary veins, superior caval vein, and coronary sinus of adult hearts irrespective of sex, age, and medical history. In the fetal heart, prominent desmin labeling was observed at the sinoatrial nodal region and in the myocardial extensions around the superior caval vein. Contrarily, atrial and ventricular working myocardium exhibited low desmin immunoreactivity in both adults and fetuses. These differences were confirmed by immunohistochemical quantitative analysis. In conclusion, this study indicates that desmin is abundant in the conduction system and venous myocardial sleeves of human hearts.

KEYWORDS
arrhythmia, caval vein, conduction system, coronary sinus, desmin, pulmonary vein

1 | INTRODUCTION

Atrial fibrillation is the most common sustained cardiac arrhythmia. It can associate with serious complications such as ischemic stroke and heart failure. Several pathophysiological factors have been reported in the background of atrial fibrillation, namely atrial fibrosis (Gal & Marrouche, 2017; Haemers et al., 2017; Lau et al., 2016; Nattel, 2017), epicardial adipose tissue (Haemers et al., 2017; Lau

DOI:10.14753/SE.2025.3172

et al., 2016), inflammatory mechanisms (Haemers et al., 2017; Yao & Veleva, 2018), autonomic nerve activity (Chen et al., 2014; Lau et al., 2016), electrophysiological mechanisms (Lau et al., 2016; Nadadur et al., 2016; Waks & Josephson, 2014) and presence of arrhythmogenic foci (Haïssaguerre et al., 1998; Santangeli & Marchlinski, 2017).

Left atrial myocardium extending into the wall of pulmonary veins and forming myocardial sleeves are well-known sources of supraventricular tachyarrhythmias. Electrophysiological studies indicate that myocardial extensions into caval veins and coronary sinus exhibit similar feature (Chang et al., 2013; Lee et al., 2005; Lin et al., 2003; Santangeli et al., 2016; Santangeli & Marchlinski, 2017; Yamaguchi et al., 2010). Arrhythmogenicity of these regions has a well-established developmental background (Christoffels et al., 2010; Christoffels & Moorman, 2009; Weerd & Christoffels, 2016). However, human studies investigating histologic properties of these structures are limited.

Previously, we examined the connexin 45 immunoreaction to detect the cardiac conduction system and found prominent positive staining in the myocardial sleeves of pulmonary veins, superior caval vein and coronary sinus, indicating their potential pacemaker and/or conducting nature (Kugler et al., 2018). In the current study, we intended to investigate regional differences in desmin immunostaining in human hearts to provide further information about the presumed conducting phenotype of the venous myocardial sleeves. Desmin is a muscle-specific intermediate filament that plays role in maintaining the structure of sarcomeres, interconnecting the myofibrils through the Z-disks and linking them to the sarcolemma, the nucleus, and mitochondria (Capetanaki et al., 2007). Albeit desmin is not a dedicated marker for the cardiac pacemaker and conduction system, it was reported to be more abundant in the ventricular conduction system (Liu et al., 2020; Yoshimura et al., 2014) and the nodal regions (Liu et al., 2020; Mavroidis et al., 2020) than in the ventricular working myocardium of human hearts. Intermediate filaments in Purkinje fibers may play a supportive role against mechanical strain during heart contraction (Eriksson & Thornell, 1979) or they might bind glycogen particles and help maintaining the structural integrity of these large cells with peripheral myofibrils (Yoshimura et al., 2014). Impaired desmin has been documented to cause filament assembly defects and abnormal distribution of Ca^{2+} that may result in cardiac arrhythmias and conduction defects (Su et al., 2022).

2 | METHODS

2.1 | Human tissues

The work has been ethically approved by the Regional and Institutional Committee of Science and Research Ethics, Semmelweis University (Research Ethics 79 committee approval 122/2016) and the Research Ethics Committee of the Medical Research Council of Hungary (No. IV/1555-1/2021/EKU). The study was performed in accordance with the ethical standards as laid down in the 1964 Declaration of Helsinki and its later amendments or comparable ethical standards.

Demographic data, medical records of patients, and basic data of histological analyses are demonstrated in Table 1. Hearts were removed from cadavers of 15 adult humans. Clinical data were unknown in 8/15 cases. The heart of a 23-week-old fetus who was born alive but died at the early perinatal period was also investigated. Prior to death, 7 donors gave written consent for the use of their bodies for education and research {Willed (Whole) Body 77 Program - WWBP}. The remaining 9 hearts were removed from human cadavers during autopsies in possession on ethical approval. Cadavers were kept at 1–5°C until autopsies or fixation, which was performed at 12–72 h postmortem age. After removal during autopsies, hearts were immediately fixed.

Due to technical reasons, pulmonary veins were investigated in 11/16 and superior caval veins in 14/16 cases. The veins were separated from the atria at the level of their ostia and were cut transversely. Coronary sinus was investigated in 9/16 cases. Tissue samples were also obtained from sinoatrial and atrioventricular nodes, left and right atrium, left and right ventricle, and interventricular septum. Specimens were fixed either in 4% formaldehyde ($n = 14$) or in 70% ethanol ($n = 2$, including the fetal heart). After dehydration in graded concentrations of alcohol, tissue samples were embedded in paraffin and 3–6 μm sections were prepared. For general histology, paraffin sections were stained with hematoxylin–eosin and trichrome.

2.2 | Immunohistochemistry

After deparaffinization and rehydration through graded alcohols, slides were washed three times in phosphate-buffered saline (PBS).

Thereafter, desmin immunohistochemistry of ethanol-fixed sections was prepared as follows. Heat-induced citrate-based antigen retrieval method was applied (Vector Laboratories; Cat# H-3300) for 30 min. Protein blocking was carried out for 20 min with 1% bovine serum albumin in PBS, followed by overnight incubation at 4°C with mouse monoclonal antibody against human desmin (Dako; Clone D33; Cat# M0760; dilution 1:4000 for adults and 1:5000 for fetal hearts). Biotinylated horse anti-mouse IgG (Vector Laboratories; dilution 1:200) was used as a secondary antibody which was followed by an endogenous peroxidase activity-blocking step using 0,6% hydrogen peroxide (Sigma-Aldrich) in PBS for 10 min. After the formation of the avidin-biotinylated peroxidase complex (Vectastain Elite ABC kit; Vector Laboratories), the binding sites of the primary antibody were visualized by 4-chloro-1-naphthol (Sigma-Aldrich; Cat# C8890).

For desmin immunohistochemistry performed on formaldehyde-fixed, paraffin-embedded tissue sections, a heat-induced Tris-EDTA-based antigen retrieval method was applied (Dako; Target Retrieval Solution pH-9). Detection of desmin was performed by using mouse anti-human desmin monoclonal antibody (Dako; Clone D33; Cat#

TABLE 1 Demographic and medical data of patients and data of histological analyses.

Case	Age (years)	Sex	Medical history	Cause of death	Fixation	Investigated tissue	Stain	Quantitative analysis
1	Unknown	Unknown	Unknown	Unknown	Formaldehyde	SCV, RA	HE, desmin (1:200)	No
2	Unknown	Unknown	Unknown	Unknown	Formaldehyde	SCV, RA, RV	HE, desmin (1:200)	No
3	Unknown	Unknown	Unknown	Unknown	Formaldehyde	SCV, SAN, RA, IAS, RV	HE, trichrome, desmin (1:200)	No
4	Unknown	Unknown	Unknown	Unknown	Formaldehyde	SCV, CS, RA, IAS, IVS (left side), LV	HE, trichrome, desmin (1:200)	Yes
5	Unknown	Unknown	Unknown	Unknown	Formaldehyde	PV	HE, trichrome, desmin (1:200)	No
6	Unknown	Unknown	Unknown	Unknown	Formaldehyde	PV	HE, trichrome, desmin (1:200)	No
7	50	Female	Unknown	Suicide by hanging	Formaldehyde	SCV, CS, PV, SAN, RA, LA, IVS (left side), LV	HE, trichrome, desmin (1:400)	No
8	22	Female	None	Suicide by hanging	Formaldehyde	SCV, CS, PV, SAN, AVN, RA, LA, IVS (right side)	HE, trichrome, desmin (1:200)	Yes
9	86	Female	Hypertension, ischemic stroke, eversion carotid endarterectomy	Postoperative left ventricular failure due to chronic ischaemic heart disease	Formaldehyde	SCV, CS, PV, SAN, RA, LA, IVS (left side)	HE, trichrome, desmin (1:400)	No
10	54	Female	Hypertrophic obstructive cardiomyopathy (alcohol septal ablation), hypertension, ischemic stroke, liver cirrhosis, surgeries due to strangulated umbilical hernia and small bowel obstruction	Postoperative multiorgan failure and vasoplegia; congestive heart failure	Formaldehyde	SCV, CS, PV, SAN, RA, LA, IVS (left side)	HE, trichrome, desmin (1:400)	No
11	43	Male	Chronic alcohol abuse	Respiratory failure due to pneumonia; accompanying disease: left ventricular hypertrophy	Formaldehyde	SCV, CS, PV, SAN, RA, LA, IVS (left side)	HE, trichrome, desmin (1:400)	Yes
12	48	Male	Nicotinism	Left ventricular failure due to dilated cardiomyopathy	Formaldehyde	SCV, CS, PV, SAN, RA, LA, IVS (left side)	HE, trichrome, desmin (1:400)	Yes
13	52	Male	Master footballer, nicotinism	Sudden cardiac death due to acute myocardial infarction caused by severe three coronary vessel disease	Formaldehyde	SCV, CS, PV, SAN, RA, LA, IVS (left side)	HE, trichrome, desmin (1:400)	Yes
14	51	Female	None	Subarachnoid hemorrhage, respiratory sepsis	Formaldehyde	SCV, CS, PV, SAN, RA, LA, IVS (left and right side), RV	HE, trichrome, desmin (1:400)	No
15	64	Male	Unknown	Unknown	Ethanol	SCV, PV, SAN, AVN, RA, IVS (left and right side)	HE, trichrome, desmin (1:4000–1:5000), connexin 45 (1:50–1:100)	No
16	23-week old fetus	Unknown	Unknown	Unknown	Ethanol	SCV, SAN, RA, IVS, LV, RV	HE, trichrome, desmin (1:5000), connexin 45 (1:75)	No

Abbreviations: AVN, atrioventricular node; CS, coronary sinus; HE, hematoxylin–eosin; IAS, interatrial septum; IVS, interventricular septum; LV, left ventricle; PV, pulmonary vein; RA, right atrium; RV, right ventricle; SAN, sinoatrial node; SCV, superior caval vein.

DOI: 10.14753/SE.2025.3172

DOI:10.14753/SE.2025.3172

M0760; dilution 1:200 or 1:400) overnight at 4°C. Two different primary antibody concentrations were used due to the somewhat different histological characteristics of the individual specimens. Nevertheless, for different regions of a single heart, the same anti-desmin antibody dilution was applied. All the other steps of the immunohistochemical protocol (application of peroxidase and protein block, post-primary blocking, incubation with secondary antibody, applying the 3,3′-diaminobenzidine as chromogen, counterstaining of the nuclei with hematoxylin) were performed at room temperature (25°C) with Novolink™ Polymer Detection System (Leica Biosystems; Cat# RE7140-K).

Double labeling immunofluorescence analysis for connexin 45 and desmin was also prepared. Connexin 45 was detected with a rabbit polyclonal antibody (Santa Cruz Biotechnology, Inc.; Cat# sc-25716; dilution 1:50), while desmin was detected with mouse monoclonal antibody (Dako; Clone D33; Cat# M0760; dilution 1:5000). For fluorescent secondary antibodies, goat anti-rabbit IgG conjugated to Alexa Fluor 488 and goat anti-mouse IgG conjugated to Alexa Fluor 594 were applied (Invitrogen). Cell nuclei were stained with DAPI (Vector Laboratories).

Sections were covered by aqueous Poly/Mount (Polyscience, Inc.) and examined by Zeiss Axiophot photomicroscope and/or Zeiss confocal microscope system. Fluorescent images were captured with an Olympus DP50-CU digital camera (Olympus Optical Co., Ltd.), whereas an automated 3D-Histotech whole slide imaging system was used to image other sections.

2.3 | Immunohistochemical quantitative analysis

ImageJ (Image Processing and Analysis in Java) program was applied to perform a semiquantitative analysis for the intensity of desmin immunostaining at formaldehyde-fixed sections of 5 hearts. At least the ventricular subendocardial region, ventricular working myocardium, and one vein was examined in all cases but if possible, six different structures (superior caval vein, pulmonary vein, coronary sinus, sinoatrial node, ventricular conduction system, ventricular working myocardium) were investigated. For each structure, three representative regions were analyzed in the case of 4/5 hearts. Signal intensity of the immunoreactive cells of the conducting system and the extracardiac myocardial sleeves was compared with the ventricular working cardiomyocytes. For this analysis, an equal number of cardiomyocytes were chosen from every region. Difference between signal intensity at representative areas of the ventricular conduction system or myocardial sleeves and the working myocardium was also investigated. The total size of the analyzed areas was equal for each region. The Colour Deconvolution plugin was used to implement stain separation of hematoxylin-DAB stained images and the derived DAB image was chosen for quantification. Mean gray values of selected cells and areas were then measured and diagrams were created to demonstrate results. More details about quantitative analysis are documented in the Supplementary material.

3 | RESULTS

3.1 | Quantitative analysis of desmin immunostaining

Quantitative analysis of desmin labeling was prepared on the sections of formaldehyde-fixed adult hearts ($n = 5$). Investigation of one heart is detailed below (Figure 1), while quantifications of the other 4 specimens are shown in the Supplementary material (Figures S1-S10). Distinct structures of the heart were investigated (Figure 1a,d,g,j). There was a marked difference in immunopositivity between ventricular cardiomyocytes and Purkinje fibers (Figures 1b,e) and also between representative areas of the ventricular myocardium and conduction system (Figures 1c,f). Nevertheless, desmin positivity of the working myocardium was obvious. Both highly immunoreactive individual cardiomyocytes and representative region of the myocardial sleeve around the coronary sinus exhibited stronger staining than ventricular myocardium (Figures 1h,i). Myocardial sleeve of the superior caval vein displayed similarly prominent desmin labeling (Figures 1k,l). Based on the quantitative analysis, strongly immunoreactive cells of the conducting system and extracardiac myocardial sleeves exhibited much more prominent desmin signal intensity than ventricular working cardiomyocytes (Figure 1m). However, signal intensities of the examined representative areas differed less. This can be attributed to the mixture of strongly stained conducting-like cells with less immunoreactive working cardiomyocytes in the myocardial sleeves. Furthermore, non-staining connective tissue between cardiomyocytes also resulted in higher mean gray values of the examined areas (Figure 1n).

FIGURE 1 Quantitative analysis of desmin labeling for a formaldehyde-fixed heart. At the encircled region of ventricular working myocardium (a), both individual cardiomyocytes (b), and the framed area (c) exhibit moderate immunopositivity (a-inset). At the ventricular subendocardial region (d), Purkinje fibers display strong labeling (e), while some cardiomyocytes are stained weakly (f). In the myocardial sleeve of the coronary sinus (g), most cardiac cells are strongly immunopositive (h) but some cells show modest reaction (i). In myocardial extensions around the superior caval vein (j), most cardiomyocytes display prominent labeling (k), while some cells are weakly positive (l). During quantification, pronounced reduction of mean gray value for Purkinje fibers and strongly immunoreactive cells of the extracardiac myocardial sleeves indicates much stronger desmin signal intensity for these cells than ventricular working cardiomyocytes (m). There was less remarkable difference in mean gray values between representative areas of the ventricular subendocardial region or myocardial sleeves and the working myocardium (n). Scale-bars: 40 μm (a-inset), 50 μm (b, c, e, f, h, i, k, l), 1000 μm (a, d, g), 2000 μm (j).

Journal of Anatomy
DOI:10.14753/SE.2025.3172

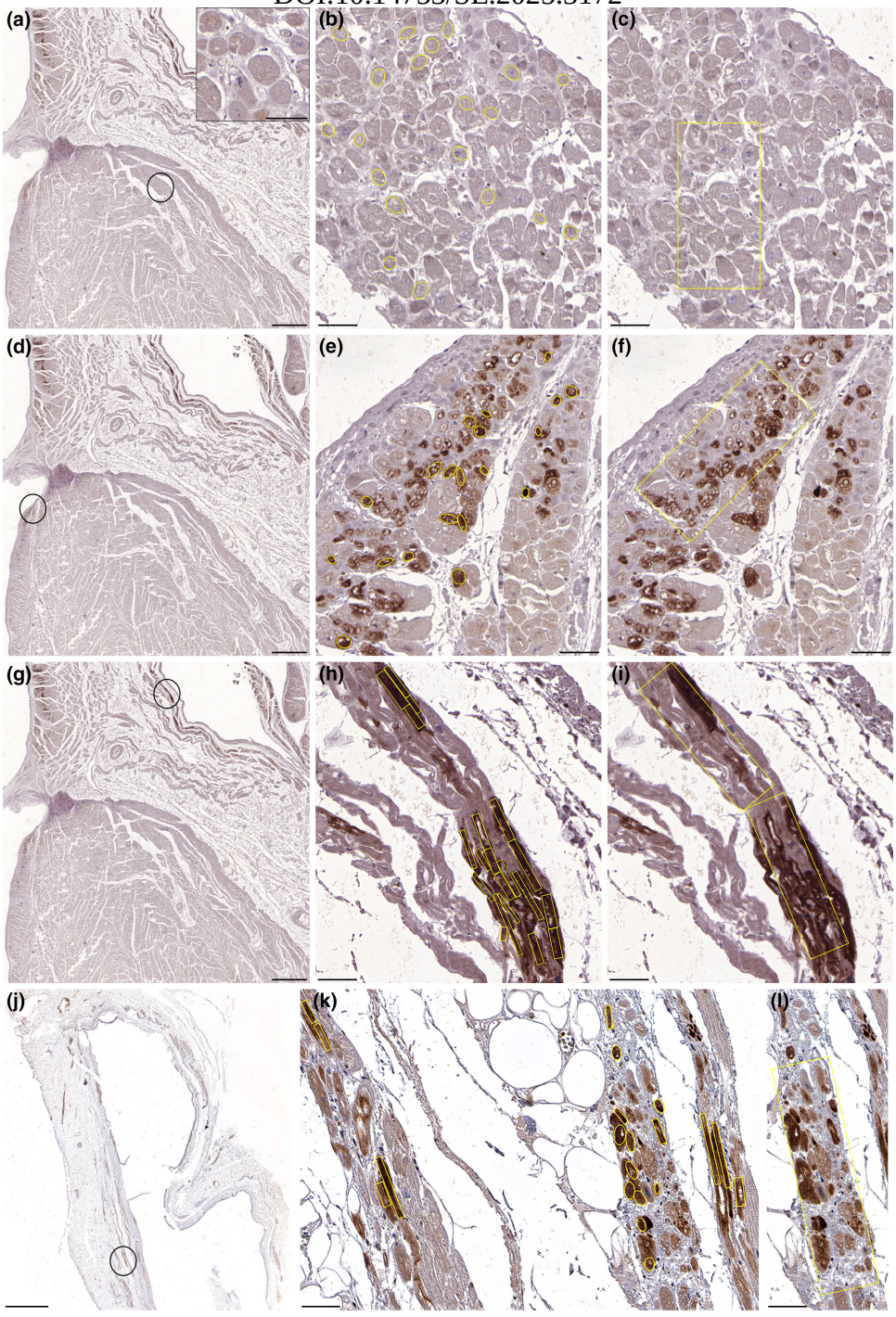

DOI:10.14753/SE.2025.3172

3.2 | Cardiac pacemaker and conduction system of the adult hearts

In the adult hearts, regions of the sinoatrial and atrioventricular nodes as well as the ventricular conduction system at the subendocardial layer of the interventricular septum could be easily identified by hematoxylin–eosin and trichrome stainings. Small pacemaker cells embedded in dense fibrous tissue around the sinoatrial nodal artery and in its adventitial layer as well were characteristic of the sinoatrial node (Figure 2a), while the apex of the triangle of Koch was the site of compact atrioventricular node embedded in the muscular part of atrioventricular septum and surrounded by elongated transitional cells (data not shown). In the ventricular conduction system, large cardiomyocytes (Purkinje fibers) possessing pale cytoplasm and peripheral

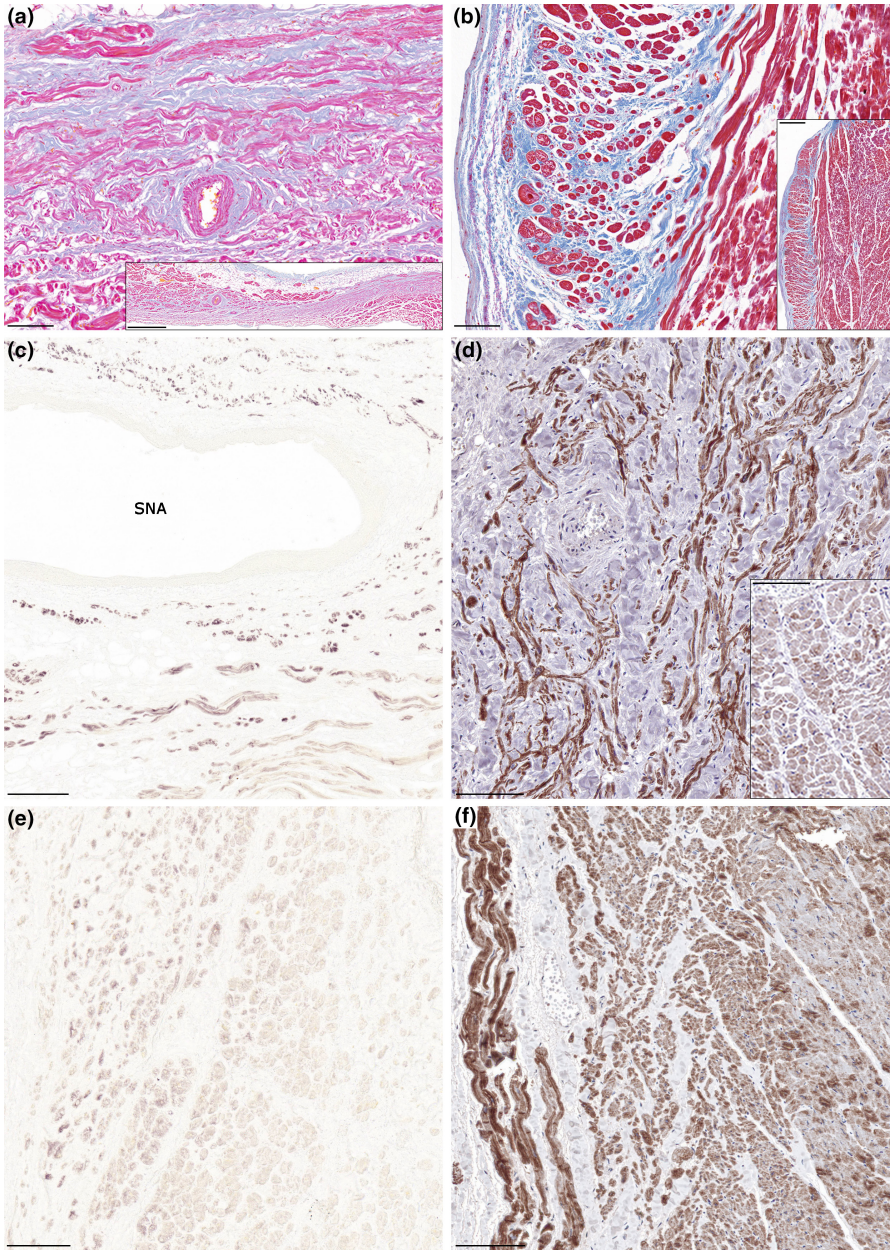

FIGURE 2 Desmin immunostaining of the cardiac pacemaker and conduction system. Representative histology images (Krutsay's trichrome) of the sinoatrial node and the ventricular septum (a, b). Small pacemaker cells embedded in dense connective tissue surrounding the sinoatrial nodal artery (a) are characteristic for the sinoatrial node (a-inset). Left ventricular working myocardium (right side) and the subendocardial conduction system (left side). Purkinje fibers exhibit large cytoplasm with peripheral myofibrils and are embedded in connective tissue (b). An extended area of the ventricular septum is shown in b-inset. Strong immunopositivity for desmin at the sinoatrial nodal region of ethanol-fixed (c) and formaldehyde-fixed (d) hearts. Adjacent atrial working myocardium exhibits weaker labeling (lower part of image [c]; d-inset). Compared to the weak staining of the working myocardium (right), desmin labeling is pronounced in the ventricular conduction system (left) of the ethanol-fixed (e) and formaldehyde-fixed (f) hearts. Label: SNA, sinoatrial nodal artery. Scale-bars: 100 μm (a, b, d, d-inset, e, f), 200 μm (c), 500 μm (b-inset), 1000 μm (a-inset).

DOI: 10.1475/SE.2025.3172

TABLE 2 Semiquantitative assessment of the prevalence of cardiomyocytes possessing the phenotype of conducting cells (pale cytoplasm, peripheral myofibrils on hematoxylin–eosin or trichrome stained sections) and cardiomyocytes exhibiting strong desmin immunoreactivity in specific regions of the examined hearts.

Case	Object of semiquantitative assessment (0, none; 1, few; 2, several; 3, abundant)	SCV	CS	PV	SAN	Subendocardium			Working myocardium		
						LV	IVS	RV	LV	IVS	RV
1	Conducting-like CMs	2	–	–	–	–	–	–	–	–	–
	CMs with strong desmin labeling	1	–	–	–	–	–	–	–	–	–
2	Conducting-like CMs	2	–	–	–	–	–	2	–	–	0
	CMs with strong desmin labeling	2	–	–	–	–	–	2	–	–	0
3	Conducting-like CMs	2	–	–	3	–	–	2	–	–	0
	CMs with strong desmin labeling	0	–	–	1	–	–	2	–	–	0
4	Conducting-like CMs	2	3	–	–	–	3	–	0	0	–
	CMs with strong desmin labeling	1	2	–	–	–	2	–	0	0	–
5	Conducting-like CMs	–	–	3	–	–	–	–	–	–	–
	CMs with strong desmin labeling	–	–	2	–	–	–	–	–	–	–
6	Conducting-like CMs	–	–	2	–	–	–	–	–	–	–
	CMs with strong desmin labeling	–	–	2	–	–	–	–	–	–	–
7	Conducting-like CMs	2	2	1	3	–	3	–	0	0	–
	CMs with strong desmin labeling	3	1	2	2	–	2	–	0	0	–
8	Conducting-like CMs	2	2	2	3	–	3	–	–	0	–
	CMs with strong desmin labeling	3	2	3	3	–	3	–	–	1	–
9	Conducting-like CMs	3	1	2	3	–	3	–	–	0	–
	CMs with strong desmin labeling	2	2	2	2	–	2	–	–	0	–
10	Conducting-like CMs	3	2	2	3	–	3	–	–	0	–
	CMs with strong desmin labeling	3	2	2	2	–	2	–	–	1	–
11	Conducting-like CMs	1	1	3	3	–	3	–	–	0	–
	CMs with strong desmin labeling	2	2	2	2	–	3	–	–	1	–
12	Conducting-like CMs	2	1	1	3	–	3	–	–	0	–
	CMs with strong desmin labeling	2	2	2	3	–	2	–	–	0	–
13	Conducting-like CMs	2	1	1	3	–	2	–	–	0	–
	CMs with strong desmin labeling	2	2	NA	3	–	2	–	–	1	–
14	Conducting-like CMs	2	1	2	3	–	2	2	–	0	0
	CMs with strong desmin labeling	2	2	3	NA	–	2	2	–	0	1
15	Conducting-like CMs	2	–	2	3	–	2	–	–	0	–
	CMs with strong desmin labeling	2	–	2	3	–	3	–	–	0	–
16	Conducting-like CMs	NA	–	–	NA	NA	NA	NA	NA	NA	NA
	CMs with strong desmin labeling	2	–	–	3	0	0	0	0	0	0

Note: Presence of conducting-like cardiomyocytes could not be clearly evaluated in case of the fetal heart. Desmin immunostaining could not be performed for the PV of case No. 13 and the SAN of case No. 14. due to technical reasons.

Abbreviations: CMs, cardiomyocytes; CS, coronary sinus; IVS, interventricular septum; LV, left ventricle; NA, not applicable; PV, pulmonary vein; RV, right ventricle; SAN, sinoatrial node; SCV, superior caval vein.

DOI:10.14753/SE.2025.3172

myofibrils were identified. These cells formed the left and right bundle branches (Figure 2b). Both pacemaker cells of the sinoatrial and atrioventricular nodes and Purkinje fibers of the ventricular conduction system exhibited strong desmin immunoreactivity compared to the weaker labeling of the surrounding atrial and ventricular working myocardium. These differences were detected at ethanol-fixed and formaldehyde-fixed sections as well (Figures 2c–f; Table 2).

3.3 | Myocardial sleeves of pulmonary veins, superior caval veins and coronary sinus in the adult hearts

Myocardial sleeves were present around all examined pulmonary vein, superior caval vein, and coronary sinus samples (Figures 3a–c). Bundles of cardiomyocytes exhibiting similar morphology to

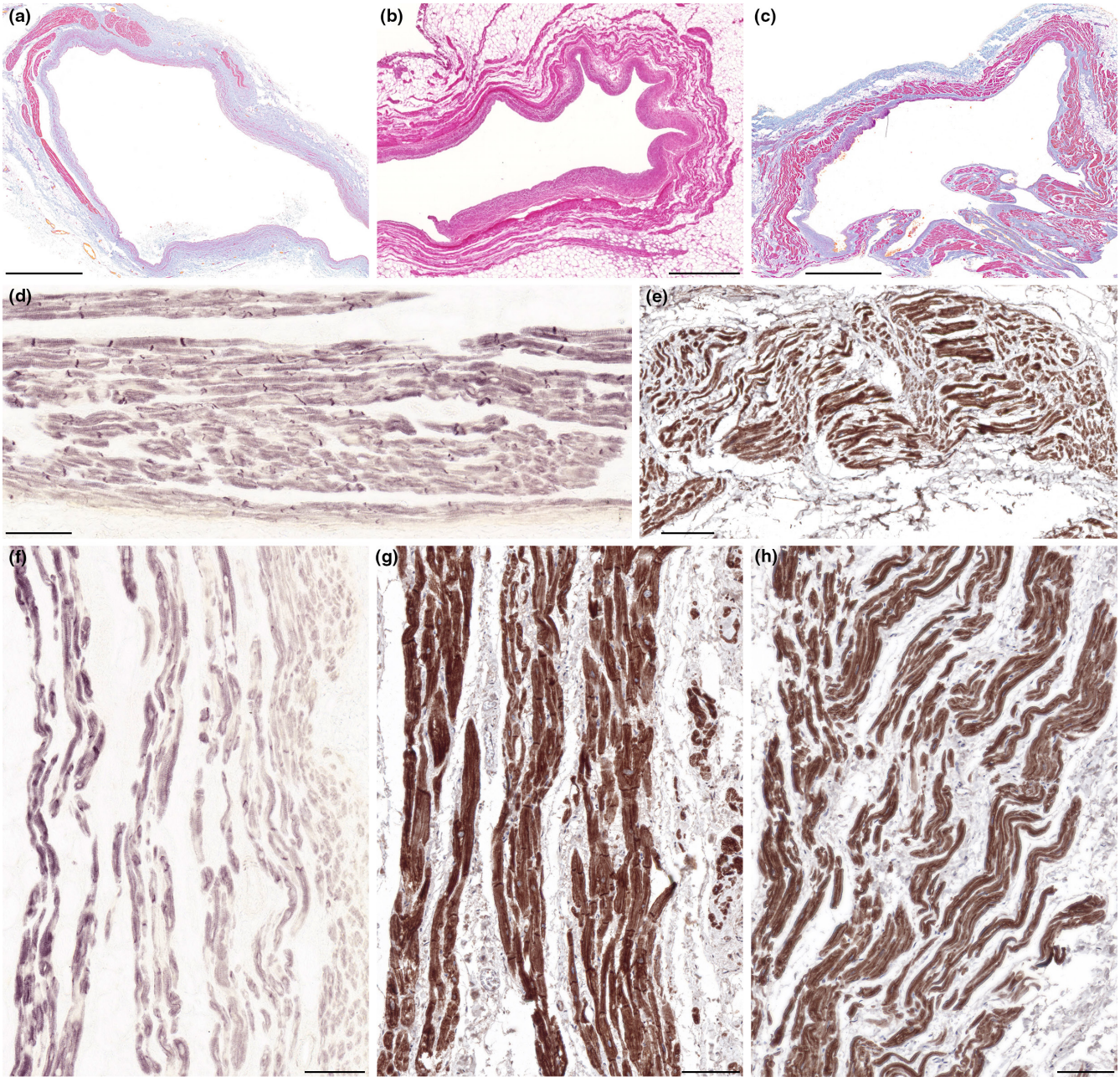

FIGURE 3 Desmin immunostaining of the venous myocardial sleeves. Representative histology images (hematoxylin–eosin [b] and Krutsay's trichrome [a, c]) of the myocardial sleeves. Cross-section of a pulmonary vein. This part of the vein is partially covered by myocardial sleeve. Cardiomyocytes are localized on the outer side of the venous adventitia (a). Cross-section of a superior caval vein with myocardial sleeve (b). Transverse section of the coronary sinus in the level of its right atrial orifice. Myocardial sleeve is present around the venous wall (c). Prominent desmin immunoreactivity was observed in the myocardial sleeves around pulmonary veins of ethanol-fixed (d) and formaldehyde-fixed (e) hearts. Desmin labeling is remarkable in myocardial extensions around both the ethanol-fixed (f) and formaldehyde-fixed (g) superior caval veins. In the myocardial sleeve of the formaldehyde-fixed coronary sinus, several cardiomyocytes show pronounced immunoreactivity for desmin as well (h). Scale-bars: 100 μm (d–h), 1000 μm (b), 2000 μm (a, c).

Journal of Anatomy
DOI:10.14753/SE.2025.3172

Purkinje fibers or pacemaker cells were present in all myocardial sleeves investigated, albeit their amount was different in each sample (Table 2). Purkinje-like cardiomyocytes were larger in size than working cardiomyocytes and possessed pale cytoplasm and peripheral myofibrils, while nodal-like cardiomyocytes had particularly small diameter. These conducting-like cells were frequently embedded in fine collagen fiber networks. Intense desmin immunoreactivity was detected in myocardial extensions into pulmonary veins of both ethanol-fixed and formaldehyde-fixed hearts (Figures 3d,e). Similarly, myocardial sleeves of superior caval veins proved to be strongly immunopositive for desmin compared to the atrial and ventricular working myocardium (Figures 3f,g). Abundant desmin labeling could be also observed in the myocardial sleeves surrounding the formaldehyde-fixed coronary sinus samples (Figure 3h). The amount of cardiomyocytes showing prominent desmin staining differed between the samples (Table 2). Strongly immunoreactive cardiomyocytes frequently displayed similar morphological phenotypes to Purkinje fibers or nodal cardiomyocytes.

3.4 | Double-immunolabeling of desmin and connexin 45 in an adult heart

Double labeling immunofluorescence analysis for desmin and conduction system marker connexin 45 showed a strong sarcomeric and junctional pattern for desmin labeling in the myocardial sleeve of the ethanol-fixed pulmonary vein (Figure 4a). Although connexin 45 immunoreactivity was also intense, it was restricted to the intercalated discs (Figure 4b) where it overlapped extensively with desmin (Figures 4c,d). The co-localisation of these two markers further supports the presumed arrhythmogenicity of this region.

3.5 | Human fetal heart

In the 23-week-old human fetus, pacemaker cells of the sinoatrial node and Purkinje fibers of the ventricular conduction system could not be differentiated clearly from working cardiomyocytes. However, the sinoatrial nodal region could be identified based on its localization and its artery. Myocardial extensions into the superior caval vein could be observed (Figures 5a,b). Similarly to human adults, prominent desmin labeling was detected in the myocardial sleeve of the fetal superior caval vein. Immunoreaction for desmin was also intense at the sinoatrial nodal region (Figure 5c).

4 | DISCUSSION

Although there is a growing knowledge of the possible pathomechanisms of supraventricular tachyarrhythmias, the histologic characteristics of the arrhythmogenic regions are still obscure. Based on previous human (Kugler et al., 2018; Nguyen et al., 2009; Perez-Lugones et al., 2003) and animal (Masani, 1986) studies, it seems that cardiomyocytes with a similar phenotype to the cardiac pacemaker or conduction cells are present in the myocardial sleeves around pulmonary veins, caval veins and coronary sinus. Few data are available

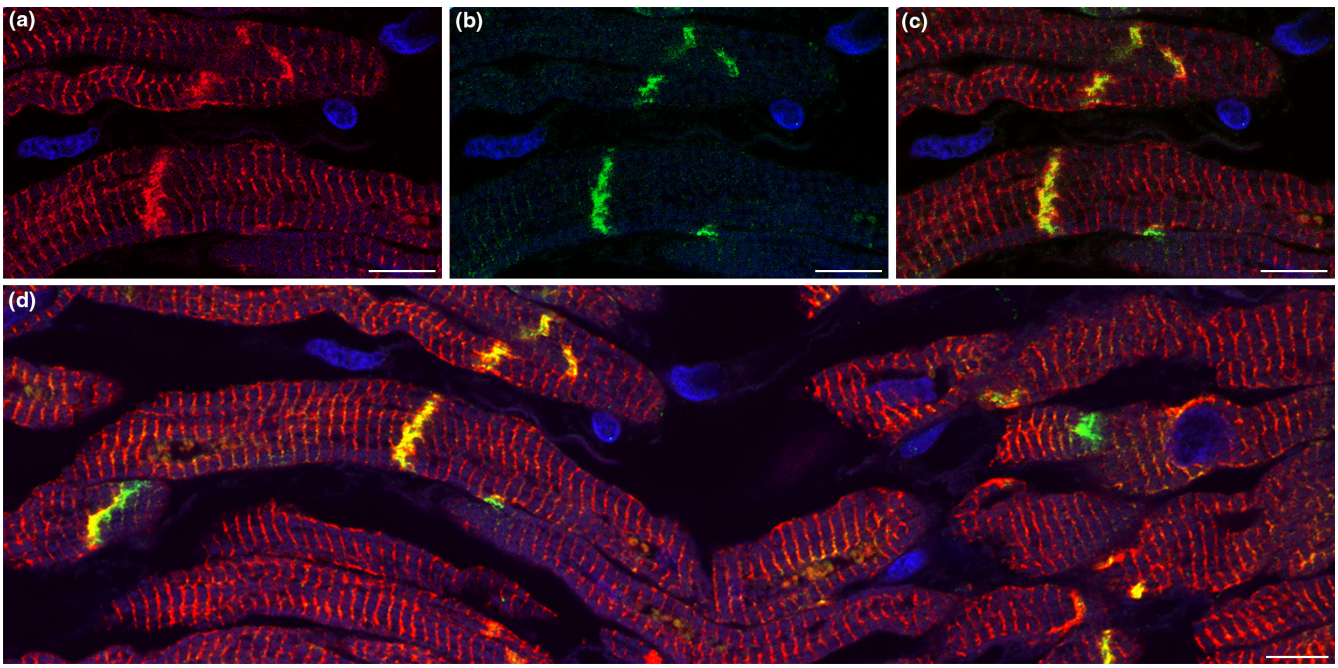

FIGURE 4 Double-labeling of desmin and connexin 45 in the myocardial sleeve of a pulmonary vein. Cardiomyocytes display intense red fluorescence which means strong positivity for desmin (a). Connexin 45 expression (green) is detected only between neighboring cardiomyocytes (b) where it colocalizes with desmin resulting in yellow fluorescent signal (c). Double-immunolabeling of desmin and connexin 45 is also demonstrated at a more extensive area (d). Nuclei are stained with DAPI (blue). Scale-bars: 10 μm (a–d).

DOI:10.14753/SE.2025.3172

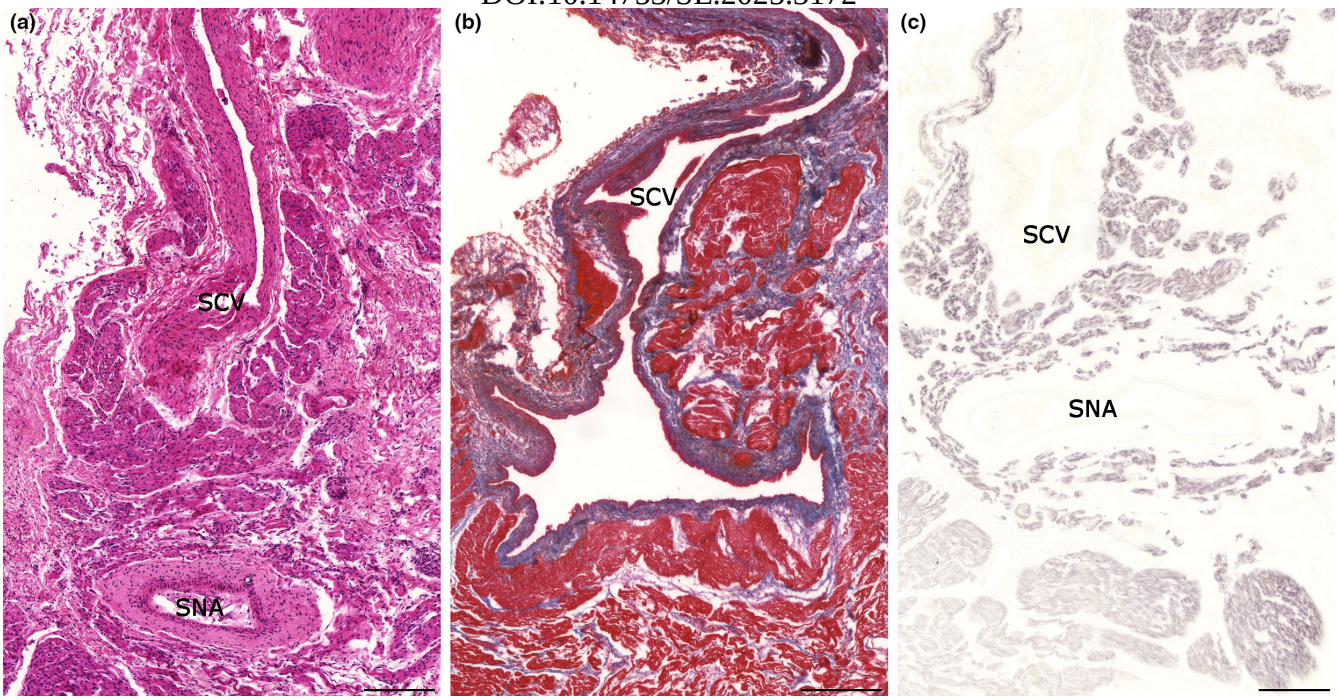

FIGURE 5 Histology of a 23-week old human fetal heart. Longitudinal section of superior caval vein. Myocardial extensions can be observed around the wall of the vein. Sinoatrial node with its artery is localized near to the right atrial orifice of the superior caval vein. Hematoxylin–eosin (a). Krutsay's trichrome staining indicates that the myocardial sleeve (red) is localized outside of the venous adventitia (blue) (b). Compared to the adjacent atrial myocardium, desmin immunoreactivity is strongly positive in both the myocardial sleeve around the superior caval vein and the sinoatrial node (c). Labels: SNA, sinoatrial nodal artery; SCV, superior caval vein. Scale bars: 200 μm (a, c), 400 μm (b).

about the immunohistologic features of these regions in humans (Blom et al., 1999; Kholová et al., 2003; Kugler et al., 2018; Nguyen et al., 2009) and animals (Yamamoto et al., 2006; Yeh et al., 2001; Yeh et al., 2003).

In the current study, we aimed to further characterize the myocardial sleeves with the comparative examination of a general marker of myocytes, the desmin. In the left ventricular myocardium, progressively increased desmin intensity was reported with increasing fetal age in humans (Kim, 1996). It was also found that bovine Purkinje fibers possess numerous intermediate filaments but less myofibrils compared to working cardiomyocytes (Eriksson et al., 1978; Eriksson & Thornell, 1979; Thornell & Eriksson, 1981). Later mammalian studies verified stronger desmin immunoreactivity for the ventricular conduction system compared to the working cardiomyocytes both during the prenatal development (Franco & Icardo, 2001; Ya et al., 1997) and in adults (Vitadello et al., 1990; Ya et al., 1997). Abundant desmin labeling was detected also in the Purkinje fibers of humans (Yoshimura et al., 2014). Obvious difference in desmin immunostaining was observed between ventricular working cardiomyocytes and Purkinje fibers during the current research as well. Intense desmin labeling was reported in the developing human sinoatrial and atrioventricular nodes (Liu et al., 2020). In adult mice and human samples, a high amount of desmin was found in the sinoatrial node as well (Mavroidis et al., 2020). Similarly, stronger desmin immunoreactivity was detected in the sinoatrial node compared to the atrial working myocardium in our study. The atrioventricular conductive axis of rabbits could be easily distinguished by prominent desmin immunostaining within the cytoplasm of conducting cardiomyocytes (Ko et al., 2004).

Conducting phenotype of the myocardial sleeves might be explained by developmental factors. Embryonic systemic veins have a substantial overlap in gene expression with the future sinus node. Tbx3 and Hcn4 expressing venous pole of the primary heart tube exhibits high pacemaker activity while later it confines to the sinoatrial node. Incomplete atrialization of sinus venosus-derived structures, such as superior caval vein (right sinus horn), crista terminalis (right venous valve), coronary sinus ostium (atrial entrance of the left sinus horn), and ligament of Marshall (remnant of the left sinus horn) may result in the persistence of focal automatic activity. Development of the pulmonary venous myocardium is different as it forms independently from the sinus venosus, and displays an atrial working myocardial phenotype and gene program (Tbx18/Hcn4-negative; Christoffels & Moorman, 2009; Christoffels et al., 2010; Weerd & Christoffels, 2016).

Data about desmin labeling of extranodal supraventricular regions is sparse. In fetal rats, strong desmin immunoreactivity was noted in the sinoatrial node, the superior caval vein, and the myocardium along pulmonary veins (Ya et al., 1997). Interatrial conducting pathway was reported to exhibit strong desmin immunolabeling compared to working cardiomyocytes in monkeys and sheeps (Yamaguchi et al., 2009). However, description of desmin expressing supraventricular structures in human adults is lacking. Only fetal data are available which indicates that similarly to the ventricular

Journal of Anatomy
DOI:10.14753/SE.2025.3172

conduction system, atrial walls, pulmonary veins, caval veins, and coronary sinus are strongly positive for desmin, while the left ventricle is immunonegative. Mechanical stress caused by involvement of the venous walls in atrial development was thought to induce desmin expression (Yamamoto et al., 2011). Studies on human embryos (Liu et al., 2020) and fetuses (Grigore et al., 2012) reported strong desmin immunoreactivity of the atria compared to weaker (Grigore et al., 2012) or absent (Liu et al., 2020) signal at the ventricular (compact) myocardium.

Based on the lacking data for desmin expression in supraventricular regions of human adults, we examined specimens both from fetal and adult hearts. Strong labeling for desmin in the myocardial sleeve of the fetal superior caval vein is in agreement with Yamamoto et al.'s (2011) report but interestingly, prominent desmin immunoreactivity was found in the pulmonary and non-pulmonary venous myocardial sleeves of adults as well. Consequently, it is likely that desmin highlights not only the pacemaker and conduction system but also those supraventricular regions which may trigger atrial tachyarrhythmias. Quantification of desmin labeling verified a considerable difference in signal intensity between the ventricular subendocardial region or venous myocardial sleeves and the working myocardium supporting the theory that desmin marks the supraventricular regions in which arrhythmogenic foci may appear. Interestingly enough, cardiomyocytes exhibiting conducting-like phenotype and strong desmin immunoreactivity were identified in the venous myocardial sleeves of all hearts irrespective of age and cardiovascular history. It is also of note that albeit working myocardium displayed weaker signal intensity than the conduction system, its desmin positivity was obvious. Therefore application of desmin as a selective marker for pacemaker or conducting cardiomyocytes does not seem to be plausible.

5 | CONCLUSIONS

Based on the results of the current study on human hearts, we conclude that immunostaining of desmin intermediate filaments is obviously stronger for the ventricular conduction system as well as for supraventricular arrhythmogenic regions than for ventricular working myocardium. Although desmin cannot be applied as a selective marker for the cardiac pacemaker and conduction systems, but prominent desmin immunoreaction coincides with the territory of pulmonary and nonpulmonary myocardial sleeves, the sites of arrhythmogenic foci.

AUTHOR CONTRIBUTIONS

S.K. substantially contributed to the design of the study, acquisition, and analysis of data, revision of the literature, and selection of relevant articles. She was also a major contributor in drafting the manuscript. A.M.T. and N.N. contributed to the design of the study, acquisition, and analysis of data, particularly to the immunohistochemistry staining, and revised the manuscript. A.F., K.D., K.T., and G.R. prepared and provided human cardiac samples in possession of ethical approval and revised the manuscript. M.S. figured out the method of sinoatrial node preparation and revised the manuscript. Á.N. substantially contributed to the conception and design of the study, analysis, and interpretation of data, selection of articles and revision of the manuscript. All authors read and approved the final manuscript.

ACKNOWLEDGMENTS

The authors wish to express their gratitude to those who donated their bodies to the University of Semmelweis for anatomical education and research. We are also grateful to Ákos Lukáts MD, PhD, Rita Padányi MD, PhD, Eszter Regős MD, PhD, Gertrúd Forika MD, PhD, Kata Pálos MD, Noémi Jákob MD, Erzsébet Kovács, Viktória Halasy, Judit Fogarasi, Lili Orbán, Ferenc Kilin, Dorottya Csernus-Horváth, Eszter Pál, Balázs Szalay, Rita Körtvélyessy, Rebeka Bertalan for their excellent technical assistance during tissue preparation and immunohistochemistry studies.

FUNDING INFORMATION

This study was funded by institutional funds and by István Apáthy Foundation's Research Grant. N.N. is supported by the Research Excellence Programme of the Ministry for Innovation and Technology in Hungary, within the framework of the TKP2021-EGA-25 thematic programme of the Semmelweis University, and by the Hungarian Science Foundation NKFI grant (138664).

CONFLICT OF INTEREST STATEMENT

The authors have no relevant financial or non-financial interests to disclose.

DATA AVAILABILITY STATEMENT

The most relevant data generated during the current study are included in this published article. Other data are available from the corresponding author on reasonable request.

ORCID

Szilvia Kugler https://orcid.org/0000-0002-1504-4861

REFERENCES

Blom, N.A., Gittenberger-de Groot, A.C., DeRuiter, M.C., Poelmann, R.E., Mentink, M.M.T. & Ottenkamp, J. (1999) Development of the cardiac conduction tissue in human embryos using HNK-1 antigen expression: possible relevance for understanding of abnormal atrial automaticity. *Circulation*, 99, 800–806. Available from: https://doi.org/10.1161/01.cir.99.6.800

Capetanaki, Y., Bloch, R.J., Kouloumenta, A., Mavroidis, M. & Psarras, S. (2007) Muscle intermediate filaments and their links to membranes and membranous organelles. *Experimental Cell Research*, 313, 2063–2076. Available from: https://doi.org/10.1016/j.yexcr.2007.03.033

Chang, H.Y., Lo, L.W., Lin, Y.J., Chang, S.L., Hu, Y.F., Li, C.H. et al. (2013) Long-term outcome of catheter ablation in patients with atrial fibrillation originating from non pulmonary vein ectopy. *Journal of Cardiovascular Electrophysiology*, 24, 250–258. Available from: https://doi.org/10.1111/jce.12036

Chen, P.S., Chen, L.S., Fishbein, M.C., Lin, S.F. & Nattel, S. (2014) Role of the autonomic nervous system in atrial

DOI:10.14753/SE.2025.3172

fibrillation. Pathophysiology and Therapy. *Circulation Research*, 114, 1500–1515. Available from: https://doi.org/10.1161/CIRCRESAHA.114.303772

Christoffels, V.M. & Moorman, A.F.M. (2009) Development of the cardiac conduction system: why are some regions of the heart more arrhythmogenic than others? *Circulation Arrhythmia and Electrophysiology*, 2, 195–207. Available from: https://doi.org/10.1161/CIRCEP.108.829341

Christoffels, V.M., Smits, G.J., Kispert, A. & Moorman, A.F.M. (2010) Development of the pacemaker tissues of the heart. *Circulation Research*, 106, 240–254. Available from: https://doi.org/10.1161/CIRCRESAHA.109.205419

Eriksson, A. & Thornell, L.E. (1979) Intermediate (skeletin) filaments in heart Purkinje fibers. A correlative morphological and biochemical identification with evidence of a cytoskeletal function. *The Journal of Cell Biology*, 80, 231–247. Available from: https://doi.org/10.1083/jcb.80.2.231

Eriksson, A., Thornell, L.E. & Stigbrand, T. (1978) Cytoskeletal filaments of heart conducting system localized by antibody against a 55,000 Dalton protein. *Experientia*, 34, 792–794. Available from: https://doi.org/10.1007/BF01947331

Franco, D. & Icardo, J.M. (2001) Molecular characterization of the ventricular conduction system in the developing mouse heart: topographical correlation in normal and congenitally malformed hearts. *Cardiovascular Research*, 49, 417–429. Available from: https://doi.org/10.1016/s0008-6363(00)00252-2

Gal, P. & Marrouche, N.F. (2017) Magnetic resonance imaging of atrial fibrosis: redefining atrial fibrillation to a syndrome. *European Heart Journal*, 38, 14–19. Available from: https://doi.org/10.1093/eurheartj/ehv514

Grigore, A., Arsene, D., Filipoiu, F., Cionca, F., Enache, S., Ceauşu, M. et al. (2012) Cellular immunophenotypes in human embryonic, fetal and adult heart. *Romanian Journal of Morphology and Embryology*, 53, 299–311.

Haemers, P., Hamdi, H., Guedj, K., Suffee, N., Farahmand, P., Popovic, N. et al. (2017) Atrial fibrillation is associated with the fibrotic remodelling of adipose tissue in the subepicardium of human and sheep atria. *European Heart Journal*, 38, 53–61. Available from: https://doi.org/10.1093/eurheartj/ehv625

Haïssaguerre, M., Jaïs, P., Shah, D.C., Takahashi, A., Hocini, M., Quiniou, G. et al. (1998) Spontaneous initiation of atrial fibrillation by ectopic beats originating in the pulmonary veins. *The New England Journal of Medicine*, 339, 659–666. Available from: https://doi.org/10.1056/NEJM199809033391003

Kholová, I., Niessen, H.W.M. & Kautzner, J. (2003) Expression of Leu-7 in myocardial sleeves around human pulmonary veins. *Cardiovascular Pathology*, 12, 263–266. Available from: https://doi.org/10.1016/s1054-8807(03)00078-4

Kim, H.D. (1996) Expression of intermediate filament desmin and vimentin in the human fetal heart. *The Anatomical Record*, 246, 271–278. Available from: https://doi.org/10.1002/(SICI)1097-0185(199610)246:2<271::AID-AR13>3.0.CO;2-L

Ko, Y.S., Yeh, H.I., Ko, Y.L., Hsu, Y.C., Chen, C.F., Wu, S. et al. (2004) Three-dimensional reconstruction of the rabbit atrioventricular conduction axis by combining histological, desmin, and connexin mapping data. *Circulation*, 109, 1172–1179. Available from: https://doi.org/10.1161/01.CIR.0000117233.57190.BD

Kugler, S., Nagy, N., Rácz, G., Tőkés, A.M., Dorogi, B. & Nemeskéri, Á. (2018) Presence of cardiomyocytes exhibiting Purkinje-type morphology and prominent connexin45 immunoreactivity in the myocardial sleeves of cardiac veins. *Heart Rhythm*, 15, 258–264. Available from: https://doi.org/10.1016/j.hrthm.2017.09.044

Lau, D.H., Schotten, U., Mahajan, R., Antic, N.A., Hatem, S.N., Pathak, R.K. et al. (2016) Novel mechanisms in the pathogenesis of atrial fibrillation: practical applications. *European Heart Journal*, 37, 1573–1581. Available from: https://doi.org/10.1093/eurheartj/ehv375

Lee, S.H., Tai, C.T., Hsieh, M.H., Tsao, H.M., Lin, Y.J., Chang, S.L. et al. (2005) Predictors of non-pulmonary vein ectopic beats initiating paroxysmal atrial fibrillation: implication for catheter ablation. *Journal of the American College of Cardiology*, 46, 1054–1059. Available from: https://doi.org/10.1016/j.jacc.2005.06.016

Lin, W.S., Tai, C.T., Hsieh, M.H., Tsai, C.F., Lin, Y.K., Tsao, H.M. et al. (2003) Catheter ablation of paroxysmal atrial fibrillation initiated by non-pulmonary vein ectopy. *Circulation*, 107, 3176–3183. Available from: https://doi.org/10.1161/01.CIR.0000074206.52056.2D

Liu, H.X., Jing, Y.X., Wang, J.J., Yang, Y.P., Wang, Y.X., Li, H.R. et al. (2020) Expression patterns of intermediate filament proteins desmin and Lamin a in the developing conduction system of early human embryonic hearts. *Journal of Anatomy*, 236, 540–548. Available from: https://doi.org/10.1111/joa.13108

Masani, F. (1986) Node-like cells in the myocardial layer of the pulmonary vein of rats: an ultrastructural study. *Journal of Anatomy*, 145, 133–142.

Mavroidis, M., Athanasiadis, N.C., Rigas, P., Kostavasili, I., Kloukina, I., te Rijdt, W.P. et al. (2020) Desmin is essential for the structure and function of the sinoatrial node: implications for increased arrhythmogenesis. *American Journal of Physiology. Heart and Circulatory Physiology*, 319, 557–570. Available from: https://doi.org/10.1152/ajpheart.00594.2019

Nadadur, R.D., Broman, M.T., Boukens, B., Mazurek, S.R., Yang, X., van den Boogaard, M. et al. (2016) Pitx2 modulates a Tbx5-dependent gene regulatory network to maintain atrial rhythm. *Science Translational Medicine*, 8, 354ra115. Available from: https://doi.org/10.1126/scitranslmed.aaf4891

Nattel, S. (2017) Molecular and cellular mechanisms of atrial fibrosis in atrial fibrillation. *JACC Clin Electrophysiol*, 3, 425–435. Available from: https://doi.org/10.1016/j.jacep.2017.03.002

Nguyen, B.L., Fishbein, M.C., Chen, L.S., Chen, P.S. & Masroor, S. (2009) Histopathological substrate for chronic atrial fibrillation in humans. *Heart Rhythm*, 6, 454–460. Available from: https://doi.org/10.1016/j.hrthm.2009.01.010

Perez-Lugones, A., McMahon, J.T., Ratliff, N.B., Saliba, W.I., Schweikert, R.A., Marrouche, N.F. et al. (2003) Evidence of specialized conduction cells in human pulmonary veins of patients with atrial fibrillation. *Journal of Cardiovascular Electrophysiology*, 14, 803–809. Available from: https://doi.org/10.1046/j.1540-8167.2003.03075.x

Santangeli, P. & Marchlinski, F.E. (2017) Techniques for the provocation, localization, and ablation of non-pulmonary vein triggers for atrial fibrillation. *Heart Rhythm*, 14, 1087–1096. Available from: https://doi.org/10.1016/j.hrthm.2017.02.030

Santangeli, P., Zado, E.S., Hutchinson, M.D., Riley, M.P., Lin, D., Frankel, D.S. et al. (2016) Prevalence and distribution of focal triggers in persistent and long-standing persistent atrial fibrillation. *Heart Rhythm*, 13, 374–382. Available from: https://doi.org/10.1016/j.hrthm.2015.10.023

Su, W., van Wijk, S.W. & Brundel, B.J.J.M. (2022) Desmin variants: trigger for cardiac arrhythmias? *Frontiers in Cell and Development Biology*, 10, 986718. Available from: https://doi.org/10.3389/fcell.2022.986718

Thornell, L.E. & Eriksson, A. (1981) Filament systems in the Purkinje fibers of the heart. *The American Journal of Physiology*, 241, 291–305. Available from: https://doi.org/10.1152/ajpheart.1981.241.3.H291

Vitadello, M., Matteoli, M. & Gorza, L. (1990) Neurofilament proteins are co-expressed with desmin in heart conduction system myocytes. *Journal of Cell Science*, 97, 11–21. Available from: https://doi.org/10.1242/jcs.97.1.11

Waks, J.W. & Josephson, M.E. (2014) Mechanisms of atrial fibrillation—reentry, rotors and reality. *Arrhythmia & Electrophysiology Review (AER)*, 3, 90–100. Available from: https://doi.org/10.15420/aer.2014.3.2.90

Weerd, J.H. & Christoffels, V.M. (2016) The formation and function of the cardiac conduction system. *Development*, 143, 197–210. Available from: https://doi.org/10.1242/dev.124883

Journal of Anatomy
DOI:10.14753/SE.2025.3172

Ya, J., Markman, M.W., Wagenaar, G.T., Blommaart, P.J., Moorman, A.F. & Lamers, W.H. (1997) Expression of the smooth-muscle proteins alpha-smooth-muscle Actin and calponin, and of the intermediate filament protein desmin are parameters of cardiomyocyte maturation in the prenatal rat heart. *The Anatomical Record*, 249, 495–505. Available from: https://doi.org/10.1002/(SICI)1097-0185(199712)249:4<495::AID-AR9>3.0.CO;2-Q

Yamaguchi, T., Tsuchiya, T., Miyamoto, K., Nagamoto, Y. & Takahashi, N. (2010) Characterization of non-pulmonary vein foci with an EnSite array in patients with paroxysmal atrial fibrillation. *Europace*, 12, 1698–1706. Available from: https://doi.org/10.1093/europace/euq326

Yamaguchi, T., Yi, S.Q., Tanaka, S., Ono, K. & Shimada, T. (2009) Ultrastructure and cytoarchitecture of Bachmann's bundle in the mammalian heart. *Journal of Arrhythmia*, 25, 24–31. Available from: https://doi.org/10.4020/jhrs.25.24

Yamamoto, M., Abe, S., Rodríguez-Vázquez, J.F., Fujimiya, M., Murakami, G. & Ide, Y. (2011) Immunohistochemical distribution of desmin in the human fetal heart. *Journal of Anatomy*, 219, 253–258. Available from: https://doi.org/10.1111/j.1469-7580.2011.01382.x

Yamamoto, M., Dobrzynski, H., Tellez, J., Niwa, R., Billeter, R., Honjo, H. et al. (2006) Extended atrial conduction system characterised by the expression of the HCN4 channel and connexin45. *Cardiovascular Research*, 72, 271–281. Available from: https://doi.org/10.1016/j.cardiores.2006.07.026

Yao, C. & Veleva, T. (2018) Enhanced cardiomyocyte NLRP3 inflammasome signaling promotes atrial fibrillation. *Circulation*, 138, 2227–2242. Available from: https://doi.org/10.1161/CIRCULATIONAHA.118.035202

Yeh, H.I., Lai, Y.J., Lee, S.H., Lee, Y.N., Ko, Y.S., Chen, S.A. et al. (2001) Heterogeneity of myocardial sleeve morphology and gap junctions in canine superior vena cava. *Circulation*, 104, 3152–3157. Available from: https://doi.org/10.1161/hc5001.100836

Yeh, H.I., Lai, Y.J., Lee, Y.N., Chen, Y.J., Chen, Y.C., Chen, C.C. et al. (2003) Differential expression of connexin43 gap junctions in cardiomyocytes isolated from canine thoracic veins. *The Journal of Histochemistry and Cytochemistry*, 51, 259–266. Available from: https://doi.org/10.1177/002215540305100215

Yoshimura, A., Yamaguchi, T., Kawazato, H., Takahashi, N. & Shimada, T. (2014) Immuno-histochemistry and three-dimensional architecture of the intermediate filaments in Purkinje cells in mammalian hearts. *Medical Molecular Morphology*, 47, 233–239. Available from: https://doi.org/10.1007/s00795-014-0069-9

SUPPORTING INFORMATION

Additional supporting information can be found online in the Supporting Information section at the end of this article.

How to cite this article: Kugler, S., Tőkés, A.-M., Nagy, N., Fintha, A., Danics, K., Sághi, M. et al. (2023) Strong desmin immunoreactivity in the myocardial sleeves around pulmonary veins, superior caval vein and coronary sinus supports the presumed arrhythmogenicity of these regions. *Journal of Anatomy*, 00, 1–13. Available from: https://doi.org/10.1111/joa.13947

DOI:10.14753/SE.2025.3172

Supplementary material

Detailed immunohistochemical quantitative analysis of four specimens

Detailed immunohistochemical quantitative analysis for desmin was performed in the case of four hearts (Case No. 8, No. 11, No. 12 and No. 13). Six different structures (ventricular working myocardium and conduction system, sinoatrial node, superior caval vein, pulmonary vein, coronary sinus) were investigated in each case except one sample where pulmonary vein myocardium could not be examined due to technical reasons. For each structure of a given heart, three distinct regions with the same sizes were analysed. These regions were chosen to be representative for the whole section regarding the proportion of conducting-like cardiomyocytes exhibiting strong desmin expression and weakly immunopositive working cardiomyocytes. At first, signal intensity of the strongly immunoreactive cells of the conducting system and the extracardiac myocardial sleeves was compared with the weaker labeled ventricular working cardiomyocytes. For this analysis, twenty cardiomyocytes were chosen from each region (Figure S1.a). Those regions where less than twenty strongly immunoreactive cells could be counted were excluded from this analysis. Thereafter, difference between signal intensity at representative areas of the ventricular conduction system or myocardial sleeves and the working myocardium was also investigated (Figure S1.b). The total size of the analysed areas were equal for each region.

Below we demonstrate the analysis of one of the four hearts (Case No. 12) step by step (Figures S2-S6) and present the diagrams of desmin signal intensity in the labeled cells and in the labeled areas of all hearts (Figures S7-S10). ImageJ (Image Processing and Analysis in Java) program was applied to perform semiquantitative analyses for the intensity of desmin immunostaining. The Colour Deconvolution plugin was used to implement stain separation of hematoxylin-DAB stained images and the derived DAB image was chosen for quantification. Lower mean gray value indicates stronger desmin signal intensity.

As demonstrated by the diagrams below, differences in mean gray values were prominent between the strongly immunoreactive cardiomyocytes and the ventricular working cardiomyocytes (Figures S7.a, S8.a, S9.a, S10a). However, signal intensities of the examined representative areas differed less and larger error bars marked the higher heterogeneities of the calculated values. This can be explained by the intermingling of strongly stained conducting-like cells and less immunoreactive working cardiomyocytes in the myocardial sleeves.

DOI:10.14753/SE.2025.3172

Furthermore, extensive connective tissue between cardiomyocytes could also result in the higher mean gray value of an area especially in the case of sinoatrial nodal samples (Figures S7.b, S8.b, S9.b, S10b).

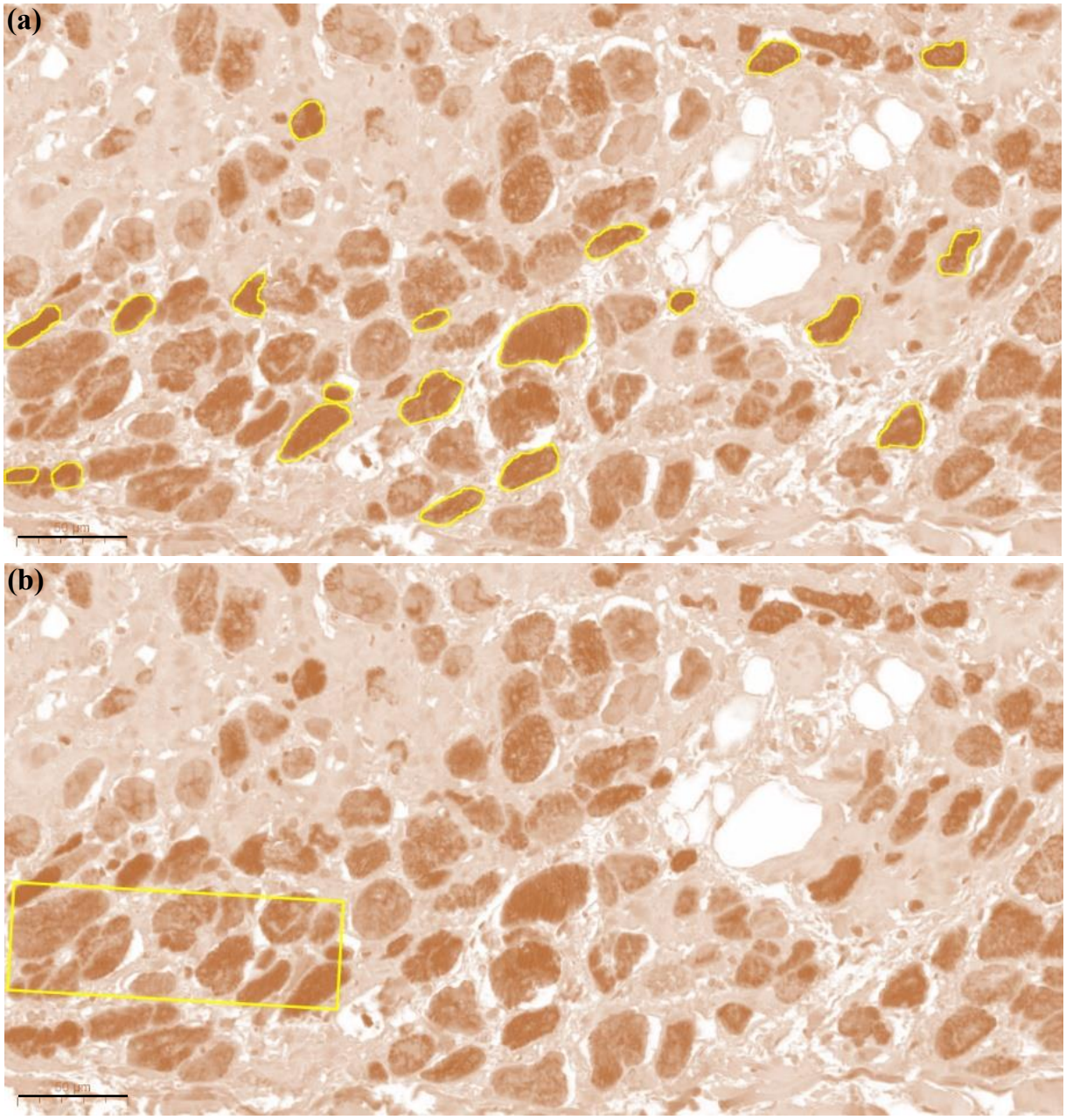

Figure S1. Quantitative analysis of desmin immunostaining for a superior caval vein sample. Mean gray values of twenty cells displaying strong desmin immunoreactivity framed by yellow were measured and averaged for the sample (a). Thereafter the mean gray value of a representative area with a given size marked by yellow square was calculated (b). Scale-bars: 50 µm

DOI:10.14753/SE.2025.3172

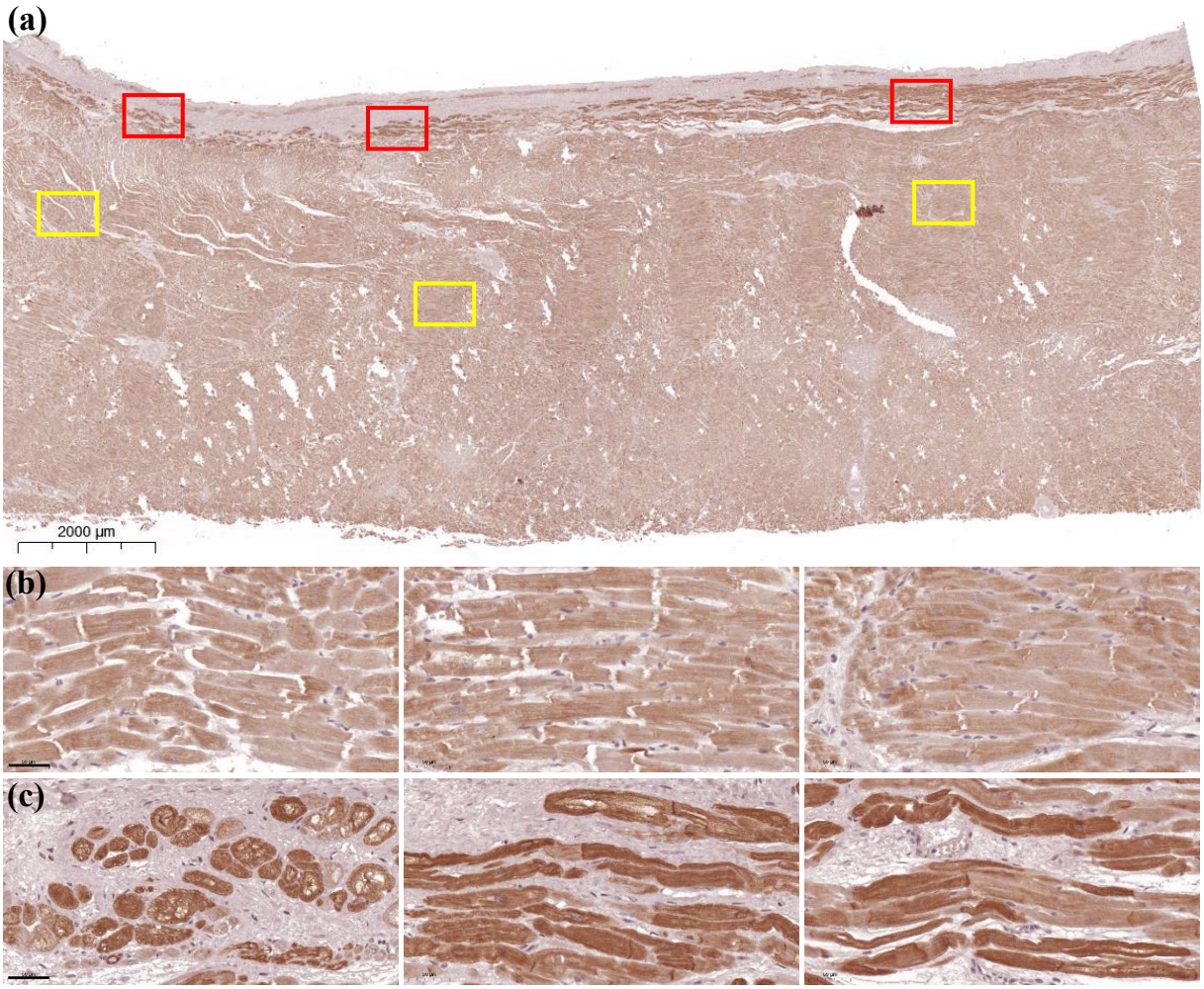

Figure S2. Case No. 12, interventricular septum, left side. Analysed regions are marked by red squares in case of the left ventricular subendocardium and by yellow squares in case of the working myocardium (a). Ventricular working cardiomyocytes of the three regions displayed weak immunopositivity (b), while conducting cardiomyocytes at the subendocardial region exhibited notably stronger desmin labeling (c). Scale-bars: 2000 µm (a), 50 µm (b, c)

DOI:10.14753/SE.2025.3172

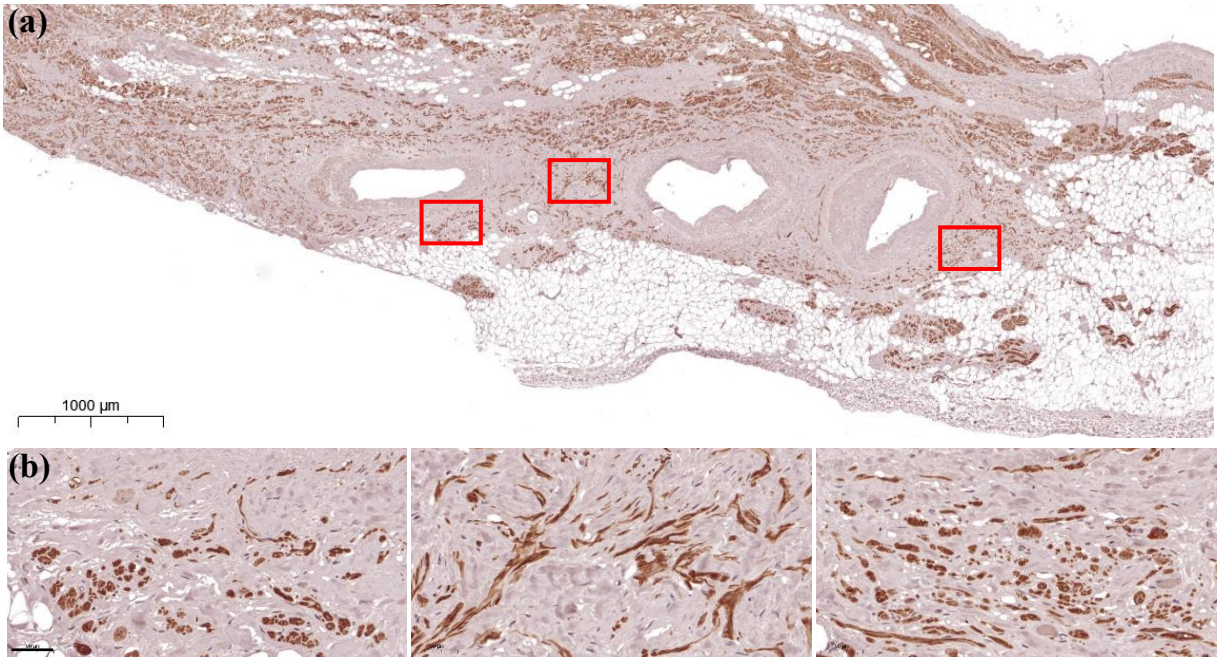

Figure S3. Case No. 12, sinoatrial node. Analysed regions of the sinoatrial node are marked by red squares (a). Pacemaker cells of the three regions displayed prominent immunopositivity (b). Scale-bars: 1000 µm (a), 50 µm (b, c)

DOI:10.14753/SE.2025.3172

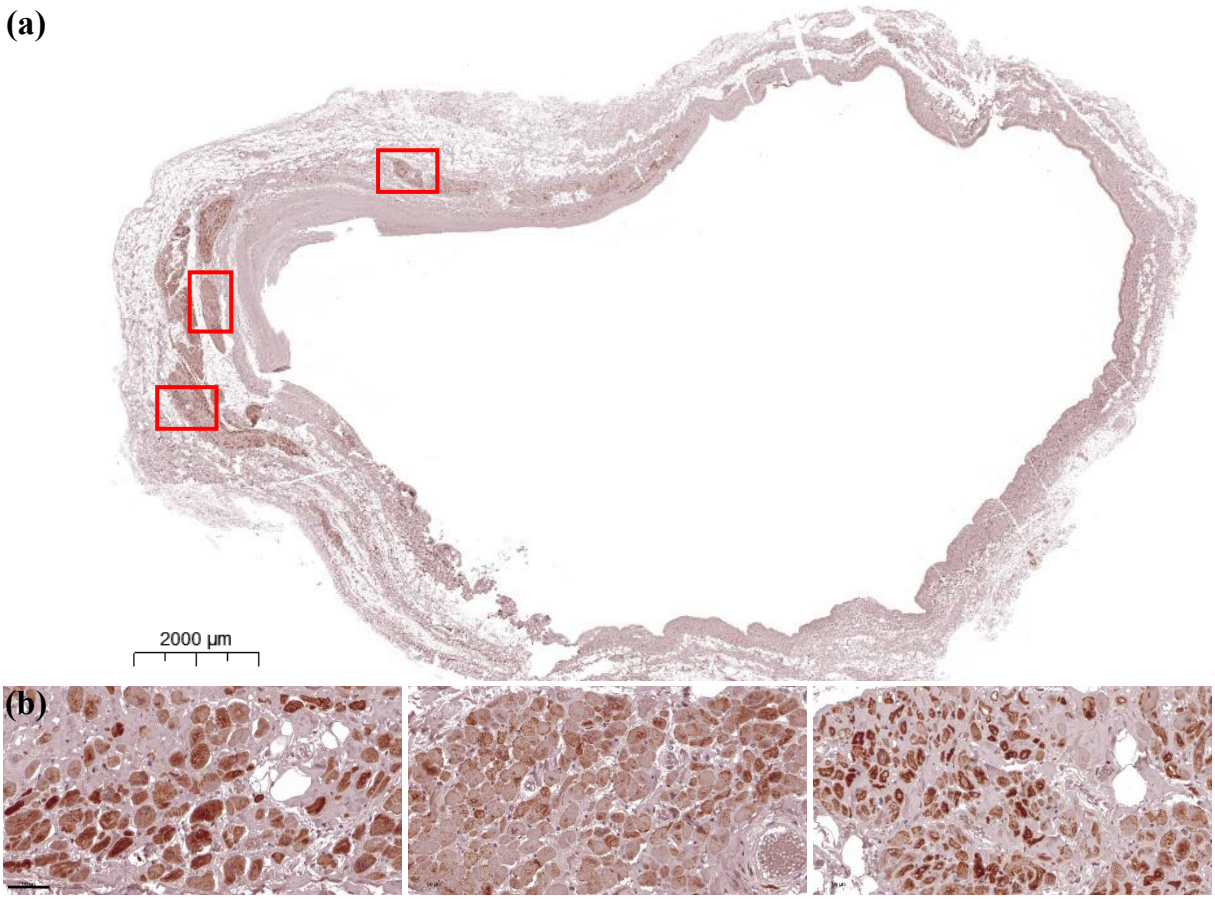

Figure S4. Case No. 12, superior caval vein. Analysed regions of the superior caval vein are marked by red squares (a). Although several cardiomyocytes of the three regions displayed prominent desmin labeling, regions showing less immunoreactive cells were also detected (b). Scale-bars: 2000 µm (a), 50 µm (b, c)

DOI:10.14753/SE.2025.3172

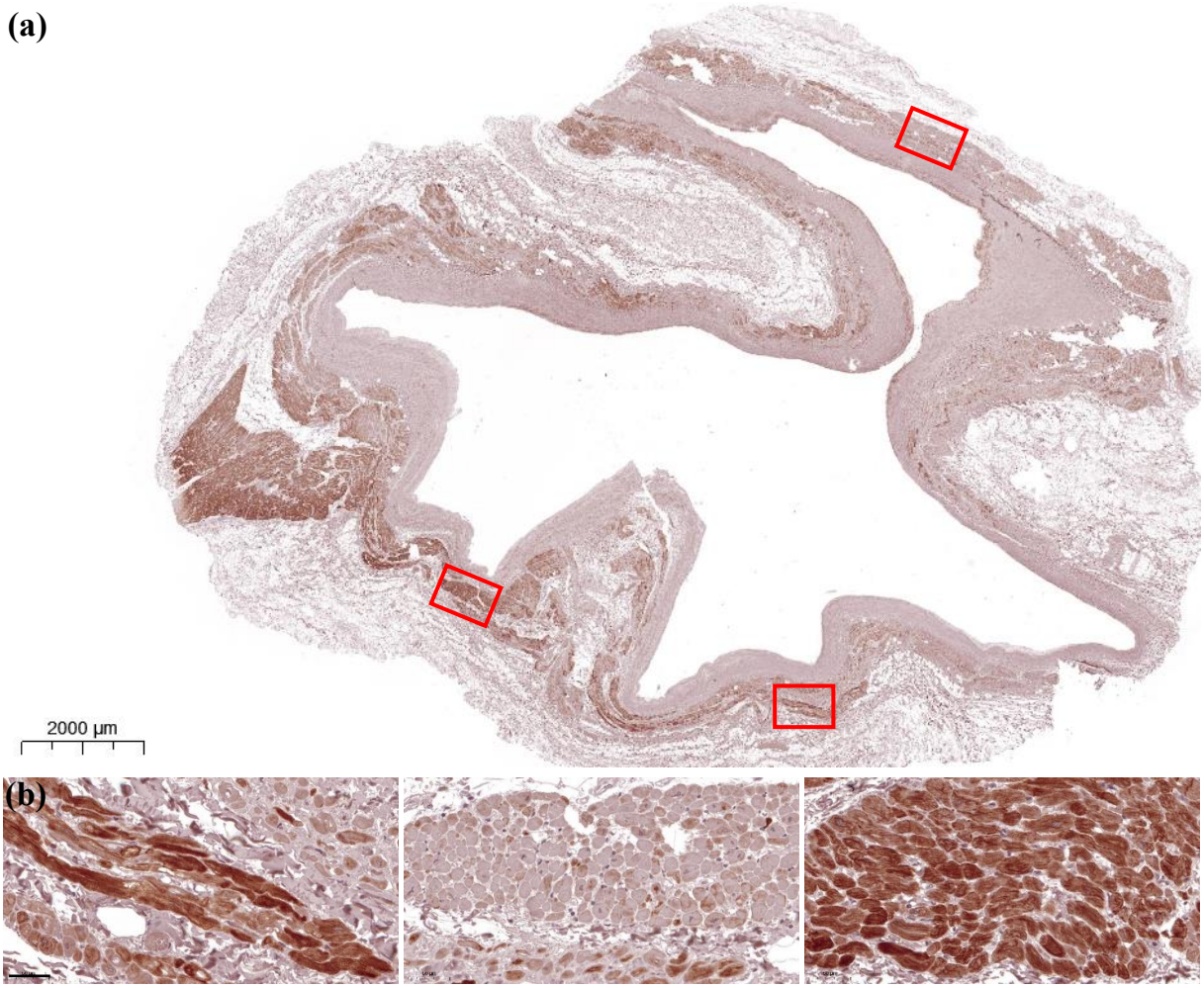

Figure S5. Case No. 12, pulmonary vein. Analysed regions of the pulmonary vein are marked by red squares (a). Although several cardiomyocytes of the three regions displayed prominent desmin labeling, regions showing less immunoreactive cells were also detected (b). Scale-bars: 2000 µm (a), 50 µm (b, c)

DOI:10.14753/SE.2025.3172

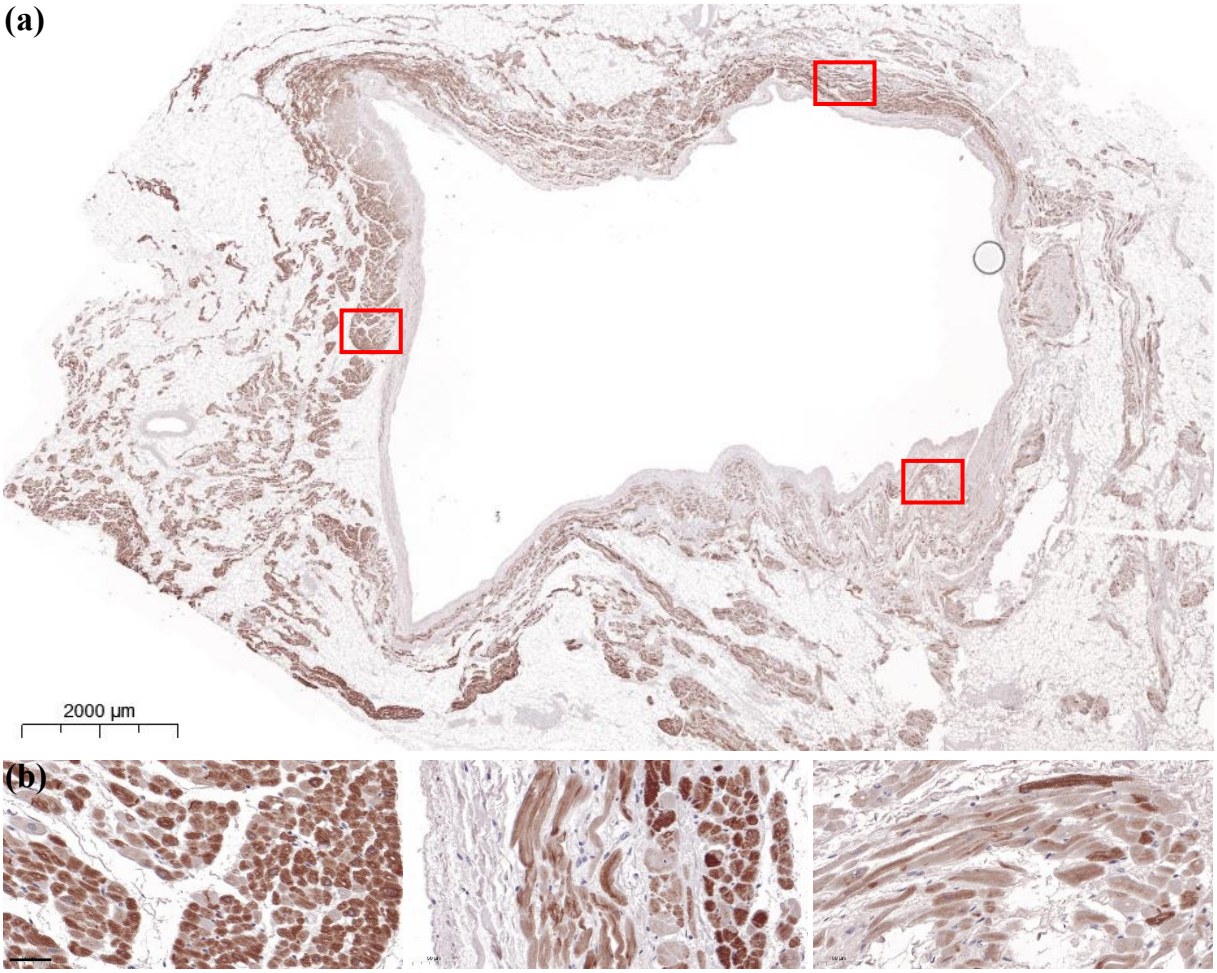

Figure S6. Case No. 12, coronary sinus. Analysed regions of the coronary sinus are marked by red squares (a). Although several cardiomyocytes of the three regions displayed prominent desmin labeling, regions showing less immunoreactive cells were also detected (b). Scale-bars: 2000 µm (a), 50 µm (b, c)

DOI:10.14753/SE.2025.3172

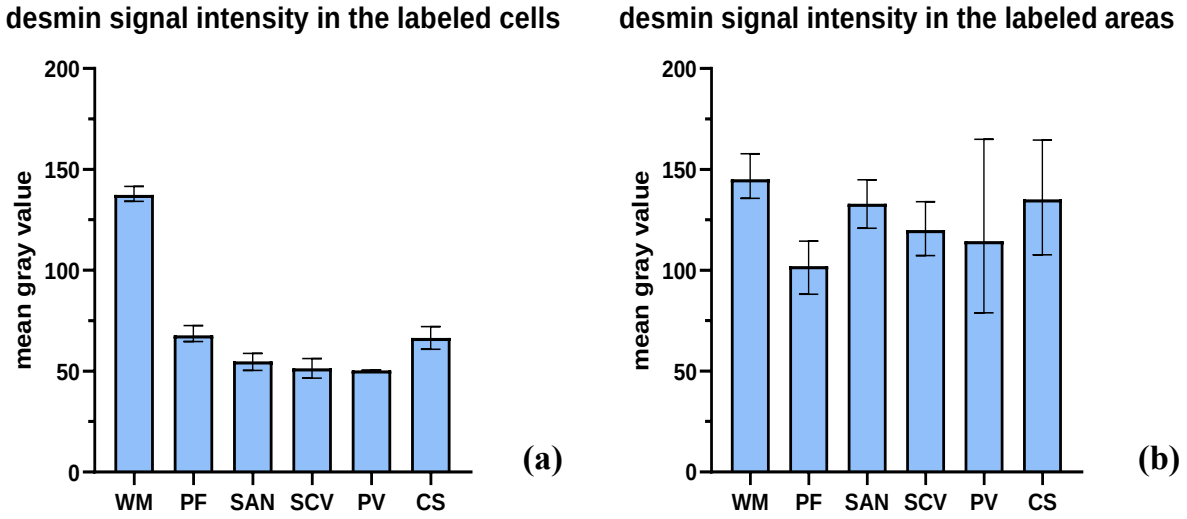

Figure S7. Quantitative analysis for all examined structures of Case No 12. Average mean gray values are presented for each structure as well as mean gray value ranges marked by error bars. Lower mean gray value indicates stronger desmin signal intensity. Differences in desmin signal intensity were more prominent between ventricular working cardiomyocytes and the conducting cardiomyocytes or highly immunoreactive cells of the venous myocardial sleeves (a) while less pronounced differences were verified between mean gray values of the representative areas (b).

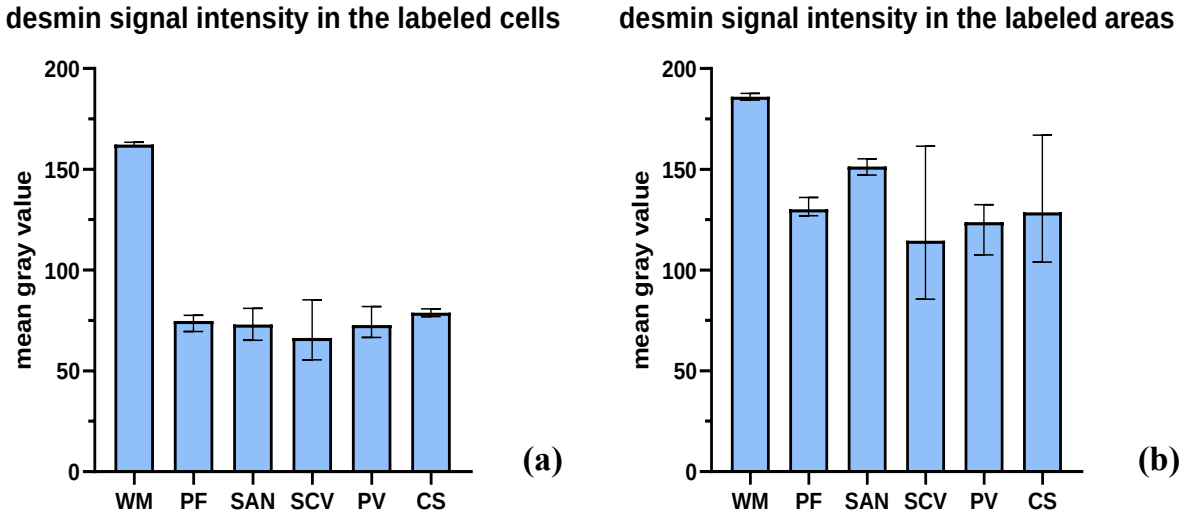

Figure S8. Quantitative analysis for all examined structures of Case No. 8. Average mean gray values are presented for each structure as well as mean gray value ranges marked by error bars. Lower mean gray value indicates stronger desmin signal intensity. Differences in desmin signal intensity were more prominent between ventricular working cardiomyocytes and the conducting cardiomyocytes or highly immunoreactive cells of the venous myocardial sleeves (a) while less pronounced differences were verified between mean gray values of the representative areas (b).

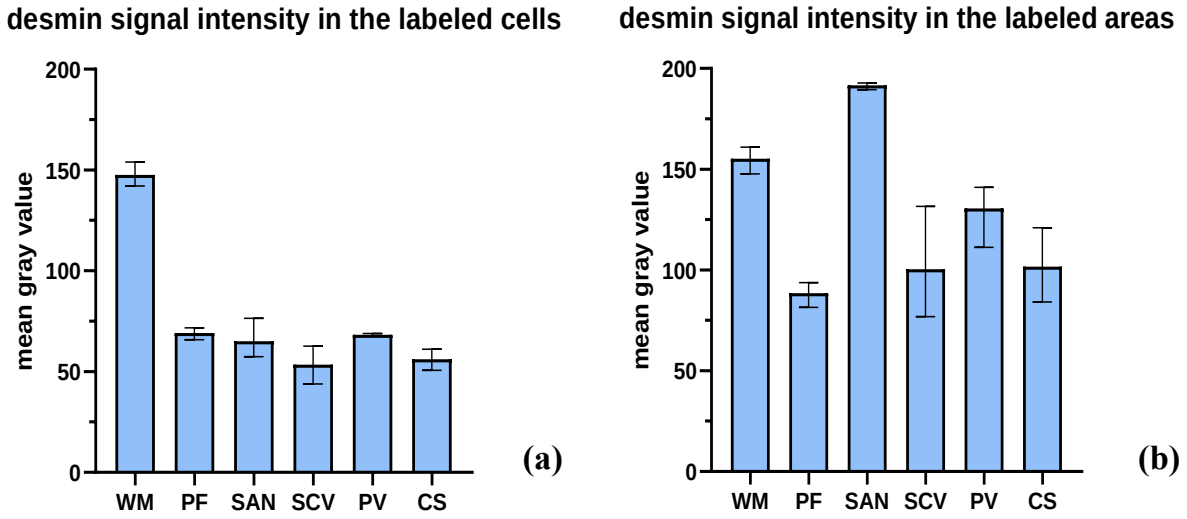

Figure S9. Quantitative analysis for all examined structures of Case No. 11. Average mean gray values are presented for each structure as well as mean gray value ranges marked by error bars. Lower mean gray value indicates stronger desmin signal intensity. Differences in desmin signal intensity were more prominent between ventricular working cardiomyocytes and the conducting cardiomyocytes or highly immunoreactive cells of the venous myocardial sleeves (a) while less pronounced differences were verified between mean gray values of the representative areas (b).

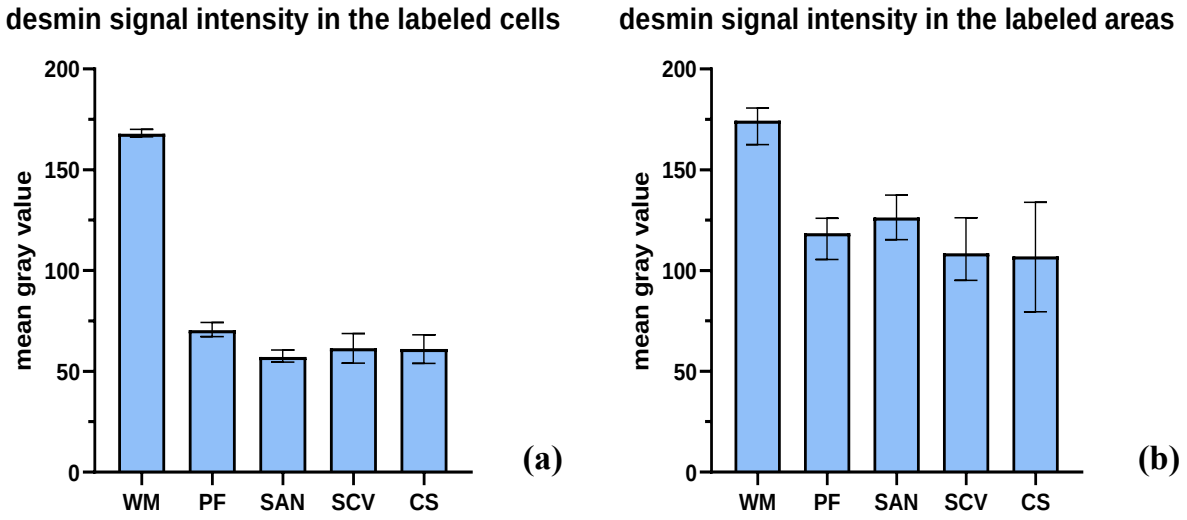

Figure S10. Quantitative analysis for all examined structures of Case No. 13. Average mean gray values are presented for each structure as well as mean gray value ranges marked by error bars. Lower mean gray value indicates stronger desmin signal intensity. Differences in desmin signal intensity were more prominent between ventricular working cardiomyocytes and the conducting cardiomyocytes or highly immunoreactive cells of the venous myocardial sleeves (a) while less pronounced differences were verified between mean gray values of the representative areas (b).